Electrochemistry as a Powerful Tool for Investigations of Antineoplastic Agents
A Comprehensive Review

Brycht, Mariola; Poltorak, Lukasz; Baluchová, Simona; Sipa, Karolina; Borgul, Paulina; Rudnicki, Konrad; Skrzypek, Sławomira

DOI
10.1080/10408347.2022.2106117

Publication date
2022

Document Version
Accepted author manuscript

Published in
Critical Reviews in Analytical Chemistry

Electrochemistry as a powerful tool for investigations of antineoplastic agents: a comprehensive review

Mariola Brycht[1,*], Lukasz Poltorak[1], Simona Baluchová[2,3], Karolina Sipa[1], Paulina Borgul[1], Konrad Rudnicki[1], Sławomira Skrzypek[1]

[1] University of Lodz, Faculty of Chemistry, Department of Inorganic and Analytical Chemistry, Tamka 12, 91-403 Lodz, Poland

[2] Charles University, Faculty of Science, Department of Analytical Chemistry, UNESCO Laboratory of Environmental Electrochemistry, Albertov 6, 128 00 Prague 2, Czechia

[3] Delft University of Technology, Department of Precision and Microsystems Engineering, Mekelweg 2, 2628 CD Delft, The Netherlands

* Corresponding author: mariola.brycht@chemia.uni.lodz.pl

Abstract

Cancer is most frequently treated with antineoplastic agents (ANAs) that are hazardous to patients undergoing chemotherapy and the healthcare workers who handle ANAs in the course of their duties. All aspects related to hazardous oncological drugs illustrate that the monitoring of ANAs is essential to minimize the risks associated with these drugs. Among all analytical techniques used to test ANAs, electrochemistry holds an important position. This review, for the first time, comprehensively describes the progress done in electrochemistry of ANAs by means of a variety of bare or modified (bio)sensors over the last four decades (in the period of 1982-2021). Attention is paid not only to the development of electrochemical sensing protocols of ANAs in various biological, environmental, and pharmaceutical matrices but also to achievements of electrochemical techniques in the examination of the interactions of ANAs with deoxyribonucleic acid (DNA), carcinogenic cells, biomimetic membranes, peptides, and enzymes. Other aspects, including the enantiopurity studies, differentiation between single-stranded and double-stranded DNA without using any label or tag, studies on ANAs degradation, and their pharmacokinetics, by means of electrochemical techniques are also commented. Finally, concluding remarks that underline the existence of a significant niche for the basic electrochemical research that should be filled in the future are presented.

Keywords

electrochemical (bio)sensors; anticancer drugs; electroanalysis; drugs-DNA interactions; drugs-cancer cells interactions.

Abbreviations

A – adenine

A-549 – human lung adenocarcinoma cell line

AdSV – adsorptive stripping voltammetry

AgNPs – silver nanoparticles

ANAs – antineoplastic agents

ATC – anatomical therapeutic chemical

AuE – gold electrode

AuNPs – gold nanoparticles

AuNRs – gold nanorods

BAX – B-cell lymphoma-2-associated X expressions

B-cells – B-lymphoblast-like Burkitt's lymphoma Raji cells

BCL-2 – B-cell lymphoma-2 expressions

BDDE – boron-doped diamond electrode

C – cytosine

C2 –2-mercaptoethanol

C4 –4-mercapto-1-butanol

C6 –6-mercapto-1-hexanol

CA – chronoamperometry

C_{dl} – double-layer capacitance

CdSe – cadmium selenide

CdSeQDs – cadmium selenide core-shell quantum dots

CEA – carcinoembryonic antigen

CHIT – chitosan

CPE – carbon paste electrode

CQDs – carbon quantum dots

$Cu(OH)_2$NTs – copper hydroxide nanotubes

Cu-TPA – copper-doped terephthalic acid

CV – cyclic voltammetry

CyA – cysteamine

DDD – defined daily dose

DH^+ – protonated daunorubicin

DME – dropping mercury electrode

DNA – deoxyribonucleic acid

DPV – differential pulse voltammetry

dsDNA – double-stranded deoxyribonucleic acid

DTT – dithiothreitol

Du-145 – prostate metastatic cancer cells

ECL – electrochemiluminescence

EIS – electrochemical impedance spectroscopy

(Eu^{3+}-Cu_2O)NPs – europium(III)-doped copper(I) oxide nanoparticles

(Eu^{3+}-NiO)NPs – europium(III)-doped nickel(II) oxide nanoparticles

ERGO – electrochemically reduced graphene oxide

FaDu – hypopharyngeal carcinoma cell line

Fe_2O_3NPs – ferrite nanoparticles

Fe_3O_4NPs – magnetite nanoparticles

G – guanine

GCE – glassy carbon electrode

GO – graphene oxide

GONRBs – graphene oxide nanoribbons

GQDs – graphene quantum dots

GTA – glutaraldehyde

HBNNSs – hexagonal boron-nitrate nanosheets

HMDE – hanging mercury drop electrode

HOPGE – highly oriented pyrolytic graphite electrode

HT-1080 – fibrosarcoma cell line

IgG-Mtx-Ab – immunoglobulin G methotrexate antibody

IL – ionic liquid

ITIES – interface between two immiscible electrolyte solutions

ITOE – indium tin oxide electrode

K-562 – chronic myeloid leukemia cell line

LMTB – leucomethylene blue

LOD – limit of detection

LR – linear range

LSV – linear sweep voltammetry

MCF-7 – breast cancer cell line

MIP – molecularly imprinted polymer

MOF – metal organic framework

MoS_2NFLs – molybdenum disulfide nanoflowers

MPA – 3-mercaptopropionic acid

MT – metallothionein

MTB – methylene blue

MWCNTs – multi-walled carbon nanotubes

N,S-ARGO – nitrogen and sulfur co-doped activated reduced graphene oxide

NADH – reduced form of nicotinamide adenine dinucleotide

NAF – Nafion

N-CQDs – nitrogen-doped carbon quantum dots

NFBs – carbon nanofibers

N-GQDs-COCl – acrylated nitrogen-doped graphene quantum dots

NiONPs – nickel(II) oxide nanoparticles

NPs – nanoparticles

N-RGO – nitrogen-doped reduced graphene oxide

NRs – nanorods

OA – oxalic acid

p-(L-Cys) – poly-(L-cysteine)

p-ANFBs – poly-acrylonitrile nanofibers

p-ANI – poly-aniline

p-ATPh – p-aminothiophenol

p-BCP – poly-bromocresol purple

PdNPs – palladium nanoparticles

p-EI – poly-ethyleneimine

p-ET – poly-ethylene terephthalate

PGE – pencil graphite electrode

PKI – protein kinase inhibitors

p-MAA – poly-methacrylic acid

p-Py – poly-pyrrole

PSA – potentiometric stripping analysis

PTC – perylene tetracarboxylic derivative

PtE – platinum electrode

pTHMMAA – N-[tris(hydroxyl-methyl)methyl]acrylamide

PtNPs – platinum nanoparticles

QCM – quartz crystal microbalance

RGO – reduced graphene oxide

SAEs – solid amalgam electrodes

SAM – self-assembled monolayer

SDS – sodium dodecyl sulfate

SERS – surface-enhanced Raman spectroscopy

SMDE – static mercury drop electrode

SPCE – screen-printed carbon electrode

SPE – screen-printed electrode

ssDNA – single-stranded deoxyribonucleic acid

SWCNTs – single-walled carbon nanotubes

SWV – square-wave voltammetry

T – thymine

TCEP – tris(2-carboxyethyl)phosphine

TiO_2NPs – titanium dioxide nanoparticles

TUB – tubulin

U-937 – histiocytic lymphoma cell line

WHO – World Health Organization

WHOCC – WHO Collaborating Centre

WI-38 – human lung fibroblast cell line

ZnO – zinc oxide

ZnONPs – zinc oxide nanoparticles

ZnOQDs– zinc oxide core-shell quantum dots

Zr(IV)-MOF – zirconium(IV)-based metal organic framework

ZrO_2NPs – zirconium dioxide nanoparticles

β-CD – β-cyclodextrin

1. Introduction

Estimates of cancer incidence and cancer mortality by the World Health Organization (WHO) indicated that cancer (also referred to as neoplastic disease) represents one of the most serious problems of the whole population, regardless of social status or wealth [1]. Over the past decade, nearly every country has seen an increase in cancer cases [2]. WHO warns that the global cancer burden is significant and is rapidly growing worldwide. Almost 19.3 million new cases and nearly 10 million (!) cancer-related deaths have been estimated in 2020 worldwide [3], and over the next two decades, the global cancer incidence will rise to 29.4 million [2].

Due to an increase in the number of new cancer cases that will further add to the workload of healthcare workers, there is a growing demand for modern treatment modalities for cancer. The most commonly applied oncological treatments are divided into two groups, *i.e.,* topical (also called local or localized) and systemic therapy, which can be used alone or in combination to increase the effectiveness of cancer treatment. Both schemes are usually applied together with supportive therapies aiming at reducing the side effects (*e.g.,* medications to reduce nausea, protect against organ damage from chemotherapy or radiation, or stimulate blood cell production)[4]. Topical therapy is a treatment directed to a specific organ or limited area of the body (*e.g.,* surgery, radiotherapy, heat or chemical ablation, and cryotherapy), whereas systemic therapy is a treatment using drugs that, when introduced into the bloodstream, reach and affect cells all over the body. Their pharmacological activity follows different mechanisms of action (*e.g.,* chemotherapy, hormonal therapy, immune therapy, and targeted therapy) [4]. Among all oncological approaches, the most often applied type of treatment of neoplastic diseases is probably chemotherapy which uses drugs referred to as antineoplastic agents (ANAs) that inhibit the growth of tumor cells by disrupting their division and rapidly killing growing cells [5]. However, ANAs are hazardous to patients undergoing chemotherapy (the toxicity of ANAs is well known since the 1940s when they began to be used in the oncological field [6]), since many are mutagenic, teratogenic, and carcinogenic [7]. In addition, ANAs are not selective in their mechanism of action; meaning that these drugs cannot distinguish between cancerous and healthy cells, thus damaging both [8]. As a result, several severe, unintended, and undesirable side effects, including cardiotoxicity, hematopoietic toxicity, pulmonary toxicity, ototoxicity, immunotoxicity, hepatic and renal toxicity, dermal toxicity, and secondary malignancies (*e.g.,* leukemia and bladder cancer) in patients who had previously received ANAs, were observed [9]. Another serious issue related to chemotherapy is the so-called medication error which is an unintended failure in the drug treatment process that can cause harmful effects to the patient [10]. The

appropriate dosing of ANAs is essential as overdosing can cause permanent and life-threatening adverse effects, while underdosing may compromise the success of chemotherapy [10, 11]. Nevertheless, the most tragic consequences are associated with the potential risk of overdose [12].

Many studies have shown the occupational exposure of ANAs to medical personnel involved in the manufacturing, administration, transport, distribution, receipt, storage, preparation, and even waste management [8, 9, 13]. Particularly vulnerable to ANAs exposure are nurses and pharmacists [14]. The first evidence describing an increase in mutagenicity in nurses working with ANAs was reported in the 1970s [15]. Acute health effects in healthcare workers who handle ANAs include headaches, hair loss, skin irritation, abdominal pain, vomiting, jaundice, eye inflammation, sore throat as well as teratogenic and adverse reproductive outcomes including spontaneous abortion, temporary or permanent infertility, and congenital malformations, and last but not least, leukemia or other neoplastic diseases [8, 9, 16, 17]. Many reports have shown the contamination by ANAs of healthcare workers and workplaces, thus, occupational, and environmental exposure to ANAs, with detectable levels of these drugs in the air, on surfaces, gloves, on different body sites, and in urine [16]. The main cause of workplace contamination with ANAs is due to failure to handle these drugs according to the safety rules/guidelines developed by many institutions, *e.g.,* National Institute of Occupational Safety and Health, International Society of Oncology Pharmacy Practitioners, the Oncology Nursing Society, Occupational Safety and Health Administration. The main routes of exposure of healthcare workers to ANAs occur by inhalation (*via* droplets and particulates especially in a form of an aerosol, dust formed from crushed tablets), dermal (*via* direct contact with skin through contaminated surfaces and formulations containing ANAs), or oral (*via* hand-to-mouth contact) route [9, 16]. Exposure to ANAs can also originate from accidental ingestion (when food or beverages are prepared, stored, or consumed in the workplace) or injection [9].

ANAs comprise a wide and heterogeneous group of chemicals with different structures, origins, and pharmacological activity. The list encompassing ANAs used in daily clinical practice contains more than 200 agents. Thus, ANAs can be categorized in a variety of ways. WHO Collaborating Centre (WHOCC) for Drug Statistics Methodology established the Anatomical Therapeutic Chemical (ATC) Classification System together with a technical unit of measurement called the Defined Daily Dose (DDD). According to the ATC/DDD system [18], ANAs can be divided into 7 groups: (i) alkylating agents, (ii) antimetabolites, (iii) plant alkaloids and other natural products, (iv) cytotoxic antibiotics and related substances, (v) protein kinase inhibitors, (vi) monoclonal antibodies and antibody drug conjugates, and (vii) other ANAs. In turn, International Agency of Research on Cancer provides classification of many substances including ANAs,

which is divided into four groups [19]: (i) group 1: carcinogenic to humans (among which are busulfan, chlorambucil, cyclophosphamide, melphalan, treosulfan, thiotepa, semustine belonging to alkylating agents group; etoposide belonging to plant alkaloids and other natural products group), (ii) group 2A: probably carcinogenic to humans (among which are azacytidine belonging to antimetabolites group; teniposide belonging to plant alkaloids and other natural products group; doxorubicin belonging to cytotoxic antibiotics and related substances group; cisplatin, procarbazine, arsenic trioxide belonging to other ANAs group), (iii) group 2B: possibly carcinogenic to humans (among which are dacarbazine, streptozocin, prednimustine belonging to alkylating agents group; bleomycin, mitomycin, mitoxantrone, daunorubicin belonging to cytotoxic antibiotics and related substances group; amsacrine belonging to other ANAs group), and (iv) group 3: not classifiable as to its carcinogenicity to humans (among which are triaziquone belonging to alkylating agents group; methotrexate, 6-mercaptopurine, 5-fluorouracil belonging to antimetabolites group; hydroxycarbamide belonging to other ANAs group).

All aspects related to hazardous oncological drugs illustrate that their quantitative and qualitative monitoring in biological samples both *in vitro* and *in vivo* is essential to minimize the associated risks. Many analytical techniques have been used to control ANAs, and these include, *e.g.,* liquid chromatography coupled to various detectors [20–28], gas chromatography [21, 23, 24], capillary electrophoresis [25, 29], chemiluminescence [30], or spectroscopy-based methods [25, 27, 31]. Although these techniques are sensitive, specific, and accurate, they require sophisticated and expensive equipment along with trained staff. In addition, analytical protocols based on chromatography/spectrometry/spectroscopy usually require labor-intensive and time-consuming sample pretreatment which can lead to the potential loss of the analyte of interest [23]. These problems can be overcome with electroanalytical techniques assuring simplicity, fast response, low cost, reliability, and usually no need for a sample pretreatment process [28]. Electrochemical sensing units can be easily miniaturized, which enables the development of devices that can be used at the point-of-care analysis [32, 33]. In addition, the modification of the sensing interface with nanomaterials or specific affinity layers may significantly improve the selectivity and sensitivity. However, nanomaterials may lead to a possible risk to the environment and reveal toxicity towards biological systems, thus, the possible genotoxicity of nanomaterials should be taken into consideration during (bio)sensors development.

For the stated reasons, electro(analytical)chemistry has been favorably applied to study ANAs, however, only a few attempts have been made to summarize and critically discuss the achieved progress. To the best of our knowledge, only three review papers covering the topic of selected electroanalytical

applications for the determination of some ANAs in the period of (mostly) 2011-2015 [34], 2013-2018 [28], and 2016-2019 [25], can be found in the literature. However, each work discusses less than 30 publications related to electrochemical sensing of only selected ANAs. Although some aspects of electrochemistry of ANAs can be found in the aforementioned works, undoubtedly these are insufficiently addressed and well beyond the current state of the art.

Herein, we discuss existing knowledge derived from the electrochemical works focused on ANAs that have been studied at a variety of bare and modified (bio)sensors over the last (nearly) four decades (in the period of 1982-2021). This review is focused on ANAs that were tested electrochemically broken down on the basis of a selection made by the WHOCC [18] (*i.e.,* 76 compounds out of 266 classified by WHOCC). Based on our survey, we concluded the topic of ANAs electrochemistry attracted the attention of the scientific community only recently since more than 80% of publications cited in this review (over 320 publications out of 390 publications) appeared in the last 10 years (in the period of 2011-2021) (see Fig. 1). A comprehensive overview of ANAs electroanalysis is divided into discussion, chosen superior sensing examples that are underlined, tabulated electroanalytical parameters (covering methodology, type of modification, sensing mechanism, selectivity aspects along with sensitivity and detection limits) together with concluding remarks and further directions. Also, significant attention was given to the detection mechanism (direct-indirect, type of a charge transfer) and sensing environments (biological and environmental matrices as well as pharmaceutical formulations). Our critical approach was based on the highest analytical standards. In addition, the interactions of ANAs with single-stranded (ss) and double-stranded (ds) deoxyribonucleic acid (DNA), and various carcinogenic cell lines studied by electrochemical techniques are commented. Finally, other aspects including interactions of ANAs with biomimetic membranes, peptides, and enzymes, enantiopurity study, differentiation between ss- and ds-DNA without using any label or tag, other studies on ANAs degradation, and pharmacokinetics study, are also discussed. This review fills the existing literature niche and offers a comprehensive overview of the proposed topic.

----------Here in Fig. 1----------

2. Electrochemistry of ANAs

2.1. Alkylating agents

The first section is focused on alkylating agents (also referred to as alkylators), which are a diverse class of ANAs that cause the alkylation of nucleic acids, which in consequence inhibits protein synthesis. They are widely used in the chemotherapy of numerous neoplastic diseases [35]. This group of ANAs is composed of 6 subclasses including nitrogen mustard analogs, nitrosoureas, alkyl sulfonates, ethylene imines, epoxides, and other alkylating agents.

So far, only 12 out of 28 alkylating agents have been studied using electrochemical techniques, leaving more than half aside (see Table S1). This large gap should be filled in the near future. A summary of electrochemically studied alkylating agents along with their structure is provided in Table 1, which summarizes the collected data and obtained electroanalytical parameters.

The approaches used for electrochemical detection of alkylating agents can be divided into two main groups:

(i) direct oxidation or reduction on either bare or modified electrodes using sensing protocols based on sensitive voltammetric techniques; a thorough overview of all important analytical figures of merit can be found in Table 1 along with selectivity studies and media tested.

For oxidation of alkylating agents, the vast majority of reported sensing protocols employed sp^2 carbon-based electrodes further modified with different (bio)materials aiming at enhancing sensitivity, selectivity, and the limits of detection (LOD) of the proposed protocols. Typically, metal nanoparticles (NPs) [36–39], multi-walled carbon nanotubes (MWCNTs) [38, 40–44], reduced graphene oxide (RGO) [37, 45, 46] and enzymes [40], often in a combination, were used. For example, cytochrome P4503A4 and cytochrome P4502B6, which are the main enzymes catalyzing 4-hydroxylation of **ifosfamide** and **cyclophosphamide** (both *nitrogen mustard analogs*), respectively, were used to functionalize MWCNTs placed at the screen printed carbon paste electrode surface making the biosensors allowing for the sensitive detection of the mentioned ANAs within their typical pharmacological levels in human serum [40]. Also, new electrochemical detection platforms based on molecularly imprinted polymers (MIPs) were developed for direct oxidation of 5 alkylating agents, *i.e.,* **chlorambucil**, **ifosfamide**, **melphalan** (all *nitrogen mustard analogs*), **dacarbazine**, and **temozolomide** (both *other alkylating agents*) [44–49] (as indicated in Table 1). MIP represents unique molecular recognition systems possessing (usually) specific cavities matching only the template molecules (chosen alkylating agent), and when used as the electrode surface modification leads

to substantially enhanced selectivity. MIP-based sensors, supported with a range of additional modifiers, successfully overcome problems with interfering compounds, that can co-exist in physiological liquids.

On the contrary, electrochemical methods based on reduction of the selected alkylating agents, specifically, **fotemustine**, **streptozocin**, **lomustine**, **carmustine** (all *nitrosoureas*), **chlorambucil** (*nitrogen mustard analog*) and **dacarbazine** (*other alkylating agent*), usually employ bare mercury (Hg) or solid amalgam electrodes (SAEs) without any modification. These systems provide highly satisfactory analytical parameters in terms of selectivity and low LOD values. Regarding the former, this is related to the fact that most of the possible interferents (*e.g.*, dopamine, uric acid, ascorbic acid, glucose, etc.) are not reducible and provide only oxidation signals.

(ii) indirect detection through changes in electrochemical responses of redox probes or purine bases.

Cyclophosphamide (*nitrogen mustard analog*) has attracted the attention of electrochemists despite its non-electroactivity. Several indirect electrochemical sensing strategies exist for this drug:

The first strategy is derived from the MIP-based modification coupled to the gate effect. Briefly, this approach is based on following the change in the current originating from the oxidation/reduction of redox probe, in this case, ferro-/ferricyanide anions ($[Fe(CN)_6]^{3-/4-}$) effected by the analyte adsorption to the active sites in the polymeric layer. Recorded drop in currents was observed after binding of cyclophosphamide to MIP cavities (the mass transfer of the redox probe to the electrode surface is hindered when the analyte resides in MIP cavities). Since the amount of bounded molecules correlates well to the decrease in the redox currents of an indicator, this methodology can be successfully applied for sensing. Particularly, two MIP-gate effect systems have been developed for cyclophosphamide monitoring: a platform integrating MIP with a microfluid chip utilizing only a two-electrode system, *i.*e., a platinum (Pt) wire acted simultaneously as reference and counter electrode, and 3D nanoporous gold (Au) – silver (Ag) alloy microwire modified with MIP was employed as working electrode [50], and a novel sensor containing nitrogen and sulfur co-doped activated RGO (N,S-ARGO) and MIP [51] (the scheme of the sensor fabrication for cyclophosphamide sensing is presented in Fig. 2A).

The second approach employs either a pencil graphite electrode (PGE) or carbon paste electrode (CPE) modified with ss/dsDNA [52]. As already mentioned, cyclophosphamide is electrochemically inactive, however, DNA molecules provide oxidation peaks of guanine (G) and adenine (A). After incubation of both ssDNA and dsDNA-modified carbon electrodes with cyclophosphamide, an increase in A or G signal, respectively, was observed because of the interaction of cyclophosphamide with DNA. Importantly, the

differential pulse voltammetric (DPV) signals of purine bases increased gradually with the increasing concentration of cyclophosphamide, which was advantageously used to develop the electrochemical method for its determination.

The versatility of electrochemical investigation tools is further demonstrated for:

(i) interaction studies of alkylating agents with carcinogenic cell lines.

Interesting results were published in which the sensitivity of **cyclophosphamide** (*nitrogen mustard analog*) on the breast cancer cell line (MCF-7) has been evaluated using a mini-electrochemical system constructed by integrating PGE modified with threonine as the working electrode and a micropipette tip as an electrochemical cell (Fig. 2B) [53]. The voltammetric signal of the suspension of MCF-7 cells decreased visibly with increasing cyclophosphamide concentration, therefore, these results reflected the influence of cyclophosphamide on inhibition of MCF-7 cell growth. A new disposable electrochemical device with an integrated indium tin oxide electrode (ITOE) and a filter paper as the electrolytic cell was reported to study the electrochemical behavior of chronic myeloid leukemia cell line (K-562) and the effect of cyclophosphamide on cell viability and toxicity [54]. Cyclophosphamide was found to have a significant influence on the voltammetric response of K-562 cells as this decreases in the presence of the drug. The great advantage of the proposed systems [53, 54] is the possibility of using a reduced volume of cell samples (10 µL) in comparison with traditional electrochemical systems (>500 µL). In another work, the HeLa cell-based chip, which contained three gold electrodes (AuEs) patterned on a silicon substrate, was used to study cancer cell growth, viability, and cyclophosphamide-related toxicity by cyclic voltammetry (CV) and potentiometric stripping analysis (PSA) [55].

(ii) studying the interactions of alkylating agents with DNA.

The interaction of **bendamustine** (*nitrogen mustard analog*) with dsDNA in the absence and presence of quercetin as an effective radical scavenger, which exhibits anticancer activity by preventing oxidative cell damage, was studied by DPV and electrochemical impedance spectroscopy (EIS) [56]. The results indicated the interaction between dsDNA and quercetin as well as between dsDNA and bendamustine both in the absence and presence of quercetin. It was found that quercetin prevents the interaction between bendamustine and DNA as a result of its strong interaction with DNA.

The interaction between **busulfan** (*alkyl sulfonate*) and dsDNA immobilized on a screen-printed carbon electrode (SPCE) was tested by CV and DPV in the absence and presence of crystal violet which was used as an effective electroactive external redox indicator to monitor crosslinks or damage to dsDNA [57].

Busulfan was found to interact with the dsDNA immobilized on SPCE (the structure of immobilized dsDNA on the SPCE surface is damaged by the adsorbed busulfan). The interaction of busulfan with dsDNA led to a decrease in the amount of loaded crystal violet in the DNA film, and thus, to a decrease in its peak current. Therefore, the crystal violet interaction with the DNA film is hampered accordingly (crystal violet binds less preferentially to the damaged dsDNA). Interestingly, up to now, busulfan is the only compound belonging to the *alkyl sulfonates* subgroup, which has been tested electrochemically; however, an electroanalytical sensing protocol for this drug has not yet been developed.

The interaction of **dacarbazine** (*other alkylating agent*) with dsDNA in the solution was studied using SPCE by CV and DPV, and the results showed that dacarbazine binds to dsDNA by a combined effect of intercalation and electrostatic interaction (the results confirmed by UV–vis spectroscopy) [58]. The interaction of dacarbazine with ssDNA and dsDNA immobilized onto PGE was investigated by DPV and EIS [59]. It was concluded that dacarbazine interacted more effectively with ssDNA than with dsDNA since a higher decrease in redox signals originating from both, dacarbazine and G oxidation, was observed. In another work, the interaction of dacarbazine and dacarbazine–Cu^{2+} complex with ssDNA and dsDNA was studied on hanging mercury drop electrode (HMDE) using CV and square-wave voltammetry (SWV) [60]. It was found that both, dacarbazine and its complex with Cu^{2+} bind to dsDNA and ssDNA, however, the binding nature is different. The interaction of dacarbazine and dacarbazine–Cu^{2+} complex with dsDNA indicated intercalation into the base stacking domain of dsDNA double helix, whereas the interaction of dacarbazine with dsDNA in the presence of Cu^{2+} led to much stronger intercalation. The dacarbazine molecule, acting as an intercalator, is inserted into the base stacking domain of the dsDNA double helix, while the interaction mode of dacarbazine molecules with ssDNA is electrostatic attraction *via* negative phosphate on the exterior of the ssDNA.

The biomolecular binding behavior of **dacarbazine** (*other alkylating agent*) with DNA and DNA bases, *i.e.*, purines (A and G) and pyrimidines (thymine (T) and cytosine (C)) has been studied in the presence of gold NPs (AuNPs) by DPV [61], AuNPs functionalized with 3-mercaptopropionic acid and triphenylphosphine by CV [62], and titanium dioxide NPs (TiO_2NPs) by CV [63] (Fig. 2C illustrates the biomolecular binding behavior of dacarbazine in the presence of TiO_2NPs). Results indicated that the presence of AuNPs, functionalized AuNPs, and TiO_2NPs can increase the binding affinity of dacarbazine to DNA and DNA bases and efficiently enhance biomolecular recognition and facilitate the specific interaction between dacarbazine and DNA/DNA bases. Furthermore, the results indicate that the binding of purines to dacarbazine is stronger than that of pyrimidines in the order of A > G > T > C [62] or A > G > C > T [61, 63].

The electrochemical monitoring of the interaction of **temozolomide** (*other alkylating agent*) with dsDNA and ssDNA on PGE by CV and EIS is a subsequent example of bioelectrochemical investigations [64]. It was found that temozolomide could reach the purine bases more easily in the ssDNA as compared with dsDNA due to the conservative structure of dsDNA. In addition, the results have shown a preferential interaction of temozolomide with the G–C sites than A–T DNA sites. In addition, the interaction of temozolomide and its metabolites (5-aminoimidazole-4-carboxamide and methyldiazonium ion) with dsDNA was studied using DPV at the glassy carbon electrode (GCE) [65]. The results obtained revealed the decrease in the dsDNA oxidation peak currents with increasing incubation time, showing that temozolomide interacts with dsDNA, causing its condensation.

(iii) differentiation between ssDNA and dsDNA without using any label or tag.

The interaction mechanism of **temozolomide** (*other alkylating agent*) with methylated dsDNA sequences was investigated using DPV at PGE as depicted in Fig. 2D [66]. According to the results, temozolomide behaved as a hybridization indicator because of its different electrochemical behavior toward different DNA strands. After the interaction of temozolomide with DNA, hybrid dsDNA signals decreased dramatically, whereas probe ssDNA and control signals remain almost unchanged; thus, the signal differences enabled distinguishing between ssDNA and dsDNA without using a label or tag.

(iv) other studies on degradation.

Degradation of **lomustine** (*nitrosourea*) in an aqueous solution was investigated using DPV at GCE and comet assays [67]. It was proved that lomustine undergoes spontaneous degradation in aqueous solutions, being more enhanced in basic pH media, without the formation of electroactive degradation products. This instability was confirmed by high-performance liquid chromatography. However, the predominant degradation product, 2-chloroethyl carbon ion, caused alkylation of the purine bases of DNA. Indeed, the study confirmed that lomustine and its degradation products interact with dsDNA causing conformational changes in the DNA strands, double-helix condensation, and subsequent unwinding and breaking of double helix chains, as the incubation time increased. The comet assay indicated conformational changes in dsDNA induced by lomustine and its degradation product(s), complementing the results obtained using DPV.

----------Here in Fig. 2----------

----------Here in Table 1----------

2.2. Antimetabolites

The second section is focused on antimetabolites (also referred to as antimetabolic agents), which are analogs of biogenic metabolites interfering during the synthesis of DNA and RNA. They are incorporated into the DNA strand or block the catalytic activity of essential enzymes, which results in the inhibition of DNA synthesis [78]. This group of ANAs is comprised of 3 subgroups, *i.e.,* folic acid analogs, purine analogs, and pyrimidine analogs.

Importantly, antimetabolites are the most widely studied group of ANAs; specifically, 14 out of 20 compounds have already been investigated with electrochemical techniques (6 compounds left aside are listed in Table S1). The reported electrochemical sensing protocols for 13 antimetabolites, whose parameters are comprehensively presented in Table 2, can be split into three groups:

(i) direct oxidation or reduction approaches using a range of bare or modified electrodes.

The vast majority of reports fall into this group. The developed protocols utilized a wide range of conductive support, either in the unmodified or modified (with a variety of materials) form, and the selected studies are presented below (however, readers are invited to get a complete overview of the methods further summarized in Table 2).

Among all published sensing protocols for **methotrexate** (*folic acid analog*), sensor based on ITOE modified with magnetite NPs (Fe_3O_4NPs) and poly-aniline (p-ANI) provided an extremely low and unbeatable LOD value of 400.0 aM (!), and was applied for methotrexate determination in spiked blood serum and blood serum collected from patients after their treatment with methotrexate [79]. Another approach utilized multi-frequency EIS and multivariate data analysis immunosensor based on AuE modified with antibodies [80, 81]. The sensing surface preparation presented in [80] is schematically shown in Fig. 3A. The determination of methotrexate in model solution [81] and blood serum [80] was performed using a conventional three-electrode electrochemical cell and the electrochemical cell consisting of two modified electrodes placed in a poly-dimethylsiloxane flow chamber, respectively. Both platforms provided an impressively wide linear range (LR) spanning over 8 orders of magnitude and very low (comparable) LOD values of 7.0 pM and 5.0 pM, respectively. A much narrower LR but still with a competitive LOD of 100.0 pM was obtained on GCE modified with Nafion (NAF) and nickel(II) oxide NPs (NiONPs). Its selectivity was verified in the presence of potentially interfering agents (listed in Table 1) including ANAs, *i.e.,* 5-fluorouracil (belonging to antimetabolites) and mitoxantrone (belonging to cytotoxic antibiotics and related substances) [82]. Worth mentioning and especially interesting is

quantification of multianalytes, *i.e.,* methotrexate (therapeutic drug), urea, uric acid (both being side effect indicators), and lactate dehydrogenase (being excellent prognostic indicator), which has been performed in the microfluidic device equipped with electrochemical sensor array [83]. This sensing chip exhibited LOD of 35.0 nM towards methotrexate which is much lower than the minimum therapeutic human serum concentration.

The best analytical parameters for **pemetrexed** (*folic acid analog*) (LOD of 330.0 pM; good recovery from spiked real samples; selectivity study) were achieved on CPE modified with palladium NPs (PdNPs), carbon nanofibers (NFBs), ionic liquid (IL), and NAF [84].

Two MIP-based sensors applied for **6-mercaptopurine** (*purine analog*) detection are certainly worth mentioning [85, 86]. First MIP sensor based on PGE modified with core-shell zinc oxide (ZnO) - graphene quantum dots (GQDs) leads to a relatively low LOD of 5.7 nM and two LRs [85], while nanohybrid-based MIP consisting of nitrogen-doped carbon silica nanospheres, PdNPs, and IL modified PGE allowed trace level detection of 6-mercaptopurine (LOD of 722.8 pM) within a wide continuous LR [86]. Both sensors exhibited excellent selectivity to other interfering agents; however, the sensor proposed in [86] was especially selective towards ANAs, *i.e.,* chlorambucil, ifosfamide, temozolomide (which belong to alkylating agents), 5-fluorouracil, 6-thioguanine (which belong to antimetabolites). Nevertheless, other configurations, such as GCE modified with MWCNTs and cationic surfactant (hexadecyl(trimethyl)ammonium bromide) [87], CPE modified with platinum NPs (PtNPs), MWCNTs and IL [88], and SPCE modified with Fe_3O_4NPs, poly-pyrrole (p-Py) and PtNPs [89], do exist and allow the determination of 6-mercaptopurine at LOD levels < 10 nM. These examples provide simple surface modification protocols with LODs holding the same order of magnitude as the MIP-based sensor proposed in [85], while maintaining satisfactory selectivity.

Similar to the compound above, superior analytical characteristics (LOD of 119.6 pM) for **6-thioguanine** (*purine analog*) were achieved with the MIP sensor based on PGE modified with poly-neutral red and electrochemically reduced graphene oxide (ERGO) [90]. Also, notable is the work describing the determination of 6-thioguanine in the presence of folic acid on ferrocenedicarboxylic acid and MWCNTs modified CPE (LOD of 8.5 nM) [91].

Our attention was also paid to **cladribine**, **fludarabine**, and **clofarabine** (all *purine analogs*). The determination of clofarabine [92] and fludarabine [93] on bare GCE enabled the detection of these drugs with acceptable LOD values of 80 nM and 280 nM, respectively. As expected, modifying a GCE surface with a layer of functionalized MWCNTs led to a lower LOD value of 29.0 nM for fludarabine [94]. Further, a catalytic adsorptive stripping voltammetric (AdSV) method has been developed for cladribine [95] and fludarabine

[96] determination. This non-conventional approach was based on the oxidation products (adsorbed on the surface of PGEs) of the two compounds manifesting electrocatalytic activity towards reduced form of nicotinamide adenine dinucleotide (NADH) oxidation. Briefly, the obtained catalytic current of NADH was linearly dependent on the immobilized oxidation products, which were related to the concentration of the parent molecule (NADH) in the analyzed solution. The proposed sensors were successfully utilized for cladribine and fludarabine determination in blood serum [95] and urine samples [95, 96] obtained from patients treated with these drugs.

Electroanalytical sensing strategies for **5-fluorouracil** (*pyrimidine analog*) are predominantly based on its oxidation [97, 98, 107–116, 99–106], and superior analytical parameters for 5-fluorouracil were obtained on HMDE in the presence of Cu^{2+} [116]; particularly, an extremely low LOD value of 7.7 pM was obtained as a result of the ability of 5-fluorouracil to create a stable complex with Cu^{2+}, which made this protocol unbeatable compared to other described electroanalytical systems. Despite this, it is worth mentioning the report where CPE modified with praseodymium-erbium(III) tungstate NPs enables the detection of 5-fluorouracil at the LOD of 980.0 pM [111]. In addition, the determination of 5-fluorouracil on GCEs modified with p-ANI, zinc oxide NPs (ZnONPs), and GQDs [99], as well as with nitrogen-doped carbon quantum dots (N-CQDs), ferrite NPs (Fe_2O_3NPs), and MWCNTs (for preparation see Fig. 3B) [101] was possible in the presence of ANA, *i.e.*, irinotecan (which belongs to plant alkaloids and other natural products) [99], as well as uric acid and xanthine [101].

Capecitabine (*pyrimidine analog*) sensing protocol based on its oxidation signal was proposed on poly-propylene hollow fiber PGE modified with functionalized MWCNTs and poly-(hydroxy urethane) [117]. The sensor exhibited not only a low LOD value of 110.0 nM but also enabled capecitabine determination in the presence of ANA, *i.e.,* erlotinib (which belongs to protein kinase inhibitors; see Chapter 5).

Rather limited attention has been drawn from the point of view of electroanalysis to the determination of **cytarabine** (*pyrimidine analog*). Sensing protocol based on direct oxidation of this molecule was proposed and is based on MIP sensor prepared on PGE modified with Au nanorods (AuNRs) [118]. The MIP-based sensor was very selective, especially towards ANAs, *i.e.*, 6-mercaptopurine, 6-thioguanine, 5-fluorouracil (which belong to antimetabolites).

Amperometric determination of **floxuridine** (*pyrimidine analog*) was performed with the use of a static mercury drop electrode (SMDE) [119]. The analytical utility of the mentioned report is rather low since the LOD value and selectivity studies are simply missing.

Amperometric sensing of **gemcitabine** (*pyrimidine analog*) carried out on a bare boron-doped diamond electrode (BDDE) allowed the drug detection with a relatively low LOD value of 570.0 nM [120]. Although gemcitabine was stated to be not electrochemically oxidizable or reducible on bare GCE [121], its direct detection was possible on GCE modified with ERGO and bismuth NPs [122]. Better parameters (LOD of 9.0 nM) were achieved on bare CPE in the presence of anionic surfactant sodium dodecyl sulfate (SDS) [123], and MIP sensor based on dsDNA, silver NPs (AgNPs), and MWCNTs (LOD of 12.5 nM) [124].

Even though **raltitrexed** (*pyrimidine analog*) can be directly irreversibly oxidized on GCE under a pH-dependent and predominantly diffusion-controlled process [125], to the best of our knowledge, there is no electroanalytical sensing protocol for this drug.

For more than half of the antimetabolites studied up to now (*i.e.,* 8), also reduction signal was favorably used to develop a reliable voltammetric method for their electroanalysis. A range of electrodes was tested and most of them provided truly impressive parameters, predominantly in the form of very low LOD values, while the major drawback of most of the approaches based on reduction signals remains poorer selectivity (this issue was tackled for some compounds as discussed below).

Impressively low LOD values (nM or even pM) for **methotrexate** (*folic acid analog*) have been reported for electrodes using Hg, either in (i) a pure form, *i.e.* HMDE [126–128], (ii) in combination with silver to form silver SAEs, after polishing [129], or in a form of meniscus [130], or (iii) as a modifier to prepare Hg film-coated carbon fiber ultramicroelectrode [131]. Similarly, determinations of **6-thioguanine** [132], **nelarabine** [133] (both *purine analogs*), **5-fluorouracil** [68] (*pyrimidine analog*) were carried out only on traditional Hg dropping electrodes. However, the more advanced approach based on polypyridyl cobalt complexes used as modifiers [134, 135] was utilized for **6-mercaptopurine** (*purine analog*) detection. Also, one sensing protocol utilized the reduction signal of the 6-mercaptopurine-Cu^{2+} complex, which was formed on a hanging copper amalgam drop electrode [136]. The formation of such complex at the electrode surface decreased the LOD value to unbeatable 120.0 pM, allowed the analysis of 6-mercaptopurine to be performed in the presence of 6-thioguanine (belonging to the same group of purine analogs). Next, **capecitabine** (*pyrimidine analog*) was electrochemically reduced on a bare GCE [137], however, improved LOD (by one order of magnitude) values were obtained when a modification layer, either consisting of ZnONPs and functionalized MWCNTs [138] or AuNPs and graphene NFBs [139], was applied to a surface of CPE or GCE, respectively. Nevertheless, the lowest LOD of 324.0 pM was achieved on the MIP sensor based on GCE modified with Fe_3O_4NPs and graphene oxide (GO). The sensor was found to be selective towards other compounds including ANA, *i.e.,* 5-fluorouracil (which belongs to antimetabolites) [140]. Sensing protocol

based on direct reduction of cytarabine was carried out using GCE coated with a Hg film, and a very low LOD value of 551.0 pM was achieved [141]. In addition, this drug can be successfully detected in the presence of potentially interfering organic compounds, *e.g.,* ascorbic acid and uric acid, at the same time being problematic in the presence of some metal ions. Finally, a complex MIP-based sensor utilizing electropolymerized metal organic framework (MOF) [142] (Fig. 3C) was developed for the detection of **gemcitabine** (*pyrimidine analog*) based on its reduction signal. Importantly, an impressively low LOD equal to 3.0 fM (!) was reported, and hence, this sensor completely outperformed other procedures proposed for the detection of this drug. Even though the methodology was successfully verified in spiked diluted serum and pharmaceutical formulation, the weakness of this work originates from missing studies focused on influence of potentially interfering substances on the gemcitabine signal.

(ii) indirect detection on dsDNA biosensors by monitoring a decrease in the oxidation peak currents of purine bases.

Indirect approaches have been employed for 5 antimetabolic agents. Two sensing protocols for indirect determination of **methotrexate** (*folic acid analogs*) were proposed and are based on dsDNA modified GCE [143] and DNA-based GCE modified with GO [144]. The results revealed that the sensor used in [144] showed improved analytical parameters (LOD of 7.6 nM; good recovery in pharmaceutical formulation and spiked urine samples; selectivity study) when compared to [143]. Indirect determination of three antimetabolites, namely **6-mercaptopurine** (*purine analog*) [145], **5-fluorouracil** [146], and **cytarabine** [147] (both *pyrimidine analogs*), was performed on DNA sensors based on PGE modified with p-Py, 4-dodecylbenzenesulfonic acid, and functionalized MWCNTs [145], GCE modified with poly-bromocresol purple (p-BCP) [146], and CPE modified with europium(III)-doped copper(I) oxide NPs ((Eu^{3+}-Cu_2O)NPs) [147], respectively. Moreover, two electroanalytical systems for indirect **gemcitabine** (*pyrimidine analog*) detection were developed, also using dsDNA sensors based on GCE modified with poly-(2,6-pyridinedicarboxylic acid) [148] and CPE modified with AgNPs, MWCNTs, and MIP [124]. Despite the addition of a modifier, the proposed sensors performed averagely, compared to other protocols presented in Table 2. It should be pointed out that in the case of 5-fluorouracil, the indirect method enabled its determination within the widest LR spanning over 5 orders of magnitude [146].

(iii) electrochemiluminescence reactions.

Electrochemiluminescent (ECL) biosensors were proposed for **methotrexate** (*folic acid analog*) detection [149, 150], giving very wide LR (7 orders of magnitude) and impressive LOD values of 150.0 fM [149] and 270.0 fM [150], respectively. Such incredible parameters originate from the electrochemiluminescence reaction

between poly-ethyleneimine (p-Ei) functionalized perylene tetracarboxylic derivative (PTC) [149] or graphite-like carbon nitride [150] and peroxysulfate ion ($S_2O_8^{2-}$) through catalyzing the electroreduction of the $S_2O_8^{2-}$ to produce sulfate radical anions (the biosensor preparation proposed in [149] is presented in Fig. 3D). Methotrexate had an inhibitory effect on these ECL systems; in principle, in the presence of methotrexate less sulfate radical anions are produced, which then subsequently decreases the intensity of the used ECL emitters. Also, the ECL biosensors showed enhanced selectivity.

Furthermore, electrochemical techniques were favorably used for detailed investigation of:

(i) enantiopurity of selected antimetabolites.

Interestingly, 10 amperometric biosensors based on different enzymes (immobilized on CPE) were proposed for the individual determination of L- and D- enantiomers of **methotrexate** (*folic acid analog*) [151], having substantially different pharmacokinetic performance. D-methotrexate has much lower anticancer effect than its L- antipode. All designed enzyme-based biosensors had exceptional enantioselective characteristics, which thus enabled performing the enantiopurity analysis of L- and D-methotrexate in various pharmaceutical formulations. Extremely low LOD values for the L- (4.0 fM) and D-methotrexate assay (10.0 fM) were obtained using biosensors based on L-glutamate and L-amino acid oxidase, respectively.

(ii) the interactions of antimetabolic agents with ss-/ds-DNA molecules.

In situ evaluation of the interaction of **methotrexate** (*folic acid analog*) with dsDNA was carried out using DPV on a highly oriented pyrolytic graphite electrode (HOPGE) showing that the dsDNA-methotrexate interaction leads to structural modifications of dsDNA in a time-dependent manner [152]. The dsDNA bending process imposes kinking of the strands, which facilitates the methotrexate intercalation between dsDNA base pairs, causing unwinding of the dsDNA structure and exposing the purine bases to HOPGE surface (thus, the increase of purine oxidation peaks is observed). Besides, the preferred affinity of methotrexate for A-rich segments (explained by the weakness of the H-bonds between A and T) was confirmed using ssDNA. The dsDNA modified HOPGE was characterized by atomic force microscopy, and the reorganization of the DNA self-assembled network on the HOPGE surface after incubation with methotrexate and the formation of a more densely packed and slightly thicker methotrexate-dsDNA lattice with many aggregates embedded into the network film was observed.

The study performed using a multilayer dsDNA-based biosensor proved that **raltitrexed** (*folic acid analog*) strongly interacts and binds to the dsDNA by various interaction modes, suggesting intercalation in between the DNA base pairs leading to defects in DNA structure [125].

Several modified electrodes have been employed to study the interaction of **6-mercaptopurine** (*purine analog*) with dsDNA; particularly: carbositall electrode modified by AuNPs, chitosan (CHIT), GO and IL (by CV) [153], PGE modified with p-Py and functionalized MWCNTs (by DPV) [145], and GCE modified with MWCNTs and CHIT (by DPV) [154]. The results confirmed that 6-mercaptopurine binds to the dsDNA causing its serious damage (the damage to A was more severe than to G), and the interaction process mainly occurs through the intercalation mode, rather than the electrostatic interactions.

The results obtained on bare PGE by DPV [155], PGE modified with single-walled carbon nanotubes (SWCNTs) by DPV [156], and HMDE by SWV [132] indicated that **6-thioguanine** (*purine analog*) interacts and bonds with DNA, and the most probable interaction mechanism is an intercalation mode, which partially neutralizes the negatively charged phosphate backbone in dsDNA.

The interactions of **clofarabine** [92], **fludarabine** [93], and **cladribine** [157] (all *purine analogs*) with dsDNA in incubated solutions using dsDNA modified GCE were investigated by DPV. All three compounds interacted with dsDNA and caused morphological changes and strand breaking in the structure of dsDNA in a time-dependent manner (condensation of the dsDNA structure), however, these drugs did not cause dsDNA oxidative damage.

Moreover, an examination performed by DPV on dsDNA sensor based on p-BCP modified GCE revealed that **5-fluorouracil** (*pyrimidine analog*) interacts and binds to the G base, and the binding mode is mainly based on intercalation (hydrophobic interaction) and partially on the electrostatic effect [146].

Also, Hg film modified GCE and Osteryoung square-wave anodic AdSV method were used to study the interaction of ssDNA with **cytarabine** (*pyrimidine analog*) [141]. The results revealed that ssDNA strongly interacts with the oxidized form of cytarabine, and the carbonyl group - in the oxidized form - is the predominant functionality responsible for ssDNA-cytarabine interaction. Moreover, the elucidation of the interaction mechanism of dsDNA with cytarabine was made using CPE modified with dsDNA and (Eu^{3+}-Cu_2O)NPs by DPV [147]. Results showed condensation of the DNA double helix being a consequence of a complex formation. Authors pointed out that the binding mode of cytarabine to dsDNA cannot occur *via* intercalative binding or electrostatic interaction. Thus, the groove binding mechanism of cytarabine with

dsDNA was indicated based on the results obtained by UV-vis spectroscopy, viscosimetric, and docking results.

Finally, the interaction of **gemcitabine** (*pyrimidine analog*) with dsDNA and DNA bases was investigated using GCE modified with dsDNA [121] and dsDNA-based GCE modified with functionalized MWCNTs [158]. It was found that gemcitabine caused modifications in the morphological structure of DNA and did not induce its oxidative damage. The interaction mechanism occurred in two consecutive steps: the initial process was independent of the DNA sequence and led to the condensation/aggregation followed by the formation of a rigid structure; this promoted a second step that favors the interaction between the hydrogen atom of G in the C–G base pair and the fluorine atoms in the gemcitabine ribose moiety and causes the release and/or exposure of G residues to the DNA modified GCE surface.

(iii) detection of cancer cells.

A sensor fabricated by conjugating **raltitrexed** (*folic acid analog*) with a positively charged lipid phosphatidylcholine was used for quantitative electrochemical detection of acute human T-cell leukemia cells (using both chronoamperometry (CA) and EIS) [159]. It was found that the raltitrexed lipid-modified sensor could detect cancer cells (without the aid of any indicator molecule) and differentiate between low concentrations of cancerous leukemia cells and healthy cells.

----------Here in Fig. 3----------

----------Here in Table 2----------

2.3. Plant alkaloids and other natural products

The third section is focused on plant alkaloids and other natural products. This group is composed of 6 subgroups, namely vinca alkaloids and analogs, podophyllotoxin derivatives, colchicine derivatives, taxanes, topoisomerase 1 inhibitors, and other plant alkaloids and natural products. The alkaloids derived from plants affect cancer cells by stabilizing microtubules, which influence DNA replication and/or protein synthesis, causing apoptosis of these cells [197].

This group represents a relatively small part of ANAs as it involves only 18 compounds, while 7 of them have been studied with electrochemical techniques so far. A comprehensive summary of the electroanalytical parameters for the tested compounds is provided in Table 3. Clearly, a large electroanalytical gap consisting of more than half of the representatives of plant alkaloids and other natural products (presented in Table S1) exists. As such, we strongly encourage the electroanalytical society to fill missing knowledge in the near future.

Electrochemical detection of plant alkaloids and other natural products was carried out:

(i) predominantly directly (30 out of 38 sensing protocols), using either oxidation or reduction processes, on both non-modified and modified electrodes.

For electrooxidation of selected compounds, which is a substantially prevalent approach (27 direct oxidations *vs*. 4 reductions according to Table 3), most commonly sp^2 carbon-based electrodes were employed along with, however to a lesser extent, metallic (micro)electrodes. The majority of developed procedures include various modifications; interestingly, two dominant modifiers are NPs and MWCNTs, sometimes even combined within one sensing protocol. For example, modification of GCE with AuNPs and MWCNTs resulted in a sensor for **docetaxel** (*taxane*) determination (the only example reported in the literature up to now) with LOD value of 12.0 nM and satisfactory selectivity, verified in spiked urine and serum samples [198].

Among all sensing protocols reported for **etoposide** (*podophyllotoxin derivative*) determination, particularly noteworthy is a sensor based on PGE modified with poly-(L-cysteine) (p-(L-Cys)) and nanocomposite consisting of RGO, AuNPs, and PdNPs (see Fig. 4A). This sensor not only offered a very low LOD value for etoposide individual sensing, but also allowed simultaneous determination of etoposide and ifosfamide (group of alkylating agents) [199].

The best result for **paclitaxel** (*taxane*) was obtained on PGE modified with functionalized MWCNTs, TiO_2NPs, zirconium dioxide NPs (ZrO_2NPs) and CHIT (LOD of 10.0 pM) [200].

Impressive analytical parameters for **topotecan** (*topoisomerase 1 inhibitor*) sensing were obtained on wax impregnated CPE in the presence of SDS surfactant (LOD of 640.0 fM) [201], and on glassy carbon paste electrode modified with AuNPs and acetylene black NPs (LOD of 16.4 pM) [202]. However, in [202] reported LOD is questionable since it is 2 orders of magnitude lower than the first (still impressively low for such straightforward surface modification protocol) studied concentration equal to 2.0 nM.

For **irinotecan** (*topoisomerase 1 inhibitor*), the most significant results were achieved on Au microelectrode by fast Fourier transform continuous CV with accumulation step [203]. Although interesting, missing selectivity studies must be completed to evaluate the proposed protocol utility.

Moreover, sensing procedures based on the reduction signals have been described for **irinotecan** (*topoisomerase 1 inhibitor*), **vincristine** (*vinca alkaloids and analogs*), and **paclitaxel** (*taxane*). Particularly, irinotecan electroreduction was carried out on SMDE [204] and bare PGE [205] providing comparable parameters. However, for [204] the real samples analysis and/or selectivity studies were missing, while in [205] possible determination of irinotecan in the presence of flutamide was verified. Reduction of vincristine [206] and paclitaxel [207] was performed on dropping mercury electrode (DME) and HMDE, respectively, at highly negative potentials.

(ii) indirectly (7 sensing protocols) *via* three different approaches: a change in impedance of a redox probe, a change in peak currents of purine bases, and enzyme inhibition.

Indirect determination of **vincristine** [208] and **vinblastine** [209] (both *vinca alkaloids and analogs*) was realized by the monitoring of the increasing resistance of $[Fe(CN)_6]^{3-/4-}$ redox reaction. Vinblastine determination was performed with an impedimetric biosensor based on a GCE modified with AuNPs, 3-mercaptopropionic acid (MPA) with attached TUB. The schematic representation of the sensor preparation is shown in Fig. 4B [209]. Given protocol allowed for the vinblastine determination with LOD of 84.0 pM. In another report, MIP sensor based on GCE modified with RGO and AuNPs nanocomposite allowed for vincristine determination down to 26.0 nM [208]. Although very good analytical parameters were achieved for both compounds, the selectivity studies were not satisfactory.

Indirect sensing of **paclitaxel** (*taxane*) was performed by monitoring a decrease in oxidation peak currents of G [210–212] and/or A [210] on modified DNA-based electrodes, and the best result was obtained on AuE with dsDNA immobilized onto the 1-azidohexane-6-thiol based self-assembled monolayer (SAM) [211].

Similarly, indirect **irinotecan** (*topoisomerase 1 inhibitor*) sensing by monitoring a decrease in G oxidation current on dsDNA-based modified PGE has been proposed. Irinotecan determination was carried out in spiked blood serum [213]; however, it should be emphasized that dsDNA-modified PGE did not show improved LOD value when compared to bare PGE [205], and the selectivity of the sensor was not tested.

Interesting work aims at providing a tool for indirect chronoamperometric **irinotecan** (*topoisomerase 1 inhibitor*) monitoring which is based on two cascade reactions: (i) acetylcholine conversion to choline *via* the action of acetylcholine esterase and further (ii) choline conversion to betaine aldehyde and H_2O_2 detectable at the platinum electrode (PtE) [214]. The working principle of the sensor was based on the acetylcholine esterase inhibition by irinotecan monitored by dropping H_2O_2 oxidation current. In addition, the applicability of the proposed sensor in fetal bovine serum was verified and the influence of potential interferents including irinotecan metabolites was investigated.

(iii) *via* ionic currents monitoring at the interface between two immiscible electrolyte solutions.

Electrochemically controlled simple ion transfer reaction occurring at the electrified soft interface – electrified liquid-liquid interface – formed between acidified water phase (assuring protonation of the tertiary amine or nitrogen heterocycle present within topotecan structure) and gelled solution of 2-nitrophenyloctyl ether was employed to develop an alternative electroanalytical procedure for **topotecan** (*topoisomerase 1 inhibitor*) sensing [215]. In addition to electroanalytical study, Mehdinia *et al.* provided pharmacochemical understanding of the topotecan derived from its interfacial behavior. The final sensing platform was constructed from the poly-ethylene terephthalate (p-ET) film punched with a sharp needle (Fig. 4C shows the miniaturization protocol).

Besides developing sensing protocols, electrochemical approaches were favorably used to study:

(i) interactions with tubulin.

The binding of **vincristine** (*vinca alkaloids and analogs*) to TUB was examined by linear sweep voltammetry (LSV) and CV [206]. The results showed that (i) vincristine and TUB create an electrochemically active complex (dimer) prone to surface adsorption; (ii) the reduction of vincristine-TUB dimer complex is irreversible.

The binding mechanism of **paclitaxel** (*taxane*) to TUB dimer was identified with LSV-based methodology [216]. Based on the obtained results Yu and Li concluded that TUB dimer has two binding sites

for paclitaxel resulting in electrochemically inactive 2:2 complex units. In addition, the experiment showed that paclitaxel interacts with bovine serum albumin in a ratio equal to 2:1.

(ii) interactions with DNA molecules.

The interaction of **etoposide** (*podophyllotoxin derivative*) with dsDNA was studied on dsDNA modified SPCE by DPV and CV [217] (UV–vis spectroscopy was also employed). The results indicated that etoposide binds to a double helix of DNA through the combined effect of intercalation and electrostatic interaction with the anionic phosphate group, and 1:1 complex of etoposide with DNA is formed.

The interaction between **paclitaxel** (*taxane*) and dsDNA at (a) the AuE modified with dsDNA immobilized onto the SAM [211], (b) dsDNA-based PGE modified with functionalized MWCNTs, TiO_2NPs, ZrO_2NPs, and CHIT [200], (c) PGE decorated with dsDNA, MWCNTs and poly-(3,4-ethylenedioxythiophene) [212], and finally, (d) PGE modified with dsDNA [210] has been studied by DPV. All studies (a-d) indicated that paclitaxel strongly interacts with dsDNA. In some works, the mode of interaction between paclitaxel and dsDNA helix is considered as groove binding [200, 211] (the finding further confirmed by UV-vis spectroscopy [211]), whereas others indicated possible intercalation [210]. Interestingly, the contrary findings were proposed by Yu and Li who investigated the interaction of paclitaxel and dsDNA on DME [216]. They have stated that the DNA cannot bind to paclitaxel as the change in the paclitaxel reduction peak current was unaffected.

The interaction between dsDNA and **irinotecan** (*topoisomerase 1 inhibitor*) and evaluation of the formed complex binding constant were studied by DPV on dsDNA modified PGE [213]. The results clearly showed that the interaction between irinotecan and dsDNA leads to condensation of the DNA double helix, and a groove binding of drug within dsDNA mainly *via* electrostatic interactions (the results confirmed by UV–vis spectroscopy).

Electrochemical investigation of **topotecan** (*topoisomerase 1 inhibitor*) by DPV at the dsDNA-based CPE sensor modified with GQDs and IL (Fig. 4D) provided an alternative electrified bio-interface [218]. The results revealed the topotecan intercalation activity into DNA double helix, which was manifested by the topotecan peak current decrease recorded in the presence of dsDNA. This is related to a significant decrease in apparent diffusion coefficient caused by the "*crowding effect*" and resulting from topotecan gradual intercalation into bulky DNA molecules. Moreover, topotecan was labeled *via* iodogen method with iodine-131 (^{131}I; radioactive isotope of iodine that emits radiation and is used for medical purposes was subjected to interactions with dsDNA isolated from healthy and cancerous cells). This model system

was then investigated using SPCE with immobilized dsDNA by EIS [219]. Although the ^{131}I-topotecan affected the structure of both, DNA isolated from healthy and cancerous cells, the latter were affected in a significantly more effective manner. This conclusion was derived from the impedimetric results that were in good agreement with the results obtained by intracellular uptake study with human lung adenocarcinoma cell line (A-549) and human lung fibroblast cell line (WI-38)). In addition, ^{131}I-topotecan impacted the structure of cancerous DNA to a greater extent than non-labeled topotecan, and in both cases, the specific interaction between topotecan and ^{131}I- topotecan and cancerous DNA was a result of the damage caused by the drug intercalation into dsDNA helix. As such, it can be concluded that ^{131}I-topotecan can be used as a better anticancer drug and a promising agent in nuclear imaging for lung cancer.

(iii) pharmacokinetics.

Interestingly, the development of a specially prepared electrochemical aptamer-based sensor for *in-vivo* **irinotecan** (*topoisomerase 1 inhibitor*) sensing, that upon drug binding folds into G-quadruplex consequently positioning methylene blue (MTB) redox probe (present at the aptamer terminus) close to the electrode surface, was described [220]. The developed aptamer-based sensor achieves 20 s-resolved, multi-hour measurements of irinotecan when emplaced in the jugular veins of living rats, thus providing an unprecedentedly high-precision view into the pharmacokinetics of this class of chemotherapeutics.

----------Here in Fig. 4----------

----------Here in Table 3----------

2.4. Cytotoxic antibiotics and related substances

The fourth section is focused on cytotoxic antibiotics and related substances group which is composed of 3 subgroups, namely: actinomycines, anthracyclines and related substances, and other cytotoxic antibiotics. These compounds possess different mechanisms of action; however, a common theme, which connects the display to chemotherapy, is based on the damage of the structure of DNA, production of free radicals and direct damage to the plasma membrane of cancerous cells [236].

In total, 16 compounds belong to cytotoxic antibiotics and related substances, and so far, 10 have been tested using electrochemical techniques. The comprehensive summary of the electroanalytical parameters obtained for this group of chemical species is provided in Table 4 (while untested drugs are listed in Table S1). In addition, Table 4 clearly shows that different approaches have been employed to develop reliable sensing procedures, which can be, in principle, divided into 3 groups:

(i) direct sensing protocols based on oxidation and/or reduction signals of studied compounds.

Interestingly, for 9 out of 10 studied cytotoxic antibiotics and related substances, procedures based on oxidation and/or reduction signals have been developed and the first part of this section discusses the detection based on the oxidation signals.

A large number of works have been reported for **doxorubicin** (*anthracyclines and related substances*) which is the most frequently studied compound from this subgroup of ANAs. Particularly noteworthy are works with relatively simple modification procedures to design reliable and sensitive doxorubicin sensors: GCE modified with AuNPs and functionalized MWCNTs [237] or poly-(2-amino-5-mercapto-1,3,4-thiadiazole), AuNPs, and RGO [238] were developed, which enabled the determination of doxorubicin at low LOD of 6.5 pM and 9.0 pM, respectively. Also, CPE modified with cobalt-doped Fe_2O_3NPs and functionalized MWCNTs [239] allowed for a low LOD value of 10.0 pM. Another interesting solution for the determination of doxorubicin is a sensor with GCE modified by electrodepositing copper nanowires on magnesium-aluminum layered double hydroxide which resulted in an impressive LOD of 20.0 pM [240]. It is also worth mentioning that LOD of 78.8 pM, obtained using the unmodified GCE [241], is an astonishing result, especially since several subsequent studies, even with the use of complex GCE surface modifications, did not provide such low LOD values. Contrarily, regardless of the electrode used in the methods reported for determination of **epirubicin** (*anthracyclines and related substances*), the LOD values were in the range of 1.0 nM – 79.1 nM, and the lowest LOD of 1.0 nM was obtained on GCE modified with a composite composed of AgNPs and functionalized MWCNTs [242]. Worth mentioning are also sensing

protocols that are focused on the simultaneous determination of epirubicin and ANAs, *i.e.,* topotecan (belonging to plant alkaloids and other natural products) [233] and methotrexate (belonging to cytotoxic antibiotics) [163, 177].

The protocols using CPE modified with various types of metallic NPs allowed the detection of **idarubicin** [243] and **valrubicin** [244] (both *anthracyclines and related substances*) at the nM levels (LOD of 3.0 nM and 1.6 nM, respectively). In contrast, for **mitoxantrone** (*anthracyclines and related substances*) sensing, unmodified CPE was employed [245] giving a very low LOD of 50.0 pM, however, the results showed rather a poor sensor selectivity. The platform which is based on the MIP prepared by electrochemical polymerization of β-cyclodextrin (β-CD) and mitoxantrone on GCE surface was developed for mitoxantrone [246]. The schematic representation of the sensor preparation is shown in Fig. 5A. A great advantage of this MIP-based sensor is that the template molecules could be easily removed by voltammetric cycling, and moreover, good reproducibility, repeatability, and stability of the sensor were obtained. In addition, the selectivity of this sensor has been the most widely studied (compared to other papers within this group of ANAs), and the results proved that the produced MIP-based sensor possesses excellent recognition ability towards template.

Two electroanalytical approaches for **bleomycin** (*other cytotoxic antibiotic*) determination were based on bleomycin-Fe^{2+} complex oxidation and utilized a DNA probe labeled with MTB at the 5' terminus modified ITOE [247] and ferrocene-labelled ssDNA, zirconium(IV)-based MOF (Zr(IV)-MOF) modified GCE [248]. The modified electrodes allowed to reach low LOD values of 33.0 pM and 4.0 pM, respectively, and the detection of bleomycin was successfully tested in spiked blood serum and in the presence of potentially interfering species including ANAs, *i.e.*, mitomycin, daunorubicin, and dactinomycin (belonging to cytotoxic antibiotics and related substances).

As already mentioned, cytotoxic antibiotics and related substances are also reducible. In fact, the best analytical assay for simultaneous detection of four compounds, namely **doxorubicin, daunorubicin, idarubicin**, and **mitoxantrone** (all *anthracyclines and related substances*) was developed using their reduction signal [249]. Specifically, a microfluidic device was proposed, which integrated pre-concentration, electrokinetic separation, and finally electrochemical detection in an amperometric biosensors configuration on a modified screen-printed electrode (SPE) (Fig. 5B). Besides achieving excellent selectivity, the proposed sensor provided extremely low LOD values (!) of 3.6 fM for doxorubicin, 5.5 fM for daunorubicin, 2.2 fM for idarubicin, and and 1.2 fM for mitoxantrone, which enabled to detect these

ANAs in trace quantities. Moreover, the usefulness of the developed method was successfully tested in spiked urine samples.

Naturally, more protocols have been focused on the individual target analytes sensing. In this respect, 8 methods have been proposed for **doxorubicin** (*anthracyclines and related substances*) using conventional Hg-based electrodes [250, 251], carbon electrodes [237, 252–255], and AuE [256]. An interesting solution for doxorubicin sensing was proposed and is based on dsDNA modified basal-plane pyrolytic graphite electrode [255]. *Ex situ* doxorubicin sensing was carried out using stripping CA and the determination was based on the catalytic reduction of oxygen which allowed to detect doxorubicin at LOD of 10.0 pM. Generally, bare carbon electrodes demonstrated superior characteristics towards doxorubicin, *e.g.,* a non-modified GCE provided a low LOD value of 400.0 pM [252], which was further decreased to 6.5 pM in the presence of modifiers composed of AuNPs and functionalized MWCNTs [237]. AuNPs and/or MWCNTs were also advantageously employed in the preparation of other two relatively complex sensors for reductive detection of **daunorubicin** [257] and **valrubicin** [258] (both *anthracyclines and related substances*). All three relevant **pirarubicin** (*anthracyclines and related substances*) sensing protocols are based on the reduction signal [259–261], and the most sensitive determination was performed on "direct writing" carbon electrode modified with dsDNA on which LOD of 112.0 pM was obtained [261]. Determination of **bleomycin** [262] and **mitomycin** [263] (both *other cytotoxic antibiotics*) was carried out on a traditional HMDE. In the case of bleomycin, LOD reached a low concentration level of 500.0 pM, and its detection was successfully performed in spiked mouse serum [262], whereas mitomycin was determined separately as well as in the presence of other ANAs, *i.e.*, 5-fluorouracil (belonging to antimetabolites) and cisplatin (belonging to other ANAs), using stripping voltammetry, and the achieved LOD value was 10.0 nM (which makes it so far the best published sensing protocol for mitomycin) [263].

(ii) indirect detection through variations in electrochemical signals of guanine and a redox probe.

Surprisingly, many reported protocols (19 in total) are based on indirect sensing of cytotoxic antibiotics and related compounds. Their main characteristics are typically advanced modification procedures further pushing the LOD values towards lower concentrations (especially required for detecting drugs in biological fluids).

Superior electroanalytical output towards indirect determination of **doxorubicin** (*anthracyclines and related substances*) was achieved by monitoring the impedance of the redox reaction ($[Fe(CN)_6]^{3-/4-}$) at AuE surface modified with sol-gel functionalized with thiol functional groups further decorated with AuNPs and monoclonal antibody (mAb) [264]. This complicated and time-consuming surface modification

protocol consisting of several steps (schematically shown in Fig. 5C) provided an impressive sensing LOD of 165.9 fM. A different approach incorporated doxorubicin into a complex sensing layer that in a final configuration allowed for the indirect detection of doxorubicin by monitoring the increase of penicillin binding protein 2a signal [265]. Although the sensor design is complex, the proposed immunosensor provides a very low LOD value of 1.2 pM and sets an innovative path that can be used in the development of biodetection tests for other important species. Moreover, the proposed bioconjugate also promotes the pattern for *in vivo* doxorubicin delivery in anticancer therapy.

Enhanced analytical performance was reported for sensors recording the alterations in redox peaks provided by $[Fe(CN)_6]^{3-/4-}$ redox probe; worth mentioning is impedimetric DNA sensor based on GCE modified with poly-proflavine for indirect **doxorubicin** and **daunorubicin** (both *anthracyclines and related substances*) individual sensing by monitoring the redox reaction of $[Fe(CN)_6]^{3-/4-}$ after intercalation of the selected antibiotic into DNA helix [266]. This sensor enabled the determination of doxorubicin and daunorubicin at very low LOD values of 300 pM and 1.0 pM, respectively. In addition, dsDNA-based GCE modified with p-ANI in the presence of oxalic acid (OA) as a doping agent enabled achieving low LOD levels of 10, 100, and 200 pM for individual detection of **doxorubicin, daunorubicin**, and **idarubicin**, respectively [267]. However, the sensor proposed in [267] cannot be used for more than one time due to the accumulation of tested ANAs at its surface (all attempts to remove the analyte from the surface layer were unsuccessful). In the case of **bleomycin** (*other cytotoxic antibiotic*), the indirect approach using DNA with a thiol group at the 5' terminus modified AuE resulted in LOD of 740.0 fM. The only sensing protocol reported for **plicamycin** (*other cytotoxic antibiotic*) was performed indirectly *via* recording signals of a redox probe before and after DNA interaction with the target analyte [268].

Finally, label-free DNA biosensors were employed for indirect determination of **epirubicin** (schematic representation is depicted in Fig. 5D) [269], **mitoxantrone** [270] (both *anthracyclines and related substances*), and **mitomycin** (*other cytotoxic antibiotic*) [212] through monitoring a decrease in oxidation peak of G, at the same time reaching LOD within nM concentration level [269].

(iii) ion transfer across the interface formed between two immiscible electrolyte solutions.

An electroanalytical approach based on the polarized liquid-liquid interface has been proposed for **doxorubicin** [250] and **daunorubicin** [271] (both *anthracyclines and related substances*) detection. Here, analyte sensing mechanism was based on an interfacial ion transfer between two immiscible electrolyte solutions (ITIES). Although low LOD value of 840 nM was obtained for doxorubicin, this methodology failed during drugs determination in body fluids even at μM concentration. This was mainly due to the presence

of interfering compounds (*e.g*., chlorides) and charged lipophilic compounds (*e.g.*, amines, amino acids) co-existing in the aqueous phase [250]. Similarly, for daunorubicin a LOD value of 800.0 nM was reported along with serious interfering effects of amino acids (aspartic acid, lysine, arginine), and inorganic cations (Mg^{2+}, Zn^{2+}, K^{+}) [271].

Noticeably, electrochemical techniques have been extensively used in studies regarding interactions of cytotoxic antibiotics and related substances with DNA molecules, cancer cells, and cell membranes:

(i) interactions with ssDNA and dsDNA molecules.

The majority of cytotoxic antibiotics and related substances have been exposed to the interactions with DNA molecules and various electrochemical techniques have been utilized to elucidate the nature and mechanism of such interaction.

Generally, **doxorubicin, daunorubicin, epirubicin, idarubicin, valrubicin,** and **mitoxantrone** (all *anthracyclines and related substances*) interact with DNA *via* predominantly intercalative mode (aromatic ring present in the structure of indicated compounds is expected to facilitate intercalation into the DNA double helix).

Particularly, investigation of the interaction of **doxorubicin** (*anthracyclines and related substances*) with dsDNA was investigated in incubation solution, using dsDNA-based GCE modified with p-ANI in the presence of OA as a doping agent [267], and SPCE modified with PtNPs and AgNPs [272] by means of EIS [267] and DPV [272]. The doxorubicin-DNA interaction was also studied on SMDE by CV, and it was proved that the mode of binding of doxorubicin to DNA is by electrostatic attraction and intercalation during which the electrochemically non-active supramolecular doxorubicin-DNA complex is formed [273]. Moreover, an electrochemical biosensor based on AuE modified with the thiolated DNA probes and labeled with AgNPs conjugated with doxorubicin (a well-known DNA intercalator) was successfully utilized for the electrochemical (CV) detection of DNA [274].

The surface-confined interaction between **daunorubicin** (*anthracyclines and related substances*) and DNA was investigated on DNA-based GCE [275], GCE modified with PtNPs and SWCNTs [276], and p-ANI in the presence of OA as a doping agent [267], PGE modified with RGO [277] and CHIT [278], CPE modified with 4-aminothiophenol, AgNPs and functionalized MWCNTs [279]. In addition to intercalating into the double helix, daunorubicin causes morphological changes (but not oxidative damage) in the DNA structure. Besides, daunorubicin has a moderately toxic effect on DNA (the results confirmed by EIS) [277]. Interestingly, the interaction between dsDNA and daunorubicin was examined using DPV at ITIES [280]. The

interaction of protonated daunorubicin (DH^+) with dsDNA was evaluated from the voltammetric response of DH^+ direct transfer across the electrified water – 1,6-dichlorohexane interface. The results showed the formation of complex and intercalation between DH^+ and DNA base pairs and implied that electrostatic binding plays an important contribution in the DH^+–DNA complex formation (the electrochemical results confirmed by the UV-vis spectroscopy). The effect of β-CD modified with non-toxic lipoic acid on the interaction of daunorubicin with dsDNA was studied by SWV, and UV–vis spectroscopy [281]. Both spectroscopic and electrochemical results revealed that complexing daunorubicin with this β-CD derivative increases the intercalation efficiency of daunorubicin into dsDNA (the native β-CD only slightly enhances the intercalation of daunorubicin to DNA, whereas the modification of the β-CD drug carrier with a lipoic acid significantly promotes daunorubicin-DNA intercalation).

The DNA-based CPE [282], PGE modified with p-Py and nitrogen-doped RGO (N-RGO) (Fig. 5D) [269], SPCE surface modified with PtNPs and AgNPs [272], and SPCE modified with Au nanocubes [283] were applied to obtain information about the intercalative interaction of **epirubicin** (*anthracyclines and related substances*) with DNA [269, 272, 282]. Moreover, the obtained results confirmed the specific binding affinity of epirubicin to dsDNA compared to ssDNA [283].

The interaction between **valrubicin** (*anthracyclines and related substances*) and DNA was studied by CV [244, 258, 284]. The obtained results revealed that valrubicin strongly binds to dsDNA with a high binding constant, and valrubicin-dsDNA interaction is attributed to the intercalation of valrubicin into the DNA double-helix [244]. UV–vis spectroscopy has proved that valrubicin-dsDNA interaction is a combination of intercalation and electrostatic interaction due to the flat structure of the drug and the positive charge of the valrubicin molecule within the studied pH range [284]. In addition, it was found that oligonucleotides containing C and G sequences as well as an increase in the length of DNA probe led to the strong interaction between valrubicin and ssDNA [258].

Similarly, the interaction of **idarubicin** (*anthracyclines and related substances*) with dsDNA resulted in changes in the DNA morphological structure but without triggering any oxidative DNA damage. These studies were performed in incubation solution and using dsDNA-based bare GCE [285], GCE modified with p-ANI in the presence of OA as a doping agent [267], and SPCE modified with PtNPs and AgNPs [272].

In the case of **mitoxantrone** (*anthracyclines and related substances*), the interaction with DNA was evaluated on dsDNA and ssDNA modified GCE [286] and CPE modified with dsDNA [270]. Opposing to daunorubicin and idarubicin, mitoxantrone not only intercalates into DNA [270, 286] but also causes DNA damage (damage occurs with time which suggests that mitoxantrone slowly interacts with DNA causing

some breaking of the H-bonds) [286]. The results showed that mitoxantrone more preferentially interacts with ssDNA than dsDNA [286]. In addition, the docked model revealed that the hydrogen and oxygen atoms participate as the donor and acceptor, respectively, to form four intermolecular H-bonds with base pairs of DNA [270].

The monitoring of surface confined interaction of **bleomycin** (*other cytotoxic antibiotic*) with ssDNA and dsDNA was performed by EIS at DNA-modified PGE [287]. It was found that bleomycin interacts with DNA without using any extra co-factors like metal ions and may induce more damage to dsDNA than ssDNA. This is most likely due to bleomycin intercalation into the base pairs of dsDNA (preferentially G-rich sites) causing the strand breakage [287]. On the contrary, Heydari-Bafrooei *et al.* tested the DNA damage induced by bleomycin in the absence and presence of some metal ions such as Fe(II), Fe(III), Cu(I), Cu(II), Zn(II), Mn(II) and Co(II) by EIS and DPV at dsDNA-based PGE modified with AuNPs and Zn(II)-Schiff base complex [288]. It was found that bleomycin itself did not interact with DNA, in contrast to its complex formed with some metal ions. The results revealed that among investigated metal ions, only divalent species (except Cu(II)) activated bleomycin in the order Fe(II) ≫ Mn(II) > Co(II) > Zn(II).

A different type of interaction mode (not intercalation) with DNA molecule was uncovered for **mitomycin** and **plicamycin** (both *other cytotoxic antibiotics*). In most of the reported studies, only G oxidation signal was evaluated for DNA-drug interactions [289–295], while only two works effectively used both G and A oxidation peaks [212, 296]. It was shown that mitomycin interacts with DNA by binding (cross-linking) to the bases, especially G-C pairs of dsDNA, and causes their damage [212, 289–296]. Interesting work showing contradictory results to the one previously described, was published by Ensafi *et al.* [297] where it was shown that mitomycin requires activation to interact with DNA. Specifically, mitomycin can bind to DNA in more than one way after its acidic and electrochemical activation (different adducts are generated), consequently causing alterations in DNA structure and its electrochemical properties. The specificity of the interaction of **plicamycin** with dsDNA-based AuE modified with AuNPs was investigated by EIS [268]. It was found that plicamycin binds selectively to the minor groove of DNA sequences through a combination of close van der Waals contact, hydrogen bonding, electrostatic attraction, and hydrophobic interaction.

(ii) interactions with cancer cells.

The interaction of histiocytic lymphoma cell line (U-937) and **daunorubicin** (*anthracyclines and related substances*) with an arginine-rich peptide (both daunorubicin and several arginine-rich peptides exhibit a high degree of permeability through U-937 cells walls) was monitored on GCE using DPV [298]. The results showed that the cell membrane permeability of daunorubicin with arginine-rich peptide probe was

improved when compared to daunorubicin alone. Thus, this concept could be applied to cell sensing and the monitoring of the drug delivery process.

Noteworthy is also an approach allowing a high throughput and quantitative analysis of cells chemosensitivity in a 3D environment [299]. Cells encapsulated in the hydrogel were cultured in the microwells on a paper substrate, and the viability of two human hepatoma cell lines, *i.e.,* Huh-7 and Hep-G2, was quantified with EIS under the treatment of **doxorubicin** (*anthracyclines and related substances*) and etoposide (belonging to the plant alkaloids and other natural products). The results revealed the higher drug resistance of Huh-7 cells than Hep-G2 cells, and doxorubicin was proved to be more effective in the treatment of hepatocellular carcinoma than etoposide.

Moreover, the combined effect of the initial cell density and the concentration of **doxorubicin** on HeLa cells was tested by performing time-dependent cytotoxicity assays using real-time impedimetric study in a static environment [300] and in microfluidic conditions [301] on a microelectrode chip with an array of 12 interdigitated microelectrodes, which were coated with laminin to promote cell adhesion. It was revealed that key factors influencing the doxorubicin-induced cytotoxicity, *i.e.,* the initial cell density, the drug concentration, and the exposure time, are interdependent. In addition, the impedimetric results were compared with those obtained from standard colorimetric end-point assay, and the results indicated that these two methods provided different time-dependence of cytotoxicity. EIS measurements detected the cellular response to doxorubicin earlier than end-point assay (EIS detection reveals cytotoxic events undetectable when using the end-point assay), thus highlighting the importance of combining impedance detection with traditional drug toxicity assays towards a more accurate understanding of the effect of ANAs on *in-vitro* assays. It was found that the response of HeLa cells to doxorubicin-induced cytotoxicity was faster than toxicity induced by oxaliplatin (belonging to platinum compounds). In addition, the time-dependent effect of doxorubicin on HeLa cells was found to have a delayed onset of cytotoxicity in microfluidic conditions [301] when compared with static conditions [300]. The obtained results were supported by the data from the fluorescent apoptosis assay performed in microfluidic conditions, proving the potential of the developed microfluidic platform to perform both electrochemical and optical detection.

(iii) interactions with biomimetic membranes.

Cytotoxic antibiotics and related substances principally target dsDNA located inside the cancerous cells, thus, to reach the DNA molecule, the drugs must first penetrate the cell membrane. The effort was made to clarify the mechanisms of such transport through the membrane for two compounds, **doxorubicin,** and

mitoxantrone (both *anthracyclines and related substances*). **Doxorubicin** was subjected to the interactions with the Langmuir and Langmuir-Blodgett biomimetic monolayers and Langmuir-Schaeffer biomimetic bilayers prepared on the support made of poly-crystalline AuE surface. These interactions were examined by CV, EIS, quartz crystal microbalance (QCM), ellipsometry techniques [302], and surface-enhanced Raman spectroscopy (SERS) [303], and the obtained results revealed that the interactions between doxorubicin and Langmuir and Langmuir-Blodgett monolayers deposited on AuE are different than those seen at a Langmuir-Schaeffer biomimetic bilayer interface. Doxorubicin has penetrated into the hydrophobic region of the monolayer, whereas the penetration of the bilayer by doxorubicin was precluded. Also, the interactions of **mitoxantrone** with the Langmuir and Langmuir-Blodgett biomimetic monolayers were observed by electrochemical (CV and EIS) and spectroscopic (SERS) techniques [304]. Mitoxantrone was monitored during its passive partitioning/penetration through the mixed Langmuir and Langmuir-Blodgett monolayers after their transfer on AuE. The results showed that mitoxantrone affects the organization of Langmuir monolayers, whereas no substantial structural effect on the organization of Langmuir-Blodgett monolayers was observed. The rapid release of mitoxantrone from the monolayer into the aqueous medium was proved.

----------Here in Fig. 5----------

----------Here in Table 4----------

2.5. Protein kinase inhibitors

The fifth section is focused on protein kinase inhibitors (PKI), which represent a number of chemical entities that bind to and inhibit the enzymatic action of protein kinases [342, 343]. This group of ANAs is composed of 14 subclasses (as listed in Table S1).

To our surprise, only 14 out of 73 (!) PKI have been studied using electrochemical techniques, and the analytical protocols exist for only 13 examples with imatinib and dasatinib attracting the most attention. Thus, the necessity to further intensify electroanalytical and electrochemical studies focused on PKI must be strongly emphasized. The comprehensive data description presented in Table 5 summarizes the information related to the electroanalytical parameters obtained for the PKI group.

Established sensing procedures (36 in total) utilizing sensitive electrochemical techniques can be divided into two categories, *i.e.*, direct and indirect protocols:

(i) the first group comprising of direct detection methods, based on oxidation as well as reduction signals, clearly predominates as 33 (out of 36) developed procedures fall into this category.

Interestingly, 14 reported procedures employed bare electrodes (carbon-based for oxidation and HMDE for reduction) and provided analytical parameters comparable to the procedures requiring complex (and often tedious) modification of the electrode surface, which often leads to complications with reproducibility and variations in obtained signals. Besides being less time-consuming, another advantage of a bare electrode is a simple cleaning step (or renewability) of its surface, which is then manifested in high repeatability of the measurements. Nevertheless, modified electrodes still prevail for detection of the PKI agents based on their electrooxidation. In this respect, various types of metallic NPs (12 procedures), often in combination with CNTs (6 out of 12) or RGO (3 out of 12) were mainly used. Importantly, such engineered electrode surfaces helped to considerably improve the selectivity, as clearly shown in Table 5 and discussed in the paragraphs below.

Among all sensing protocols reported for **imatinib** (*BCR-ABL tyrosine kinase inhibitor*), particularly noteworthy is a sensor based on poly-acrylonitrile nanofibers (p-ANFBs), Fe_3O_4NPs, and MWCNTs modified CPE which allowed the detection of imatinib at LOD of 400.0 pM [344]. However, the results showed rather a poor selectivity towards other interfering compounds including ANAs, *i.e.,* gefitinib and sunitinib (both belonging to other ANAs). Also, a GCE modified with RGO and AgNPs was developed for imatinib determination giving a low LOD value of 1.1 nM [345]. Besides, imatinib detection down to 6.0 nM was reported on GO nanoribbons (GONRBs) sandwiched between HKUST-1 MOF and the GCE (sensing surface

with preparation steps is depicted in Fig. 6A) [346]; however, similar electroanalytical parameters (LOD of 6.3 nM) were also reported on anodically pretreated BDDE, being the simplest and still fully operational method for imatinib detection [347].

Superior electroanalytical output towards **dasatinib** (*BCR-ABL tyrosine kinase inhibitor*) was achieved on CPE modified with Fe_3O_4NPs, functionalized SWCNTs, and IL giving LOD value of 700.0 pM [348]. Also, the LOD within nM level obtained at unmodified PGE [349] and GCE [350] is an impressive result, given that several studies describing dasatinib detection at modified electrodes provided less impressive electroanalytical output (higher LOD values).

AdSV methods for the quantification of **nilotinib** (*BCR-ABL tyrosine kinase inhibitor*) [351] and **lapatinib** (*human epidermal growth factor receptor 2 tyrosine kinase inhibitor*) [352] have been effectively developed on a bare GCE in the presence of surfactants. The effect of an anionic surfactant, SDS, on the nilotinib signal was thoroughly examined, and it was confirmed that negatively charged SDS at low concentrations (*i.e.,* below critical micellar concentration) are electrostatically attracted to positively charged amine moieties present within the nilotinib structure. This in turn facilitated the nilotinib molecules diffusion to the GCE surface. As a result, when SDS was present in a supporting electrolyte, nilotinib gave higher voltammetric responses (as shown in Fig. 6B) with a low LOD value of 3.4 nM. In the absence of SDS, a ~31-fold increase in LOD value (106.0 nM) was observed [351]. Similarly, a non-ionic surfactant, Triton X-100, increased the solubility of lapatinib and ensured that more of its molecules could readily approach the electrode surface; such hydrophobic interaction is most probably the reason for the excellent LOD values of 3.5 nM (for the first oxidation peak) and 1.6 nM (for the second oxidation peak) [352].

The reported **erlotinib** (*epidermal growth factor receptor tyrosine kinase inhibitor*) sensing protocol is based on a simple surface modification utilizing drop-casting β-CD solution onto the GCE surface (see Fig. 6C) [353]. In this work, erlotinib (as a hydrophobic guest) was used to form a host-guest complex with β-CD (having a hydrophobic interior and a hydrophilic exterior). Such configuration provided very good analytical parameters with LOD of 1.1 nM. It is also worth mentioning that β-CD are water-soluble and nontoxic, they can increase solubility, chemical stability, and bioavailability of the drugs, and hence they are extensively used in drug delivery applications [354].

Direct **sunitinib** (*other protein kinase inhibitor*) determination based on the oxidation signal was proposed on CPE modified with a nanocomposite composed of p-ANFBs and nickel- and zinc-doped Fe_2O_3NPs (synthesized using an electrospinning method) [355]. The modified sensor exhibited good

electrocatalytic performance, allowed to detect the sunitinib at a very low level (LOD of 900.0 pM), and showed good selectivity towards different interfering species, including ANAs, *i.e.,* gefitinib and imatinib (belonging to PKI).

The best result (LOD of 73.8 pM) for **sorafenib** (*other protein kinase inhibitor*) was obtained on CPE modified with sodium montmorillonite clay as the result of electrocatalytic activity of modifier towards sorafenib oxidation [356].

GCE modified with rod-like copper oxide NPs synthesized by hydrothermal method and finger-like carbon material obtained from hydrothermal carbonization of waste masks was proposed as a sensor for **pazopanib** (*other protein kinase inhibitor*) direct determination and allowed its detection at a very low LOD value of 49.4 pM and within a wide LR spanning over 4 orders of magnitude [357].

A very simple modification by drop-casting functionalized MWCNTs suspension onto the GCE surface was developed for **regorafenib** (*other protein kinase inhibitor*) [358]. The LOD value dawn to 20.8 nM, and rather a good selectivity of the sensor was achieved (except for uric acid which showed a high level of interference even at the ratio of uric acid:regorafenib of 1:1). Worth mentioning is also an electrochemical sensor based on GCE modified with a nanocomposite consisting of ZrO_2NPs and RGO [359]. This was synthesized using a simple one-pot hydrothermal method, with RGO serving as supporting material for ZrO_2NPs at the same time preventing their agglomeration. The consequent platform provided excellent electrocatalytic performance toward regorafenib sensing based on its oxidation (LOD value of 17.0 nM) and allowed regorafenib detection in the presence of ascorbic acid and uric acid.

Finally, sensing procedures based on the reduction signal, utilizing a traditional HMDE and AdSV techniques, have been proposed for **imatinib** (*BCR-ABL tyrosine kinase inhibitor*) [360, 361], **gefitinib** (*epidermal growth factor receptor tyrosine kinase inhibitor*) [362], and **palbociclib** (*cyclin-dependent kinase inhibitor*) detection [363]. All protocols provided relatively good analytical parameters, manifested predominantly by low LOD values (in the range of 88.0 pM – 12.0 nM), and the possibility to be applied for real sample analysis (*e.g.*, urine or blood serum samples or pharmaceutical formulations). However, the major shortcoming of all herein proposed procedures is the lack of selectivity studies.

(ii) indirect detection through alterations in electrochemical responses of guanine and a redox probe.

Only 3 indirect approaches have been proposed for 3 various PKI compounds, *i.e.,* **dasatinib** (*BCR-ABL tyrosine kinase inhibitor*), **ruxolitinib** (*Janus-associated kinase inhibitor*), and **axitinib** (*vascular endothelial growth factor receptor tyrosine kinase inhibitor*). First, dsDNA sensor based on GCE modified with AuNPs

and RGO was developed to indirectly detect **dasatinib** *via* monitoring a decrease in the G oxidation current. Such sensor displayed a LOD value of 9.0 nM [364]. Second, MIP-based sensors with a signal originating from the decreasing $[Fe(CN)_6]^{3-/4-}$ oxidation peak current were used to develop methods for the indirect determination of **ruxolitinib** [365] and **axitinib** [366]. Both platforms provided impressive LOD values of 1.9 fM for ruxolitinib [365] and 27.0 fM for axitinib [366], making them unbeatable when compared to other electroanalytical configurations for the tested PKI. Moreover, the superior selectivity of the latter sensor was proved by comparing the binding of axitinib and ANAs, *i.e.,* erlotinib, dasatinib, nilotinib, and imatinib (belonging to PKI), and the results showed that the designed MIP-based sensor possesses high recognition abilities towards template molecule [366].

In addition, electrochemical methods have been employed for the examination of the interaction between PKI with dsDNA or cancerous cell lines:

(i) interaction with dsDNA.

Two compounds, **dasatinib** (*BCR-ABL tyrosine kinase inhibitors*) [364] and **lapatinib** (*human epidermal growth factor receptor 2 tyrosine kinase inhibitor*) (Fig. 6D) [367], were subjected to investigate their interactions with dsDNA molecules using DPV technique. For both inhibitors, the intercalation mode of interaction was confirmed; most probably facilitated by the existence of planar aromatic ring(s) in their structures. Dasatinib exhibits a high affinity to dsDNA and the intercalation process occurs through the minor or major grooves of DNA [364]. In the case of lapatinib, not only electrochemical but also spectroscopic methods (UV–vis spectroscopy and fluorescence spectroscopy) confirmed that this compound intercalates into the dsDNA helix and the resulting interaction causes the condensation of the DNA molecule [367].

(ii) interaction with carcinogenous cells.

The most frequently used compound in cell-related studies was certainly **nilotinib** (*BCR-ABL tyrosine kinase inhibitor*). First, a biocompatible film consisting of GO and poly-(L-Lysine), immobilized on GCE surface, was used to design the label-free electrochemical device for the detection of K-562 cells by EIS method [368]. In addition, the evaluation of the effectiveness of nilotinib on the K-562 cell lines was tested, and the obtained nilotinib cytotoxicity results (recorded by EIS) were satisfactory and in good agreement with those from colorimetric WST-1 assays. The second work describes the development of the photoelectrochemical biosensing platform fabricated using core-shell NPs on an ITOE to effectively monitor caspase-3 activation during K-562 cell apoptosis with great sensitivity and high stability [369].

Nilotinib was chosen as a model antileukemia drug to induce the apoptosis of K-562 cells in the photoelectrochemical detection of caspase-3. Further, a novel sandwich-type dual-signal-marked electrochemical sandwich immunosensor for simultaneous detection of B-cell lymphoma-2 (BCL-2) and BCL-2-associated X (BAX) expressions was successfully fabricated [370]. The biosensor was further used to investigate BCL-2 and BAX expressions from apoptotic K562 cells treated with nilotinib. It was found that the increase of the nilotinib dosage and incubation time increases BAX and reduces BCL-2 expression, and the rise of the BAX/BCL-2 ratio indicates the promotion of the K-562 cells apoptosis. These results show that the apoptosis level of K-562 cells could be regulated by the BCL-2 family.

At least one study concerns **vandetanib** (*other protein kinase inhibitor*). Interestingly, the impedimetric characteristics of the MCF-7 cell line were recorded using a microfabricated impedance sensing device to evaluate the cytotoxic effect of vandetanib on cellular electrical behavior [371]. Impedimetric studies provided a set of interesting findings that were translated into suppression of cells proliferation and induction of apoptosis process.

----------Here in Fig. 6----------

----------Here in Table 5----------

2.6. Monoclonal antibodies and antibody-drug conjugates

The sixth section is focused on monoclonal antibodies and antibody-drug conjugates. Monoclonal antibodies are synthetic proteins that mimic the immune system's ability to fight off harmful pathogens which can directly target tumor cells while simultaneously promoting the induction of long-lasting anti-tumor immune responses [380]. Antibody-drug conjugates are monoclonal antibodies conjugated to cytotoxic agents that use antibodies specific to tumor cell-surface proteins and, thus, have tumor specificity and potency not achievable with traditional drugs [381]. This group of ANAs is composed of 8 subclasses (as listed in Table S1).

Monoclonal antibodies and antibody-drug conjugates represent the class of chemical species that have attracted rather limited attention in a view of electrochemistry. Among 45 agents, only 5 have been studied by electrochemical techniques; each agent ((i) – (v)) is presented and discussed separately within this chapter. Moreover, when it comes to sensing applications only 3 protocols exist, this is for rituximab, trastuzumab, and cetuximab (summarized in Table 6), leaving other ANAs aside (see Table S1). As indicated in Table 6, all three approaches are based on indirect detection, even though monoclonal antibodies can be directly oxidized at the carbon-based electrodes (anodic currents are assumed to originate predominantly from the oxidation of tyrosine and/or tryptophan subunits present in the amino-acid antibody sequence). Nevertheless, direct electroanalysis is expected to be highly non-selective when it comes to real application. In this respect, the most promising electroanalytical platforms are those with monoclonal antibodies placed within carefully designed surfaces. Thus, in the future, more effort should be devoted to the development of electrified sensing interfaces decorated with antigens, their epitopes, or specially designed mimotopes. Such configurations should give very selective (or even specific) sensing interfaces and should help at filling the enormous gap consisting of 42 existing chemical compounds (however, the group is expected to be further enlarged), for which detection protocols have not yet been proposed.

(i) A sensing protocol has been developed for **rituximab** (*clusters of differentiation 20 inhibitors*); particularly, poly-amidoamine dendrimer and RGO nanocomposite modified PGE was used to fabricate an electrochemical DNA biosensor for indirect determination of rituximab [382]. Especially noteworthy are works describing the interaction between monoclonal antibodies and the cells placed at the electrified surfaces which provide direct electroanalytical output from the investigated system. In this respect, QCM-biosensor based on arginine-glycine-aspartic acid tripeptide modified AuE surface with immobilized B-lymphoblast-like Burkitt's lymphoma Raji cells (B-cells) was proposed and used to study the interaction

between B-lymphocyte antigen CD20 expressed on the surface of B-cells and rituximab by potentiometry, CV, EIS, and piezoelectric response [383]. The results confirmed the specific interaction (binding) between rituximab and B-cells. In addition, the effect of Ca^{2+} and Mn^{2+} ions on the interaction between rituximab and B-cells was studied. Experiments indicated that CD20 antigen functions as Ca^{2+} ion channel present in the cell membranes. Transport of Ca^{2+} ions into the cells accelerated the rituximab binding and resulted in the facilitated cell lysis. In other work, the SAM of peptide mimotopes of CD20 antigen modified QCM AuE sensor was designed to study the binding of peptides with rituximab by piezoelectric response, CV, and EIS [384]. Results showed that the peptide mimotopes of the CD20 antigen designated as CN-14 (CGSGSGSWPRWLEN) are the most selective and relatively sensitive for rituximab binding.

In addition, the electrochemical oxidation behavior of native rituximab was studied on GCE by CV and DPV [385]. Results showed that the electrochemical oxidation process of native rituximab is pH-dependent and involves complex electron transfer reactions. The anodic peak recorded in all pH values corresponds to the oxidation of monomeric tyrosine and/or tryptophan amino acid residues in the native rituximab structure, whereas the second peak occurred at lower pH values and most probably corresponds to the oxidation of monomeric methionine amino acid residues. Further, the electrooxidation mechanism of denatured rituximab was also investigated using the electrochemical biosensors with a thick multilayer of rituximab completely covering the GCE surface. For the concerned surface, the higher number of voltammetric signals and/or their enhanced intensity was recorded as expected after protein denaturation due to the unfolding and subsequent structural changes in the protein molecule. This in turn has led to the exposure of more electroactive amino acid residues contributing to the recorded signals. Particularly, SDS, tris(2-carboxyethyl)phosphine (TCEP), and dithiothreitol (DTT) were used as the denaturing agent (SDS) and the reductants (TCEP, DTT) to unfold the rituximab. The use of SDS and TCEP resulted in the denaturated rituximab providing one peak of enhanced intensity (compared to the native rituximab) which corresponds to the oxidation of tyrosine and tryptophan amino acid residues. In contrast, the denaturated rituximab, achieved using DTT, revealed the presence of three peaks corresponding to the oxidation of tyrosine and tryptophan amino acid residues, the second step of the oxidation of tryptophan amino acid residues, and finally oxidation of histidine amino acid residues.

Finally, the evaluation of the interaction between rituximab and dsDNA was investigated using DPV by two methodologies: (i) in incubated samples of dsDNA with rituximab, (ii) on a multilayer dsDNA-based electrochemical biosensors in an aqueous solution [382, 386]. The obtained electrochemical results were verified by gel-electrophoresis [382, 386] and UV-vis spectroscopy [382]. The results confirmed that rituximab

binds to dsDNA and: (i) a strong condensation of the dsDNA structure due to the interaction between dsDNA and rituximab was observed; (ii) no oxidative damage to the DNA base was detected [382, 386]; (iii) binding mode between the rituximab and dsDNA was governed by electrostatic interaction, and finally (iv) rituximab may interact with dsDNA *via* groove binding [382].

(ii) The label-free and reagent-free cysteine terminated peptide mimotope SAM biointerface was designed for **trastuzumab** (*human epidermal growth factor receptor 2 inhibitor*) detection [387]. The non-faradic impedance read-out of the capacitive biosensor was governed by the change in the electric double-layer capacitance (C_{dl}) affected by the trastuzumab specific surface binding. The best sensing parameters were obtained under the experimental conditions assuring low ionic strength of the buffered solution because in such case the C_{dl} governs the resulting capacitance of the modified AuE. Further, an electrochemical biosensor was developed based on AuE modified with RGO, AuNPs, and horseradish peroxidase-conjugated with trastuzumab and a cluster of differentiation 166 monoclonal antibodies. This was then used for the recognition and indirect detection of prostate metastatic cancer cells (Du-145) providing amplified signals governed by enzymatic reactions [388]. The results showed that upon the adsorption on the surface the analytical signal originating from the enzymatically formed hydrogen peroxide reduction at the underlying electrode increased. The proposed cytosensor is characterized by a high ability to capture the target cells, high sensitivity, and selectivity toward Du-145 cancer cells. Besides, an impedimetric sensor based on the carboxylic group-containing AuNPs functionalized GQDs and cobalt porphyrin binuclear framework modified GCE was designed towards the detection of human epidermal growth factor receptor 2 [389]. The carboxylic groups present in the modified GCE allowed for covalent linkage to the amino group-containing trasmatuzab *via* an amide bond. The fabricated sensor also showed good reproducibility and stability, making it a potential candidate for the human epidermal growth factor receptor 2 sensing tool in breast cancer patients.

(iii) Zinc oxide (ZnO) - cadmium selenide (CdSe) core-shell QDs-based dual-analyte biosensor was developed for the simultaneous detection of **cetuximab** (*Epidermal Growth Factor Receptor inhibitors*) and the carcinoembryonic antigen (CEA) [390]. The simultaneous detection of cetuximab (a therapeutic drug of colorectal cancer) and CEA (preferred biomarker for *in vivo* colorectal cancer) was achieved in a single run through the preparation of adsorptive surfaces that upon cetuximab (or CEA) binding leads to release of CdSeQDs (or ZnOQDs) [390].

(iv) The electrochemical behavior of native and denatured **nivolumab** (*programmed cell death protein 1/death ligand 1 inhibitor*) was studied, correspondingly, in solution and in a form of denatured

nivolumab multilayer thick film adsorbed to GCE surface, using DPV, CV, and EIS [391]. It was found that native nivolumab gives two pH-dependent anodic peaks which correspond to the oxidation of cysteine amino acid residues (first peak) and the oxidation of tyrosine and tryptophan amino acid residues (second peak). As expected, the denatured nivolumab (immobilized on the GCE surface) underwent substantial changes providing new charge transfer characteristics. The unfolding of nivolumab morphological structure upon denaturation (urea and SDS were used as denaturing agents whereas DTT and SDA as reducing agents) caused enhancement of existing and appearance of new anodic responses as compared with the native drug structure. These were attributed to the oxidation of tryptophan, methionine, and histidine amino acid residues.

Also, the nivolumab-dsDNA interaction was evaluated in incubated solutions and *in-situ* with dsDNA, poly[G]- or poly[A]-based biosensors by electrochemical methods, such as DPV, CV, EIS, and further confirmed with QCM, UV-vis spectroscopy, and gel electrophoresis [392]. The results have shown that nivolumab binds to dsDNA resulting in the formation of a nivolumab-dsDNA complex, followed by its structure relaxation/unwinding. In addition, it was proven that the nivolumab did not induce oxidative damage to DNA.

(v) The electrochemical oxidation behavior of native and denatured **bevacizumab** (*vascular endothelial growth factor inhibitors*) was investigated by CV, DPV, SWV, and EIS in solutions over a wide pH range at bevacizumab-thin film modified GCE [393]. Native bevacizumab exhibited only one pH-dependent irreversible oxidation peak which corresponds to the oxidation of tyrosine and tryptophan amino acid residues. The unfolding of the bevacizumab structure occurred upon denaturation with SDS, DTT, and SDS leading to additional oxidation peaks attributed to cysteine and histidine amino acid residues.

Moreover, the bevacizumab-dsDNA interaction was studied by DPV in incubated solutions and using dsDNA immobilized GCE [394]. The experiments showed that bevacizumab binds to the dsDNA, and this binding is driven by electrostatic forces; however, no oxidative damage to DNA by bevacizumab was detected electrochemically. Bevacizumab-dsDNA interaction leads to the formation of a complex bevacizumab-dsDNA adduct. Both, DNA and bevacizumab undergo unfolding which leads to morphological and conformational changes. For comparison, non-denaturing agarose gel-electrophoresis in incubated samples was carried out and the obtained results were in good agreement with those obtained by DPV.

----------Here in Table 6----------

2.7. Other antineoplastic agents

The last section is focused on a group composed of 8 classes of chemical constituents (listed in Table S1) used for cancer treatment classified as other antineoplastic agents.

This group lists 66 chemical species, but to our surprise, only 14 (!) have been studied electrochemically (the compounds left aside are summarized in Table S1). This underlines the existence of a significant niche for the basic electroanalytical research that should be filled in the future. Besides, the electrochemical detection strategies have been developed for 12 drugs from the concerned group, and the comprehensive summary of the electroanalytical parameters can be found in Table 7. Unlike the previous chapters, sensing protocols established for members of other ANAs are discussed together without classification. Table 7 points out unique electroanalytical configurations developed for the individual compounds and highlights the predominant availability of indirect sensing approaches.

Considering intrinsic redox properties of the *platinum compounds* the utilization of electrochemical techniques for their analytical studies is an intuitive choice. Due to the electrochemical activity of platinum-based drugs, electroanalytical methods may aspire to become routine tools even for their *in vivo* analysis (existing reports are focused mainly on cisplatin).

Inhibiting properties of **cisplatin** (*platinum compound*) on cell division were discovered accidentally during unaware PtEs electrolysis in the chlorine ions-containing solution while being placed in the *Escherichia coli* growing medium. Basic cisplatin redox reactions were also harvested electrochemically during its plating over the GCE followed by its oxidation (analytical step) [395] or direct reduction at the Hg-based electrodes [396]. Indirect sensing of cisplatin was realized on HMDE modified with metallothionein (MT) by monitoring an increase in the reduction peak of Pt^{2+}-MT protein complex [397] and on CPE with electrodeposited AgNPs [398], with the latter procedure providing a lower LOD of 3.2 nM [398]. Besides, the nanoporous GCE modified with thionine and GQDs [399] was designed, where the electrocatalytic effect of thionine on cisplatin oxidation gave the sensor operating in two LR with LOD of 90.0 nM and good selectivity [399]. Wu and Lai proposed tunable signal-off and signal-on electrochemical sensor based on AuE modified with a thiolated and low coverage MTB-terminated oligo-A-oligo-G DNA probe for cisplatin sensing (Fig. 7A shows the sensing concept). The detection strategy was based on the electrocatalytic reaction between the Pt(IV) center of cisplatin and leucomethylene blue (LMTB; MTB is firstly reduced to LMTB which then acts as the reducing agent to catalyze the reduction of the Pt(IV) center in cisplatin to Pt(II), regenerating MTB in the process). This configuration, with a rather narrow LR, allowed cisplatin detection down to 200.0 nM [400]. Interestingly, a method was established for the individual determination

of three *platinum compounds*, **cisplatin**, **carboplatin**, and **oxaliplatin**. Their indirect sensing was realized by monitoring an increase in Pt^{2+}-formazone complex reduction peak current on HMDE (complex was formed in the presence of supporting electrolyte) [401]. Such platform enabled the drugs detection at a very low LOD of 200.0 pM for cisplatin, 100.0 pM for carboplatin, and 80.0 pM for oxaliplatin; however, the selectivity study was not performed.

Further, **carboplatin** (*platinum compound*) can be directly oxidized on a bare PtE, which was used to develop a very simple electroanalytical protocol with a LOD of 30.0 μM [402]. Noticeably, the indirect determination of carboplatin in blood serum collected from the patients with ovarian cancer undergoing treatment with carboplatin by monitoring the decrease in A oxidation peak current was reported on ssDNA modified GCE with LOD of 5.7 μM [403]. In addition, the pharmacokinetic study performed in this work showed that carboplatin concentration in the blood serum decreases exponentially with time, and thus, after 72 h since the administration of the drug, the carboplatin concentration is lower than the established LOD value and cannot be detected.

The impressive sensing output for **oxaliplatin** (*platinum compound*) was achieved with a platform utilizing MIP(p-Py)-based sensor electrodeposited on the GCE surface modified with nitrogen-doped MWCNTs and AgNPs functionalized copper-doped terephthalic acid (Cu-TPA) MOF, which increased the anchoring binding sites on the polymeric film [404]. The oxaliplatin detection strategy was based on indirect oxaliplatin sensing by monitoring a decrease in the reduction signal of Cu-TPA. The developed MIP-based sensor offered outstanding sensitivity, reproducibility, and stability and gave the lowest reported LOD value for oxaliplatin equal to 40.3 pM. Obtained results showed that oxaliplatin, unlike most of the tested interfering species which are listed in Table 7, can freely diffuse into imprinted cavities existing in the polymeric network. The exceptions were structurally related Pt-containing drugs such as cisplatin, satraplatin, and carboplatin (poor selectivity reported in the presence of high concentrations above 126.0 μM). Another indirect oxaliplatin sensing platform was based on monitoring a decrease in $[Fe(CN)_6]^{3-/4-}$ oxidation peak current recorded with a sensor constructed from a combination of Zr(IV)-MOF, hexagonal boron nitride nanosheets (HBNNSs) and carbon quantum dots (CQDs) placed over GCE surface. Imprinting the oxaliplatin in the polymeric network gave excellent sensing output with very high target molecule recognition capability [405] (the sensing surface preparation is schematically shown in Fig. 7B). The sensor allowed LOD as low as 370.0 pM, showed superior selectivity toward oxaliplatin detection in the presence of interfering species at high concentration (especially other Pt-based compounds such as cisplatin, carboplatin, picoplatin, and satraplatin), as well as exhibited excellent reproducibility and stability.

Indirect sensing protocol for **amsacrine** (*other non-classified ANA*) by monitoring a decrease in G oxidation peak was proposed on CPE modified with europium(III)-doped nickel(II) oxide NPs ((Eu^{3+}-NiO)NPs) and dsDNA [406]. The sensor-enabled amsacrine detection at LOD of 50.0 nM and showed satisfactory selectivity. Direct amsacrine determination based on its oxidation signal was also carried out on CPE modified with graphene with immobilized dsDNA [407]. A relatively low LOD value of 300.0 nM was achieved, however, the selectivity of the sensor was not tested.

Among all sensing protocols for **hydroxycarbamide** (*other non-classified ANA*), worth mentioning is the work where SPCE was modified with acrylated nitrogen-doped GQDs (N-GQDs-COCl) prepared utilizing the degree of dehydration/carbonization of citric acid (carbon skeleton) and urea (nitrogen dopant), which provided an efficient platform anchoring core-shell bimetallic Au-Ag nanorods (NRs) placed in MIP sensing interface (Fig. 7C shows the nanomaterial structure) [408]. The developed MIP-based sensor allowed to push hydroxycarbamide detection down to 657.4 pM and showed excellent selectivity toward other potentially interfering substances (phenomenal imprinting effect) including ANAs (*i.e.,* temozolomide, dacarbazine, ifosfamide, and chlorambucil which belong to alkylating agents) even at high excess concentrations. In addition, the regeneration of the MIP-based sensor was possible by template retrieval approach using methanol as a solvent. The sensing surface withstood at least 20 binding-rebinding cycles.

Reports describing the determination of **celecoxib** (*other non-classified ANA*) are only based on its reduction signal. Among 5 sensing protocols developed for this drug (see Table 7), worthy of note is work where ITOE modified with p-ANI and functionalized MWCNTs was used to detect celecoxib with a very low LOD value of 10.0 pM [409]. The determination of celecoxib was also carried out on HMDE providing comprehensive electroanalytical protocol with a low LOD value of 186.0 pM, and selectivity studies performed in pharmaceutical formulation, spiked blood serum, and in the presence of interfering agents [410].

As clearly indicated in Table 7, for six compounds only one sensing protocol has been developed so far. Moreover, the proposed methods possess a common feature, represented by rather poor analytical parameters, as evidenced by the lack of selectivity studies and relatively high LOD values (the only exception is a method established for satraplatin as discussed below). Briefly, a kinetic potentiometric method was proposed for the determination of **procarbazine** (*methylhydrazines*; making the entire methylhydrazine group by itself) which was based on monitoring the reaction between 1-fluoro-2,4-dinitrobenzene and procarbazine, which resulted in the release of fluoride ions that could be detected using fluorine ion-selective electrode (FISE) (reaction and sensing mechanism is depicted in Fig. 7D) [411].

Direct determination of **tretinoin** (*retinoids for cancer treatment*) was carried out on GCE, however, obtained LOD value of 7.5 nM is questionable as lower concentration value of the reported LR equals to 1.0 μM [412]. Next, an amperometric sensor based on AuE modified with hierarchical leaf-like AuNPs electrochemically deposited using choline chloride as a shape directing agent was fabricated and used for **vorinostat** (*histone deacetylase inhibitors*) determination [413]. Moreover, sensing protocols based on cytochrome C modified BDDE (*via* monitoring a decrease in cytochrome C reduction peak) and SPCE modified with zinc-doped cobalt Fe_2O_3NPs (direct oxidation) have been reported for **arsenic trioxide** and **anagrelide** (*other non-classified ANA*), respectively.

Reagentless and reusable amperometric sensors based on AuE with immobilized MTB (which is one of the most commonly used redox labels in electrochemical biosensing applications) were prepared in three different alkanethiol diluents, *i.e.,* 2-mercaptoethanol (C2), 4-mercapto-1-butanol (C4), and 6-mercapto-1-hexanol (C6) to evaluate the effect of the chain length on the overall sensor performance, were developed and tested for **satraplatin** (*platinum compound*) sensing in 50 % bovine calf serum [414]. In this work, the detection strategy was based on the electrocatalytic reaction between the Pt(IV) center of satraplatin and LMTB (MTB is firstly reduced to LMTB which then acts as the reducing agent to catalyze the reduction of the Pt(IV) center in satraplatin to Pt(II), regenerating MTB in the process). The C2-passivated amperometric sensor has shown better performance in terms of the lowest LOD value of 1.0 μM, compared to C4- and C6-passivated sensors. In addition, the prepared sensor was proved to be highly specific for satraplatin (did not respond to other platinum compounds such as cisplatin and carboplatin), and selective enough to be employed directly in serum.

To the best of our knowledge, no sensing protocols have been proposed for two representatives of *proteasome inhibitors*, even though their electrochemical activity has been successfully manifested: **bortezomib** can be directly oxidized and reduced on GCE (both processes are pH-dependent) [415], and similarly, direct electrooxidation (under a pH-dependent and adsorption-controlled mechanism) of **carfilzomib** was performed on GCE and BDDE [416].

Moreover, electrochemical methods can throw light on the following areas of interest:

(i) interactions with ssDNA and dsDNA.

The interaction between **carboplatin** (*platinum compound*) and ssDNA was studied by DPV on ssDNA-modified GCE [403]. It was stated that carboplatin binds covalently to DNA preferentially interacting with A rather than G groups. In contrast, **cisplatin** and **oxaliplatin** (*platinum compounds*) specifically bind to G

bases in the skeleton of DNA, which was revealed based on the experiments with these drugs and dsDNA-based PGE modified with SWCNTs using DPV and EIS [417]. Moreover, the dsDNA sensors based on CPE modified either with (Eu^{3+}-NiO)NPs [406] or graphene [407] were used to investigate the interactions between **amsacrine** (*other non-classified ANA*) and dsDNA by DPV. In addition, UV–vis spectroscopy and docking measurements were also employed to investigate the amsacrine-dsDNA interaction. The results proved the effective interaction between amsacrine and dsDNA *via* intercalation at minor and major groove of dsDNA (the possibility of intercalation at major groove was proved to be higher than at minor groove).

(ii) interactions with peptides and enzymes.

The interactions between **cisplatin**, **carboplatin**, and **oxaliplatin** (all *platinum compounds*) with three synthesized peptides derived from MT proteins were studied using electrochemistry [401]. Briefly, MT belongs to the group of intracellular and low molecular mass proteins that are rich in cysteine and have no aromatic amino acids. The overexpression of MT in tumor cells is one of the generally accepted mechanisms of resistance development to these drugs. Therefore, such interactions between platinum compounds and metal-binding peptide fragments of MT proteins were examined using flow-injection analysis with amperometric detection on HMDE. As evident from the obtained data, interactions proceeded differently, with oxaliplatin demonstrating the highest ability to form Pt^{2+}-MT complex.

In addition, the mechanism of action of **bortezomib** (*20S proteasome inhibitor*) was examined using electrochemical assays based on 20S proteasome enzyme [418, 419]. In particular, two assays were established: (a) 20S proteasome was immobilized on GCE, and its electrochemical activity was monitored by DPV (and fluorescence spectroscopy for comparative purposes) [418], and (b) GCE with immobilized 20S proteasome and a monoclonal antibody specific to the β5 subunits of the 20S proteasome, whose activity was observed by CA [419]. In both works, the detection principle was based on the electrochemical oxidation of the electroactive probe commonly used in the study of proteases, 7-amino-4-methylcoumarin, released from the enzymatic substrate of chymotrypsin-like activity upon proteolysis. It was demonstrated that the proposed electrochemical assays are reliable and can be used to assess the 20S proteasome activity as well as to effectively investigate the inhibition mechanism of bortezomib.

(iii) interactions with cancer cells.

HeLa cell lines have been frequently used to elucidate:

(a) the effect of different **cisplatin** (*platinum compound*) loaded liposomes on HeLa cells by simple CV [420]. The results showed that cisplatin decreased the voltammetric response of HeLa cells in a time- and

concentration-dependent manner and a decrease in peak current was in line with the nuclear damage and the loss of mitochondrial membrane potential additionally revealed by two-photon laser scanning microscopy and confocal laser scanning microscopy.

(b) real-time and time-dependent impedimetric cytotoxicity of **oxaliplatin** (*platinum compound*) and liposome-encapsulated oxaliplatin (developed for targeted drug delivery) [301]. For this purpose, "plug-in" microfluidic chip with the microelectrode array consisting of 12 interdigitated microelectrodes coated with laminin was developed. It was found that the response of HeLa cells to oxaliplatin-induced cytotoxicity was slower than toxicity induced by doxorubicin. In addition, it was possible to differentiate between the effect of free oxaliplatin and liposome-encapsulated oxaliplatin on the induction of the cell death in fibrosarcoma cell line (HT-1080) that produce matrix metalloproteinases needed for degradation of drug-loaded liposomes (the metalloproteinases-dependent release of oxaliplatin from the liposomes was confirmed using hypopharyngeal carcinoma cell line (FaDu) that do not express metalloproteinases).

(c) cell growth, viability, and **hydroxycarbamide** (*other non-classified ANA*)-related toxicity; this investigation was carried out by CV and PSA on the HeLa cell-based chip, which contained three AuEs patterned on a silicon substrate [55].

Also, PtE was used to monitor **carboplatin** (*platinum compound*) consumption (carboplatin removal from the solution by cells uptake and binding) by drug-susceptible and drug-resistant ovarian cancer cells using electrochemical methods [402]. Interestingly, the obtained results demonstrated a similar consumption of carboplatin by both, susceptible and resistant, cell lines.

Finally, the electrochemical behavior of K-562 and the effect of **arsenic trioxide** (*other non-classified ANA*) on cell viability and toxicity was investigated on a new disposable electrochemical device with an integrated ITOE and a filter paper used as the electrochemical cell [54]. The results revealed that arsenic trioxide considerably affects the voltammetric response of K-562 cells, which decreased significantly in the presence of the drug. In addition, the system enabled the use of a very small volume of cell samples of 10 µL, which is significantly reduced when compared to traditional electrochemical systems (>500 µL).

----------Here in Fig. 7----------

----------Here in Table 7----------

3. Conclusion and outlook

In this review, the versatility and powerfulness of electrochemistry for studying ANAs, a wide and structurally heterogeneous group of pharmaceuticals, have been demonstrated. The progress made in (i) electrochemical sensing of ANAs over the last four decades and (ii) investigation of interactions of ANAs with complex structures, such as DNA, cancerous cells, biomimetic membranes, peptides, and enzymes by means of electrochemical techniques has been comprehensively documented. Moreover, perspectives for applications of electrochemical approaches towards enantiopurity study, differentiation between ssDNA and dsDNA without using any label or tag, degradation, and pharmacokinetic studies on ANAs, are shown and commented.

The core of this review is based on the selection of *ca.* 350 most relevant publications; importantly, *ca.* 300 are from the last decade (*i.e.*, period of 2011-2021), which illustrates increasing interest in electrochemical studies of ANAs. It is expected that the research on ANAs will intensify, considering that no electrochemical data are available for more than 70% (!) of currently known compounds: WHOCC lists 266 ANAs in total, however, only 76 have been tested electrochemically so far, and even though electroactivity of some ANAs have been confirmed, the sensing protocols have not yet been established (such information may facilitate the development of sensing solutions for the concerned molecules). This leaves a huge gap to be filled in the coming years, bearing in mind that fast and reliable monitoring of ANAs in cancer patients undergoing chemotherapy as well as in exposed medical personnel was, is, and will be crucial to diminish the health risks associated with these drugs.

Up to date, the sensing protocols for ANAs are frequently based on relatively straightforward modifications of carbon-based electrode surfaces with a simple type of nano-/micro-objects, resuting in analytical methodology providing an impressive LOD values reaching the nM range. Some sensing scenarious are fully applicable for the monitoring of therapeutic concentrations of ANAs in physiological fluids of patients and healthcare workers. Methods that were not verified by real samples analysis or at least exposed to potentially interfering chemical species are of limited usefulness for clinical applications. If such reports aim to be applicable and relevant, the missing knowledge gap must be filled. Further effort is also needed to improve the selectivity, at the same time remaining one of the biggest challenges, of the electrochemical sensing of ANAs. This aspect can be addressed *via* the following actions:

(i) One of the most common solutions has been the development of MIP-based sensors for a wide range of ANAs. A considerable amount of developed MIP-based configurations demonstrated impressive sensing output and very high selectivity. This approach should be considered, despite being quite tedious,

for other drugs sensing. Another advantage of MIP-based sensors is their applicability for non-electroactive compounds detection when combined with an indirect approach based on a redox marker. This also further expands the possibility of using electroanalytical techniques for ANAs detection.

(ii) Incorporation of the electrokinetic separation step before electrochemical detection as successfully reported for four cytotoxic antibiotics in [248]. Such an approach demonstrated, besides excellent selectivity, the ability to detect the selected compounds in trace quantities (fM range).

(iii) Biosensing, especially enzymatic, aptamer-/immune-based, attracted very limited attention in a view of ANAs sensing. As frequently reported in the literature, these approaches may lead to a very high selectivity or even, in some cases, very much desired sensing specificity.

Further, it is expected that ion transfer voltammetry will be utilized to a much greater extent. Until now, the analytical protocols based on the interfacial ion transfer reaction exist only for a limited amount of ANAs. All drugs possessing ionizable or permanently charged functional groups are potentially active at the electrified liquid-liquid interface, and hence, can be detected using this methodology. Also, an important advantage of electrochemical system (in general) is their susceptibility to miniaturization. As such, the future development will be heading towards portablility and the possibility to be used for point-of-care testing. The miniaturized sensor requires small sample for analysis, which is convenient when, *e.g.*, working with limited amounts of physiological fluids. A few interesting reports exist where electroanalytical techniques were used to monitor the concentration levels of selected ANAs in real blood serum or urine samples collected directly from the treated cancer patients. Similar studies should become more frequent as it is beneficial for both patients/healthcare workers and researchers who can verify and validate the developed (bio)sensors in clinical practice. In this respect, the cooperation between the electrochemical community and medical centers should be intensified.

As demonstrated in this review, electrochemical techniques provide a set of powerful tools which may be used to study ANAs interactions with complex structures, including DNA and carcinogenic cell lines. However, the interaction between some drugs and DNA is inconclusive since contrary data pointing towards different interaction mechanisms exist in the literature. Therefore, experimental verification of the published results is a must. Besides, not all electrochemically tested ANAs have been subjected to such investigations, even though “DNA-drug interaction” examination has great importance in predicting the mechanism of action of individual ANA as a genotoxic anticancer drug and understanding its biological activity and toxicity *in vivo*.

Although a few exciting works describing interesting electrochemical platforms for studying ANAs interactions with cancerous cells already exist, more attention should be given to developing similar platforms since simple electroanalytical readout may serve as the information which can be translated into the most appropriate cancer treatment scheme. Such platforms may also create a bedrock for further development and fabrication of even more sophisticated devices based on lab-on-the-chip and organ-on-the-chip technology.

In conclusion, this review highlights the relevance and importance of electrochemistry in investigations of ANAs, summarizes the most significant achievements and applications, points out future research aims, that will fill the existing literature niche on the proposed topic.

Acknowledgements

MB acknowledge the financial support of the University of Lodz, IDUB, (Grant no. B2211101000089.07).

Declaration of competing interest

The authors declare that they have no known competing financial interests or personal relationships that could have appeared to influence the work reported in this paper.

Appendix A. Supplementary material

Supplementary material contains a table listing ANAs which were not subjected to electrochemical studies.

References

[1] World Health Organization. *Global Health Estimates 2020: Deaths by Cause, Age, Sex, by Country and by Region, 2000-2019*; Geneva, 2020.

[2] World Health Organization. *WHO Report on Cancer: Setting Priorities, Investing Wisely and Providing Care for All*; World Health Organization: Licence: CC BY-NC-SA 3.0 IGO, 2020.

[3] The Global Cancer Observatory. *International Agency for Research on Cancer, World Health Organization, Fact Sheet on All Cancers*; 2020; Vol. 419.

[4] American Cancer Society. *Cancer Treatment and Survivorship Facts and Figures 2019-2021*; Atlanta, 2019.

[5] Aristizabal-Pachon, A. F.; Castillo William Orlando. Genotoxic Evaluation of Occupational Exposure to Antineoplastic Drugs. *Toxicol. Res.*, **2020**, *36*, 29–36. https://doi.org/10.1007/s43188-019-00003-7.

[6] Goodman, L. S.; Wintrobe, M. M.; Dameshek, W.; Goodman, M. J.; Gilman, A.; McLennan, M. T. Nitrogen Mustard Therapy; Use of Methyl-Bis (Beta-Chloroethyl) Amine Hydrochloride and Tris (Beta-Chloroethyl) Amine Hydrochloride for Hodgkin's Disease, Lymphosarcoma, Leukemia and Certain Allied and Miscellaneous Disorders. *J. Am. Med. Assoc.*, **1946**, *132*, 126–132. https://doi.org/10.1001/jama.1946.02870380008004.

[7] Connor, T. H.; MacKenzie, B. A.; DeBord, D. G.; Trout, D. B.; O'Callaghan, J. P. NIOSH List of Antineoplastic and Other Hazardous Drugs in Healthcare Settings. *U.S. Dep. Heal. Hum. Serv. Centers Dis. Control Prev. Natl. Inst. Occup. Saf. Heal.*, **2016**, *2016–161*, 1–34.

[8] Al-Azzam, S. I.; Awawdeh, B. T.; Alzoubi, K. H.; Khader, Y. S.; Alkafajei, A. M. Compliance with Safe Handling Guidelines of Antineoplastic Drugs in Jordanian Hospitals. *J. Oncol. Pharm. Pract.*, **2015**, *21* (1), 3–9. https://doi.org/10.1177/1078155213517128.

[9] Connor, T. H.; McDiarmid, M. A. Preventing Occupational Exposures to Antineoplastic Drugs in Health Care Settings. *CA. Cancer J. Clin.*, **2006**, *56* (6), 354–365. https://doi.org/10.3322/canjclin.56.6.354.

[10] Reinhardt, H.; Otte, P.; Eggleton, A. G.; Ruch, M.; Wöhrl, S.; Ajayi, S.; Duyster, J.; Jung, M.; Hug, M. J.; Engelhardt, M. Avoiding Chemotherapy Prescribing Errors: Analysis and Innovative Strategies. *Cancer*, **2019**, *125* (9), 1547–1557. https://doi.org/10.1002/cncr.31950.

[11] Tjokrowidjaja, A.; Hovey, E.; Lewis, C. R. Let's Talk about Cytotoxic Chemotherapy Dosing: Unravelling Adjustments and off-Protocol Prescribing. *Med. J. Aust.*, **2019**, *210* (2), 65–66. https://doi.org/10.5694/mja2.12072.

[12] Nelson, W. K.; Moore, J.; Grasso, J. A.; Barbarotta, L.; Fischer, D. S. Development of a Policy and Procedure for Accidental Chemotherapy Overdose. *Clin. J. Oncol. Nurs.*, **2014**, *18* (4), 414–420. https://doi.org/10.1188/14.CJON.18-04AP.

[13] Bernabeu-Martínez, M. A.; Merino, M. R.; Santos Gago, J. M.; Alvarez Sabucedo, L. M.; Wanden-Berghe, C.; Sanz-Valero, J. Guidelines for Safe Handling of Hazardous Drugs: A Systematic Review. *PLoS One*, **2018**, *13* (5), 1–24. https://doi.org/10.1371/journal.pone.0197172.

[14] Nouri, A.; Seyed Javadi, M.; Iranijam, E.; Aghamohammadi, M. Improving Nurses' Performance in the Safe Handling of Antineoplastic Agents: A Quasi-Experimental Study. *BMC Nurs.*, **2021**, *20* (1), 247. https://doi.org/10.1186/s12912-021-00771-4.

[15] Falck, K.; Gröhn, P.; Sorsa, M.; Vainio, H.; Heinonen, E.; Holsti, L. R. Mutagenicity in Urine of Nurses Handling Cytostatic Drugs. *Lancet*, **1979**, *313* (8128), 1250–1251. https://doi.org/10.1016/S0140-6736(79)91939-1.

[16] Villarini, M.; Gianfredi, V.; Levorato, S.; Vannini, S.; Salvatori, T.; Moretti, M. Occupational Exposure to Cytostatic/Antineoplastic Drugs and Cytogenetic Damage Measured Using the Lymphocyte Cytokinesis-Block Micronucleus Assay: A Systematic Review of the Literature and

Meta-Analysis. *Mutat. Res. - Rev. Mutat. Res.*, **2016**, *770*, 35–45. https://doi.org/10.1016/j.mrrev.2016.05.001.

[17] Mahmoodi, M.; Soleyman-Jahi, S.; Zendehdel, K.; Mozdarani, H.; Azimi, C.; Farzanfar, F.; Safari, Z.; Mohagheghi, M. A.; Khaleghian, M.; Divsalar, K.; et al. Chromosomal Aberrations, Sister Chromatid Exchanges, and Micronuclei in Lymphocytes of Oncology Department Personnel Handling Anti-Neoplastic Drugs. *Drug Chem. Toxicol.*, **2017**, *40* (2), 235–240. https://doi.org/10.1080/01480545.2016.1209678.

[18] World Health Organization Collaborating Centre for Drug Statistics Methodology. Anatomical Therapeutic Chemical Classification System together with a technical unit of measurement called the Defined Daily Dose https://www.whocc.no/atc_ddd_index/?code=L.

[19] IARC (International Agency for Research on Cancer). Agents Classified by the IARC Monographs. *IARC Press*, **2021**, *1–130*.

[20] Jain, S.; Jadav, T.; Sahu, A. K.; Kalia, K.; Sengupta, P. An Exploration of Advancement in Analytical Methodology for Quantification of Anticancer Drugs in Biomatrices. *Anal. Sci.*, **2019**, *35* (7), 719–732. https://doi.org/10.2116/analsci.19R002.

[21] Guichard, N.; Guillarme, D.; Bonnabry, P.; Fleury-Souverain, S. Antineoplastic Drugs and Their Analysis: A State of the Art Review. *Analyst*, **2017**, *142* (13), 2273–2321. https://doi.org/10.1039/c7an00367f.

[22] Mathias, P. I.; Connor, T. H.; B'Hymer, C. A Review of High Performance Liquid Chromatographic-Mass Spectrometric Urinary Methods for Anticancer Drug Exposure of Health Care Workers. *J. Chromatogr. B Anal. Technol. Biomed. Life Sci.*, **2017**, *1060* (April), 316–324. https://doi.org/10.1016/j.jchromb.2017.06.028.

[23] Nussbaumer, S.; Bonnabry, P.; Veuthey, J. L.; Fleury-Souverain, S. Analysis of Anticancer Drugs: A Review. *Talanta*, **2011**, *85* (5), 2265–2289. https://doi.org/10.1016/j.talanta.2011.08.034.

[24] Turci, R.; Sottani, C.; Spagnoli, G.; Minoia, C. Biological and Environmental Monitoring of Hospital Personnel Exposed to Antineoplastic Agents: A Review of Analytical Methods. *J. Chromatogr. B Anal. Technol. Biomed. Life Sci.*, **2003**, *789* (2), 169–209. https://doi.org/10.1016/s1570-0232(03)00100-4.

[25] Safaei, M.; Shishehbore, M. R. A Review on Analytical Methods with Special Reference to Electroanalytical Methods for the Determination of Some Anticancer Drugs in Pharmaceutical and Biological Samples. *Talanta*, **2021**, *229* (March), 122247. https://doi.org/10.1016/j.talanta.2021.122247.

[26] Sabourian, R.; Mirjalili, S. Z.; Namini, N.; Chavoshy, F.; Hajimahmoodi, M.; Safavi, M. HPLC Methods for Quantifying Anticancer Drugs in Human Samples: A Systematic Review. *Anal. Biochem.*, **2020**, *610* (August), 113891. https://doi.org/10.1016/j.ab.2020.113891.

[27] Pashaei, Y.; Mehrabi, M.; Shekarchi, M. A Review on Various Analytical Methods for Determination of Anthracyclines and Their Metabolites as Anti–Cancer Chemotherapy Drugs in Different Matrices over the Last Four Decades. *TrAC - Trends Anal. Chem.*, **2020**, *130*, 115991. https://doi.org/10.1016/j.trac.2020.115991.

[28] Kurbanoglu, S.; Bakirhan, N. K.; Gumustas, M.; Ozkan, S. A. Modern Assay Techniques for Cancer Drugs: Electroanalytical and Liquid Chromatography Methods. *Crit. Rev. Anal. Chem.*, **2019**, *49* (4), 306–323. https://doi.org/10.1080/10408347.2018.1527206.

[29] Ali, I.; Haque, A.; Wani, W. A.; Saleem, K.; Al Za'abi, M. Analyses of Anticancer Drugs by Capillary Electrophoresis: A Review. *Biomed. Chromatogr.*, **2013**, *27* (10), 1296–1311. https://doi.org/10.1002/bmc.2953.

[30] Iranifam, M. Analytical Applications of Chemiluminescence Methods for Cancer Detection and Therapy. *TrAC - Trends Anal. Chem.*, **2014**, *59*, 156–183. https://doi.org/10.1016/j.trac.2014.03.010.

[31] De Castro, F.; Benedetti, M.; Del Coco, L.; Fanizzi, F. P. NMR-Based Metabolomics in Metal-Based Drug Research. *Molecules*, **2019**, *24* (12), 1–14. https://doi.org/10.3390/molecules24122240.
[32] Wang, J. Portable Electrochemical Systems. *TrAC - Trends Anal. Chem.*, **2002**, *21* (4), 226–232. https://doi.org/10.1016/S0165-9936(02)00402-8.
[33] Umapathi, R.; Ghoreishian, S. M.; Sonwal, S.; Rani, G. M.; Huh, Y. S. Portable Electrochemical Sensing Methodologies for On-Site Detection of Pesticide Residues in Fruits and Vegetables. *Coord. Chem. Rev.*, **2022**, *453*, 214305. https://doi.org/10.1016/j.ccr.2021.214305.
[34] Lima, H. R. S.; da Silva, J. S.; de Oliveira Farias, E. A.; Teixeira, P. R. S.; Eiras, C.; Nunes, L. C. C. Electrochemical Sensors and Biosensors for the Analysis of Antineoplastic Drugs. *Biosens. Bioelectron.*, **2018**, *108* (February), 27–37. https://doi.org/10.1016/j.bios.2018.02.034.
[35] Chu, C. S.; Rubin, S. C. Basic Principles of Chemotherapy. In *Clinical Gynecologic Oncology*; DiSaia, P. J., Creasman, W. T., Mannel, R. S., McMeekin, D. S., Mutch, D. G., Eds.; Elsevier, 2018; pp 449–469. https://doi.org/10.1016/B978-0-323-40067-1.00017-6.
[36] Sakthivel, K.; Muthumariappan, A.; Chen, S. M.; Li, Y. L.; Chen, T. W.; Ali, M. A. Evaluating Ternary Metal Oxide (TMO)Core-Shell Nanocomposites for the Rapid Determination of the Anti-Neoplastic Drug Chlorambucil (Leukeran™)by Electrochemical Approaches. *Mater. Sci. Eng. C*, **2019**, *103* (December 2018), 109724. https://doi.org/10.1016/j.msec.2019.05.009.
[37] Hatamluyi, B.; Lorestani, F.; Es'haghi, Z. Au/Pd@rGO Nanocomposite Decorated with Poly (L-Cysteine) as a Probe for Simultaneous Sensitive Electrochemical Determination of Anticancer Drugs, Ifosfamide and Etoposide. *Biosens. Bioelectron.*, **2018**, *120* (August), 22–29. https://doi.org/10.1016/j.bios.2018.08.008.
[38] Hasanpour, F.; Taei, M.; Fouladgar, M. A Voltammetric Sensor Based on Spinel-Structured Copper Ferrite Nanoparticles Multiwalled Carbon Nanotubes Modified Carbon Paste Electrode for Determination of Dacarbazine. *Russ. J. Electrochem.*, **2018**, *54* (1), 70–76. https://doi.org/10.1134/S1023193517110040.
[39] Ibrahim, M.; Temerk, Y.; Ibrahim, H. Fabrication of a New Biosensor Based on a Sn Doped Ceria Nanoparticle Modified Glassy Carbon Paste Electrode for the Selective Determination of the Anticancer Drug Dacarbazine in Pharmaceuticals. *RSC Adv.*, **2017**, *7* (51), 32357–32366. https://doi.org/10.1039/c7ra04331g.
[40] Baj-Rossi, C.; de Micheli, G.; Carrara, S. Electrochemical Detection of Anti-Breast-Cancer Agents in Human Serum by Cytochrome P450-Coated Carbon Nanotubes. *Sensors (Switzerland)*, **2012**, *12* (5), 6520–6537. https://doi.org/10.3390/s120506520.
[41] Kalambate, P. K.; Dhanjai; Sinha, A.; Li, Y.; Shen, Y.; Huang, Y. An Electrochemical Sensor for Ifosfamide, Acetaminophen, Domperidone, and Sumatriptan Based on Self-Assembled MXene/MWCNT/Chitosan Nanocomposite Thin Film. *Microchim. Acta*, **2020**, *187*, 402. https://doi.org/10.1007/s00604-020-04366-9.
[42] Dehdashtian, S.; Behbahanian, N.; Taherzadeh, K. M. An Ultrasensitive Electrochemical Sensor for Direct Determination of Anticancer Drug Dacarbazine Based on Multiwall Carbon Nanotube-Modified Carbon Paste Electrode and Application in Pharmaceutical Sample. *J. Iran. Chem. Soc.*, **2018**, *15* (4), 931–941. https://doi.org/10.1007/s13738-018-1291-5.
[43] Satyanarayana, M.; Yugender Goud, K.; Koteshwara Reddy, K.; Vengatajalabathy Gobi, K. Conducting Polymer-Layered Carbon Nanotube as Sensor Interface for Electrochemical Detection of Dacarbazine In-Vitro. *Electrocatalysis*, **2017**, *8* (3), 214–223. https://doi.org/10.1007/s12678-017-0357-y.
[44] Prasad, B. B.; Pathak, P. K. Development of Surface Imprinted Nanospheres Using the Inverse Suspension Polymerization Method for Electrochemical Ultra Sensing of Dacarbazine. *Anal. Chim. Acta*, **2017**, *974*, 75–86. https://doi.org/10.1016/j.aca.2017.04.001.
[45] Fatma, S.; Prasad, B. B.; Singh, K.; Singh, R.; Jaiswal, S. A Reduced Graphene Oxide Ceramic

Electrode Modified with One MoNomer Doubly Imprinted Acryloylated Tetraamine Cobalt Phthalocyanine Polymer for the Simultaneous Analysis of Anticancerous Drugs. *Sensors Actuators, B Chem.*, **2019**, *281* (October 2018), 139–149. https://doi.org/10.1016/j.snb.2018.10.070.

[46] Pathak, P. K.; Kumar, A.; Prasad, B. B. A Novel Electrocatalytic Nanocomposite of Reduced Graphene Oxide/Silver Nanocube Hybrid Decorated Imprinted Polymer for Ultra-Trace Sensing of Temozolomide. *New J. Chem.*, **2018**, *42* (16), 13486–13496. https://doi.org/10.1039/c8nj01824c.

[47] Prasad, B. B.; Singh, R.; Kumar, A. Synthesis of Fullerene (C60-Monoadduct)-Based Water-Compatible Imprinted Micelles for Electrochemical Determination of Chlorambucil. *Biosens. Bioelectron.*, **2017**, *94* (January), 115–123. https://doi.org/10.1016/j.bios.2017.02.040.

[48] Bali Prasad, B.; Kumar, A.; Singh, R. Synthesis of Novel Monomeric Graphene Quantum Dots and Corresponding Nanocomposite with Molecularly Imprinted Polymer for Electrochemical Detection of an Anticancerous Ifosfamide Drug. *Biosens. Bioelectron.*, **2017**, *94*, 1–9. https://doi.org/10.1016/j.bios.2017.02.028.

[49] Kumar Singh, A.; Singh, M. QCM Sensing of Melphalan via Electropolymerized Molecularly Imprinted Polythiophene Films. *Biosens. Bioelectron.*, **2015**, *74*, 711–717. https://doi.org/10.1016/j.bios.2015.07.027.

[50] Liu, J.; Zhang, Y.; Jiang, M.; Tian, L.; Sun, S.; Zhao, N.; Zhao, F.; Li, Y. Electrochemical Microfluidic Chip Based on Molecular Imprinting Technique Applied for Therapeutic Drug Monitoring. *Biosens. Bioelectron.*, **2017**, *91* (January), 714–720. https://doi.org/10.1016/j.bios.2017.01.037.

[51] Huang, B.; Xiao, L.; Dong, H.; Zhang, X.; Gan, W.; Mahboob, S.; Al-Ghanim, K. A.; Yuan, Q.; Li, Y. Electrochemical Sensing Platform Based on Molecularly Imprinted Polymer Decorated N,S Co-Doped Activated Graphene for Ultrasensitive and Selective Determination of Cyclophosphamide. *Talanta*, **2017**, *164* (October 2016), 601–607. https://doi.org/10.1016/j.talanta.2016.11.009.

[52] Palaska, P.; Aritzoglou, E.; Girousi, S. Sensitive Detection of Cyclophosphamide Using DNA-Modified Carbon Paste, Pencil Graphite and Hanging Mercury Drop Electrodes. *Talanta*, **2007**, *72* (3), 1199–1206. https://doi.org/10.1016/j.talanta.2007.01.013.

[53] Guo, X.; Wang, Q.; Li, J.; Cui, J.; Zhou, S.; Hao, S.; Wu, D. A Mini-Electrochemical System Integrated Micropipet Tip and Pencil Graphite Electrode for Detection of Anticancer Drug Sensitivity in Vitro. *Biosens. Bioelectron.*, **2015**, *64*, 594–596. https://doi.org/10.1016/j.bios.2014.09.086.

[54] Yu, C.; Zhu, Z.; Wang, L.; Wang, Q.; Bao, N.; Gu, H. A New Disposable Electrode for Electrochemical Study of Leukemia K562 Cells and Anticancer Drug Sensitivity Test. *Biosens. Bioelectron.*, **2014**, *53*, 142–147. https://doi.org/10.1016/j.bios.2013.09.044.

[55] El-Said, W. A.; Yea, C. H.; Kim, H.; Oh, B. K.; Choi, J. W. Cell-Based Chip for the Detection of Anticancer Effect on HeLa Cells Using Cyclic Voltammetry. *Biosens. Bioelectron.*, **2009**, *24* (5), 1259–1265. https://doi.org/10.1016/j.bios.2008.07.037.

[56] Erol, A.; Akpınar, F.; Muti, M. Electrochemical Determination of Anticancer Drug Bendamustine and Its Interaction with Double Strand DNA in the Absence and Presence of Quercetin. *Colloids Surfaces B Biointerfaces*, **2021**, *205*, 111884. https://doi.org/10.1016/j.colsurfb.2021.111884.

[57] Radi, A. E.; Nassef, H. M.; Eissa, A. Electrochemical Study of the Interaction of the Alkylating Agent Busulfan with Double Strand DNA. *Electroanalysis*, **2013**, *25* (11), 2463–2469. https://doi.org/10.1002/elan.201300294.

[58] Radi, A. E.; Eissa, A.; Nassef, H. M. Voltammetric and Spectroscopic Studies on the Binding of the Antitumor Drug Dacarbazine with DNA. *J. Electroanal. Chem.*, **2014**, *717–718*, 24–28. https://doi.org/10.1016/j.jelechem.2014.01.007.

[59] Eksin, E.; Polat, D.; Erdem, A. Voltammetric and Impedimetric Detection of Interaction Between Dacarbazine and Nucleic Acids. *Electroanalysis*, **2019**, *31* (10), 2012–2019. https://doi.org/10.1002/elan.201900284.

[60] Temerk, Y.; Ibrahim, H. Binding Mode and Thermodynamic Studies on the Interaction of the

Anticancer Drug Dacarbazine and Dacarbazine-Cu(II) Complex with Single and Double Stranded DNA. *J. Pharm. Biomed. Anal.*, **2014**, *95*, 26–33. https://doi.org/10.1016/j.jpba.2014.02.010.

[61] Zhang, R.; Wang, X.; Gong, S. A Voltammetric Study of the Effect of Gold Nanoparticles on the Binding of DTIC to DNA Bases. *Electrochem. Solid-State Lett.*, **2004**, *7* (8), J27–J28. https://doi.org/10.1149/1.1758933.

[62] Shen, Q.; Wang, X.; Fu, D. The Amplification Effect of Functionalized Gold Nanoparticles on the Binding of Anticancer Drug Dacarbazine to DNA and DNA Bases. *Appl. Surf. Sci.*, **2008**, *255* (2), 577–580. https://doi.org/10.1016/j.apsusc.2008.06.132.

[63] Song, M.; Zhang, R.; Wang, X. Nano-Titanium Dioxide Enhanced Biosensing of the Interaction of Dacarbazine with DNA and DNA Bases. *Mater. Lett.*, **2006**, *60* (17–18), 2143–2147. https://doi.org/10.1016/j.matlet.2005.12.100.

[64] Altay, C.; Eksin, E.; Congur, G.; Erdem, A. Electrochemical Monitoring of the Interaction between Temozolamide and Nucleic Acids by Using Disposable Pencil Graphite Electrodes. *Talanta*, **2015**, *144*, 809–815. https://doi.org/10.1016/j.talanta.2015.07.017.

[65] Lopes, I. C.; Oliveira, S. C. B.; Oliveira-Brett, A. M. In Situ Electrochemical Evaluation of Anticancer Drug Temozolomide and Its Metabolites-DNA Interaction. *Anal. Bioanal. Chem.*, **2013**, *405* (11), 3783–3790. https://doi.org/10.1007/s00216-012-6546-x.

[66] Topkaya, S. N.; Serindere, G.; Ozder, M. Determination of DNA Hypermethylation Using Anti-Cancer Drug-Temozolomide. *Electroanalysis*, **2016**, *28* (5), 1052–1059. https://doi.org/10.1002/elan.201501027.

[67] de Carvalho, P. A. V.; Campelo Lopes, I.; Silva, E. H. C.; Bruzaca, E. E. S.; Alves, H. J.; Lima, M. I. S.; Tanaka, A. A. Electrochemical Behaviour of Anticancer Drug Lomustine and in Situ Evaluation of Its Interaction with DNA. *J. Pharm. Biomed. Anal.*, **2019**, *176*, 112786. https://doi.org/10.1016/j.jpba.2019.112786.

[68] Wang, J.; Lin, M. S.; Villa, V. Investigation of the Adsorptive Stripping Voltammetric Behaviour of the Anticancer Drugs Chlorambucil and 5-Fluorouracil. *Analyst*, **1987**, *112* (3), 247–251. https://doi.org/10.1039/an9871200247.

[69] Mutharani, B.; Ranganathan, P.; Chen, S. M.; Tsai, H. C. Temperature-responsive Voltammetric Sensor Based on Stimuli-Sensitive Semi-Interpenetrating Polymer Network Conductive Microgels for Reversible Switch Detection of Nitrogen Mustard Analog Chlorambucil (Leukeran™). *Electrochim. Acta*, **2021**, *374*, 137866. https://doi.org/10.1016/j.electacta.2021.137866.

[70] Barek, J.; Berka, A.; Zima, J. Determination of Melphalan Using Differential Pulse Voltammetry. *Anal. Lett.*, **1985**, *18* (20), 2581–2589. https://doi.org/10.1080/00032718508064488.

[71] Díaz De Guereñu, M. M.; Barrio, R. J.; Arranz, A.; Arranz, J. F. Use of Derivatization Reactions with Adsorptive Stripping Voltammetry for Determining Fotemustine in Biological Samples. *J. Pharm. Biomed. Anal.*, **1992**, *10* (7), 481–486. https://doi.org/10.1016/0731-7085(92)80068-X.

[72] Pecková, K.; Vrzalová, L.; Bencko, V.; Barek, J. Voltammetric and Amperometric Determination of N-Nitroso Antineoplastic Drugs at Mercury and Amalgam Electrodes. *Collect. Czechoslov. Chem. Commun.*, **2009**, *74* (11–12), 1697–1713. https://doi.org/10.1135/cccc2009112.

[73] Temerk, Y.; Ibrahim, M.; Ibrahim, H.; Kotb, M. Adsorptive Stripping Voltammetric Determination of Anticancer Drug Lomustine in Biological Fluids Using in Situ Mercury Film Coated Graphite Pencil Electrode. *J. Electroanal. Chem.*, **2016**, *760*, 135–142. https://doi.org/10.1016/j.jelechem.2015.11.026.

[74] Ordieres, A. J. M.; Garcia, A. C.; Blanco, P. T.; Smyth, W. F. An Electroanalytical Study of the Anticancer Drug Dacarbazine. *Anal. Chim. Acta*, **1987**, *202* (C), 141–149. https://doi.org/10.1016/S0003-2670(00)85909-7.

[75] Temerk, Y. M.; Kamal, M. M.; Ibrahim, M. S.; Ibrahim, H.; Schuhmann, W. Electrochemical Behaviour of the Anticancer Dacarbazine-Cu2+complex and Its Analytical Applications.

Electroanalysis, **2011**, *23* (7), 1638–1644. https://doi.org/10.1002/elan.201100038.
[76] Deepa, S.; Swamy, B. E. K.; Pai, K. V. A Surfactant SDS Modified Carbon Paste Electrode as an Enhanced and Effective Electrochemical Sensor for the Determination of Doxorubicin and Dacarbazine Its Applications: A Voltammetric Study. *J. Electroanal. Chem.*, **2020**, *879*, 114748. https://doi.org/10.1016/j.jelechem.2020.114748.
[77] Abdel-aal, F. A. M.; Ali, M. F. B. Eco-Friendly Fabricated Electrochemical Sensor Using Red Cabbage Extract for Electrochemical Determination of Dacarbazine with the Aid of Factorial Design Approach. *J. Electrochem. Soc.*, **2017**, *164* (14), H1053–H1063. https://doi.org/10.1149/2.0581714jes.
[78] Chiao, J.; Beitz, J.; DeLap, R. J. Antimetabolic Agents. In *Current cancer therapeutics*; Kirkwood, J. M., Lotze, M. Y., Yaskao, J. M., Eds.; Current Medicine Group: London, 2001; pp 37–40. https://doi.org/https://doi.org/10.1007/978-1-4613-1099-0_2.
[79] El-Said, W. A.; Abdel-Rahman, M. A.; Sayed, E. M.; Abdel-Wahab, A. M. A. Electrochemical Monitoring of Methotrexate Anticancer Drug in Human Blood Serum by Using in Situ Solvothermal Synthesized Fe3O4/ITO Electrode. *Electroanalysis*, **2019**, *31* (5), 829–837. https://doi.org/10.1002/elan.201800798.
[80] Phal, S.; Lindholm-Sethson, B.; Geladi, P.; Shchukarev, A.; Tesfalidet, S. Determination of Methotrexate in Spiked Human Blood Serum Using Multi-Frequency Electrochemical Immittance Spectroscopy and Multivariate Data Analysis. *Anal. Chim. Acta*, **2017**, *987*, 15–24. https://doi.org/10.1016/j.aca.2017.08.034.
[81] Phal, S.; Shatri, B.; Berisha, A.; Geladi, P.; Lindholm-Sethson, B.; Tesfalidet, S. Covalently Electrografted Carboxyphenyl Layers onto Gold Surface Serving as a Platform for the Construction of an Immunosensor for Detection of Methotrexate. *J. Electroanal. Chem.*, **2018**, *812*, 235–243. https://doi.org/10.1016/j.jelechem.2017.12.072.
[82] Khand, A. A.; Lakho, S. A.; Tahira, A.; Ubaidullah, M.; Alothman, A. A.; Aljadoa, K.; Nafady, A.; Ibupoto, Z. H. Facile Electrochemical Determination of Methotrexate (MTX) Using Glassy Carbon Electrode-Modified with Electronically Disordered NiO Nanostructures. *Nanomaterials*, **2021**, *11* (5), 1266. https://doi.org/10.3390/nano11051266.
[83] Zhu, L.; Liu, X.; Yang, J.; He, Y.; Li, Y. Application of Multiplex Microfluidic Electrochemical Sensors in Monitoring Hematological Tumor Biomarkers. *Anal. Chem.*, **2020**, *92* (17), 11981–11986. https://doi.org/10.1021/acs.analchem.0c02430.
[84] Afzali, M.; Mostafavi, A.; Nekooie, R.; Jahromi, Z. A Novel Voltammetric Sensor Based on Palladium Nanoparticles/Carbon Nanofibers/Ionic Liquid Modified Carbon Paste Electrode for Sensitive Determination of Anti-Cancer Drug Pemetrexed. *J. Mol. Liq.*, **2019**, *282*, 456–465. https://doi.org/10.1016/j.molliq.2019.03.041.
[85] Hatamluyi, B.; Es'haghi, Z. Electrochemical Biosensing Platform Based on Molecularly Imprinted Polymer Reinforced by ZnO–Graphene Capped Quantum Dots for 6-Mercaptopurine Detection. *Electrochim. Acta*, **2018**, *283*, 1170–1177. https://doi.org/10.1016/j.electacta.2018.07.068.
[86] Kumar, A.; Pathak, P. K.; Prasad, B. B. Electrocatalytic Imprinted Polymer of N-Doped Hollow Carbon Nanosphere-Palladium Nanocomposite for Ultratrace Detection of Anticancer Drug 6-Mercaptopurine. *ACS Appl. Mater. Interfaces*, **2019**, *11* (17), 16065–16074. https://doi.org/10.1021/acsami.9b02947.
[87] Gowda, J. I.; Mallappa, M. M.; Nandibewoor, S. T. CTAB Functionalized Multiwalled Carbon Nanotube Composite Modified Electrode for the Determination of 6-Mercaptopurine. *Sens. Bio-Sensing Res.*, **2017**, *12*, 1–7. https://doi.org/10.1016/j.sbsr.2016.11.002.
[88] Karimi-Maleh, H.; Shojaei, A. F.; Tabatabaeian, K.; Karimi, F.; Shakeri, S.; Moradi, R. Simultaneous Determination of 6-Mercaptopruine, 6-Thioguanine and Dasatinib as Three Important Anticancer Drugs Using Nanostructure Voltammetric Sensor Employing Pt/MWCNTs and 1-Butyl-3-

Methylimidazolium Hexafluoro Phosphate. *Biosens. Bioelectron.*, **2016**, *86*, 879–884. https://doi.org/10.1016/j.bios.2016.07.086.

[89] Tajik, S.; Beitollahi, H.; Jang, H. W.; Shokouhimehr, M. A Screen Printed Electrode Modified with Fe3O4@polypyrrole-Pt Core-Shell Nanoparticles for Electrochemical Detection of 6-Mercaptopurine and 6-Thioguanine. *Talanta*, **2021**, *232*, 122379. https://doi.org/10.1016/j.talanta.2021.122379.

[90] Prasad, B. B.; Singh, R.; Kumar, A. Development of Imprinted Polyneutral Red/Electrochemically Reduced Graphene Oxide Composite for Ultra-Trace Sensing of 6-Thioguanine. *Carbon N. Y.*, **2016**, *102*, 86–96. https://doi.org/10.1016/j.carbon.2016.02.031.

[91] Ensafi, A. A.; Karimi-Maleh, H. Modified Multiwall Carbon Nanotubes Paste Electrode as a Sensor for Simultaneous Determination of 6-Thioguanine and Folic Acid Using Ferrocenedicarboxylic Acid as a Mediator. *J. Electroanal. Chem.*, **2010**, *640* (1–2), 75–83. https://doi.org/10.1016/j.jelechem.2010.01.010.

[92] Satana, H. E.; Pontinha, A. D. R.; Diculescu, V. C.; Oliveira-Brett, A. M. Nucleoside Analogue Electrochemical Behaviour and in Situ Evaluation of DNA-Clofarabine Interaction. *Bioelectrochemistry*, **2012**, *87*, 3–8. https://doi.org/10.1016/j.bioelechem.2011.07.004.

[93] Satana, E. H.; Oliveira-Brett, A. M. In Situ Evaluation of Fludarabine-DNA Interaction Using a DNA-Electrochemical Biosensor. *Int. J. Electrochem.*, **2011**, *2011* (Artcled ID 340239), 1–8. https://doi.org/10.4061/2011/340239.

[94] Dogan-Topal, B.; Bakirhan, N. K.; Tok, T. T.; Ozkan, S. A. Electrochemical Determination and in Silico Studies of Fludarabine on NH2 Functionalized Multiwalled Carbon Nanotube Modified Glassy Carbon Electrode. *Electroanalysis*, **2020**, *32* (1), 37–49. https://doi.org/10.1002/elan.201900347.

[95] De-Los-Santos-Álvarez, N.; Lobo-Castañón, M. J.; Miranda-Ordieres, A. J.; Tuñón-Blanco, P. Catalytic Voltammetric Determination of Cladribine in Biological Samples. *Electroanalysis*, **2003**, *15* (5–6), 441–446. https://doi.org/10.1002/elan.200390051.

[96] De-Los-Santos-Álvarez, N.; Lobo-Castañón, M. J.; Miranda-Ordieres, A. J.; Tuñón-Blanco, P. Electrocatalytic Adsorptive Voltammetry for Fludarabine Determination in Urine. *Anal. Chim. Acta*, **2004**, *504* (2), 271–277. https://doi.org/10.1016/j.aca.2003.10.055.

[97] Pattar, V. P.; Nandibewoor, S. T. Electroanalytical Method for the Determination of 5-Fluorouracil Using a Reduced Graphene Oxide/Chitosan Modified Sensor. *RSC Adv.*, **2015**, *5* (43), 34292–34301. https://doi.org/10.1039/c5ra04396d.

[98] Hua, X.; Hou, X.; Gong, X.; Shen, G. Electrochemical Behavior of 5-Fluorouracil on a Glassy Carbon Electrode Modified with Bromothymol Blue and Multi-Walled Carbon Nanotubes. *Anal. Methods*, **2013**, *5* (10), 2470–2476. https://doi.org/10.1039/c3ay40149a.

[99] Hatamluyi, B.; Es'haghi, Z.; Modarres Zahed, F.; Darroudi, M. A Novel Electrochemical Sensor Based on GQDs-PANI/ZnO-NCs Modified Glassy Carbon Electrode for Simultaneous Determination of Irinotecan and 5-Fluorouracil in Biological Samples. *Sensors Actuators, B Chem.*, **2019**, *286*, 540–549. https://doi.org/10.1016/j.snb.2019.02.017.

[100] Satyanarayana, M.; Goud, K. Y.; Reddy, K. K.; Gobi, K. V. Biopolymer Stabilized Nanogold Particles on Carbon Nanotube Support as Sensing Platform for Electrochemical Detection of 5-Fluorouracil in-Vitro. *Electrochim. Acta*, **2015**, *178*, 608–616. https://doi.org/10.1016/j.electacta.2015.08.036.

[101] Ganesan, M.; Ramadhass, K. D.; Chuang, H. C.; Gopalakrishnan, G. Synthesis of Nitrogen-Doped Carbon Quantum Dots@Fe2O3/Multiwall Carbon Nanotubes Ternary Nanocomposite for the Simultaneous Electrochemical Detection of 5-Fluorouracil, Uric Acid, and Xanthine. *J. Mol. Liq.*, **2021**, *331*, 115768. https://doi.org/10.1016/j.molliq.2021.115768.

[102] Mariyappan, V.; Keerthi, M.; Chen, S.-M.; Boopathy, G. Facile Synthesis of α-Sm2S3/MoS2 Bimetallic Sulfide as a High-Performance Electrochemical Sensor for the Detection of

Antineoplastic Drug 5-Fluorouracil in a Biological Samples. *J. Electrochem. Soc.*, **2020**, *167* (11), 117506. https://doi.org/10.1149/1945-7111/aba1a5.

[103] Vishnu S. K, D.; Ranganathan, P.; Rwei, S. P.; Pattamaprom, C.; Kavitha, T.; Sarojini, P. New Reductant-Free Synthesis of Gold Nanoparticles-Doped Chitosan-Based Semi-IPN Nanogel: A Robust Nanoreactor for Exclusively Sensitive 5-Fluorouracil Sensor. *Int. J. Biol. Macromol.*, **2020**, *148*, 79–88. https://doi.org/10.1016/j.ijbiomac.2020.01.108.

[104] Mutharani, B.; Ranganathan, P.; Chen, S.-M. Temperature-Reversible Switched Antineoplastic Drug 5-Fluorouracil Electrochemical Sensor Based on Adaptable Thermo-Sensitive Microgel Encapsulated PEDOT. *Sensors Actuators, B Chem.*, **2020**, *304*, 127361. https://doi.org/https://doi.org/10.1016/j.snb.2019.127361.

[105] Zahed, F. M.; Hatamluyi, B.; Lorestani, F.; Es'haghi, Z. Silver Nanoparticles Decorated Polyaniline Nanocomposite Based Electrochemical Sensor for the Determination of Anticancer Drug 5-Fluorouracil. *J. Pharm. Biomed. Anal.*, **2018**, *161*, 12–19. https://doi.org/10.1016/j.jpba.2018.08.004.

[106] Hadi, M.; Mollaei, T.; Ehsani, A. Graphene Oxides/Multi-Walled Carbon Nanotubes Hybrid-Modified Carbon Electrodes for Fast and Sensitive Voltammetric Determination of the Anticancer Drug 5-Fluorouracil in Spiked Human Plasma Samples. *Chem. Pap.*, **2018**, *72* (2), 431–439. https://doi.org/10.1007/s11696-017-0295-4.

[107] Bukkitgar, S. D.; Shetti, N. P. Electrochemical Behavior of an Anticancer Drug 5-Fluorouracil at Methylene Blue Modified Carbon Paste Electrode. *Mater. Sci. Eng. C*, **2016**, *65*, 262–268. https://doi.org/10.1016/j.msec.2016.04.045.

[108] Bukkitgar, S. D.; Shetti, N. P. Electrochemical Sensor for the Determination of Anticancer Drug 5-Fluorouracil at Glucose Modified Electrode. *ChemistrySelect*, **2016**, *1* (4), 771–777. https://doi.org/10.1002/slct.201600197.

[109] Zhan, T.; Cao, L.; Sun, W.; Hou, W. Electrochemical Behavior of 5-Fluoro-1H-Pyrimidine-2 on an Ionic Liquid Modified Carbon Paste Electrode. *Anal. Methods*, **2011**, *3* (11), 2651–2656. https://doi.org/10.1039/c1ay05454f.

[110] Fallah Shojaei, A.; Tabatabaeian, K.; Shakeri, S.; Karimi, F. A Novel 5-Fluorouracile Anticancer Drug Sensor Based on ZnFe2O4 Magnetic Nanoparticles Ionic Liquids Carbon Paste Electrode. *Sensors Actuators, B Chem.*, **2016**, *230*, 607–614. https://doi.org/10.1016/j.snb.2016.02.082.

[111] Rahimi-Nasrabadi, M.; Ahmadi, F.; Beigizadeh, H.; Karimi, M. S.; Sobhani-Nasab, A.; Joseph, Y.; Ehrlich, H.; Ganjali, M. R. A Modified Sensitive Carbon Paste Electrode for 5-Fluorouracil Based Using a Composite of Praseodymium Erbium Tungstate. *Microchem. J.*, **2020**, *154*, 104654. https://doi.org/10.1016/j.microc.2020.104654.

[112] Abbar, J. C.; Shetti, N. P.; Nandibewoor, S. T. Development of Voltammetric Method for the Determination of an Anticancer Drug, 5-Flurouracil, at a Multiwalled Carbon Nanotubes Paste Electrode. *Synth. React. Inorganic, Met. Nano-Metal Chem.*, **2016**, *46* (6), 814–820. https://doi.org/10.1080/15533174.2014.989586.

[113] Lima, D.; Calaça, G. N.; Viana, A. G.; Pessôa, C. A. Porphyran-Capped Gold Nanoparticles Modified Carbon Paste Electrode: A Simple and Efficient Electrochemical Sensor for the Sensitive Determination of 5-Fluorouracil. *Appl. Surf. Sci.*, **2018**, *427*, 742–753. https://doi.org/10.1016/j.apsusc.2017.08.228.

[114] Prasad, B. B.; Kumar, A. Development of Molecularly Imprinted Polymer Nanoarrays of N-Acryloyl-2-Mercaptobenzamide on a Silver Electrode for Ultratrace Sensing of Uracil and 5-Fluorouracil. *J. Mater. Chem. B*, **2015**, *3* (28), 5864–5876. https://doi.org/10.1039/c5tb00678c.

[115] Prasad, B. B.; Kumar, D.; Madhuri, R.; Tiwari, M. P. Nonhydrolytic Sol-Gel Derived Imprinted Polymer-Multiwalled Carbon Nanotubes Composite Fiber Sensors for Electrochemical Sensing of Uracil and 5-Fluorouracil. *Electrochim. Acta*, **2012**, *71*, 106–115.

https://doi.org/10.1016/j.electacta.2012.03.110.
[116] Mirčeski, V.; Gulaboski, R.; Jordanoski, B.; Komorsky-Lovrić, Š. Square-Wave Voltammetry of 5-Fluorouracil. *J. Electroanal. Chem.*, **2000**, *490* (1), 37–47. https://doi.org/10.1016/S0022-0728(00)00203-5.
[117] Es'haghi, Z.; Moeinpour, F. Carbon Nanotube/Polyurethane Modified Hollow Fiber-Pencil Graphite Electrode for in Situ Concentration and Electrochemical Quantification of Anticancer Drugs Capecitabine and Erlotinib. *Eng. Life Sci.*, **2019**, *19* (4), 302–314. https://doi.org/10.1002/elsc.201800167.
[118] Prasad, B. B.; Singh, R.; Kumar, A. Gold Nanorods: Vs. Gold Nanoparticles: Application in Electrochemical Sensing of Cytosine β-d-Arabinoside Using Metal Ion Mediated Molecularly Imprinted Polymer. *RSC Adv.*, **2016**, *6* (84), 80679–80691. https://doi.org/10.1039/c6ra14097a.
[119] Bouzid, B.; Macdonald, A. M. G. Flow-Injection Methods for the Determination of Uracil Derivatives with Voltammetric Detection. *Anal. Chim. Acta*, **1988**, *211* (C), 175–193. https://doi.org/10.1016/S0003-2670(00)83678-8.
[120] Rus, I.; Pusta, A.; Tertiș, M.; Barbălată, C.; Tomuță, I.; Săndulescu, R.; Cristea, C. Gemcitabine Direct Electrochemical Detection from Pharmaceutical Formulations Using a Boron-Doped Diamond Electrode. *Pharmaceuticals*, **2021**, *14*, 912. https://doi.org/10.3390/ph14090912.
[121] Buoro, R. M.; Lopes, I. C.; Diculescu, V. C.; Serrano, S. H. P.; Lemos, L.; Oliveira-Brett, A. M. In Situ Evaluation of Gemcitabine-DNA Interaction Using a DNA-Electrochemical Biosensor. *Bioelectrochemistry*, **2014**, *99*, 40–45. https://doi.org/10.1016/j.bioelechem.2014.05.005.
[122] Tandel, R.; Teradal, N.; Satpati, A.; Jaldappagari, S. Fabrication of the Electrochemically Reduced Graphene Oxide-Bismuth Nanoparticles Composite and Its Analytical Application for an Anticancer Drug Gemcitabine. *Chinese Chem. Lett.*, **2017**, *28* (7), 1429–1437. https://doi.org/10.1016/j.cclet.2016.11.028.
[123] Teradal, N. L.; Kalanur, S. S.; Prashanth, S. N.; Seetharamappa, J. Electrochemical Investigations of an Anticancer Drug in the Presence of Sodium Dodecyl Sulfate as an Enhancing Agent at Carbon Paste Electrode. *J. Appl. Electrochem.*, **2012**, *42* (11), 917–923. https://doi.org/10.1007/s10800-012-0473-6.
[124] Shoja, Y.; Kermanpur, A.; Karimzadeh, F.; Ghodsi, J.; Rafati, A. A.; Adhami, S. Electrochemical Molecularly Bioimprinted Siloxane Biosensor on the Basis of Core/Shell Silver Nanoparticles/EGFR Exon 21 L858R Point Mutant Gene/Siloxane Film for Ultra-Sensing of Gemcitabine as a Lung Cancer Chemotherapy Medication. *Biosens. Bioelectron.*, **2019**, *145*, 111611. https://doi.org/10.1016/j.bios.2019.111611.
[125] Queiroz, N. L.; Nascimento, M. L.; Nascimento, J. A. M.; Nascimento, V. B.; Oliveira, S. C. B. Electrochemistry Study of Antineoplastic Raltitrexed Oxidation Mechanism and Its Interaction with DNA. *Electroanalysis*, **2018**, *30* (6), 1184–1191. https://doi.org/10.1002/elan.201800087.
[126] Wang, J.; Tuzhi, P.; Lin, M. S.; Tapia, T. Trace Measurements of the Antineoplastic Agent Methotrexate by Adsorptive Stripping Voltammetry. *Talanta*, **1986**, *33* (9), 707–712. https://doi.org/10.1016/0039-9140(86)80170-9.
[127] Cataldi, T. R. I.; Guerrieri, A.; Palmisano, F.; Zambonin, P. G. Adsorptive Cathodic Stripping Voltammetry of Amethopterine at a Static Mercury Drop Electrode and Its Application to Serum Drug Determination. *Analyst*, **1988**, *113* (6), 869–873. https://doi.org/10.1039/AN9881300869.
[128] Temizer, A.; Nur Onar, A. Determination of Methotrexate in Human Blood Plasma by Adsorptive Stripping Voltammetry. *Talanta*, **1988**, *35* (10), 805–806. https://doi.org/10.1016/0039-9140(88)80188-7.
[129] Janíková-Bandžuchová, L.; Šelešovská, R. Determination of Methotrexate at a Silver Solid Amalgam Electrode by Differential Pulse Voltammetry. *Anal. Lett.*, **2016**, *49* (1), 122–134. https://doi.org/10.1080/00032719.2014.996812.

[130] Šelešovská, R.; Bandžuchová, L.; Navrátil, T. Voltammetric Behavior of Methotrexate Using Mercury Meniscus Modified Silver Solid Amalgam Electrode. *Electroanalysis*, **2011**, *23* (1), 177–187. https://doi.org/10.1002/elan.201000440.
[131] del Pozo, J. A.; García, A. C.; Blanco, P. T. Adsorptive Stripping Voltammetry on Mercury-Coated Carbon Fibre Ultramicroelectrodes. *Anal. Chim. Acta*, **1993**, *273* (1–2), 101–109. https://doi.org/10.1016/0003-2670(93)80149-F.
[132] Mirmomtaz, E.; Ensafi, A. A. Voltammetric Determination of Trace Quantities of 6-Thioguanine Based on the Interaction with DNA at a Mercury Electrode. *Electrochim. Acta*, **2009**, *54* (18), 4353–4358. https://doi.org/10.1016/j.electacta.2009.03.004.
[133] Nageswara Reddy, C.; Reddy Prasad, P.; Sreedhar, N. Y. Determination of Nelarabine in Pharmaceutical Formulations and Urine Samples by Adsorptive Stripping Voltammetry. *Int. J. PharmTech Res.*, **2011**, *3* (2), 1125–1131.
[134] Yan, Z.; Li, H. Voltammetric Determination of 6-Mercaptopurine at Co(III) Trisphenanthroline Complex and DNA Decorated with Grpahene Oxide Modified Glassy Carbon Electrode. *Int. J. Electrochem. Sci.*, **2015**, *10* (10), 8714–8726.
[135] Zhou, P.; He, L.; Gan, G.; Ni, S.; Li, H.; Li, W. Fabrication and Evaluation of [Co(Phen)2L]3+-Modified DNA-MWCNT and SDS-MWCNT Electrodes for Electrochemical Detection of 6-Mercaptopurine. *J. Electroanal. Chem.*, **2012**, *665*, 63–69. https://doi.org/10.1016/j.jelechem.2011.11.026.
[136] Gu, H. Y.; Sun, D. M.; Yu, A. M.; Chen, H. Y. Electrochemical Behavior of 6-Mercapto-Purine at Hanging Copper Amalgam Dropping Electrode and Its Trace Determination by Differential Pulse Adsorption Cathodic Stripping Voltammetry. *Anal. Lett.*, **1996**, *29* (15), 2743–2753. https://doi.org/10.1080/00032719608002277.
[137] Kalanur, S. S.; Seetharamappa, J.; Mamatha, G. P.; Hadagali, M. D.; Kandagal, P. B. Electrochemical Behavior of an Anti-Cancer Drug at Glassy Carbon Electrode and Its Determination in Pharmaceutical Formulations. *Int. J. Electrochem. Sci.*, **2008**, *3* (7), 756–767.
[138] Madrakian, T.; Ghasemi, H.; Haghshenas, E.; Afkhami, A. Preparation of a ZnO Nanoparticles/Multiwalled Carbon Nanotubes/Carbon Paste Electrode as a Sensitive Tool for Capecitabine Determination in Real Samples. *RSC Adv.*, **2016**, *6* (40), 33851–33856. https://doi.org/10.1039/c6ra03666j.
[139] Zhang, Q.; Shan, X.; Fu, Y.; Liu, P.; Li, X.; Liu, B.; Zhang, L.; Li, D. Electrochemical Determination of the Anticancer Drug Capecitabine Based on a Graphene-Gold Nanocomposite-Modified Glassy Carbon Electrode. *Int. J. Electrochem. Sci.*, **2017**, *12* (11), 10773–10782. https://doi.org/10.20964/2017.11.36.
[140] Afzali, M.; Mostafavi, A.; Shamspur, T. A Novel Electrochemical Sensor Based on Magnetic Core@shell Molecularly Imprinted Nanocomposite (Fe3O4@graphene Oxide@MIP) for Sensitive and Selective Determination of Anticancer Drug Capecitabine. *Arab. J. Chem.*, **2020**, *13* (8), 6626–6638. https://doi.org/10.1016/j.arabjc.2020.06.018.
[141] Abd El-Hady, D.; Abdel-Hamid, M. I.; Seliem, M. M.; Andrisano, V.; Abo El-Maali, N. Osteryoung Square Wave Stripping Voltammetry at Mercury Film Electrode for Monitoring Ultra Trace Levels of Tarabine PFS and Its Interaction with SsDNA. *J. Pharm. Biomed. Anal.*, **2004**, *34* (5), 879–890. https://doi.org/10.1016/j.jpba.2003.12.001.
[142] Florea, A.; Guo, Z.; Cristea, C.; Bessueille, F.; Vocanson, F.; Goutaland, F.; Dzyadevych, S.; Səndulescu, R.; Jaffrezic-Renault, N. Anticancer Drug Detection Using a Highly Sensitive Molecularly Imprinted Electrochemical Sensor Based on an Electropolymerized Microporous Metal Organic Framework. *Talanta*, **2015**, *138*, 71–76. https://doi.org/10.1016/j.talanta.2015.01.013.
[143] Rafique, B.; Khalid, A. M.; Akhtar, K.; Jabbar, A. Interaction of Anticancer Drug Methotrexate with

DNA Analyzed by Electrochemical and Spectroscopic Methods. *Biosens. Bioelectron.*, **2013**, *44* (1), 21–26. https://doi.org/10.1016/j.bios.2012.12.028.

[144] Chen, J.; Fu, B.; Liu, T.; Yan, Z.; Li, K. A Graphene Oxide-DNA Electrochemical Sensor Based on Glassy Carbon Electrode for Sensitive Determination of Methotrexate. *Electroanalysis*, **2018**, *30* (2), 288–295. https://doi.org/10.1002/elan.201700615.

[145] Karimi-Maleh, H.; Tahernejad-Javazmi, F.; Atar, N.; Yola, M. L.; Gupta, V. K.; Ensafi, A. A. A Novel DNA Biosensor Based on a Pencil Graphite Electrode Modified with Polypyrrole/Functionalized Multiwalled Carbon Nanotubes for Determination of 6-Mercaptopurine Anticancer Drug. *Ind. Eng. Chem. Res.*, **2015**, *54* (14), 3634–3639. https://doi.org/10.1021/ie504438z.

[146] Koyuncu Zeybek, D.; Demir, B.; Zeybek, B.; Pekyardimci, Ş. A Sensitive Electrochemical DNA Biosensor for Antineoplastic Drug 5-Fluorouracil Based on Glassy Carbon Electrode Modified with Poly(Bromocresol Purple). *Talanta*, **2015**, *144*, 793–800. https://doi.org/10.1016/j.talanta.2015.06.077.

[147] Foroughi, M. M.; Jahani, S.; Aramesh-Broujeni, Z.; Rostaminasab Dolatabad, M. A Label-Free Electrochemical Biosensor Based on 3D Cubic Eu3+/Cu2O Nanostructures with Clover-like Faces for the Determination of Anticancer Drug Cytarabine. *RSC Adv.*, **2021**, *11* (28), 17514–17525. https://doi.org/10.1039/d1ra01372f.

[148] Tiğ, G. A.; Zeybek, B.; PekyardImcI, Ş. Electrochemical DNA Biosensor Based on Poly(2,6-Pyridinedicarboxylic Acid) Modified Glassy Carbon Electrode for the Determination of Anticancer Drug Gemcitabine. *Talanta*, **2016**, *154*, 312–321. https://doi.org/10.1016/j.talanta.2016.03.049.

[149] Wang, P.; Wu, Q.; Wang, C.; Pu, Y.; Zhou, M.; Zhang, M. 3D Flower-Like MoS 2 Nanomaterial as Signal-Promoter of PTC-PEI/S2O82− System for Fabricating a Sensitive Electrochemiluminescence Methotrexate Sensor. *J. Electrochem. Soc.*, **2020**, *167* (10), 107505. https://doi.org/10.1149/1945-7111/ab98ac.

[150] Zhou, M.; Pu, Y.; Wu, Q.; Wang, P.; Liu, T.; Zhang, M. 2D Hexagonal SnS2 Nanoplates as Novel Co-Reaction Accelerator for Construction of Ultrasensitive g-C3N4-Based Electrochemiluminescent Biosensor. *Sensors Actuators, B Chem.*, **2020**, *319*, 128298. https://doi.org/10.1016/j.snb.2020.128298.

[151] Stefan, R. I.; Bokretsion, R. G.; Van Staden, J. F.; Aboul-Enein, H. Y. Determination of L- and D-Enantiomers of Methotrexate Using Amperometric Biosensors. *Talanta*, **2003**, *60* (5), 983–990. https://doi.org/10.1016/S0039-9140(03)00177-2.

[152] Pontinha, A. D. R.; Jorge, S. M. A.; Chiorcea Paquim, A. M.; Diculescu, V. C.; Oliveira-Brett, A. M. In Situ Evaluation of Anticancer Drug Methotrexate-DNA Interaction Using a DNA-Electrochemical Biosensor and AFM Characterization. *Phys. Chem. Chem. Phys.*, **2011**, *13* (12), 5227–5234. https://doi.org/10.1039/c0cp02377a.

[153] Shpigun, L. K.; Andryukhina, E. Y. A New Electrochemical Sensor for Direct Detection of Purine Antimetabolites and DNA Degradation. *J. Anal. Methods Chem.*, **2019**, *2019*, Article ID 1572526. https://doi.org/10.1155/2019/1572526.

[154] Tang, W.; Li, W.; Li, Y.; Zhang, M.; Zeng, X. Electrochemical Sensors Based on Multi-Walled Nanotubes for Investigating the Damage and Action of 6-Mercaptopurine on Double-Stranded DNA. *New J. Chem.*, **2015**, *39* (11), 8454–8460. https://doi.org/10.1039/c5nj01303h.

[155] Unal, D. N.; Eksin, E.; Erdem, A. Electrochemical Determination of 6-Thioguanine and Its Interaction with DNA Oligonucleotides Using Disposable Graphite Pencil Electrodes. *Anal. Lett.*, **2018**, *51* (1–2), 265–278. https://doi.org/10.1080/00032719.2017.1338714.

[156] Unal, D. N.; Eksin, E.; Erdem, A. Carbon Nanotubes Modified Graphite Electrodes for Monitoring of Biointeraction Between 6-Thioguanine and DNA. *Electroanalysis*, **2017**, *29* (10), 2292–2299. https://doi.org/10.1002/elan.201700270.

[157] Pontinha, A. D. R.; Satana, H. E.; Diculescu, V. C.; Oliveira-Brett, A. M. Anodic Oxidation of

Cladribine and in Situ Evaluation of DNA-Cladribine Interaction. *Electroanalysis*, **2011**, *23* (11), 2651–2657. https://doi.org/10.1002/elan.201100320.

[158] Shahzad, S.; Karadurmus, L.; Dogan-Topal, B.; Taskin-Tok, T.; Shah, A.; Ozkan, S. A. Sensitive Nucleic Acid Detection at NH2-MWCNTs Modified Glassy Carbon Electrode and Its Application for Monitoring of Gemcitabine-DNA Interaction. *Electroanalysis*, **2020**, *32* (5), 912–922. https://doi.org/10.1002/elan.201900597.

[159] Gurudatt, N. G.; Naveen, M. H.; Ban, C.; Shim, Y. B. Enhanced Electrochemical Sensing of Leukemia Cells Using Drug/Lipid Co-Immobilized on the Conducting Polymer Layer. *Biosens. Bioelectron.*, **2016**, *86*, 33–40. https://doi.org/10.1016/j.bios.2016.06.029.

[160] Šelešovská, R.; Janíková-Bandžuchová, L.; Chýlková, J. Sensitive Voltammetric Sensor Based on Boron-Doped Diamond Electrode for Determination of the Chemotherapeutic Drug Methotrexate in Pharmaceutical and Biological Samples. *Electroanalysis*, **2015**, *27* (1), 42–51. https://doi.org/10.1002/elan.201400326.

[161] Gao, L.; Wu, Y.; Liu, J.; Ye, B. Anodic Voltammetric Behaviors of Methotrexate at a Glassy Carbon Electrode and Its Determination in Spiked Human Urine. *J. Electroanal. Chem.*, **2007**, *610* (2), 131–136. https://doi.org/10.1016/j.jelechem.2007.07.030.

[162] Asadian, E.; Shahrokhian, S.; Iraji Zad, A.; Ghorbani-Bidkorbeh, F. Glassy Carbon Electrode Modified with 3D Graphene–Carbon Nanotube Network for Sensitive Electrochemical Determination of Methotrexate. *Sensors Actuators, B Chem.*, **2017**, *239*, 617–627. https://doi.org/10.1016/j.snb.2016.08.064.

[163] Jandaghi, N.; Jahani, S.; Foroughi, M. M.; Kazemipour, M.; Ansari, M. Cerium-Doped Flower-Shaped ZnO Nano-Crystallites as a Sensing Component for Simultaneous Electrochemical Determination of Epirubicin and Methotrexate. *Microchim. Acta*, **2020**, *187* (1), 24. https://doi.org/10.1007/s00604-019-4016-2.

[164] Materon, E. M.; Wong, A.; Fatibello-Filho, O.; Faria, R. C. Development of a Simple Electrochemical Sensor for the Simultaneous Detection of Anticancer Drugs. *J. Electroanal. Chem.*, **2018**, *827*, 64–72. https://doi.org/10.1016/j.jelechem.2018.09.010.

[165] Ghadimi, H.; Nasiri-Tabrizi, B.; Nia, P. M.; Basirun, W. J.; Tehrani, R. M. A.; Lorestani, F. Nanocomposites of Nitrogen-Doped Graphene Decorated with a Palladium Silver Bimetallic Alloy for Use as a Biosensor for Methotrexate Detection. *RSC Adv.*, **2015**, *5* (120), 99555–99565. https://doi.org/10.1039/c5ra18109g.

[166] Ensafi, A. A.; Rezaloo, F.; Rezaei, B. CoFe2O4/Reduced Graphene Oxide/Ionic Liquid Modified Glassy Carbon Electrode, a Selective and Sensitive Electrochemical Sensor for Determination of Methotrexate. *J. Taiwan Inst. Chem. Eng.*, **2017**, *78*, 45–50. https://doi.org/10.1016/j.jtice.2017.05.031.

[167] Zhu, Z.; Wang, F.; Wang, F.; Xi, L. Simultaneous Determination of Methotrexate and Calcium Folinate with Electrochemical Method Based on a Poly-ABSA/Functionalized MWNTs Composite Film Modified Electrode. *J. Electroanal. Chem.*, **2013**, *708*, 13–19. https://doi.org/10.1016/j.jelechem.2013.09.004.

[168] Wei, Y.; Luo, L.; Ding, Y.; Si, X.; Ning, Y. Highly Sensitive Determination of Methotrexate at Poly (l-Lysine) Modified Electrode in the Presence of Sodium Dodecyl Benzene Sulfonate. *Bioelectrochemistry*, **2014**, *98*, 70–75. https://doi.org/10.1016/j.bioelechem.2014.03.005.

[169] Wang, F.; Wang, Y.; Lu, K.; Wei, X.; Ye, B. Sensitive Determination of Methotrexate at Nano-Au Self-Assembled Monolayer Modified Electrode. *J. Electroanal. Chem.*, **2012**, *674*, 83–89. https://doi.org/10.1016/j.jelechem.2012.04.010.

[170] Mutharani, B.; Ranganathan, P.; Chen, S. M.; Sireesha, P. Ultrasound-Induced Radicals Initiated the Formation of Inorganic–Organic Pr2O3/Polystyrene Hybrid Composite for Electro-Oxidative Determination of Chemotherapeutic Drug Methotrexate. *Ultrason. Sonochem.*, **2019**, *56*, 410–

421. https://doi.org/10.1016/j.ultsonch.2019.04.029.
[171] Li, J.; Chen, D.; Zhang, T.; Chen, G. Highly Sensitive Electrochemical Determination of Methotrexate Based on a N-Doped Hollow Nanocarbon Sphere Modified Electrode. *Anal. Methods*, **2021**, *13* (1), 117–123. https://doi.org/10.1039/d0ay01996h.
[172] Fathi, Z.; Jahani, S.; Zandi, M. S.; Foroughi, M. M. Synthesis of Bifunctional Cabbage Flower–like Ho3+/NiO Nanostructures as a Modifier for Simultaneous Determination of Methotrexate and Carbamazepine. *Anal. Bioanal. Chem.*, **2020**, *412* (4), 1011–1024. https://doi.org/10.1007/s00216-019-02326-8.
[173] Guo, Y.; Chen, Y.; Zhao, Q.; Shuang, S.; Dong, C. Electrochemical Sensor for Ultrasensitive Determination of Doxorubicin and Methotrexate Based on Cyclodextrin-Graphene Hybrid Nanosheets. *Electroanalysis*, **2011**, *23* (10), 2400–2407. https://doi.org/10.1002/elan.201100259.
[174] Huang, D.; Wu, H.; Zhu, Y.; Su, H.; Zhang, H.; Sheng, L.; Liu, Z.; Xu, H.; Song, C. Sensitive Determination of Anticancer Drug Methotrexate Using Graphite Oxide-Nafion Modified Glassy Carbon Electrode. *Int. J. Electrochem. Sci.*, **2019**, *14* (4), 3792–3804. https://doi.org/10.20964/2019.04.03.
[175] Wang, F.; Wu, Y.; Liu, J.; Ye, B. DNA Langmuir-Blodgett Modified Glassy Carbon Electrode as Voltammetric Sensor for Determinate of Methotrexate. *Electrochim. Acta*, **2009**, *54* (5), 1408–1413. https://doi.org/10.1016/j.electacta.2008.09.027.
[176] Wang, Y.; Liu, H.; Wang, F.; Gao, Y. Electrochemical Oxidation Behavior of Methotrexate at DNA/SWCNT/Nafion Composite Film-Modified Glassy Carbon Electrode. *J. Solid State Electrochem.*, **2012**, *16* (10), 3227–3235. https://doi.org/10.1007/s10008-012-1763-y.
[177] Wang, Y.; Xie, J.; Tao, L.; Tian, H.; Wang, S.; Ding, H. Simultaneous Electrochemical Determination of Epirubicin and Methotrexate in Human Blood Using a Disposable Electrode Modified with Nano-Au/MWNTs-ZnO Composites. *Sensors Actuators, B Chem.*, **2014**, *204*, 360–367. https://doi.org/10.1016/j.snb.2014.07.099.
[178] Zhou, H.; Ran, G.; Masson, J. F.; Wang, C.; Zhao, Y.; Song, Q. Novel Tungsten Phosphide Embedded Nitrogen-Doped Carbon Nanotubes: A Portable and Renewable Monitoring Platform for Anticancer Drug in Whole Blood. *Biosens. Bioelectron.*, **2018**, *105*, 226–235. https://doi.org/10.1016/j.bios.2018.01.045.
[179] Kummari, S.; Kumar, V. S.; Satyanarayana, M.; Gobi, K. V. Direct Electrochemical Determination of Methotrexate Using Functionalized Carbon Nanotube Paste Electrode as Biosensor for In-Vitro Analysis of Urine and Dilute Serum Samples. *Microchem. J.*, **2019**, *148*, 626–633. https://doi.org/10.1016/j.microc.2019.05.054.
[180] Salandari-Jolge, N.; Ensafi, A. A.; Rezaei, B. A Novel Three-Dimensional Network of CuCr2O4/CuO Nanofibers for Voltammetric Determination of Anticancer Drug Methotrexate. *Anal. Bioanal. Chem.*, **2020**, *412* (11), 2443–2453. https://doi.org/10.1007/s00216-020-02461-7.
[181] Asbahr, D.; Figueiredo-Filho, L. C. S.; Vicentini, F. C.; Oliveira, G. G.; Fatibello-Filho, O.; Banks, C. E. Differential Pulse Adsorptive Stripping Voltammetric Determination of Nanomolar Levels of Methotrexate Utilizing Bismuth Film Modified Electrodes. *Sensors Actuators, B Chem.*, **2013**, *188*, 334–339. https://doi.org/10.1016/j.snb.2013.07.027.
[182] Tesfalidet, S.; Geladi, P.; Shimizu, K.; Lindholm-Sethson, B. Detection of Methotrexate in a Flow System Using Electrochemical Impedance Spectroscopy and Multivariate Data Analysis. *Anal. Chim. Acta*, **2016**, *914*, 1–6. https://doi.org/10.1016/j.aca.2016.02.012.
[183] Lima, H. R. S.; Airton de Oliveira Farias, E.; Teixeira, P. R. S.; Eiras, C.; Nunes, L. C. C. Blend Films Based on Biopolymers Extracted from Babassu Mesocarp (Orbignya Phalerata) for the Electrochemical Detection of Methotrexate Antineoplastic Drug. *J. Solid State Electrochem.*, **2019**, *23* (11), 3153–3164. https://doi.org/10.1007/s10008-019-04406-2.
[184] Karadas, N.; Ozkan, S. A. Electrochemical Preparation of Sodium Dodecylsulfate Doped Over-

Oxidized Polypyrrole/Multi-Walled Carbon Nanotube Composite on Glassy Carbon Electrode and Its Application on Sensitive and Selective Determination of Anticancer Drug: Pemetrexed. *Talanta*, **2014**, *119*, 248–254. https://doi.org/10.1016/j.talanta.2013.10.065.

[185] Ozcelikay, G.; Karadas-Bakirhan, N.; Taskin-Tok, T.; Ozkan, S. A. A Selective and Molecular Imaging Approach for Anticancer Drug: Pemetrexed by Nanoparticle Accelerated Molecularly Imprinting Polymer. *Electrochim. Acta*, **2020**, *354*, 136665. https://doi.org/10.1016/j.electacta.2020.136665.

[186] Hanko, M.; Švorc, Ľ.; Planková, A.; Mikuš, P. Novel Electrochemical Strategy for Determination of 6-Mercaptopurine Using Anodically Pretreated Boron-Doped Diamond Electrode. *J. Electroanal. Chem.*, **2019**, *840*, 295–304. https://doi.org/10.1016/j.jelechem.2019.03.067.

[187] Shpigun, L. K.; Andryukhina, E. Y. Electrochemical Sensor Based on Nanocomposite of Ionic Liquid Modified Graphene Oxide – Chitosan and Its Application for Flow Injection Detection of Anticancer Thiopurine Drugs. *Electroanalysis*, **2018**, *30* (10), 2356–2365. https://doi.org/10.1002/elan.201800358.

[188] Keyvanfard, M.; Khosravi, V.; Karimi-Maleh, H.; Alizad, K.; Rezaei, B. Voltammetric Determination of 6-Mercaptopurine Using a Multiwall Carbon Nanotubes Paste Electrode in the Presence of Isoprenaline as a Mediator. *J. Mol. Liq.*, **2013**, *177*, 182–189. https://doi.org/10.1016/j.molliq.2012.10.020.

[189] Beitollahi, H.; Ivari, S. G.; Torkzadeh-Mahani, M. A Double Electrochemical Platform for Ultrasensitive and Simultaneous Determination of 6-Mercaptopurine and Folic Acid Based on a Carbon Paste Electrode Modified with ZnO-CuO Nanoplates and 2-Chlorobenzoyl Ferrocene. *ECS J. Solid State Sci. Technol.*, **2017**, *6* (4), M29–M35. https://doi.org/10.1149/2.0201704jss.

[190] Ensafi, A. A.; Karimi-Maleh, H. Determination of 6-Mercaptopurine in the Presence of Uric Acid Using Modified Multiwall Carbon Nanotubes-TiO2 as a Voltammetric Sensor. *Drug Test. Anal.*, **2012**, *4* (12), 970–977. https://doi.org/10.1002/dta.286.

[191] Vinita; Tiwari, M.; Agnihotri, N.; Singh, M.; Singh, A. K.; Prakash, R. Nanonetwork of Coordination Polymer AHMT-Ag for the Effective and Broad Spectrum Detection of 6-Mercaptopurine in Urine and Blood Serum. *ACS Omega*, **2019**, *4* (16), 16733–16742. https://doi.org/10.1021/acsomega.9b01122.

[192] Shahrokhian, S.; Ghorbani-Bidkorbeh, F.; Mohammadi, A.; Dinarvand, R. Electrochemical Determinations of 6-Mercaptopurine on the Surface of a Carbon Nanotube-Paste Electrode Modified with a Cobalt Salophen Complex. *J. Solid State Electrochem.*, **2012**, *16* (4), 1643–1650. https://doi.org/10.1007/s10008-011-1575-5.

[193] Mirmomtaz, E.; Ensafi, A. A.; Karimi-Maleh, H. Electrocatalytic Determination of 6-Tioguanine at a p-Aminophenol Modified Carbon Paste Electrode. *Electroanalysis*, **2008**, *20* (18), 1973–1979. https://doi.org/10.1002/elan.200804273.

[194] Smarzewska, S.; Pokora, J.; Leniart, A.; Festinger, N.; Ciesielski, W. Carbon Paste Electrodes Modified with Graphene Oxides – Comparative Electrochemical Studies of Thioguanine. *Electroanalysis*, **2016**, *28* (7), 1562–1569. https://doi.org/10.1002/elan.201501101.

[195] Mohammadi, S.; Taher, M. A.; Beitollahi, H.; Hosseinzadeh, R. Voltammetric Mixture Analysis of 6-Thioguanine and Folic Acid Using Ionic Liquid-Carbon Paste Electrode Modified by Nano Petal-Like MoWS 2 and N-(Ferrocenylmethylidene)Fluoren-2-Amine. *J. Electrochem. Soc.*, **2020**, *167* (4), 047520. https://doi.org/10.1149/1945-7111/ab6f59.

[196] Naik, K. M.; Nandibewoor, S. T. Electro-Oxidation and Determination of Gemcitabine Hydrochloride, an Anticancer Drug at Gold Electrode. *J. Ind. Eng. Chem.*, **2013**, *19* (6), 1933–1938. https://doi.org/10.1016/j.jiec.2013.02.040.

[197] Isah, T. Anticancer Alkaloids from Trees: Development into Drugs. *Pharmacogn. Rev.*, **2016**, *10* (20), 90–99. https://doi.org/10.4103/0973-7847.194047.

[198] Najari, S.; Bagheri, H.; Monsef-Khoshhesab, Z.; Hajian, A.; Afkhami, A. Electrochemical Sensor

Based on Gold Nanoparticle-Multiwall Carbon Nanotube Nanocomposite for the Sensitive Determination of Docetaxel as an Anticancer Drug. *Ionics (Kiel).*, **2018**, *24* (10), 3209–3219. https://doi.org/10.1007/s11581-018-2517-3.

[199] Hatamluyi, B.; Lorestani, F.; Es'haghi, Z. Au/Pd@rGO Nanocomposite Decorated with Poly (L-Cysteine) as a Probe for Simultaneous Sensitive Electrochemical Determination of Anticancer Drugs, Ifosfamide and Etoposide. *Biosens. Bioelectron.*, **2018**, *120*, 22–29. https://doi.org/10.1016/j.bios.2018.08.008.

[200] Taei, M.; Hassanpour, F.; Salavati, H.; Sadeghi, Z.; Alvandi, H. Highly Selective Electrochemical Determination of Taxol Based on Ds-DNA-Modified Pencil Electrode. *Appl. Biochem. Biotechnol.*, **2015**, *176* (2), 344–358. https://doi.org/10.1007/s12010-015-1578-2.

[201] Li, H.; Li, J.; Yang, Z.; Xu, Q.; Hu, X. Sodium Dodecyl Sulfate Sensitized Electrochemical Method for Sub-Picomole Level Determination of Topotecan Hydrochloride at a Novel Disposable Electrode. *Sci. China Chem.*, **2011**, *54* (1), 217–222. https://doi.org/10.1007/s11426-010-4089-6.

[202] Ibrahim, M.; Ibrahim, H.; Almandil, N. B.; Kawde, A. N. A Novel Nanocomposite Based on Gold Nanoparticles Loaded on Acetylene Black for Electrochemical Sensing of the Anticancer Drug Topotecan in the Presence of High Concentration of Uric Acid. *J. Electroanal. Chem.*, **2018**, *824*, 22–31. https://doi.org/10.1016/j.jelechem.2018.07.031.

[203] Norouzi, P.; Qomi, M.; Nemati, A.; Ganjali, M. R. Determination of Anti Colon Cancer Drug, Irinotecan by Fast Fourier Transforms Continuous Cyclic Voltammetry. *Int. J. Electrochem. Sci.*, **2009**, *4* (9), 1248–1261.

[204] Novak Jovanović, I.; Komorsky-Lovrić, Š.; Lucić Vrdoljak, A.; Popović, A. R.; Neuberg, M. Voltammetric Characterisation of Anticancer Drug Irinotecan. *Electroanalysis*, **2018**, *30* (2), 336–344. https://doi.org/10.1002/elan.201700593.

[205] Temerk, Y. M.; Ibrahim, H.; Schuhmann, W. Square Wave Cathodic Adsorptive Stripping Voltammetric Determination of the Anticancer Drugs Flutamide and Irinotecan in Biological Fluids Using Renewable Pencil Graphite Electrodes. *Electroanalysis*, **2016**, *28* (2), 372–379. https://doi.org/10.1002/elan.201500329.

[206] Yu, Y.; Li, Q. L. Electrochemical Study on Interaction of Vincristine with Tubulin. *Chinese J. Chem.*, **2001**, *19* (11), 1084–1088. https://doi.org/10.1002/cjoc.20010191114.

[207] Holgado, T. M.; Quintana, M. C.; Pinilla, J. M. Electrochemical Study of Taxol (Paclitaxel) by Cathodic Stripping Voltammetry: Determination in Human Urine. *Microchem. J.*, **2003**, *74* (1), 99–104. https://doi.org/10.1016/S0026-265X(02)00175-3.

[208] Zhang, Y.; Zheng, J.; Guo, M. Preparation of Molecularly Imprinted Electrochemical Sensor for Detection of Vincristine Based on Reduced Graphene Oxide/Gold Nanoparticle Composite Film. *Chinese J. Chem.*, **2016**, *34* (12), 1268–1276. https://doi.org/10.1002/cjoc.201600582.

[209] Haghshenas, E.; Madrakian, T.; Afkhami, A.; Saify Nabiabad, H. A Label-Free Electrochemical Biosensor Based on Tubulin Immobilized on Gold Nanoparticle/Glassy Carbon Electrode for the Determination of Vinblastine. *Anal. Bioanal. Chem.*, **2017**, *409* (22), 5269–5278. https://doi.org/10.1007/s00216-017-0471-y.

[210] Tajik, S.; Taher, M. A.; Beitollahi, H.; Torkzadeh-Mahani, M. Electrochemical Determination of the Anticancer Drug Taxol at a Ds-DNA Modified Pencil-Graphite Electrode and Its Application as a Label-Free Electrochemical Biosensor. *Talanta*, **2015**, *134*, 60–64. https://doi.org/10.1016/j.talanta.2014.10.063.

[211] Mehdinia, A.; Habib Kazemi, S.; Zahra Bathaie, S.; Alizadeh, A.; Shamsipur, M.; Mousavi, M. F. Electrochemical Studies of DNA Immobilization onto the Azide-Terminated Monolayers and Its Interaction with Taxol. *Anal. Biochem.*, **2008**, *375* (2), 331–338. https://doi.org/10.1016/j.ab.2008.01.006.

[212] Kuralay, F.; Dükar, N.; Bayramlı, Y. Designing Functional Materials: DNA/Poly(3,4-

Ethylenedioxythiophene) Interfaces for Advanced DNA Direct Electrochemistry and DNA-Drug Interaction Detection. *Mater. Sci. Eng. B Solid-State Mater. Adv. Technol.*, **2021**, *272* (July), 115382. https://doi.org/10.1016/j.mseb.2021.115382.

[213] Bolat, G. Investigation of Poly(CTAB-MWCNTs) Composite Based Electrochemical DNA Biosensor and Interaction Study with Anticancer Drug Irinotecan. *Microchem. J.*, **2020**, *159*, 105426. https://doi.org/10.1016/j.microc.2020.105426.

[214] Alvau, M. D.; Tartaggia, S.; Meneghello, A.; Casetta, B.; Calia, G.; Serra, P. A.; Polo, F.; Toffoli, G. Enzyme-Based Electrochemical Biosensor for Therapeutic Drug Monitoring of Anticancer Drug Irinotecan. *Anal. Chem.*, **2018**, *90* (10), 6012–6019. https://doi.org/10.1021/acs.analchem.7b04357.

[215] Kim, H. R.; Pereira, C. M.; Han, H. Y.; Lee, H. J. Voltammetric Studies of Topotecan Transfer across Liquid/Liquid Interfaces and Sensing Applications. *Anal. Chem.*, **2015**, *87* (10), 5356–5362. https://doi.org/10.1021/acs.analchem.5b00653.

[216] Yu, Y.; Li, Q. Studies on the Interaction of Paclitaxel with Tubulin by an Electrochemical Method. *Anal. Chim. Acta*, **2001**, *436* (1), 147–152. https://doi.org/10.1016/S0003-2670(01)00896-0.

[217] Radi, A. E.; Nassef, H. M.; Eissa, A. Voltammetric and Ultraviolet-Visible Spectroscopic Studies on the Interaction of Etoposide with Deoxyribonucleic Acid. *Electrochim. Acta*, **2013**, *113*, 164–169. https://doi.org/10.1016/j.electacta.2013.09.046.

[218] Mahmoudi-Moghaddam, H.; Tajik, S.; Beitollahi, H. A New Electrochemical DNA Biosensor Based on Modified Carbon Paste Electrode Using Graphene Quantum Dots and Ionic Liquid for Determination of Topotecan. *Microchem. J.*, **2019**, *150*, 104085. https://doi.org/10.1016/j.microc.2019.104085.

[219] Top, M.; Er, O.; Congur, G.; Erdem, A.; Lambrecht, F. Y. Intracellular Uptake Study of Radiolabeled Anticancer Drug and Impedimetric Detection of Its Interaction with DNA. *Talanta*, **2016**, *160*, 157–163. https://doi.org/10.1016/j.talanta.2016.06.058.

[220] Idili, A.; Arroyo-Currás, N.; Ploense, K. L.; Csordas, A. T.; Kuwahara, M.; Kippin, T. E.; Plaxco, K. W. Seconds-Resolved Pharmacokinetic Measurements of the Chemotherapeutic Irinotecan: In Situ in the Living Body. *Chem. Sci.*, **2019**, *10* (35), 8164–8170. https://doi.org/10.1039/c9sc01495k.

[221] Pinar, P. T.; Saka, C.; Yardim, Y. Electrochemical Behavior of the Antineoplastic Agent Etoposide at a Graphene-Based Modified Electrode: Its Square-Wave Adsorptive Stripping Voltammetric Determination in the Pharmaceutical Formulations. *Rev. Roum. Chim.*, **2018**, *63* (12), 1149–1156.

[222] Nguyen, H. V.; Richtera, L.; Moulick, A.; Xhaxhiu, K.; Kudr, J.; Cernei, N.; Polanska, H.; Heger, Z.; Masarik, M.; Kopel, P.; et al. Electrochemical Sensing of Etoposide Using Carbon Quantum Dot Modified Glassy Carbon Electrode. *Analyst*, **2016**, *141* (9), 2665–2675. https://doi.org/10.1039/c5an02476e.

[223] Vajedi, F. sadat; Dehghani, H. A High-Sensitive Electrochemical DNA Biosensor Based on a Novel ZnAl/Layered Double Hydroxide Modified Cobalt Ferrite-Graphene Oxide Nanocomposite Electrophoretically Deposited onto FTO Substrate for Electroanalytical Studies of Etoposide. *Talanta*, **2020**, *208*, 120444. https://doi.org/10.1016/j.talanta.2019.120444.

[224] Gowda, J. I.; Nandibewoor, S. T. Electrochemical Behavior of Paclitaxel and Its Determination at Glassy Carbon Electrode. *Asian J. Pharm. Sci.*, **2014**, *9* (1), 42–49. https://doi.org/10.1016/j.ajps.2013.11.007.

[225] Gowda, J. I.; Nandibewoor, S. T. Carbon Paste Sensor for the Determination of an Anticancer Drug Paclitaxel in Pharmaceuticals and Biological Fluids. *Anal. Bioanal. Electrochem.*, **2015**, *7* (5), 539–554.

[226] Gowda, J. I.; Nandibewoor, S. T. Electrochemical Characterization and Determination of Paclitaxel Drug Using Graphite Pencil Electrode. *Electrochim. Acta*, **2014**, *116*, 326–333. https://doi.org/10.1016/j.electacta.2013.11.014.

[227] Bonazza, G.; Tartaggia, S.; Toffoli, G.; Polo, F.; Daniele, S. Voltammetric Behaviour of the Anticancer Drug Irinotecan and Its Metabolites in Acetonitrile. Implications for Electrochemical Therapeutic Drug Monitoring. *Electrochim. Acta*, **2018**, *289*, 483–493. https://doi.org/10.1016/j.electacta.2018.09.094.
[228] Bonazza, G.; Tartaggia, S.; Toffoli, G.; Polo, F.; Daniele, S. A Fast Method for the Detection of Irinotecan in Plasma Samples by Combining Solid Phase Extraction and Differential Pulse Voltammetry. *Anal. Bioanal. Chem.*, **2020**, *412* (7), 1585–1595. https://doi.org/10.1007/s00216-020-02386-1.
[229] Karadas, N.; Sanli, S.; Akmese, B.; Dogan-Topal, B.; Can, A.; Ozkan, S. A. Analytical Application of Polymethylene Blue-Multiwalled Carbon Nanotubes Modified Glassy Carbon Electrode on Anticancer Drug Irinotecan and Determination of Its Ionization Constant Value. *Talanta*, **2013**, *115*, 911–919. https://doi.org/10.1016/j.talanta.2013.07.006.
[230] Cheng, Q.; Du, Y.; Wu, K.; Chen, J.; Zhou, Y. Electrochemical Detection of Anticancer Drug Topotecan Using Nano-Acetylene Black Film. *Colloids Surfaces B Biointerfaces*, **2011**, *84* (1), 135–139. https://doi.org/10.1016/j.colsurfb.2010.12.027.
[231] Saxena, S.; Shrivastava, R.; Satsangee, S. P.; Srivastava, S. TiO2/Graphene/Chitosan-Nanocomposite-Based Electrochemical Sensor for the Sensing of Anti-HIV Drug Topotecan. *J. Electrochem. Soc.*, **2014**, *161* (14), H934–H940. https://doi.org/10.1149/2.0891414jes.
[232] Mohammadian, A.; Ebrahimi, M.; Karimi-Maleh, H. Synergic Effect of 2D Nitrogen Doped Reduced Graphene Nano-Sheet and Ionic Liquid as a New Approach for Fabrication of Anticancer Drug Sensor in Analysis of Doxorubicin and Topotecan. *J. Mol. Liq.*, **2018**, *265*, 727–732. https://doi.org/10.1016/j.molliq.2018.07.026.
[233] Alavi-Tabari, S. A. R.; Khalilzadeh, M. A.; Karimi-Maleh, H.; Zareyee, D. An Amplified Platform Nanostructure Sensor for the Analysis of Epirubicin in the Presence of Topotecan as Two Important Chemotherapy Drugs for Breast Cancer Therapy. *New J. Chem.*, **2018**, *42* (5), 3828–3832. https://doi.org/10.1039/c7nj04430e.
[234] Beitollahi, H.; Dehghannoudeh, G.; Moghaddam, H. M.; Forootanfar, H. A Sensitive Electrochemical DNA Biosensor for Anticancer Drug Topotecan Based on Graphene Carbon Paste Electrode. *J. Electrochem. Soc.*, **2017**, *164* (12), H812–H817. https://doi.org/10.1149/2.0511712jes.
[235] Er, E.; Erk, N. A Novel Electrochemical Sensing Platform Based on Mono-Dispersed Gold Nanorods Modified Graphene for the Sensitive Determination of Topotecan. *Sensors Actuators, B Chem.*, **2020**, *320* (April), 128320. https://doi.org/10.1016/j.snb.2020.128320.
[236] Offermanns, S.; Rosenthal, W. *Encyclopedia of Molecular Pharmacology*, 2nd editio.; Offermanns, S., Rosenthal, W., Eds.; Springer: Berlin, 2008. https://doi.org/10.1007/978-3-540-38918-7.
[237] Sharifi, J.; Fayazfar, H. Highly Sensitive Determination of Doxorubicin Hydrochloride Antitumor Agent via a Carbon Nanotube/Gold Nanoparticle Based Nanocomposite Biosensor. *Bioelectrochemistry*, **2021**, *139*, 107741. https://doi.org/10.1016/j.bioelechem.2021.107741.
[238] Ghanbari, M. H.; Shahdost-Fard, F.; Salehzadeh, H.; Ganjali, M. R.; Iman, M.; Rahimi-Nasrabadi, M.; Ahmadi, F. A Nanocomposite Prepared from Reduced Graphene Oxide, Gold Nanoparticles and Poly(2-Amino-5-Mercapto-1,3,4-Thiadiazole) for Use in an Electrochemical Sensor for Doxorubicin. *Microchim. Acta*, **2019**, *186* (9), 641. https://doi.org/10.1007/s00604-019-3761-6.
[239] Taei, M.; Hasanpour, F.; Salavati, H.; Mohammadian, S. Fast and Sensitive Determination of Doxorubicin Using Multi-Walled Carbon Nanotubes as a Sensor and CoFe2O4 Magnetic Nanoparticles as a Mediator. *Microchim. Acta*, **2016**, *183* (1), 49–56. https://doi.org/10.1007/s00604-015-1588-3.
[240] Taei, M.; Hasanpour, F.; Dehghani, E. Electrodepositing of Copper Nanowires on Layered Double Hydroxide Film Modified Glassy Carbon Electrode for the Determination of Doxorubicin. *J. Taiwan*

Inst. Chem. Eng., **2015**, *54*, 183–190. https://doi.org/10.1016/j.jtice.2015.03.016.
[241] Oliveira-Brett, A. M.; Piedade, J. A. P.; Chiorcea, A. M. Anodic Voltammetry and AFM Imaging of Picomoles of Adriamycin Adsorbed onto Carbon Surfaces. *J. Electroanal. Chem.*, **2002**, *538–539*, 267–276. https://doi.org/10.1016/S0022-0728(02)00944-0.
[242] Shams, A.; Yari, A. A New Sensor Consisting of Ag-MWCNT Nanocomposite as the Sensing Element for Electrochemical Determination of Epirubicin. *Sensors Actuators, B Chem.*, **2019**, *286*, 131–138. https://doi.org/10.1016/j.snb.2019.01.128.
[243] Arkan, E.; Paimard, G.; Moradi, K. A Novel Electrochemical Sensor Based on Electrospun TiO2 Nanoparticles/Carbon Nanofibers for Determination of Idarubicin in Biological Samples. *J. Electroanal. Chem.*, **2017**, *801*, 480–487. https://doi.org/10.1016/j.jelechem.2017.08.034.
[244] Ibrahim, M.; Ibrahim, H.; Almandil, N. B.; Sayed, M. A.; Kawde, A. N.; Aldaqdouq, Y. A Novel Platform Based on Au−CeO2@MWCNT Functionalized Glassy Carbon Microspheres for Voltammetric Sensing of Valrubicin as Bladder Anticancer Drug and Its Interaction with DNA. *Electroanalysis*, **2020**, *32* (10), 2146–2155. https://doi.org/10.1002/elan.202060125.
[245] Villar, J. C. C.; García, A. C.; Blanco, P. T. Adsorptive Stripping Voltammetric Behaviour of Mitoxantrone on Mercury Electrodes. *Talanta*, **1993**, *40* (3), 333–339. https://doi.org/10.1016/0039-9140(93)80242-J.
[246] Liu, Y.; Wei, M.; Hu, Y.; Zhu, L.; Du, J. An Electrochemical Sensor Based on a Molecularly Imprinted Polymer for Determination of Anticancer Drug Mitoxantrone. *Sensors Actuators, B Chem.*, **2018**, *255*, 544–551. https://doi.org/10.1016/j.snb.2017.08.023.
[247] Chang, J.; Gai, P.; Li, H.; Li, F. Target-Induced Diffusivity Enhancement for Rapid and Highly Sensitive Homogeneous Electrochemical Detection of BLM in Human Serum. *Talanta*, **2018**, *190* (August), 492–497. https://doi.org/10.1016/j.talanta.2018.08.038.
[248] He, Y. Q.; Gao, Y.; Gu, H. W.; Meng, X. Z.; Yi, H. C.; Chen, Y.; Sun, W. Y. Target-Induced Activation of DNAzyme for Sensitive Detection of Bleomycin by Using a Simple MOF-Modified Electrode. *Biosens. Bioelectron.*, **2021**, *178* (December 2020), 113034. https://doi.org/10.1016/j.bios.2021.113034.
[249] Chandra, P.; Zaidi, S. A.; Noh, H. B.; Shim, Y. B. Separation and Simultaneous Detection of Anticancer Drugs in a Microfluidic Device with an Amperometric Biosensor. *Biosens. Bioelectron.*, **2011**, *28* (1), 326–332. https://doi.org/10.1016/j.bios.2011.07.038.
[250] Skalová, Š.; Langmaier, J.; Barek, J.; Vyskočil, V.; Navrátil, T. Doxorubicin Determination Using Two Novel Voltammetric Approaches: A Comparative Study. *Electrochim. Acta*, **2020**, *330*, 135180. https://doi.org/10.1016/j.electacta.2019.135180.
[251] Hahn, Y.; Lee, H. Y. Electrochemical Behavior and Square Wave Voltammetric Determination of Doxorubicin Hydrochloride. *Arch. Pharm. Res.*, **2004**, *27* (1), 31–34. https://doi.org/10.1007/BF02980041.
[252] Yu, J.; Jin, H.; Gui, R.; Wang, Z.; Ge, F. A General Strategy to Facilely Design Ratiometric Electrochemical Sensors in Electrolyte Solution by Directly Using a Bare Electrode for Dual-Signal Sensing of Analytes. *Talanta*, **2017**, *162*, 435–439. https://doi.org/10.1016/j.talanta.2016.10.084.
[253] Zhang, K.; Zhang, Y. Electrochemical Behavior of Adriamycin at an Electrode Modified with Silver Nanoparticles and Multi-Walled Carbon Nanotubes, and Its Application. *Microchim. Acta*, **2010**, *169* (1), 161–165. https://doi.org/10.1007/s00604-010-0331-3.
[254] Fei, J.; Wen, X.; Zhang, Y.; Yi, L.; Chen, X.; Cao, H. Voltammetric Determination of Trace Doxorubicin at a Nano-Titania/Nafion Composite Film Modified Electrode in the Presence of Cetyltrimethylammonium Bromide. *Microchim. Acta*, **2009**, *164* (1–2), 85–91. https://doi.org/10.1007/s00604-008-0037-y.
[255] Vacek, J.; Havran, L.; Fojta, M. Ex Situ Voltammetry and Chronopotentiometry of Doxorubicin at a Pyrolytic Graphite Electrode: Redox and Catalytic Properties and Analytical Applications.

Electroanalysis, **2009**, *21* (19), 2139–2144. https://doi.org/10.1002/elan.200904646.
[256] Lü, L. A Novel Sensitive Doxorubicin Hydrochloride Electrochemical Sensor Based on a Nickel Hexacyanoferrate/Ni-Al-LDH Modified Gold Electrode. *Anal. Sci.*, **2020**, *36* (1), 127–133. https://doi.org/10.2116/analsci.19P271.
[257] Chandra, P.; Noh, H. B.; Won, M. S.; Shim, Y. B. Detection of Daunomycin Using Phosphatidylserine and Aptamer Co-Immobilized on Au Nanoparticles Deposited Conducting Polymer. *Biosens. Bioelectron.*, **2011**, *26* (11), 4442–4449. https://doi.org/10.1016/j.bios.2011.04.060.
[258] Hajian, R.; Mehrayin, Z.; Mohagheghian, M.; Zafari, M.; Hosseini, P.; Shams, N. Fabrication of an Electrochemical Sensor Based on Carbon Nanotubes Modified with Gold Nanoparticles for Determination of Valrubicin as a Chemotherapy Drug: Valrubicin-DNA Interaction. *Mater. Sci. Eng. C*, **2015**, *49*, 769–775. https://doi.org/10.1016/j.msec.2015.01.072.
[259] Li, S.; Wei, C.; Hu, J.; Li, Q. Electrochemical Behavior and Application of Pirarubicin at Gold Nanoparticles-Modified Indium Tin Oxide Electrode. *Anal. Lett.*, **2008**, *41* (4), 582–592. https://doi.org/10.1080/00032710801910635.
[260] Li, S. Q.; Yang, Y. F.; Yang, S. Y.; Ye, S. Y.; Fang, H. Q.; Hu, J. B.; Li, Q. L. Electrochemical Reduction and Voltammetric Determination of Pirarubicin at Carboxyl Ions Implantation-Modified Indium Tin Oxide Electrode. *Chinese J. Anal. Chem.*, **2011**, *39* (7), 990–993. https://doi.org/10.1016/S1872-2040(10)60454-9.
[261] Paziewska-Nowak, A.; Jankowska-Śliwińska, J.; Dawgul, M.; Pijanowska, D. G. Selective Electrochemical Detection of Pirarubicin by Means of DNA-Modified Graphite Biosensor. *Electroanalysis*, **2017**, *29* (7), 1810–1819. https://doi.org/10.1002/elan.201700067.
[262] Tan, X.; Hu, J.; Li, Q. Adsorptive Stripping Voltammetry of Bleomycin. *Analyst*, **1997**, *122*, 991–994. https://doi.org/https://doi.org/10.1039/A700436B.
[263] Marín, D.; Pérez, P.; Teijeiro, C.; Paleček, E. Voltammetric Determination of Mitomycin C in the Presence of Other Anti-Cancer Drugs and in Urine. *Anal. Chim. Acta*, **1998**, *358* (1), 45–50. https://doi.org/10.1016/S0003-2670(97)00605-3.
[264] Rezaei, B.; Askarpour, N.; Ensafi, A. A. A Novel Sensitive Doxorubicin Impedimetric Immunosensor Based on a Specific Monoclonal Antibody-Gold Nanoaprticle-Sol-Gel Modified Electrode. *Talanta*, **2014**, *119*, 164–169. https://doi.org/10.1016/j.talanta.2013.11.017.
[265] Yang, J.; Shen, H.; Zhang, X.; Tao, Y.; Xiang, H.; Xie, G. A Novel Platform for High Sensitivity Determination of PbP2a Based on Gold Nanoparticles Composited Graphitized Mesoporous Carbon and Doxorubicin Loaded Hollow Gold Nanospheres. *Biosens. Bioelectron.*, **2016**, *77*, 1119–1125. https://doi.org/10.1016/j.bios.2015.11.009.
[266] Porfireva, A. V.; Goida, A. I.; Rogov, A. M.; Evtugyn, G. A. Impedimetric DNA Sensor Based on Poly(Proflavine) for Determination of Anthracycline Drugs. *Electroanalysis*, **2020**, *32* (4), 827–834. https://doi.org/10.1002/elan.201900653.
[267] Shamagsumova, R.; Porfireva, A.; Stepanova, V.; Osin, Y.; Evtugyn, G.; Hianik, T. Polyaniline-DNA Based Sensor for the Detection of Anthracycline Drugs. *Sensors Actuators, B Chem.*, **2015**, *220*, 573–582. https://doi.org/10.1016/j.snb.2015.05.076.
[268] Li, C. Z.; Liu, Y.; Luong, J. H. T. Impedance Sensing of DNA Binding Drugs Using Gold Substrates Modified with Gold Nanoparticles. *Anal. Chem.*, **2005**, *77* (2), 478–485. https://doi.org/10.1021/ac048672l.
[269] Khodadadi, A.; Faghih-Mirzaei, E.; Karimi-Maleh, H.; Abbaspourrad, A.; Agarwal, S.; Gupta, V. K. A New Epirubicin Biosensor Based on Amplifying DNA Interactions with Polypyrrole and Nitrogen-Doped Reduced Graphene: Experimental and Docking Theoretical Investigations. *Sensors Actuators, B Chem.*, **2019**, *284*, 568–574. https://doi.org/10.1016/j.snb.2018.12.164.
[270] Alizadeh, M.; Azar, P. A.; Mozaffari, S. A.; Karimi-Maleh, H.; Tamaddon, A. M. A DNA Based

Biosensor Amplified With ZIF-8/Ionic Liquid Composite for Determination of Mitoxantrone Anticancer Drug: An Experimental/Docking Investigation. *Front. Chem.*, **2020**, *8* (October), 1–10. https://doi.org/10.3389/fchem.2020.00814.

[271] Ribeiro, J. A.; Silva, F.; Pereira, C. M. Electrochemical Study of the Anticancer Drug Daunorubicin at a Water/Oil Interface: Drug Lipophilicity and Quantification. *Anal. Chem.*, **2013**, *85* (3), 1582–1590. https://doi.org/10.1021/ac3028245.

[272] Karadurmus, L.; Dogan-Topal, B.; Kurbanoglu, S.; Shah, A.; Ozkan, S. A. The Interaction between DNA and Three Intercalating Anthracyclines Using Electrochemical Dna Nanobiosensor Based on Metal Nanoparticles Modified Screen-Printed Electrode. *Micromachines*, **2021**, *12* (11), 1337. https://doi.org/10.3390/mi12111337.

[273] Zhang, H. M.; Li, N. Q. Electrochemical Studies of the Interaction of Adriamycin to DNA. *J. Pharm. Biomed. Anal.*, **2000**, *22* (1), 67–73. https://doi.org/10.1016/S0731-7085(99)00254-X.

[274] Ting, B. P.; Zhang, J.; Gao, Z.; Ying, J. Y. A DNA Biosensor Based on the Detection of Doxorubicin-Conjugated Ag Nanoparticle Labels Using Solid-State Voltammetry. *Biosens. Bioelectron.*, **2009**, *25* (2), 282–287. https://doi.org/10.1016/j.bios.2009.07.005.

[275] Hajian, R.; Shams, N.; Parvin, A. DNA-Binding Studies of Daunorubicin in the Presence of Methylene Blue by Spectroscopy and Voltammetry Techniques. *Chinese J. Chem.*, **2009**, *27* (6), 1055–1060. https://doi.org/10.1002/cjoc.200990176.

[276] Karimi-Maleh, H.; Alizadeh, M.; Orooji, Y.; Karimi, F.; Baghayeri, M.; Rouhi, J.; Tajik, S.; Beitollahi, H.; Agarwal, S.; Gupta, V. K.; et al. Guanine-Based DNA Biosensor Amplified with Pt/SWCNTs Nanocomposite as Analytical Tool for Nanomolar Determination of Daunorubicin as an Anticancer Drug: A Docking/Experimental Investigation. *Ind. Eng. Chem. Res.*, **2021**, *60* (2), 816–823. https://doi.org/10.1021/acs.iecr.0c04698.

[277] Eksin, E.; Zor, E.; Erdem, A.; Bingol, H. Electrochemical Monitoring of Biointeraction by Graphene-Based Material Modified Pencil Graphite Electrode. *Biosens. Bioelectron.*, **2017**, *92* (December 2016), 207–214. https://doi.org/10.1016/j.bios.2017.02.016.

[278] Congur, G.; Eksin, E.; Erdem, A. Chitosan Modified Graphite Electrodes Developed for Electrochemical Monitoring of Interaction between Daunorubicin and DNA. *Sens. Bio-Sensing Res.*, **2019**, *22* (November 2018), 100255. https://doi.org/10.1016/j.sbsr.2018.100255.

[279] Saljooqi, A.; Shamspur, T.; Mostafavi, A. Ag-4-ATP-MWCNT Electrode Modified with DsDNA as Label-Free Electrochemical Sensor for the Detection of Daunorubicin Anticancer Drug. *Bioelectrochemistry*, **2017**, *118*, 161–167. https://doi.org/10.1016/j.bioelechem.2017.08.003.

[280] Ribeiro, J. A.; Pereira, C. M.; Silva, F. Electrochemistry of the Interaction between Bioactive Drugs Daunorubicin and Dopamine and DNA at a Water/Oil Interface. *Electrochim. Acta*, **2015**, *180*, 687–694. https://doi.org/10.1016/j.electacta.2015.08.074.

[281] Krzak, A.; Swiech, O.; Majdecki, M.; Bilewicz, R. Complexing Daunorubicin with β-Cyclodextrin Derivative Increases Drug Intercalation into DNA. *Electrochim. Acta*, **2017**, *247*, 139–148. https://doi.org/10.1016/j.electacta.2017.06.140.

[282] Erdem, A.; Ozsoz, M. Interaction of the Anticancer Drug Epirubicin with DNA. *Anal. Chim. Acta*, **2001**, *437* (1), 107–114. https://doi.org/10.1016/S0003-2670(01)00942-4.

[283] Abedi, R.; Bakhsh Raoof, J.; Bagheri Hashkavayi, A.; Asghary, M. Highly Sensitive and Label-Free Electrochemical Biosensor Based on Gold Nanostructures for Studying the Interaction of Prostate Cancer Gene Sequence with Epirubicin Anti-Cancer Drug. *Microchem. J.*, **2021**, *170*, 106668. https://doi.org/10.1016/j.microc.2021.106668.

[284] Hajian, R.; Hossaini, P.; Mehrayin, Z.; Woi, P. M.; Shams, N. DNA-Binding Studies of Valrubicin as a Chemotherapy Drug Using Spectroscopy and Electrochemical Techniques. *J. Pharm. Anal.*, **2017**, *7* (3), 176–180. https://doi.org/10.1016/j.jpha.2017.01.003.

[285] Satana Kara, H. E. Redox Mechanism of Anticancer Drug Idarubicin and In-Situ Evaluation of

Interaction with DNA Using an Electrochemical Biosensor. *Bioelectrochemistry*, **2014**, *99*, 17–23. https://doi.org/10.1016/j.bioelechem.2014.06.002.
[286] Oliveira-Brett, A. M.; MacEdo, T. R. A.; Raimundo, D.; Marques, M. H.; Serrano, S. H. P. Voltammetric Behaviour of Mitoxantrone at a DNA-Biosensor. *Biosens. Bioelectron.*, **1998**, *13* (7–8), 861–867. https://doi.org/10.1016/S0956-5663(98)00053-0.
[287] Erdem, A.; Congur, G. Impedimetric Detection of in Situ Interaction between Anti-Cancer Drug Bleomycin and DNA. *Int. J. Biol. Macromol.*, **2013**, *61*, 295–301. https://doi.org/10.1016/j.ijbiomac.2013.07.012.
[288] Heydari-Bafrooei, E.; Amini, M.; Saeednia, S. Electrochemical Detection of DNA Damage Induced by Bleomycin in the Presence of Metal Ions. *J. Electroanal. Chem.*, **2017**, *803* (September), 104–110. https://doi.org/10.1016/j.jelechem.2017.09.031.
[289] Findik, M.; Bingol, H.; Erdem, A. Hybrid Nanoflowers Modified Pencil Graphite Electrodes Developed for Electrochemical Monitoring of Interaction between Mitomycin C and DNA. *Talanta*, **2021**, *222* (April 2020), 121647. https://doi.org/10.1016/j.talanta.2020.121647.
[290] Kuralay, F.; Bayramlı, Y. Electrochemical Determination of Mitomycin C and Its Interaction with Double-Stranded DNA Using a Poly(o-Phenylenediamine)-Multi-Walled Carbon Nanotube Modified Pencil Graphite Electrode. *Anal. Lett.*, **2021**, *54* (8), 1295–1308. https://doi.org/10.1080/00032719.2020.1801710.
[291] Gürsoy, S.; Dükar, N.; Yaman, Y. T.; Abaci, S.; Kuralay, F. Electroactive Polyglycine Coatings for Nanobiosensing Applications: Label-Free DNA Hybridization, DNA-Antitumor Agent Interaction and Antitumor Agent Determination. *Anal. Chim. Acta*, **2019**, *1072*, 15–24. https://doi.org/10.1016/j.aca.2019.04.044.
[292] Erdem, A.; Muti, M.; Papakonstantinou, P.; Canavar, E.; Karadeniz, H.; Congur, G.; Sharma, S. Graphene Oxide Integrated Sensor for Electrochemical Monitoring of Mitomycin C-DNA Interaction. *Analyst*, **2012**, *137* (9), 2129–2135. https://doi.org/10.1039/c2an16011k.
[293] Eksin, E.; Muti, M.; Erdem, A. Chitosan/Ionic Liquid Composite Electrode for Electrochemical Monitoring of the Surface-Confined Interaction between Mitomycin C and DNA. *Electroanalysis*, **2013**, *25* (10), 2321–2329. https://doi.org/10.1002/elan.201300188.
[294] Sengiz, C.; Congur, G.; Eksin, E.; Erdem, A. Multiwalled Carbon Nanotubes-Chitosan Modified Single-Use Biosensors for Electrochemical Monitoring of Drug-DNA Interactions. *Electroanalysis*, **2015**, *27* (8), 1855–1863. https://doi.org/10.1002/elan.201500107.
[295] Ozkan, D.; Karadeniz, H.; Erdem, A.; Mascini, M.; Ozsoz, M. Electrochemical Genosensor for Mitomycin C-DNA Interaction Based on Guanine Signal. *J. Pharm. Biomed. Anal.*, **2004**, *35* (4), 905–912. https://doi.org/10.1016/j.jpba.2004.03.001.
[296] Kuralay, F.; Demirci, S.; Kiristi, M.; Oksuz, L.; Oksuz, A. U. Poly(3,4-Ethylenedioxythiophene) Coated Chitosan Modified Disposable Electrodes for DNA and DNA-Drug Interaction Sensing. *Colloids Surfaces B Biointerfaces*, **2014**, *123*, 825–830. https://doi.org/10.1016/j.colsurfb.2014.10.021.
[297] Ensafi, A. A.; Amini, M.; Rezaei, B. Impedimetric DNA-Biosensor for the Study of Anti-Cancer Action of Mitomycin C: Comparison between Acid and Electroreductive Activation. *Biosens. Bioelectron.*, **2014**, *59*, 282–288. https://doi.org/10.1016/j.bios.2014.03.041.
[298] Sugawara, K.; Kadoya, T.; Kuramitz, H. Monitoring of the Interaction between U937 Cells and Electroactive Daunomycin with an Arginine-Rich Peptide. *Bioelectrochemistry*, **2015**, *105*, 95–102. https://doi.org/10.1016/j.bioelechem.2015.05.012.
[299] Lei, K. F.; Liu, T. K.; Tsang, N. M. Towards a High Throughput Impedimetric Screening of Chemosensitivity of Cancer Cells Suspended in Hydrogel and Cultured in a Paper Substrate. *Biosens. Bioelectron.*, **2018**, *100* (259), 355–360. https://doi.org/10.1016/j.bios.2017.09.029.
[300] Caviglia, C.; Zór, K.; Canepa, S.; Carminati, M.; Larsen, L. B.; Raiteri, R.; Andresen, T. L.; Heiskanen,

A.; Emnéus, J. Interdependence of Initial Cell Density, Drug Concentration and Exposure Time Revealed by Real-Time Impedance Spectroscopic Cytotoxicity Assay. *Analyst*, **2015**, *140* (10), 3623–3629. https://doi.org/10.1039/c5an00097a.

[301] Caviglia, C.; Zór, K.; Montini, L.; Tilli, V.; Canepa, S.; Melander, F.; Muhammad, H. B.; Carminati, M.; Ferrari, G.; Raiteri, R.; et al. Impedimetric Toxicity Assay in Microfluidics Using Free and Liposome-Encapsulated Anticancer Drugs. *Anal. Chem.*, **2015**, *87* (4), 2204–2212. https://doi.org/10.1021/ac503621d.

[302] Nieciecka, D.; Joniec, A.; Blanchard, G. J.; Krysinski, P. Interactions of Doxorubicin with Organized Interfacial Assemblies. 1. Electrochemical Characterization. *Langmuir*, **2013**, *29* (47), 14560–14569. https://doi.org/10.1021/la403765w.

[303] Nieciecka, D.; Królikowska, A.; Setiawan, I.; Krysinski, P.; Blanchard, G. J. Interactions of Doxorubicin with Organized Interfacial Assemblies. 2. Spectroscopic Characterization. *Langmuir*, **2013**, *29* (47), 14570–14579. https://doi.org/10.1021/la4037666.

[304] Nieciecka, D.; Królikowska, A.; Krysinski, P. Probing the Interactions of Mitoxantrone with Biomimetic Membranes with Electrochemical and Spectroscopic Techniques. *Electrochim. Acta*, **2015**, *165*, 430–442. https://doi.org/10.1016/j.electacta.2015.02.223.

[305] Haghshenas, E.; Madrakian, T.; Afkhami, A. Electrochemically Oxidized Multiwalled Carbon Nanotube/Glassy Carbon Electrode as a Probe for Simultaneous Determination of Dopamine and Doxorubicin in Biological Samples. *Anal. Bioanal. Chem.*, **2016**, *408* (10), 2577–2586. https://doi.org/10.1007/s00216-016-9361-y.

[306] Hashemzadeh, N.; Hasanzadeh, M.; Shadjou, N.; Eivazi-Ziaei, J.; Khoubnasabjafari, M.; Jouyban, A. Graphene Quantum Dot Modified Glassy Carbon Electrode for the Determination of Doxorubicin Hydrochloride in Human Plasma. *J. Pharm. Anal.*, **2016**, *6* (4), 235–241. https://doi.org/10.1016/j.jpha.2016.03.003.

[307] Hasanzadeh, M.; Hashemzadeh, N.; Shadjou, N.; Eivazi-Ziaei, J.; Khoubnasabjafari, M.; Jouyban, A. Sensing of Doxorubicin Hydrochloride Using Graphene Quantum Dot Modified Glassy Carbon Electrode. *J. Mol. Liq.*, **2016**, *221*, 354–357. https://doi.org/10.1016/j.molliq.2016.05.082.

[308] Ehsani, M.; Soleymani, J.; Mohammadalizadeh, P.; Hasanzadeh, M.; Jouyban, A.; Khoubnasabjafari, M.; Vaez-Gharamaleki, Y. Low Potential Detection of Doxorubicin Using a Sensitive Electrochemical Sensor Based on Glassy Carbon Electrode Modified with Silver Nanoparticles-Supported Poly(Chitosan): A New Platform in Pharmaceutical Analysis. *Microchem. J.*, **2021**, *165* (February), 106101. https://doi.org/10.1016/j.microc.2021.106101.

[309] Ehsani, M.; Soleymani, J.; Hasanzadeh, M.; Vaez-Gharamaleki, Y.; Khoubnasabjafari, M.; Jouyban, A. Sensitive Monitoring of Doxorubicin in Plasma of Patients, MDA-MB-231 and 4T1 Cell Lysates Using Electroanalysis Method. *J. Pharm. Biomed. Anal.*, **2021**, *192*, 113701. https://doi.org/10.1016/j.jpba.2020.113701.

[310] Guo, H.; Jin, H.; Gui, R.; Wang, Z.; Xia, J.; Zhang, F. Electrodeposition One-Step Preparation of Silver Nanoparticles/Carbon Dots/Reduced Graphene Oxide Ternary Dendritic Nanocomposites for Sensitive Detection of Doxorubicin. *Sensors Actuators, B Chem.*, **2017**, *253*, 50–57. https://doi.org/10.1016/j.snb.2017.06.095.

[311] Kalambate, P. K.; Li, Y.; Shen, Y.; Huang, Y. Mesoporous Pd@Pt Core-Shell Nanoparticles Supported on Multi-Walled Carbon Nanotubes as a Sensing Platform: Application in Simultaneous Electrochemical Detection of Anticancer Drugs Doxorubicin and Dasatinib. *Anal. Methods*, **2019**, *11* (4), 443–453. https://doi.org/10.1039/c8ay02381f.

[312] Behravan, M.; Aghaie, H.; Giahi, M.; Maleknia, L. Determination of Doxorubicin by Reduced Graphene Oxide/Gold/Polypyrrole Modified Glassy Carbon Electrode: A New Preparation Strategy. *Diam. Relat. Mater.*, **2021**, *117* (May), 108478. https://doi.org/10.1016/j.diamond.2021.108478.

[313] Materon, E. M.; Wong, A.; Fatibello-Filho, O.; Faria, R. C. Development of a Simple Electrochemical Sensor for the Simultaneous Detection of Anticancer Drugs. *J. Electroanal. Chem.*, **2018**, *827* (August), 64–72. https://doi.org/10.1016/j.jelechem.2018.09.010.
[314] Rajaji, U.; Yogesh Kumar, K.; Chen, S. M.; Raghu, M. S.; Parashuram, L.; Alzahrani, F. M.; Alsaiari, N. S.; Ouladsmane, M. Deep Eutectic Solvent Synthesis of Iron Vanadate-Decorated Sulfur-Doped Carbon Nanofiber Nanocomposite: Electrochemical Sensing Tool for Doxorubicin. *Microchim. Acta*, **2021**, *188* (9), 303. https://doi.org/10.1007/s00604-021-04950-7.
[315] Soleymani, J.; Hasanzadeh, M.; Shadjou, N.; Khoubnasab Jafari, M.; Gharamaleki, J. V.; Yadollahi, M.; Jouyban, A. A New Kinetic-Mechanistic Approach to Elucidate Electrooxidation of Doxorubicin Hydrochloride in Unprocessed Human Fluids Using Magnetic Graphene Based Nanocomposite Modified Glassy Carbon Electrode. *Mater. Sci. Eng. C*, **2016**, *61*, 638–650. https://doi.org/10.1016/j.msec.2016.01.003.
[316] Soleymani, J.; Hasanzadeh, M.; Eskandani, M.; Khoubnasabjafari, M.; Shadjou, N.; Jouyban, A. Electrochemical Sensing of Doxorubicin in Unprocessed Whole Blood, Cell Lysate, and Human Plasma Samples Using Thin Film of Poly-Arginine Modified Glassy Carbon Electrode. *Mater. Sci. Eng. C*, **2017**, *77*, 790–802. https://doi.org/10.1016/j.msec.2017.03.257.
[317] Ghanbari, M. H.; Norouzi, Z. A New Nanostructure Consisting of Nitrogen-Doped Carbon Nanoonions for an Electrochemical Sensor to the Determination of Doxorubicin. *Microchem. J.*, **2020**, *157* (May), 105098. https://doi.org/10.1016/j.microc.2020.105098.
[318] Yan, F.; Chen, J.; Jin, Q.; Zhou, H.; Sailjoi, A.; Liu, J.; Tang, W. Fast One-Step Fabrication of a Vertically-Ordered Mesoporous Silica-Nanochannel Film on Graphene for Direct and Sensitive Detection of Doxorubicin in Human Whole Blood. *J. Mater. Chem. C*, **2020**, *8* (21), 7113–7119. https://doi.org/10.1039/d0tc00744g.
[319] Vetri Selvi, S.; Prasannan, A.; Chen, S. M.; Vadivelmurugan, A.; Tsai, H. C.; Lai, J. Y. Glutathione and Cystamine Functionalized MoS2core-Shell Nanoparticles for Enhanced Electrochemical Detection of Doxorubicin. *Microchim. Acta*, **2021**, *188* (2), 35. https://doi.org/10.1007/s00604-020-04642-8.
[320] Wang, M.; Lin, J.; Gong, J.; Ma, M.; Tang, H.; Liu, J.; Yan, F. Rapid and Sensitive Determination of Doxorubicin in Human Whole Blood by Vertically-Ordered Mesoporous Silica Film Modified Electrochemically Pretreated Glassy Carbon Electrodes. *RSC Adv.*, **2021**, *11* (15), 9021–9028. https://doi.org/10.1039/d0ra10000e.
[321] Chaney, E. N.; Baldwin, R. P. Electrochemical Determination of Adriamycin Compounds in Urine by Preconcentration at Carbon Paste Electrodes. *Anal. Chem.*, **1982**, *54* (14), 2556–2560. https://doi.org/10.1021/ac00251a034.
[322] Jemelková, Z.; Zima, J.; Barek, J. Voltammetric and Amperometric Determination of Doxorubicin Using Carbon Paste Electrodes. *Collect. Czechoslov. Chem. Commun.*, **2009**, *74* (10), 1503–1515. https://doi.org/10.1135/cccc2009081.
[323] Alavi-Tabari, S. A. R.; Khalilzadeh, M. A.; Karimi-Maleh, H. Simultaneous Determination of Doxorubicin and Dasatinib as Two Breast Anticancer Drugs Uses an Amplified Sensor with Ionic Liquid and ZnO Nanoparticle. *J. Electroanal. Chem.*, **2018**, *811*, 84–88. https://doi.org/10.1016/j.jelechem.2018.01.034.
[324] Madrakian, T.; Asl, K. D.; Ahmadi, M.; Afkhami, A. Fe3O4@Pt/MWCNT/Carbon Paste Electrode for Determination of a Doxorubicin Anticancer Drug in a Human Urine Sample. *RSC Adv.*, **2016**, *6* (76), 72803–72809. https://doi.org/10.1039/c6ra13935c.
[325] Jahandari, S.; Taher, M. A.; Karimi-Maleh, H.; Mansouri, G. Simultaneous Voltammetric Determination of Glutathione, Doxorubicin and Tyrosine Based on the Electrocatalytic Effect of a Nickel(II) Complex and of Pt:Co Nanoparticles as a Conductive Mediator. *Microchim. Acta*, **2019**, *186* (8), 493. https://doi.org/10.1007/s00604-019-3598-z.
[326] Stanković, D. M.; Milanović, Z.; Švorc, Ľ.; Stanković, V.; Janković, D.; Mirković, M.; Đurić, S. V.

Screen Printed Diamond Electrode as Efficient “Point-of-Care” Platform for Submicromolar Determination of Cytostatic Drug in Biological Fluids and Pharmaceutical Product. *Diam. Relat. Mater.*, **2021**, *113* (2020), 108277. https://doi.org/10.1016/j.diamond.2021.108277.

[327] Er, E.; Erk, N. Construction of a Sensitive Electrochemical Sensor Based on 1T-MoS2 Nanosheets Decorated with Shape-Controlled Gold Nanostructures for the Voltammetric Determination of Doxorubicin. *Microchim. Acta*, **2020**, *187* (4), 223. https://doi.org/10.1007/s00604-020-4206-y.

[328] Wang, J.; Lin, M. S.; Villa, V. Adsorptive Stripping Voltammetric Determination of Low Levels of Daunorubicin. *Analyst*, **1987**, *112* (9), 1303–1307. https://doi.org/10.1039/an9871201303.

[329] Erdem, A.; Karadeniz, H.; Caliskan, A. Dendrimer Modified Graphite Sensors for Detection of Anticancer Drug Daunorubicin by Voltammetry and Electrochemical Impedance Spectroscopy. *Analyst*, **2011**, *136* (5), 1041–1045. https://doi.org/10.1039/c0an00357c.

[330] Gao, D. M.; Hu, J. B.; Yang, M.; Li, Q. L. Determination of Daunomycin at a Novel COOH/Indium Tin Oxide Ion Implantation-Modified Electrode. *Anal. Biochem.*, **2006**, *358* (1), 70–75. https://doi.org/10.1016/j.ab.2006.06.008.

[331] Bozal-Palabiyik, B.; Kurbanoglu, S.; Gumustas, M.; Uslu, B.; Ozkan, S. A. Electrochemical Approach for the Sensitive Determination of Anticancer Drug Epirubicin in Pharmaceuticals in the Presence of Anionic Surfactant. *Rev. Roum. Chim.*, **2013**, *58* (7–8), 647–658.

[332] Abbasghorbani, M. Fe3O4 Loaded Single Wall Carbon Nanotubes and 1-Methyl-3-Octylimidazlium Chloride as Two Amplifiers for Fabrication of Highly Sensitive Voltammetric Sensor for Epirubicin Anticancer Drug Analysis. *J. Mol. Liq.*, **2018**, *266*, 176–180. https://doi.org/10.1016/j.molliq.2018.06.060.

[333] Karimi, F.; Shojaei, A. F.; Tabatabaeian, K.; Shakeri, S. CoFe2O4 Nanoparticle/Ionic Liquid Modified Carbon Paste Electrode as an Amplified Sensor for Epirubicin Analysis as an Anticancer Drug. *J. Mol. Liq.*, **2017**, *242*, 685–689. https://doi.org/10.1016/j.molliq.2017.07.067.

[334] Hashkavayi, A. B.; Raoof, J. B. Design an Aptasensor Based on Structure-Switching Aptamer on Dendritic Gold Nanostructures/Fe3O4@SiO2/DABCO Modified Screen Printed Electrode for Highly Selective Detection of Epirubicin. *Biosens. Bioelectron.*, **2017**, *91*, 650–657. https://doi.org/10.1016/j.bios.2017.01.025.

[335] Irem Kaya, S.; Kurbanoglu, S.; Yavuz, E.; Demiroglu Mustafov, S.; Sen, F.; Ozkan, S. A. Carbon-Based Ruthenium Nanomaterial-Based Electroanalytical Sensors for the Detection of Anticancer Drug Idarubicin. *Sci. Rep.*, **2020**, *10* (1), 1–12. https://doi.org/10.1038/s41598-020-68055-6.

[336] Kurbanoglu, S.; Dogan-Topal, B.; Uslu, B.; Can, A.; Ozkan, S. A. Electrochemical Investigations of the Anticancer Drug Idarubicin Using Multiwalled Carbon Nanotubes Modified Glassy Carbon and Pyrolytic Graphite Electrodes. *Electroanalysis*, **2013**, *25* (6), 1473–1482. https://doi.org/10.1002/elan.201300048.

[337] Oliveira Brett, A. M.; MacEdo, T. R. A.; Raimundo, D.; Marques, M. H.; Serrano, S. H. P. Electrochemical Oxidation of Mitoxantrone at a Glassy Carbon Electrode. *Anal. Chim. Acta*, **1999**, *385* (1–3), 401–408. https://doi.org/10.1016/S0003-2670(98)00807-1.

[338] Hasanzadeh, M.; Khalilzadeh, B.; Shadjou, N. Nanosilica Grafted by Sulfonic Acid: A Novel Nanocomposite towards Amplification of Mitoxantrone Electrooxidation Signals. *Nanocomposites*, **2016**, *2* (2), 76–83. https://doi.org/10.1080/20550324.2016.1200286.

[339] Villar, J. C. C.; García, A. C.; Blanco, P. T. Determination of Mitoxantrone Using Phase-Selective a.c. Adsorptive Stripping Voltammetry in a Flow System with Selectivity Enhancement. *Anal. Chim. Acta*, **1992**, *256* (2), 231–236. https://doi.org/10.1016/0003-2670(92)85348-A.

[340] Mao, Y.; Hu, J.; Li, Q.; Xue, P. Study of the Electrochemical Behavior of Mitoxantrone and Its Determination at a Co-C Modified Ultramicroelectrode. *Analyst*, **2000**, *125* (12), 2299–2302. https://doi.org/10.1039/b006865i.

[341] Lu, S.; Yang, M.; Li, X.; Liu, X.; Yin, Y.; Cao, Y. Amplified Detection of Bleomycin Based on an

Electrochemically Driven Recycling Strategy. *Anal. Methods*, **2014**, *6* (15), 5573–5577. https://doi.org/10.1039/c4ay00989d.
[342] Lawrence, D. S.; Niu, J. Protein Kinase Inhibitors: The Tyrosine-Specific Protein Kinases. *Pharmacol. Ther.*, **1998**, *77* (2), 81–114. https://doi.org/10.1016/S0163-7258(97)00052-1.
[343] Brycht, M.; Leniart, A.; Skrzypek, S. Application of Solid Carbon Electrodes in Voltammetric (Bio)Analysis of Selected Cytostatic Drugs. In *Handbook of Bioanalytics*; Buszewski, B., Baranowska, I., Eds.; Springer Nature: Switzerland, 2020. https://doi.org/https://doi.org/10.1007/978-3-030-95660-8.
[344] Ghapanvari, M.; Madrakian, T.; Afkhami, A.; Ghoorchian, A. A Modified Carbon Paste Electrode Based on Fe3O4@multi-Walled Carbon Nanotubes@polyacrylonitrile Nanofibers for Determination of Imatinib Anticancer Drug. *J. Appl. Electrochem.*, **2020**, *50* (2), 281–294. https://doi.org/10.1007/s10800-019-01388-x.
[345] Wu, Z.; Liu, J.; Liang, M.; Zheng, H.; Zhu, C.; Wang, Y. Detection of Imatinib Based on Electrochemical Sensor Constructed Using Biosynthesized Graphene-Silver Nanocomposite. *Front. Chem.*, **2021**, *9* (April), 1–7. https://doi.org/10.3389/fchem.2021.670074.
[346] Rezvani Jalal, N.; Madrakian, T.; Afkhami, A.; Ghoorchian, A. In Situ Growth of Metal-Organic Framework HKUST-1 on Graphene Oxide Nanoribbons with High Electrochemical Sensing Performance in Imatinib Determination. *ACS Appl. Mater. Interfaces*, **2020**, *12* (4), 4859–4869. https://doi.org/10.1021/acsami.9b18097.
[347] Brycht, M.; Kaczmarska, K.; Uslu, B.; Ozkan, S. A.; Skrzypek, S. Sensitive Determination of Anticancer Drug Imatinib in Spiked Human Urine Samples by Differential Pulse Voltammetry on Anodically Pretreated Boron-Doped Diamond Electrode. *Diam. Relat. Mater.*, **2016**, *68*, 13–22. https://doi.org/10.1016/j.diamond.2016.05.007.
[348] Moghaddam, A.; Zamani, H. A.; Karimi-maleh, H. A New Electrochemical Platform for Dasatinib Anticancer Drug Sensing Using Fe3O4-SWCTs/Ionic Liquid Paste Sensor. *Micromachines*, **2021**, *12* (4), 437. https://doi.org/10.3390/mi12040437.
[349] Eskiköy Bayraktepe, D.; Polat, K.; Yazan, Z. Electrochemical Oxidation Pathway of the Anti-Cancer Agent Dasatinib Using Disposable Pencil Graphite Electrode and Its Adsorptive Stripping Voltammetric Determination in Biological Samples. *J. Turkish Chem. Soc. Sect. A Chem.*, **2018**, *5* (2), 381–392. https://doi.org/10.18596/jotcsa.345238.
[350] Jesus, C. S. H.; Diculescu, V. C. Redox Mechanism, Spectrophotometrical Characterisation and Voltammetric Determination in Serum Samples of Kinases Inhibitor and Anticancer Drug Dasatinib. *J. Electroanal. Chem.*, **2015**, *752*, 47–53. https://doi.org/10.1016/j.jelechem.2015.06.006.
[351] Sener, C. E.; Dogan Topal, B.; Ozkan, S. A. Effect of Monomer Structure of Anionic Surfactant on Voltammetric Signals of an Anticancer Drug: Rapid, Simple, and Sensitive Electroanalysis of Nilotinib in Biological Samples. *Anal. Bioanal. Chem.*, **2020**, *412* (29), 8073–8081. https://doi.org/10.1007/s00216-020-02934-9.
[352] Aksoz, B. E.; Dogan Topal, B. Effect of Triton X-100 on the Electrochemical Behavior of Hydrophobic Lapatinib Used in the Treatment of Breast Cancer: A First Electroanalytical Study. *J. Electrochem. Soc.*, **2021**, *168* (7), 076506. https://doi.org/10.1149/1945-7111/ac0ec3.
[353] Bakirhan, N. K.; Tok, T. T.; Ozkan, S. A. The Redox Mechanism Investigation of Non-Small Cell Lung Cancer Drug: Erlotinib via Theoretical and Experimental Techniques and Its Host–Guest Detection by B-Cyclodextrin Nanoparticles Modified Glassy Carbon Electrode. *Sensors Actuators, B Chem.*, **2019**, *278*, 172–180. https://doi.org/10.1016/j.snb.2018.09.090.
[354] Sharma, N.; Baldi, A. Exploring Versatile Applications of Cyclodextrins: An Overview. *Drug Deliv.*, **2016**, *23* (3), 729–747. https://doi.org/10.3109/10717544.2014.938839.
[355] Yarahmadi, A.; Madrakian, T.; Afkhami, A.; Jalal, N. R. Electrochemical Determination of Sunitinib

in Biological Samples Using Polyacrylonitrile Nanofibers/Nickel-Zinc-Ferrite Nanocomposite/Carbon Paste Electrode. *J. Electrochem. Soc.*, **2019**, *166* (14), B1268–B1275. https://doi.org/10.1149/2.0371914jes.

[356] Ghoneim, M. M.; El-Desoky, H. S.; Ahmed, H. M.; El-badawy, F. M. Nano Determination of Kinase I Nhibitor Sorafenib Drug in Pharmaceutical Formulation and Human Blood at a Modified Carbon Paste Electrode. *J. Electrochem. Soc.*, **2016**, *163* (6), B215–B226. https://doi.org/10.1149/2.0471606jes.

[357] Bilge, S.; Dogan-Topal, B.; Atici, E. B.; Sınağ, A.; Ozkan, S. A. Rod-like CuO Nanoparticles/Waste Masks Carbon Modified Glassy Carbon Electrode as a Voltammetric Nanosensor for the Sensitive Determination of Anti-Cancer Drug Pazopanib in Biological and Pharmaceutical Samples. *Sensors Actuators, B Chem.*, **2021**, *343* (March), 130109. https://doi.org/10.1016/j.snb.2021.130109.

[358] Doulache, M.; Kaya, S. I.; Cetinkaya, A.; K Bakirhan, N.; Trari, M.; Ozkan, S. A. Detailed Electrochemical Behavior and Thermodynamic Parameters of Anticancer Drug Regorafenib and Its Sensitive Electroanalytical Assay in Biological and Pharmaceutical Samples. *Microchem. J.*, **2021**, *170* (August), 106717. https://doi.org/10.1016/j.microc.2021.106717.

[359] Venu, M.; Venkateswarlu, S.; Reddy, Y. V. M.; Seshadri Reddy, A.; Gupta, V. K.; Yoon, M.; Madhavi, G. Highly Sensitive Electrochemical Sensor for Anticancer Drug by a Zirconia Nanoparticle-Decorated Reduced Graphene Oxide Nanocomposite. *ACS Omega*, **2018**, *3* (11), 14597–14605. https://doi.org/10.1021/acsomega.8b02129.

[360] Rodríguez, J.; Berzas, J. J.; Castañeda, G.; Rodríguez, N. Voltammetric Determination of Imatinib (Gleevec) and Its Main Metabolite Using Square-Wave and Adsorptive Stripping Square-Wave Techniques in Urine Samples. *Talanta*, **2005**, *66* (1), 202–209. https://doi.org/10.1016/j.talanta.2004.11.010.

[361] Hammam, E.; El-Desoky, H. S.; Tawfik, A.; Ghoneim, M. M. Voltammetric Behavior and Quantification of the Anti-Leukemia Drug Imatinib in Bulk Form, Pharmaceutical Formulation, and Human Serum at a Mercury Electrode. *Can. J. Chem.*, **2004**, *82* (7), 1203–1209. https://doi.org/10.1139/v04-060.

[362] Nageswara Reddy, C.; Reddy Prasad, P.; Sreedhar, N. Y. Voltammetric Behavior of Gefitinib and Its Adsorptive Stripping Voltammetric Determination in Pharmaceutical Formulations and Urine Samples. *Int. J. Pharm. Pharm. Sci.*, **2011**, *3* (SUPPL. 3), 141–145.

[363] Alghamdi, A. F.; Hefnawy, M.; Al-Rashood, S. Development and Validation of Electrochemical Method for Quantification of Palbociclib (Anticancer Agent) in Biological Matrices Using Square Wave-Adsorptive Stripping Voltammetry. *Int. J. Electrochem. Sci.*, **2020**, *15*, 3517–3533. https://doi.org/10.20964/2020.04.31.

[364] Tahernejad-Javazmi, F.; Shabani-Nooshabadi, M.; Karimi-Maleh, H. Gold Nanoparticles and Reduced Graphene Oxide-Amplified Label-Free DNA Biosensor for Dasatinib Detection. *New J. Chem.*, **2018**, *42* (19), 16378–16383. https://doi.org/10.1039/C8NJ03783C.

[365] Çorman, M. E.; Cetinkaya, A.; Ozcelikay, G.; Özgür, E.; Atici, E. B.; Uzun, L.; Ozkan, S. A. A Porous Molecularly Imprinted Nanofilm for Selective and Sensitive Sensing of an Anticancer Drug Ruxolitinib. *Anal. Chim. Acta*, **2021**, *1187*, 339143. https://doi.org/10.1016/j.aca.2021.339143.

[366] Cetinkaya, A.; Topal, B. D.; Atici, E. B.; Ozkan, S. A. Simple and Highly Sensitive Assay of Axitinib in Dosage Form and Biological Samples and Its Electrochemical Behavior on the Boron-Doped Diamond and Glassy Carbon Electrodes. *Electrochim. Acta*, **2021**, *386*, 138443. https://doi.org/10.1016/j.electacta.2021.138443.

[367] Dogan-Topal, B.; Bozal-Palabiyik, B.; Ozkan, S. A.; Uslu, B. Investigation of Anticancer Drug Lapatinib and Its Interaction with DsDNA by Electrochemical and Spectroscopic Techniques. *Sensors Actuators, B Chem.*, **2014**, *194*, 185–194. https://doi.org/10.1016/j.snb.2013.12.088.

[368] Zhang, D.; Zhang, Y.; Zheng, L.; Zhan, Y.; He, L. Graphene Oxide/Poly-l-Lysine Assembled Layer for

Adhesion and Electrochemical Impedance Detection of Leukemia K562 Cancer Cells. *Biosens. Bioelectron.*, **2013**, *42* (1), 112–118. https://doi.org/10.1016/j.bios.2012.10.057.
[369] Zhou, S.; Kong, Y.; Shen, Q.; Ren, X.; Zhang, J. R.; Zhu, J. J. Chronic Myeloid Leukemia Drug Evaluation Using a Multisignal Amplified Photoelectrochemical Sensing Platform. *Anal. Chem.*, **2014**, *86* (23), 11680–11689. https://doi.org/10.1021/ac502969x.
[370] Zhou, S.; Wang, Y.; Zhu, J. J. Simultaneous Detection of Tumor Cell Apoptosis Regulators Bcl-2 and Bax through a Dual-Signal-Marked Electrochemical Immunosensor. *ACS Appl. Mater. Interfaces*, **2016**, *8* (12), 7674–7682. https://doi.org/10.1021/acsami.6b01010.
[371] Pradhan, R.; Rajput, S.; Mandal, M.; Mitra, A.; Das, S. Frequency Dependent Impedimetric Cytotoxic Evaluation of Anticancer Drug on Breast Cancer Cell. *Biosens. Bioelectron.*, **2014**, *55*, 44–50. https://doi.org/10.1016/j.bios.2013.11.060.
[372] Chen, H.; Luo, K.; Li, K. A Facile Electrochemical Sensor Based on NiO-ZnO/MWCNT-COOH Modified GCE for Simultaneous Quantification of Imatinib and Itraconazole. *J. Electrochem. Soc.*, **2019**, *166* (8), B697–B707. https://doi.org/10.1149/2.1071908jes.
[373] Hassan Pour, B.; Haghnazari, N.; Keshavarzi, F.; Ahmadi, E.; Rahimian Zarif, B. High Sensitive Electrochemical Sensor for Imatinib Based on Metal-Organic Frameworks and Multiwall Carbon Nanotubes Nanocomposite. *Microchem. J.*, **2021**, *165* (August 2020), 106147. https://doi.org/10.1016/j.microc.2021.106147.
[374] Hatamluyi, B.; Es'haghi, Z. A Layer-by-Layer Sensing Architecture Based on Dendrimer and Ionic Liquid Supported Reduced Graphene Oxide for Simultaneous Hollow-Fiber Solid Phase Microextraction and Electrochemical Determination of Anti-Cancer Drug Imatinib in Biological Samples. *J. Electroanal. Chem.*, **2017**, *801* (March), 439–449. https://doi.org/10.1016/j.jelechem.2017.08.032.
[375] Rodríguez, J.; Castañeda, G.; Lizcano, I. Electrochemical Sensor for Leukemia Drug Imatinib Determination in Urine by Adsorptive Striping Square Wave Voltammetry Using Modified Screen-Printed Electrodes. *Electrochim. Acta*, **2018**, *269*, 668–675. https://doi.org/10.1016/j.electacta.2018.03.051.
[376] Cetinkaya, A.; Kaya, S. I.; Ozcelikay, G.; Atici, E. B.; Ozkan, S. A. A Molecularly Imprinted Electrochemical Sensor Based on Highly Selective and an Ultra-Trace Assay of Anti-Cancer Drug Axitinib in Its Dosage Form and Biological Samples. *Talanta*, **2021**, *233* (June), 122569. https://doi.org/10.1016/j.talanta.2021.122569.
[377] Karadas-Bakirhan, N.; Patris, S.; Ozkan, S. A.; Can, A.; Kauffmann, J. M. Determination of the Anticancer Drug Sorafenib in Serum by Adsorptive Stripping Differential Pulse Voltammetry Using a Chitosan/Multiwall Carbon Nanotube Modified Glassy Carbon Electrode. *Electroanalysis*, **2016**, *28* (2), 358–365. https://doi.org/10.1002/elan.201500384.
[378] Ghoneim, M. M.; El-Desoky, H. S.; Ahmed, H. M.; El-badawy, F. M. Nano Determination of Kinase I Nhibitor Sorafenib Drug in Pharmaceutical Formulation and Human Blood at a Modified Carbon Paste Electrode . *J. Electrochem. Soc.*, **2016**, *163* (6), B215–B226. https://doi.org/10.1149/2.0471606jes.
[379] Aydoğmuş, Z.; Aslan, S. S.; Yildiz, G.; Senocak, A. Differential Pulse Voltammetric Determination of Anticancer Drug Regorafenib at a Carbon Paste Electrode: Electrochemical Study and Density Functional Theory Computations. *J. Anal. Chem.*, **2020**, *75* (5), 691–700. https://doi.org/10.1134/S1061934820050032.
[380] Zahavi, D.; Weiner, L. Monoclonal Antibodies in Cancer Therapy. *Antibodies*, **2020**, *9*, 34. https://doi.org/10.3390/antib9030034.
[381] Thomas, A.; Teicher, B. A.; Hassan, R. Antibody–Drug Conjugates for Cancer Therapy. *Lancet Oncol.*, **2016**, *17* (6), e254-262. https://doi.org/10.1016/S1470-2045(16)30030-4.
[382] Hatamluyi, B.; Es'haghi, Z. Quantitative Biodetection of Anticancer Drug Rituxan with DNA

Biosensor Modified PAMAM Dendrimer/Reduced Graphene Oxide Nanocomposite. *Electroanalysis*, **2018**, *30* (8), 1651–1660. https://doi.org/10.1002/elan.201800014.
[383] Tan, L.; Lin, P.; Chisti, M. M.; Rehman, A.; Zeng, X. Real Time Analysis of Binding between Rituximab (Anti-CD20 Antibody) and B Lymphoma Cells. *Anal. Chem.*, **2013**, *85* (18), 8543–8551. https://doi.org/10.1021/ac400062v.
[384] Leo, N.; Shang, Y.; Yu, J. J.; Zeng, X. Characterization of Self-Assembled Monolayers of Peptide Mimotopes of CD20 Antigen and Their Binding with Rituximab. *Langmuir*, **2015**, *31* (51), 13764–13772. https://doi.org/10.1021/acs.langmuir.5b02605.
[385] Oliveira, S. C. B.; Santarino, I. B.; Oliveira-Brett, A. M. Direct Electrochemistry of Native and Denatured Anticancer Antibody Rituximab at a Glassy Carbon Electrode. *Electroanalysis*, **2013**, *25* (4), 1029–1034. https://doi.org/10.1002/elan.201200552.
[386] Santarino, I. B.; Oliveira, S. C. B.; Oliveira-Brett, A. M. In Situ Evaluation of the Anticancer Antibody Rituximab-DsDNA Interaction Using a DNA-Electrochemical Biosensor. *Electroanalysis*, **2014**, *26* (6), 1304–1311. https://doi.org/10.1002/elan.201300488.
[387] Liu, J.; Chisti, M. M.; Zeng, X. General Signal Amplification Strategy for Nonfaradic Impedimetric Sensing: Trastuzumab Detection Employing a Peptide Immunosensor. *Anal. Chem.*, **2017**, *89* (7), 4013–4020. https://doi.org/10.1021/acs.analchem.6b04570.
[388] Yadegari, A.; Omidi, M.; Yazdian, F.; Zali, H.; Tayebi, L. An Electrochemical Cytosensor for Ultrasensitive Detection of Cancer Cells Using Modified Graphene-Gold Nanostructures. *RSC Adv.*, **2017**, *7* (4), 2365–2372. https://doi.org/10.1039/c6ra25938c.
[389] Centane, S.; Nyokong, T. The Antibody Assisted Detection of HER2 on a Cobalt Porphyrin Binuclear Framework and Gold Functionalized Graphene Quantum Dots Modified Electrode. *J. Electroanal. Chem.*, **2021**, *880*, 114908. https://doi.org/10.1016/j.jelechem.2020.114908.
[390] Yang, C.; Xu, C.; Wang, X.; Hu, X. Quantum-Dot-Based Biosensor for Simultaneous Detection of Biomarker and Therapeutic Drug: First Steps toward an Assay for Quantitative Pharmacology. *Analyst*, **2012**, *137* (5), 1205–1209. https://doi.org/10.1039/c2an15894a.
[391] Machini, W. B. S.; Marques, N. V.; Oliveira-Brett, A. M. Nivolumab Anticancer Monoclonal Antibody Native and Denatured Direct Electrochemistry at a Glassy Carbon Electrode. *J. Electroanal. Chem.*, **2019**, *851*, 113251. https://doi.org/10.1016/j.jelechem.2019.113251.
[392] Machini, W. B. S.; Marques, N. V.; Oliveira-Brett, A. M. In Situ Evaluation of Anticancer Monoclonal Antibody Nivolumab-DNA Interaction Using a DNA-Electrochemical Biosensor. *ChemElectroChem*, **2019**, *6* (17), 4608–4616. https://doi.org/10.1002/celc.201901005.
[393] Issaad, F. Z.; Tomé, L. I. N.; Marques, N. V.; Mouats, C.; Diculescu, V. C.; Oliveira-Brett, A. M. Bevacizumab Anticancer Monoclonal Antibody: Native and Denatured Redox Behaviour. *Electrochim. Acta*, **2016**, *206*, 246–253. https://doi.org/10.1016/j.electacta.2016.04.097.
[394] Tomé, L. I. N.; Marques, N. V.; Diculescu, V. C.; Oliveira-Brett, A. M. In Situ DsDNA-Bevacizumab Anticancer Monoclonal Antibody Interaction Electrochemical Evaluation. *Anal. Chim. Acta*, **2015**, *898*, 28–33. https://doi.org/10.1016/j.aca.2015.09.049.
[395] Schmid, G. M.; Atherton, D. R. Voltammetric Determination of Platinum from Aqueous Solutions and from Urine. *Anal. Chem.*, **1986**, *58* (9), 1956–1959. https://doi.org/10.1021/ac00122a009.
[396] Wang, J.; Peng, T.; Lin, M. S. Voltammetric Measurement of Cis-Dichlorodiammineplatinum(II) Following Interfacial Accumulation at Mercury Electrodes. *Bioelectrochemistry Bioenerg.*, **1986**, *16* (3), 395–406. https://doi.org/10.1016/0302-4598(86)80062-9.
[397] Petrlova, J.; Potesil, D.; Zehnalek, J.; Sures, B.; Adam, V.; Trnkova, L.; Kizek, R. Cisplatin Electrochemical Biosensor. *Electrochim. Acta*, **2006**, *51* (24), 5169–5173. https://doi.org/10.1016/j.electacta.2006.03.077.
[398] Hernández-Santos, D.; González-García, M. B.; Costa-García, A. Effect of Metals on Silver Electrodeposition: Application to the Detection of Cisplatin. *Electrochim. Acta*, **2005**, *50* (9), 1895–

1902. https://doi.org/10.1016/j.electacta.2004.08.042.
[399] Gholivand, M. B.; Ahmadi, E.; Mavaei, M. A Novel Voltammetric Sensor Based on Graphene Quantum Dots-Thionine/Nano-Porous Glassy Carbon Electrode for Detection of Cisplatin as an Anti-Cancer Drug. *Sensors Actuators, B Chem.*, **2019**, *299*, 126975. https://doi.org/10.1016/j.snb.2019.126975.
[400] Wu, Y.; Lai, R. Y. Tunable Signal-Off and Signal-On Electrochemical Cisplatin Sensor. *Anal. Chem.*, **2017**, *89* (18), 9984–9989. https://doi.org/10.1021/acs.analchem.7b02353.
[401] Kensova, R.; Kremplova, M.; Smerkova, K.; Zitka, O.; Hynek, D.; Adam, V.; Beklova, M.; Trnkova, L.; Stiborova, M.; Eckschlager, T.; et al. Interactions of Platinum-Based Cytostatics with Metallothionein Revealed by Electrochemistry. *Int. J. Electrochem. Sci.*, **2013**, *8* (4), 4472–4484.
[402] Luu, H. T. Le; Nachtigal, M. W.; Kuss, S. Electrochemical Characterization of Carboplatin at Unmodified Platinum Electrodes and Its Application to Drug Consumption Studies in Ovarian Cancer Cells. *J. Electroanal. Chem.*, **2020**, *872*, 114253. https://doi.org/10.1016/j.jelechem.2020.114253.
[403] Oliveira Brett, A. M.; Serrano, S. H. P.; Macedo, T. A.; Raimundo, D.; Marques, M. H.; La-Scalea, M. A. Electrochemical Determination of Carboplatin in Serum Using a DNA-Modified Glassy Carbon Electrode. *Electroanalysis*, **1996**, *8* (11), 992–995. https://doi.org/10.1002/elan.1140081104.
[404] Mahnashi, M. H.; Mahmoud, A. M.; Alhazzani, K.; Alanazi, A. Z.; Alaseem, A. M.; Algahtani, M. M.; El-Wekil, M. M. Ultrasensitive and Selective Molecularly Imprinted Electrochemical Oxaliplatin Sensor Based on a Novel Nitrogen-Doped Carbon Nanotubes/Ag@cu MOF as a Signal Enhancer and Reporter Nanohybrid. *Microchim. Acta*, **2021**, *188* (4), 124. https://doi.org/10.1007/s00604-021-04781-6.
[405] Hatamluyi, B.; Hashemzadeh, A.; Darroudi, M. A Novel Molecularly Imprinted Polymer Decorated by CQDs@HBNNS Nanocomposite and UiO-66-NH2 for Ultra-Selective Electrochemical Sensing of Oxaliplatin in Biological Samples. *Sensors Actuators, B Chem.*, **2020**, *307*, 127614. https://doi.org/10.1016/j.snb.2019.127614.
[406] Akbari Javar, H.; Garkani-Nejad, Z.; Dehghannoudeh, G.; Mahmoudi-Moghaddam, H. Development of a New Electrochemical DNA Biosensor Based on Eu3+−doped NiO for Determination of Amsacrine as an Anti-Cancer Drug: Electrochemical, Spectroscopic and Docking Studies. *Anal. Chim. Acta*, **2020**, *1133*, 48–57. https://doi.org/10.1016/j.aca.2020.07.071.
[407] Moghaddam, H. M.; Beitollahi, H.; Dehghannoudeh, G.; Forootanfar, H. Electrochemical Determination of Amsacrine at a Ds-DNA Modified Graphene Carbon Paste Electrode and Its Application as a Label-Free Electrochemical Biosensor. *Int. J. Electrochem. Sci.*, **2017**, *12* (11), 9958–9971. https://doi.org/10.20964/2017.11.39.
[408] Pathak, P. K.; Kumar, A.; Prasad, B. B. Functionalized Nitrogen Doped Graphene Quantum Dots and Bimetallic Au/Ag Core-Shell Decorated Imprinted Polymer for Electrochemical Sensing of Anticancerous Hydroxyurea. *Biosens. Bioelectron.*, **2019**, *127*, 10–18. https://doi.org/10.1016/j.bios.2018.11.055.
[409] Manesh, K. M.; Santhosh, P.; Komathi, S.; Kim, N. H.; Park, J. W.; Gopalan, A. I.; Lee, K. P. Electrochemical Detection of Celecoxib at a Polyaniline Grafted Multiwall Carbon Nanotubes Modified Electrode. *Anal. Chim. Acta*, **2008**, *626* (1), 1–9. https://doi.org/10.1016/j.aca.2008.07.050.
[410] Ghoneim, M. M.; Beltagi, A. M. Adsorptive Stripping Voltammetric Determination of the Anti-Inflammatory Drug Celecoxib in Pharmaceutical Formulation and Human Serum. *Talanta*, **2003**, *60* (5), 911–921. https://doi.org/10.1016/S0039-9140(03)00151-6.
[411] Athanasiou-Malaki, E.; Koupparis, M. A. Kinetic Study of the Determination of Hydrazines, Isoniazid and Sodium Azide by Monitoring Their Reactions with 1-Fluoro-2,4-Dinitrobenzene, by Means of a Fluoride-Selective Electrode. *Talanta*, **1989**, *36* (4), 431–436.

https://doi.org/10.1016/0039-9140(89)80224-3.
[412] Alghamdi, A. F. Development and Validation of Anodic Stripping Voltammetry Method for the Determination of Tretinoin in Human Urine and Plasma Using Glassy Carbon Electrode. *J. King Saud Univ. - Sci.*, **2020**, *32* (5), 2635–2640. https://doi.org/10.1016/j.jksus.2020.05.005.
[413] Vais, R. D.; Karimian, K.; Heli, H. Electrooxidation and Amperometric Determination of Vorinostat on Hierarchical Leaf-like Gold Nanolayers. *Talanta*, **2018**, *178*, 704–709. https://doi.org/10.1016/j.talanta.2017.10.001.
[414] Wu, Y.; Lai, R. Y. Electrochemical Detection of Platinum(IV) Prodrug Satraplatin in Serum. *Anal. Chem.*, **2015**, *87* (21), 11092–11097. https://doi.org/10.1021/acs.analchem.5b03215.
[415] Golea, D. A.; Diculescu, V. C.; Tugulea, L.; OliveiraBrett, A. M. Proteasome Inhibitor Anticancer Drug Bortezomib Redox Behaviour at a Glassy Carbon Electrode. *Electroanalysis*, **2012**, *24* (10), 1915–1921. https://doi.org/10.1002/elan.201200307.
[416] Henriques de Jesus, C. S. H.; Enache, T. A.; Diculescu, V. C. Charge Transfer Reaction Mechanisms of Epoxyketone and Boronated Peptides at Glassy Carbon and Boron Doped Diamond Electrodes. *J. Electroanal. Chem.*, **2020**, *878*, 114733. https://doi.org/10.1016/j.jelechem.2020.114733.
[417] Yapasan, E.; Caliskan, A.; Karadeniz, H.; Erdem, A. Electrochemical Investigation of Biomolecular Interactions between Platinum Derivatives and DNA by Carbon Nanotubes Modified Sensors. *Mater. Sci. Eng. B Solid-State Mater. Adv. Technol.*, **2010**, *169* (1–3), 169–173. https://doi.org/10.1016/j.mseb.2009.10.024.
[418] Henriques de Jesus, C. S.; Chiorcea-Paquim, A. M.; Barsan, M. M.; Diculescu, V. C. Electrochemical Assay for 20S Proteasome Activity and Inhibition with Anti-Cancer Drugs. *Talanta*, **2019**, *199* (December 2018), 32–39. https://doi.org/10.1016/j.talanta.2019.02.052.
[419] Barsan, M. M.; Diculescu, V. C. An Antibody-Based Amperometric Biosensor for 20S Proteasome Activity and Inhibitor Screening. *Analyst*, **2021**, *146* (10), 3216–3224. https://doi.org/10.1039/d0an02426k.
[420] Ci, Y. X.; Zhai, Q.; Wang, S.; Chang, W. B.; Zhang, C. Y.; Ma, H.; Chen, D. Y.; Zhao, M. Z.; Hu, S. W. Voltammetric Studies of the Effect of Cisplatin-Liposome on Hela Cells. *Talanta*, **2001**, *55* (4), 693–698. https://doi.org/10.1016/S0039-9140(01)00480-5.
[421] Dospivova, D.; Smerkova, K.; Ryvolova, M.; Hynek, D.; Adam, V.; Kopel, P.; Stiborova, M.; Eckschlager, T.; Hubalek, J.; Kizek, R. Catalytic Electrochemical Analysis of Platinum in Pt-DNA Adducts. *Int. J. Electrochem. Sci.*, **2012**, *7* (4), 3072–3088.
[422] Materon, E. M.; Jimmy Huang, P. J.; Wong, A.; Pupim Ferreira, A. A.; Sotomayor, M. D. P. T.; Liu, J. Glutathione-s-Transferase Modified Electrodes for Detecting Anticancer Drugs. *Biosens. Bioelectron.*, **2014**, *58*, 232–236. https://doi.org/10.1016/j.bios.2014.02.070.
[423] Materon, E. M.; Wong, A.; Klein, S. I.; Liu, J.; Sotomayor, M. D. P. T. Multi-Walled Carbon Nanotubes Modified Screen-Printed Electrodes for Cisplatin Detection. *Electrochim. Acta*, **2015**, *158*, 271–276. https://doi.org/10.1016/j.electacta.2015.01.184.
[424] Naik, K. M.; Alagur, M. M.; Nandibewoor, S. T. Electrochemical Response of Hydroxyurea by Different Voltammetric Techniques at Carbon Paste Electrode. *Anal. Methods*, **2013**, *5* (24), 6947–6953. https://doi.org/10.1039/c3ay41680a.
[425] Torkzadeh-Mahani, A.; Mohammadi, A.; Torkzadeh-Mahani, M.; Mohamadi, M. Voltammetric Determination of the Anticancer Drug Hydroxyurea Using a Carbon Paste Electrode Incorporating TiO2 Nanoparticles. *Anal. Bioanal. Electrochem.*, **2017**, *9* (1), 117–125.
[426] Cazelles, R.; Shukla, R. P.; Ware, R. E.; Vinks, A. A.; Ben-Yoav, H. Electrochemical Determination of Hydroxyurea in a Complex Biological Matrix Using Mos2-Modified Electrodes and Chemometrics. *Biomedicines*, **2021**, *9* (1), 1–17. https://doi.org/10.3390/biomedicines9010006.
[427] Haghshenas, M.; Mazloum-Ardakani, M.; Alizadeh, Z.; Vajhadin, F.; Naeimi, H. A Sensing Platform Using Ag/Pt Core-Shell Nanostructures Supported on Multiwalled Carbon Nanotubes to Detect

Hydroxyurea. *Electroanalysis*, **2020**, *32* (10), 2137–2145. https://doi.org/10.1002/elan.202060020.
[428] Naik, K. M.; Ashi, C. R.; Nandibewoor, S. T. Anodic Voltammetric Behavior of Hydroxyurea and Its Electroanalytical Determination in Pharmaceutical Dosage Form and Urine. *J. Electroanal. Chem.*, **2015**, *755*, 109–114. https://doi.org/10.1016/j.jelechem.2015.07.038.
[429] Fuku, X.; Iftikar, F.; Hess, E.; Iwuoha, E.; Baker, P. Cytochrome c Biosensor for Determination of Trace Levels of Cyanide and Arsenic Compounds. *Anal. Chim. Acta*, **2012**, *730*, 49–59. https://doi.org/10.1016/j.aca.2012.02.025.
[430] Arkan, E.; Karimi, Z.; Shamsipur, M.; Saber, R. Electrochemical Determination of Celecoxib on a Graphene Based Carbon Ionic Liquid Electrode Modified with Gold Nanoparticles and Its Application to Pharmaceutical Analysis. *Anal. Sci.*, **2013**, *29* (8), 855–860. https://doi.org/10.2116/analsci.29.855.
[431] Parsaee, Z.; Karachi, N.; Abrishamifar, S. M.; Kahkha, M. R. R.; Razavi, R. Silver-Choline Chloride Modified Graphene Oxide: Novel Nano-Bioelectrochemical Sensor for Celecoxib Detection and CCD-RSM Model. *Ultrason. Sonochem.*, **2018**, *45*, 106–115. https://doi.org/10.1016/j.ultsonch.2018.03.009.
[432] Nezhadali, A.; Sadeghzadeh, S. Experimental Design-Artificial Neural Network-Genetic Algorithm Optimization and Computer-Assisted Design of Celecoxib Molecularly Imprinted Polymer/Carbon Nanotube Sensor. *J. Electroanal. Chem.*, **2017**, *795*, 32–40. https://doi.org/10.1016/j.jelechem.2017.04.032.
[433] Abdel Maksoud, M. I. A.; El-Sayyad, G. S.; Ashour, A. H.; El-Batal, A. I.; Abd-Elmonem, M. S.; Hendawy, H. A. M.; Abdel-Khalek, E. K.; Labib, S.; Abdeltwab, E.; El-Okr, M. M. Synthesis and Characterization of Metals-Substituted Cobalt Ferrite [Mx Co(1-x) Fe2O4; (M = Zn, Cu and Mn; x = 0 and 0.5)] Nanoparticles as Antimicrobial Agents and Sensors for Anagrelide Determination in Biological Samples. *Mater. Sci. Eng. C*, **2018**, *92*, 644–656. https://doi.org/10.1016/j.msec.2018.07.007.

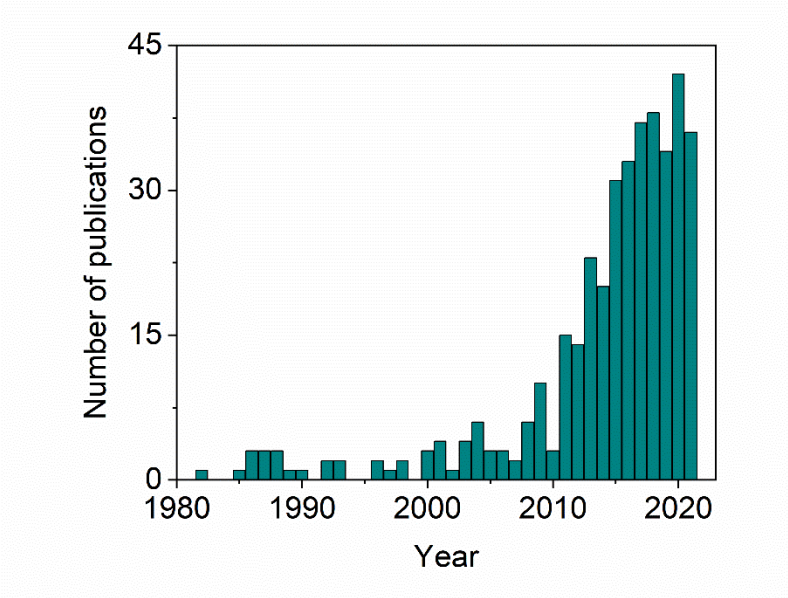

Fig. 1. Number of publications from the last (nearly) four decades (in the period 1982-2021) related to the topic of ANAs electrochemistry that were cited in this review: 390 publications.

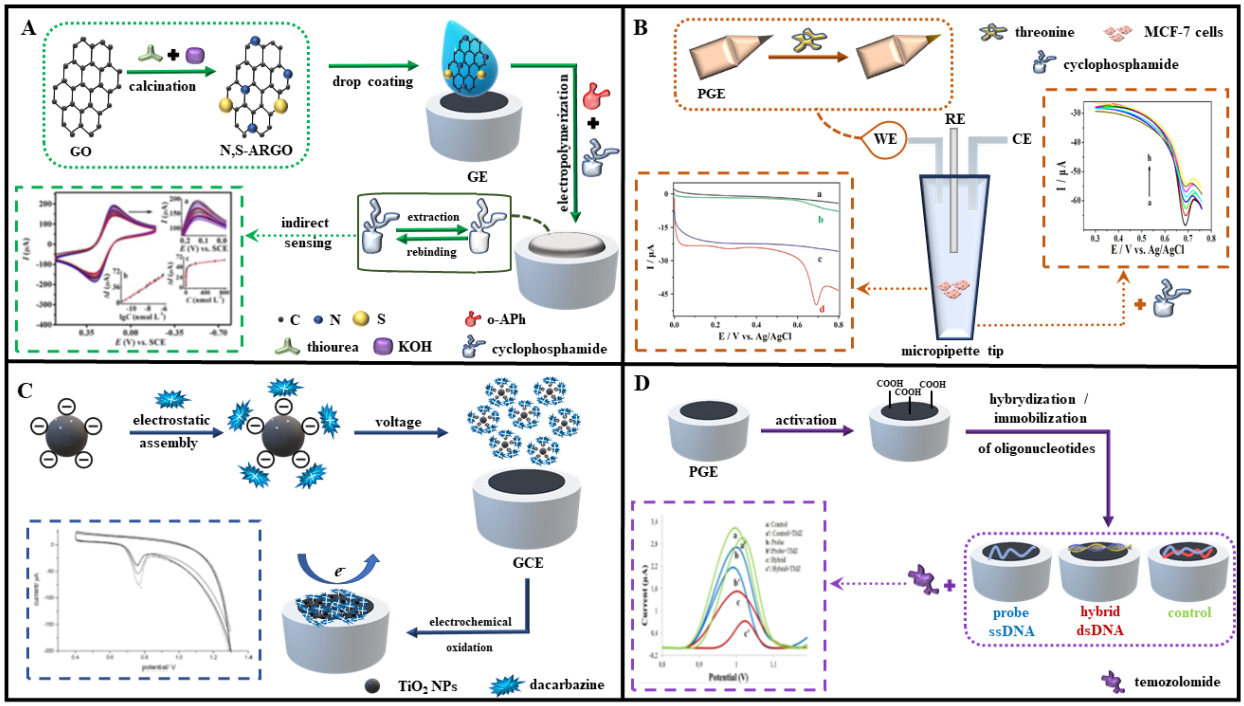

Fig. 2. (A) The scheme showing the preparation of the sensor based on the graphite electrode (GE) containing N,S-ARGO and MIP with o-aminophenol (o-APh) as a functional monomer developed for cyclophosphamide sensing. Voltammograms were reprinted from [51] with permission from Elsevier; **(B)** The schematic draw of the mini-electrochemical system constructed by integrating PGE modified with threonine as the working electrode and a micropipette tip having sealed ending as an electrochemical cell used for the investigation of the sensitivity of cyclophosphamide on the MCF-7 cells. Voltammograms were reprinted from [53] with permission from Elsevier; **(C)** The schematic representation of the biomolecular binding behavior of dacarbazine with DNA in the presence of the TiO_2NPs. Voltammograms reprinted from [63] with permission from Elsevier; **(D)** The preparation of DNA biosensor based on anodically pretreated PGE developed for the investigation of the electrochemical interaction between methylated DNA sequences and temozolomide. The voltammetric signal differences enabled distinguishing ssDNA and dsDNA without using a label or tag. Voltammograms were reprinted from [66] with permission from Wiley.

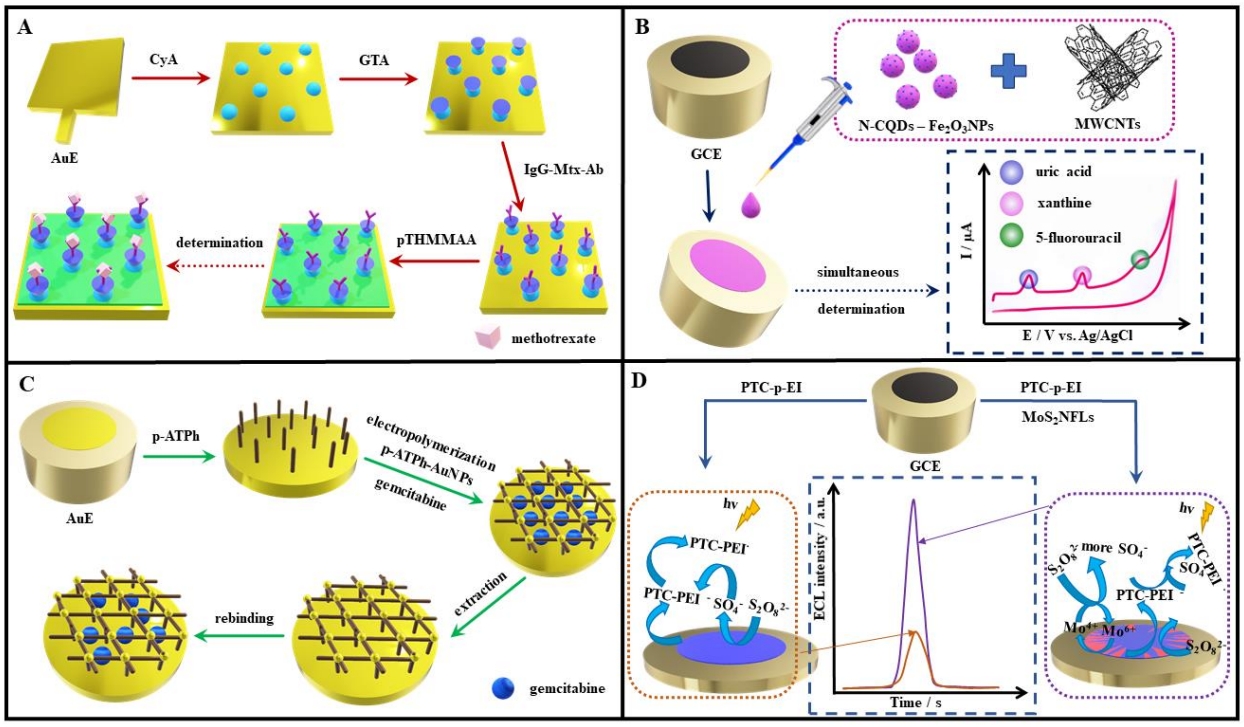

Fig. 3. (A) The steps of the preparation of immunosensor based on AuE modified with cysteamine (CyA), glutaraldehyde (GTA) as a linker, immunoglobulin G methotrexate antibody (IgG-Mtx-Ab), and N-[tris(hydroxyl-methyl)methyl]acrylamide (pTHMMAA) to block pinholes. The immunosensor was used for the methotrexate sensing. Prepared based on [80]; **(B)** Schematic representation of the GCE surface modification procedure with N-CQDs, Fe_2O_3NPs, and MWCNTs used for the simultaneous electrochemical detection of 5-fluorouracil, uric acid, and xanthine. Voltammograms reprinted from [101] with permission from Elsevier; **(C)** MIP sensor based on electropolymerized molecularly imprinted MOF used for the detection of gemcitabine. The sensor was prepared by immersing the AuE in p-aminothiophenol (p-ATPh) solution, and further by electropolymerization of the aniline moieties of p-ATPh functionalized with AuNPs on AuE modified with p-ATPh in the presence of gemcitabine as a template molecule. Prepared based on [142]; **(D)** Molybdenum disulfide nanoflowers (MoS_2NFLs) as signal-promoter of p-EI functionalized PTC and $S_2O_8^{2-}$ system for fabricating an electrochemiluminescence methotrexate sensor. Prepared based on [149].

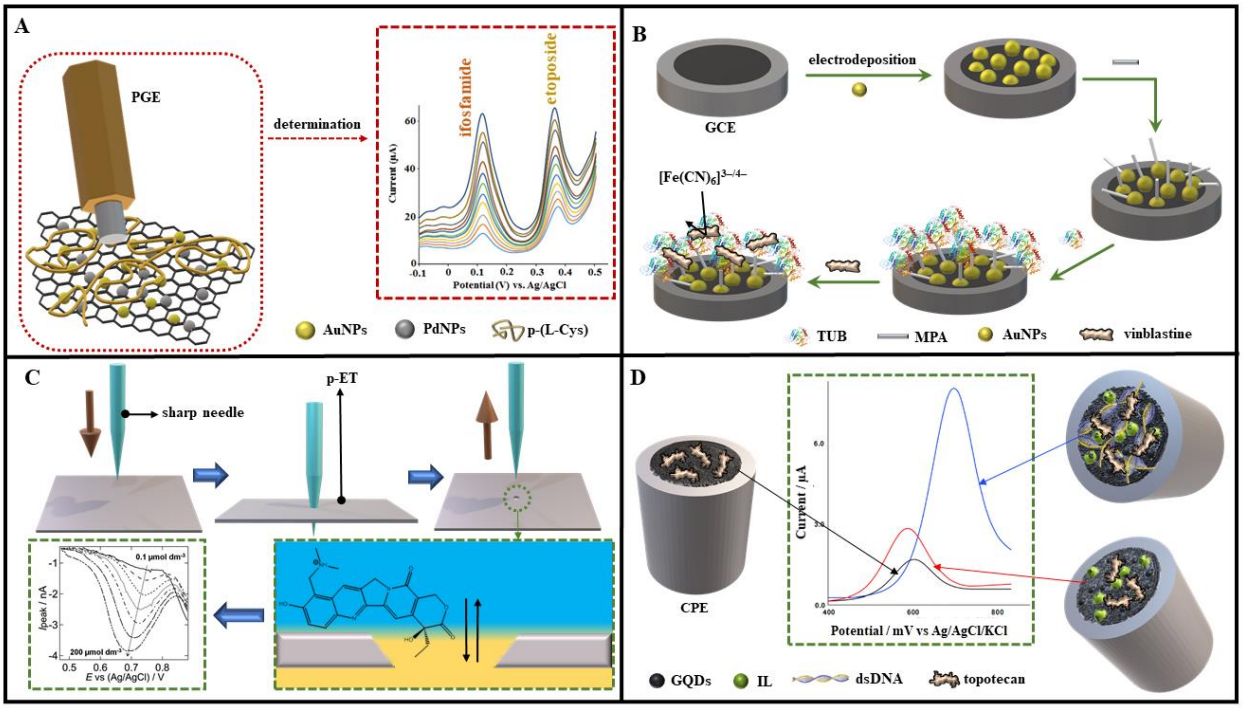

Fig. 4. (A) Scheme depicting the PGE modified with RGO further decorated with AuNPs, PdNPs, and p-(L-Cys used for the simultaneous determination of ifosfamide and etoposide. DP voltammograms reprinted from [199] with permission from Elsevier; **(B)** GCE surface sequential modification with AuNPs, MPA layer further used as the TUB anchor. The presented architecture was employed as the impedimetric vinblastine sensor. Prepared based on [209]; **(C)** Electrified liquid-liquid interface miniaturization protocol based on p-ET film micro punched with a sharp needle. Formed micro aperture served as the support for the soft junction. The signals recorded at the corresponding DP voltammograms originate from the topotecan simple interfacial ion transfer reaction. Voltammograms reprinted from [215] with permission from American Chemical Society; **(D)** Series of DP voltammograms for topotecan recorded at bare CPE (bottom left corner) and bulk-modified CPE with IL and GQDs (bottom right corner) and additionally decorated with dsDNA (upper right corner). DP voltammograms reprinted from [218] with permission from Elsevier.

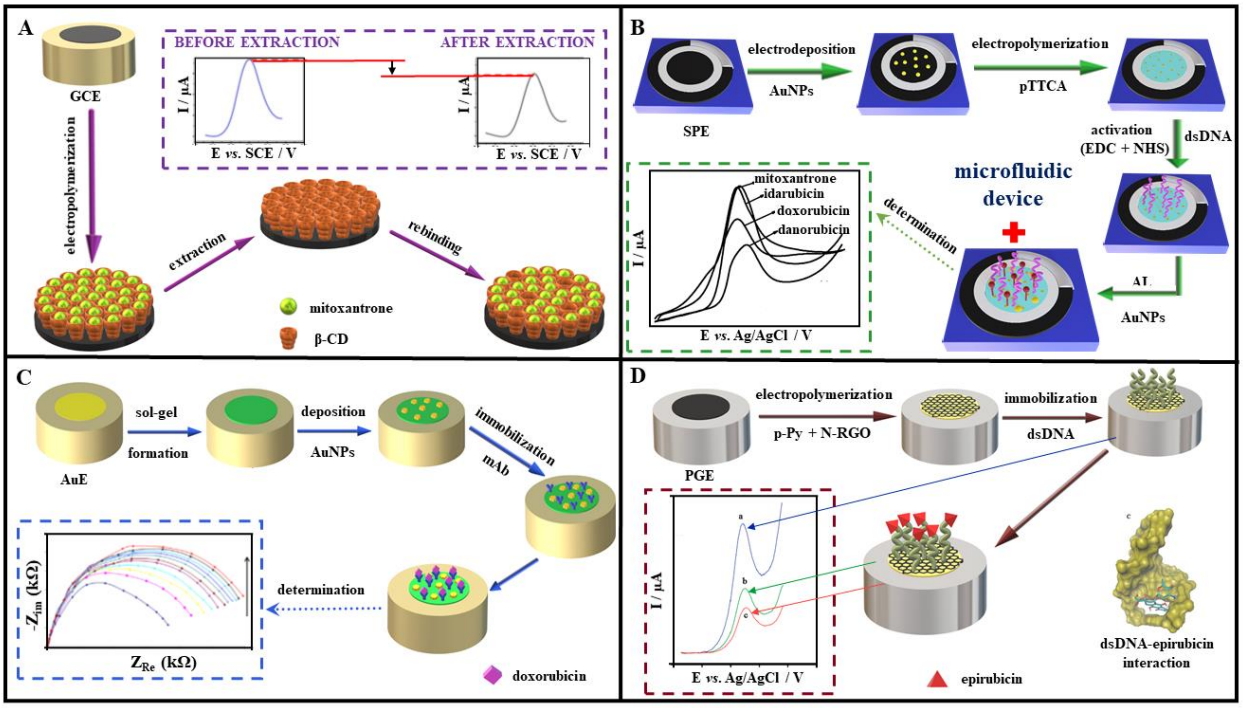

Fig. 5. (A) The GCE modified with MIP sensor based on β-CD for mitoxantrone detection. Voltammograms were reprinted from [246] with permission from Elsevier; **(B)** The steps of the preparation of a microfluidic device, which integrated pre-concentration, separation, and simultaneous detection of doxorubicin, daunorubicin, idarubicin, and mitoxantrone by utilizing electrokinetic separation and electrochemical detection method, using amperometric biosensors based on a modified SPE. Voltammograms were reprinted from [249] with permission from Elsevier; **(C)** The schematic representation of AuE modified with sol-gel functionalized with thiol functional groups, AuNPs, and mAb for the doxorubicin impedimetric detection. EIS spectra reprinted from [264] with permission from Elsevier; **(D)** The PGE modified with dsDNA, N-RGO, and p-Py for indirect detection of epirubicin. Voltammograms were reprinted from [269] with permission from Elsevier.

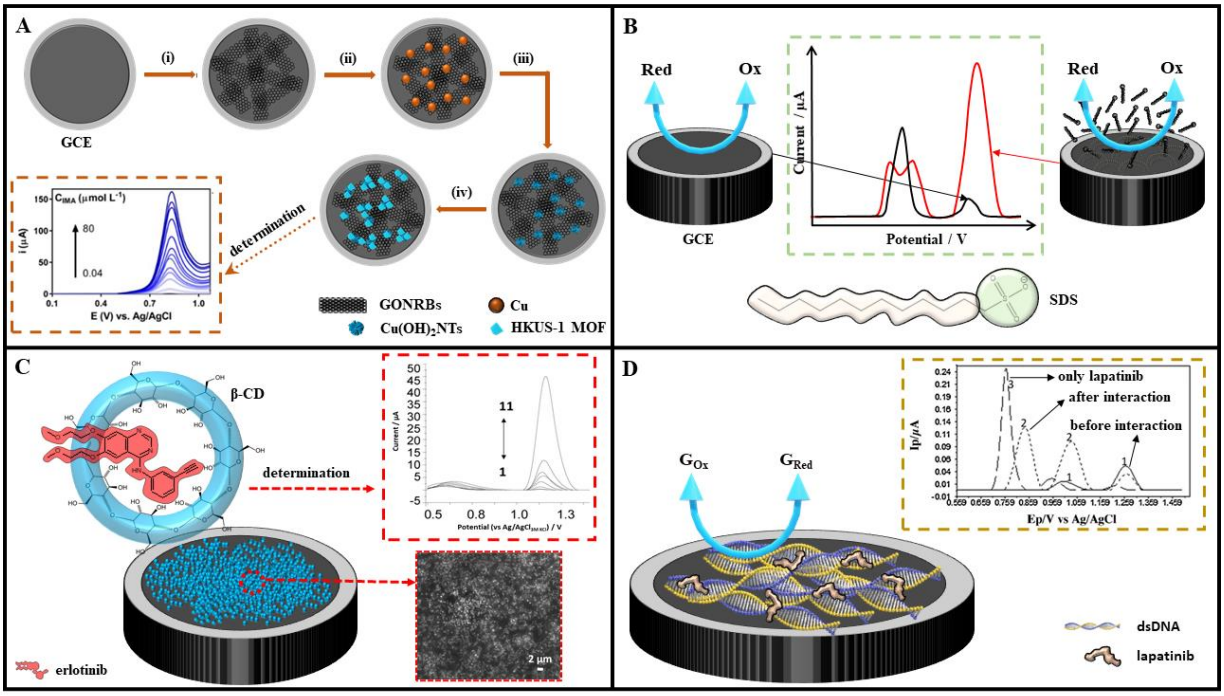

Fig. 6. **(A)** The GCE surface decoration protocol for imatinib sensing: (i) drop-casting of GONRBs suspension on the GCE surface, (ii) metallic Cu electrodeposition, (iii) treatment with NaOH for the oxidation of the elemental Cu to copper hydroxide nanotubes ($Cu(OH)_2NTs$), (iv) MOF formation step. Voltammograms reprinted from [346] with permission from American Chemical Society; **(B)** Simple GCE-based sensing of the nilotinib in the absence and presence of surfactant (SDS) species. Prepared based on [351]; **(C)** erlotinib electroanalytical sensing at β-CD modified GCE using electrochemically optimized stripping SWV sensing protocol. Voltammograms reprinted from [353] with permission from Elsevier; **(D)** Studying the interaction between dsDNA and lapatinib using G oxidation as the electroanalytical signal. Voltammograms reprinted from [367] with permission from Elsevier.

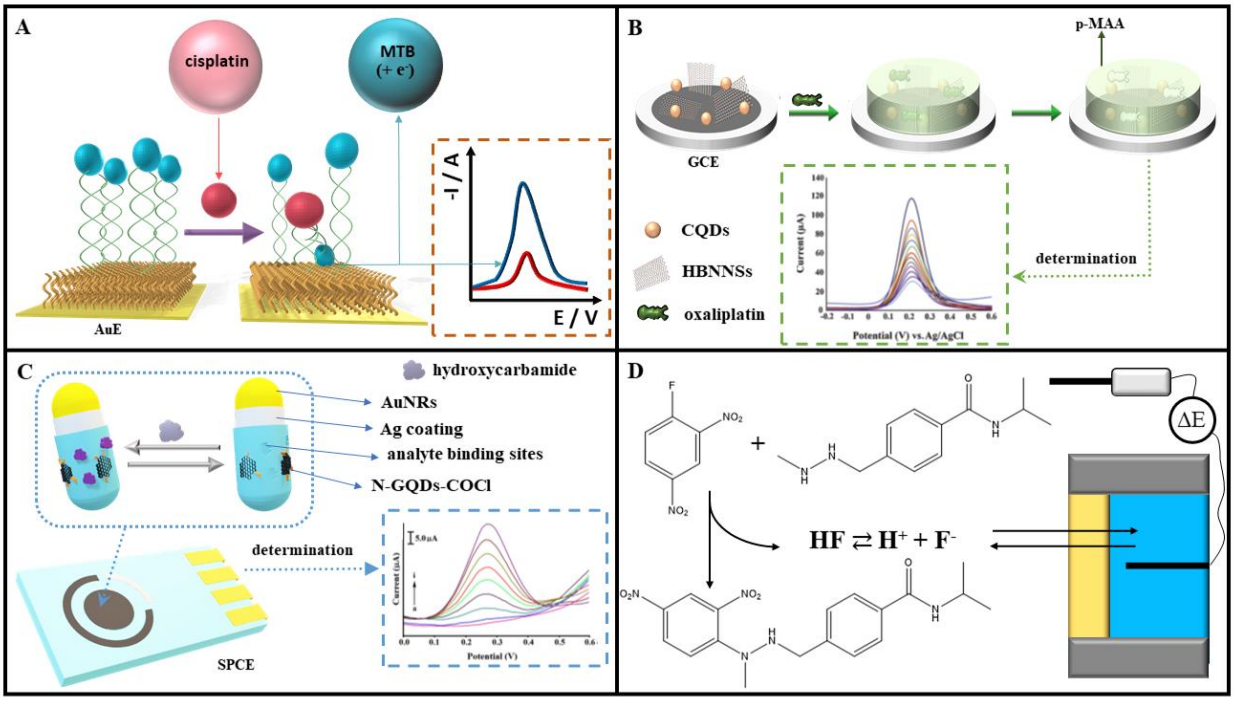

Fig. 7. (A) Cisplatin sensors constructed at the AuE surface modified with thiolated MTB-terminated DNA strands. The analytical signal originates from the DNA conformational changes triggered upon cisplatin (red sphere) binding. Prepared based on [400]; **(B)** Protocol for the oxaliplatin imprinting in a blend composed of CQDs, HBNNSs, and Zr(IV)-MOF in a poly-methacrylic acid (p-MAA) MIP. DP voltammograms reprinted from [405] with permission from Elsevier; **(C)** SPCE decorated with a nanomaterial derived from gold NRs (AuNRs) further modified with Ag coating and N-GQDs-COCl containing MIP used for the hydroxycarbamide sensing. DP voltammograms reprinted from [408] with permission from Elsevier; **(D)** The scheme showing indirect, potentiometric detection of procarbazine using FISE. Fluoride ions are the side project of the procarbazine reaction with 1-fluoro-2,4-nitrobenze reagent. Prepared based on [411].

Table 1. Comprehensive electroanalytical overview for the ANAs belonging to the group of alkylating agents.

Drug and its structure	Modification / Electrode	Technique	Medium	Linear range	LOD/LOQ	Application	Selectivity	Comments	Ref.
Nitrogen mustard analogs									
cyclophosphamide 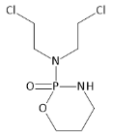	dsDNA / AP-CPE	DPAdSV	200.0 mM AcB, pH 4.8, containing 20.0 mM NaCl	30.0 nM – 70.0 nM	LOD = 30.0 nM	The interaction with dsDNA.	N/A	**Analytical signal:** indirect cyclophosphamide sensing by monitoring the increase in guanine oxidation peak currents ($E_{p\ guanine}$ ≈ +1.0 V *vs* Ag|AgCl|KCl_{3M}).	[52]
	ssDNA / AP-CPE	DPAdSV	200.0 mM AcB, pH 4.8, containing 20.0 mM NaCl	8.0 nM – 80.0 nM	LOD = 8.0 nM	The interaction with ssDNA.	N/A	**Analytical signal:** indirect cyclophosphamide sensing by monitoring the increase in oxidation peak currents of guanine ($E_{p\ guanine}$ ≈ +1.0 V *vs* Ag|AgCl|KCl_{3M}) and adenine ($E_{p\ adenine}$ ≈ +1.25 V *vs*. Ag|AgCl|KCl_{3M}).	[52]
	dsDNA / AP-PGE	DPAdSV	200.0 mM AcB, pH 4.8, containing 20.0 mM NaCl	10.0 nM – 80.0 nM	LOD = 10.0 nM	The interaction with dsDNA.	N/A	**Analytical signal:** indirect cyclophosphamide sensing by monitoring the increase in oxidation peak currents of guanine ($E_{p\ guanine}$ ≈ +1.0 V *vs* Ag|AgCl|KCl_{3M}) and adenine ($E_{p\ adenine}$ ≈ +1.25 V *vs* Ag|AgCl|KCl_{3M}).	[52]
	ssDNA / AP-PGE	DPAdSV	200.0 mM AcB, pH 4.8, containing 20.0 mM NaCl	1.0 nM – 70.0 nM	LOD = 1.0 nM	The interaction with ssDNA.	N/A	**Analytical signal:** indirect cyclophosphamide sensing by monitoring the increase in guanine oxidation peak currents ($E_{p\ guanine}$ ≈ +1.0 V *vs* Ag|AgCl|KCl_{3M}).	[52]
	MIP(p-(o-APh)) – N,S-ARGO / GE	CV	100.0 mM KCl	8.0 pM – 800.0 nM	LOD = 3.4 pM	**Real sample:** spiked rabbit serum.	**Tested interfering agents**: Ca^{2+}, Na^{+}, NH_4^{+}, K^{+}, Cl^{-}, NO_3^{-}.	**Analytical signal:** indirect cyclophosphamide sensing by monitoring the decrease in $[Fe(CN)_6]^{3-/4-}$ oxidation current ($E_{p\ [Fe(CN)6]3-/4-}$ ≈ +0.15 V *vs* SCE).	[51]
	CYP2B6 – f(-COOH)MWCNTs / SPCPE	CV	100.0 mM PBS, pH 7.4	2.7 µM – 76.6 µM	LOD = 4.9 µM	**Real sample:** spiked blood serum.	N/A	**Analytical signal:** cyclophosphamide oxidation (E_p ≈ –0.45 V *vs* Ag|AgCl).	[40]
	MIP(p-(o-APh)) / (Pd-Ag)A-MW	CV	100.0 mM KNO_3	20.0 fM – 10.0 pM	LOD = 8.0 fM	N/A	N/A	**Analytical signal:** indirect cyclophosphamide sensing by monitoring the decrease in $[Fe(CN)_6]^{3-/4-}$ reduction current ($E_{p\ [Fe(CN)6]3-/4-}$ ≈ +0.15 V *vs* SCE).	[50]
chlorambucil	SMDE	AdSV	AcB, pH 5.4	200.0 nM – 1.0 µM	LOD = 30.0 nM	N/A	**Tested interfering agents:** uric acid, ascorbic acid, 5-fluorouracil, methotrexate.	**Analytical signal:** chlorambucil reduction (E_p ≈ –1.3 V *vs* Ag|AgCl).	[68]
	$(MnO_2$-$NiFe_2O_4)$NPs / GCE	DPV	100.0 mM PBS, pH 5.0	25.0 nM – 574.5 µM	LOD = 4.7 nM	**Real sample:** pharmaceutical formulation, spiked urine, spiked drinking water.	**Tested interfering agents:** dopamine, uric acid, glucose, mercury, diphenylamine, sodium, potassium, nitrite, diuron.	**Analytical signal:** chlorambucil oxidation (E_p ≈ +0.6 V *vs* Ag|AgCl).	[36]

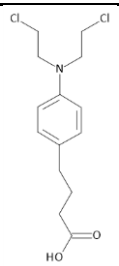	(p-NVCL-p-Py)MGs / GCE	DPV	100 mM PB, pH 7.0	20.0 nM – 420.0 µM	LOD = 2.0 nM	**Real sample:** spiked blood serum, spiked urine.	**Tested interfering agents**: dopamine, uric acid, diuron, naproxen, acetaminophen, ascorbic acid, theophylline, acyclovir, Mg^{2+}, K^{+}, Na^{+}, Zn^{2+}, Cu^{2+}.	**Analytical signal:** chlorambucil oxidation (E_p ≈ +0.8 V *vs* Ag|AgCl).	[69]
	MIP(MBAA – SDS – Vi-C_{60}-MA) – IL(BMIM-BF_4) / CCE	DPASV	100.0 mM PB, pH 5.5	4.8 nM – 812.6 nM	LOD = 1.2 nM	**Real sample:** pharmaceutical formulation, spiked blood plasma, spiked urine.	**Tested interfering agents**: dacarbazine, ifosfamide, cytarabine, 5-flurouracil, temozolomide, melphalan, glucose, uric acid, dopamine.	**Analytical signal:** chlorambucil oxidation (E_p ≈ +0.45 V *vs* Ag|AgCl|KCl_{3M}).	[47]
	OMNiDIP (aTACoPC – AIBN) – RGO / CCE	DPASV	100.0 mM BB, pH 5.0	516.1 pM – 107.9 nM	LOD = 115.1 pM	**Real sample:** pharmaceutical formulation, spiked blood serum, spiked urine.	**Tested interfering agents**: cytarabine, 5-fluorouracil, ifosfamide, melphalan, temozolomide, alanine, ascorbic acid, cysteine, glutamic acid, histidine, phenylalanine, glucose, uric acid, dopamine.	**Analytical signal:** chlorambucil oxidation (E_p ≈ +0.4 V *vs* Ag|AgCl). Possible simultaneous determination of chlorambucil with dacarbazine.	[45]
ifosfamide 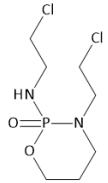	p-(L-Cys) – RGO – (Au-Pd)NPs / AP-PGE	DPV	BRB, pH 6.0	10.0 nM – 10.0 µM 10.0 µM – 115.0 µM	LOD = 9.2 nM	**Real sample:** pharmaceutical formulation, spiked blood serum, spiked urine.	**Tested interfering agents**: glucose, sucrose, ascorbic acid, uric acid, citric acid, Na^{+}, K^{+}, Mg^{2+}, SO_4^{2-}, CO_3^{2-}, NO_3^{-}.	**Analytical signal:** ifosfamide oxidation (E_p ≈ +0.15 V *vs* Ag|AgCl|KCl_{sat}). Possible determination of ifosfamide in the presence of etoposide.	[37]
	CYP3A4 – f(-COOH)MWCNTs / SPCPE	CV	100.0 mM PBS, pH 7.4	10.0 µM – 160.0 µM	LOD = 2.8 µM	**Real sample:** spiked blood serum.	N/A	**Analytical signal:** ifosfamide oxidation (E_p ≈ –0.45 V *vs* Ag|AgCl).	[40]
	MIP(EGDMA – AIBN – N-ABA) – f(-COCl)GQDs / SPCE	DPASV	100.0 mM PB, pH 4.7	957.5 pM – 464.8 nM	LOD = 306.4 pM	**Real sample:** pharmaceutical formulation (injection), spiked blood plasma, spiked urine.	**Tested interfering agents**: 5-fluorouracil, cyclophosphamide, chlorambucil, cytarabine, ascorbic acid, dopamine, cysteine, uric acid.	**Analytical signal:** ifosfamide oxidation (E_p ≈ +0.05 V *vs* AgE).	[48]
	Ti_3C_2 – MX – MWCNTs – Chit / GCE	DPAdSV	400. mM BRB, pH 4.0	1.1 nM – 1.0 µM	LOD = 310.0 pM LOQ = 1.3 nM	**Real sample:** spiked urine, spiked blood serum.	**Tested interfering agents**: cyclophosphamide, 5-fluorouracil, ascorbic acid, uric acid, citric acid, bovine serum albumin, glucose, starch, Na^{+}, K^{+}, Mg^{2+}, NH_4^{+}, Cl^{-}, PO_4^{3-}.	**Analytical signal:** ifosfamide oxidation (E_p ≈ +0.25 V *vs* Ag|AgCl|KCl_{sat}).	[41]
melphalan 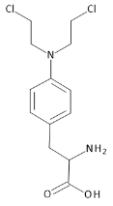	RD-GCE	DPV	100.0 mM H_2SO_4	1.0 µM – 10.0 µM 10.0 µM – 100.0 µM 100.0 µM – 1.0 mM	LOD = 1.0 µM	N/A	N/A	**Analytical signal:** melphalan oxidation (E_p ≈ +0.8 V *vs* SCE).	[70]
	MIP(p-(3-TAA)) / AuE	DPV	KCl	N/A	LOD = 17.7 nM	**Real sample:** pharmaceutical formulation.	**Tested interfering agents**: baclofen, 3-aminosalicylic acid, L-phenylalanine, 4-aminosalicylic acid, 5-aminosalicylic acid.	**Analytical signal:** melphalan oxidation (E_p ≈ +0.2 V *vs* Ag|AgCl).	[49]
bendamustine	AP-PGE	DPV	100.0 mM BRB, pH 5.0	1.4 µM – 22.3 µM	LOD = 1.7 µM LOQ = 5.6 µM	The interaction of bendamustine with DNA in the absence and presence of quercetin.	N/A	**Analytical signal:** bendamustine oxidation (E_p ≈ +0.65 V *vs* Ag|AgCl|$KCl_{3M\ KCl}$).	[56]

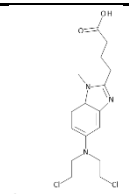									
Alkyl sulfonates									
busulfan 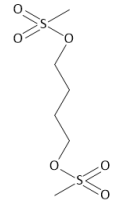	dsDNA / SPCE	CV, DPV	20.0 mM TrisB, pH 7.0, containing 100.0 mM crystal violet	N/A	N/A	The interaction between busulfan and dsDNA in the absence and presence of crystal violet.	N/A	**Analytical signal:** indirect cyclophosphamide detection by monitoring the increase in the oxidation peak currents of guanine ($E_{p\ guanine}$ ≈ +0.7 V *vs* Ag|AgCl-pseudoRE) and adenine ($E_{p\ adenine}$ ≈ +1.0 V *vs* Ag|AgCl-pseudoRE).	[57]
Nitrosoureas									
fotemustine 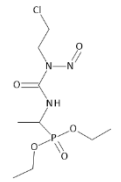	HMDE	DPAdSV	120.0 mM BB in KCl, pH 10.0	600.0 pM – 80.0 nM	LOD = 140.0 pM LOQ = 610.0 pM	**Real sample:** spiked blood serum.	N/A	**Analytical signal:** fotemustine reduction (E_p ≈ –0.5 V *vs* Ag|AgCl). The method based on the derivatization of fotemustine by means of diazotization and coupling reactions (coupling reagent: 1-naphthol).	[71]
streptozocin (streptozotocin) 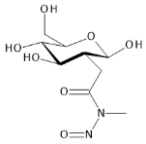	HMDE	DPV	400.0 mM BRB, pH 6.0	200.0 nM – 100.0 µM	LOD = 70.0 nM LOQ = 240.0 nM	N/A	N/A	**Analytical signal:** streptozocin reduction	[72]
lomustine 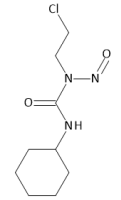	m-AgSAE	DPV	50.0 mM AcB, pH 4.0 and MeOH (9:1)	200.0 nM – 100.0 µM	LOD = 660.0 nM LOQ = 2.2 µM	**Real sample:** pharmaceutical formulation.	N/A	**Analytical signal:** lomustine reduction (E_p ≈ –0.8 V *vs* Ag|AgCl|$KCl_{1M\ KCl}$).	[72]
	HgF / PGE	SWCAdSV	BRB, pH 5.0 containing 500.0 mM SO_4^{2-}	192.0 nM – 13.6 µM	LOD = 81.3 nM LOQ = 271.0 nM	**Real sample:** spiked blood, spiked urine.	**Tested interfering agents:** oxalic acid, glutaric acid, D-sucrose, phenylalanine, ascorbic acid, uric acid, EDTA, Ca^{2+}, Fe^{3+}, Pb^{2+}, Cu^{2+}, Ni^{2+}, Zn^{2+}, Mg^{2+}.	**Analytical signal:** lomustine reduction (E_p ≈ –0.95 V *vs* Ag|AgCl|KCl_{sat}). Proposed electrochemical reduction mechanism of lomustine.	[73]
carmustine	HMDE	DPV	400.0 mM BRB, pH 2.2	200.0 nM – 100.0 µM	LOD = 190.0 nM LOQ = 620.0 nM	N/A	N/A	**Analytical signal:** carmustine reduction.	[72]
	m-AgSAE	DPV	400.0 mM BRB, pH 7.0	200.0 nM – 100.0 µM	LOD = 210.0 nM LOQ = 710.0 nM	**Real sample:** pharmaceutical formulation.	N/A	**Analytical signal:** carmustine reduction (E_p ≈ –1.05 V *vs* Ag|AgCl|$KCl_{1M\ KCl}$).	[72]

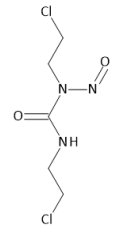									
Other alkylating agents									
dacarbazine 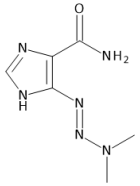	HMDE	DPAdSV	100.0 mM $HClO_4$	5.0 nM – 10.0 µM	LOD = 4.0 nM	**Real sample:** spiked blood serum.	N/A	**Analytical signal:** dacarbazine reduction (E_p ≈ –0.75 V *vs* SCE).	[74]
	HMDE	SWCSV	80.0 mM BRB, pH 7.2	400.0 pM – 21.1 nM	LOD = 277.0 pM LOQ = 923.0 pM	**Real sample:** pharmaceutical formulation, spiked urine, spiked blood serum. The interaction of dacarbazine and dacarbazine-Cu^{2+} complex with dsDNA.	**Tested interfering agents:** alanine, oxalic acid, glutaric acid, ascorbic acid, phenylalanine, Mg^{2+}, Pb^{2+}, Ni^{2+}, Cd^{2+}, Ca^{2+}, Ba^{2+}, Co^{2+}, Zn^{2+}.	**Analytical signal:** reduction of the dacarbazine-Cu^{2+} complex (E_p ≈ –0.4 V *vs* Ag|AgCl|KCl_{sat}).	[75]
	MWCNTs / CPE	DPV	100.0 mM PB, pH 2.0	400.0 pM – 40.0 nM 40 nM – 2.5 µM	LOD = 120.0 pM LOQ = 400.0 pM	**Real sample:** pharmaceutical formulation.	**Tested interfering agents**: uric acid, dopamine, ascorbic acid.	**Analytical signal:** dacarbazine oxidation (E_p ≈ +1.0 V *vs* SCE).	[42]
	MWCNTs – $(CuFe_2O_4)$NPs / CPE	DPV	100.0 mM PB, pH 5.0	100.0 nM – 76.0 µM	LOD = 80.0 nM	**Real sample:** pharmaceutical formulation, spiked blood plasma, spiked urine.	**Tested interfering agents**: glucose, ascorbic acid, cysteine, alanine, phenylalanine, methionine, sucrose, glycine, uric acid.	**Analytical signal:** dacarbazine oxidation (E_p ≈ +0.8 V *vs* Ag|AgCl|KCl_{3M}).	[38]
	SDS / CPE	DPV	200.0 mM PBS, pH 6.2	1.0 µM – 4.0 µM	LOD = 150.0 nM	N/A	**Tested interfering agents**: citric acid, oxalic acid, glucose, starch, succinic acid.	**Analytical signal:** dacarbazine oxidation (E_p ≈ +0.65 V *vs* SCE). Possible simultaneous determination of dacarbazine with doxorubicin. Proposed electrochemical oxidation mechanism of dacarbazine.	[76]
	p-ATD / f(-COOH)MWCNTsPE	DPV	BRB, pH 6.0	50.0 nM – 24.0 µM	LOD = 35.0 nM	**Real sample:** pharmaceutical formulation (injection), spiked urine.	**Tested interfering agents:** dopamine, 5-hydroxytryptamine.	**Analytical signal:** dacarbazine oxidation (E_p ≈ +0.65 V *vs* Ag|AgCl|KCl_{3M}).	[43]
	$(Sn\text{-}CeO_2)$NPs / GCPE	SWV	200.0 mM PB, pH 4.0	640.0 nM – 6.7 µM	LOD = 3.8 nM	**Real sample:** pharmaceutical formulation, spiked blood serum, spiked urine.	**Tested interfering agents**: ascorbic acid, uric acid, alanine, cysteine, glucose, citric acid, uracil, serine.	**Analytical signal:** dacarbazine oxidation (E_p ≈ +0.95 V *vs* Ag|AgCl|KCl_{sat}).	[39]
	p-Cyn – GCMPs / PGE	SWV	100.0 mM H_2SO_4	70.0 nM – 5.0 µM	LOD = 12.8 nM LOQ = 38.8 nM	N/A	**Tested interfering agents**: mannitol, citric acid, sodium chloride, dextrose.	**Analytical signal:** dacarbazine oxidation (E_p ≈ +1.0 V *vs* Ag|AgCl|KCl_{sat}).	[77]

	MIP(N-ABA – DAU – APS) – f(-COOH)MWCNTs / PGE	DPASV	100.0 mM BB, pH 5.2	548.9 pM – 278.9 nM	LOD = 109.8 pM	**Real sample:** pharmaceutical formulation, spiked blood plasma, spiked urine.	**Tested interfering agents**: ascorbic acid, glutamic acid, phenylalanine, cysteine, alanine, histidine, temozolomide, ifosfamide, chlorambucil, structurally identical typical metabolite of dacarbazine.	**Analytical signal:** dacarbazine oxidation (E_p ≈ +0.65 V *vs* Ag|AgCl).	[44]
	OMNiDIP (aTACoPC – AIBN) – RGO / CCE	DPASV	100.0 mM BB, pH 5.0	362.3 pM – 199.7 nM	LOD = 76.9 pM	**Real sample:** pharmaceutical formulation, spiked blood serum, spiked urine.	**Tested interfering agents**: cytarabine, 5-fluorouracil, ifosfamide, melphalan, temozolomide, alanine, ascorbic acid, cysteine, glutamic acid, histidine, phenylalanine, glucose, uric acid, dopamine, dacarbazine.	**Analytical signal:** dacarbazine oxidation (E_p ≈ +0.65 V *vs* Ag|AgCl). Possible simultaneous determination of dacarbazine with chlorambucil.	[45]
	dsDNA / AP-SPCE	DPV	200.0 mM PBS, pH 7.4	N/A	LOD = 20.0 nM LOQ = 59.0 nM	**Real sample:** spiked blood serum. The interaction of dacarbazine with dsDNA.	N/A	**Analytical signal:** dacarbazine oxidation (E_p ≈ +0.35 V *vs* Ag|AgCl-pseudoRE).	[58]
temozolomide 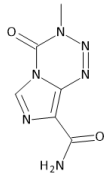	PGE	DPV	50.0 mM PB, pH 7.4, containing 20.0 mM NaCl.	206.0 µM – 515.1 µM	LOD = 31.4 µM	The interaction of temozolomide with ssDNA and dsDNA.	N/A	**Analytical signal:** temozolomide oxidation ($E_{p\ guanine}$ ≈ +0.4 V *vs* Ag|AgCl|KCl_{3M}).	[64]
	MIP(MAC – EGDMA – BDC) – RGO – AgNCs / SPCE	DPASV	100.0 mM PB, pH 7.1	5.6 nM – 742.8 nM	LOD = 824.1 pM	**Real sample:** pharmaceutical formulation, spiked human blood plasma, spiked urine.	**Tested interfering agents**: dacarbazine, ifosfamide, ascorbic acid, dopamine, cyclophosphamide, chlorambucil, histidine, cysteine, phenylalanine, 5-amino-4-imidazolecarboxamide.	**Analytical signal:** temozolomide oxidation (E_p ≈ +0.2 V *vs* Ag|AgCl-pseudoRE).	[46]

Modification: AgNCs – silver nanocubes; **AIBN** – 2-20-azobis (isobutyronitrile); **APS** – ammonium persulphate; **aTACoPC** – acryloylated tetraamine cobalt phthalocyanine; **BDC** – benzyl N,N-diethyldithiocarbamate; **BMIM-BF_4** – 1-butyl-3-methylimidazolium tetrafluoroborate; **Chit** – chitosan; **CYP2B6** –- enzyme of cytochrome P450 2B6; **CYP3A4** – cytochrome P450 3A4; **DAU** – 1, 3-diacryloylurea; **dsDNA** – double-stranded deoxyribonucleic acid; **EGDMA** – ethylene glycol dimethacrylate; **f(-COCl)GQDs** – functionalized (acyl chloride) graphene quantum dots; **f(-COOH)MWCNTs** – functionalized (carboxyl) multi-walled carbon nanotubes; **GCMPs** – glassy carbon microparticles; **HgF** – mercury film; **IL** – ionic liquid; **MAC** – N-methacryloyl-L-cysteine; **MBAA** – N,N-methylenebisacrylamide; **MIP** – molecularly imprinted polymer; **MWCNTs** – multi-walled carbon nanotubes; **MX** – MXene; **N,S-ARGO** – nitrogen and sulfur co-doped activated reduced graphene oxide; **N-ABA** – N-acryloyl-4-aminobenzamide; **N-ABA** – N-acryloylamino butyric acid; **OMNiDIP** – one MoNomer dual imprinted polymer; **p-(3-TAA)** – poly-(3-thiophene acetic acid); **p-(L-Cys)** – poly-(L-cysteine); **p-(o-APh)** – poly-(o-aminophenol); **p-ATD** – poly-(2-amino-1,3,4-thiadiazole); **p-Cyn** – poly-cyanidin; **RGO** – reduced graphene oxide; **SDS** – sodium dodecyl sulfate; **ssDNA** – single-stranded deoxyribonucleic acid; **Ti_3C_2** – titanium (IV) carbide; **Vi-C_{60}-MA** – vinylic-C_{60}-monoadduct; **(Au-Pd)NPs** – gold and palladium nanoparticles; **($CuFe_2O_4$)NPs** – copper-doped ferrite nanoparticles; **(MnO_2-$NiFe_2O_4$)NPs** – core-shell nanocomposite of manganese dioxide and nickel ferrite nanoparticles; **(p-NVCL-p-Py)MGs** – poly-(N-vinylcaprolactam) and poly-pyrrole microgels; **(Sn-CeO_2)NPs** – tin-doped cerium dioxide nanoparticles.

Electrode: AP-CPE – anodically pretreated carbon paste electrode; **AP-PGE** – anodically pretreated pencil graphite electrode; **AP-SPCE** – anodically pretreated screen-printed carbon (graphite) electrode;**AuE** – gold electrode; **CCE** – carbon (graphite) ceramic electrode; **CPE** – carbon (graphite) paste electrode; **f(-COOH)MWCNTsPE** – functionalized (carboxyl) multi-walled carbon nanotubes paste electrode; **GCE** – glassy carbon electrode; **GCPE** – glassy carbon paste electrode; **GE** – graphite electrode; **HMDE** – hanging mercury drop electrode; **m-AgSAE** – meniscus modified silver solid amalgam electrode; **PGE** – pencil graphite electrode; **RD-GCE** – rotating disk glassy carbon electrode; **SMDE** – static mercury drop electrode; **SPCE** – screen-printed carbon (graphite) electrode; **SPCPE** – screen-printed carbon (graphite) paste electrode; **(Pd-Ag)A-MW** – palladium-silver alloy microwire.

Technique: AdSV – adsorptive stripping voltammetry; **CV** – cyclic voltammetry; **DPAdSV** – differential pulse adsorptive stripping voltammetry; **DPASV** – differential pulse anodic stripping voltammetry; **DPV** – differential pulse voltammetry; **SWCAdSV** – square-wave cathodic adsorptive stripping voltammetry; **SWCSV** – square-wave cathodic stripping voltammetry; **SWV** – square-wave voltammetry.

Medium: AcB – acetate buffer; **BB** – borate buffer; **BRB** – Britton-Robinson buffer; **PB** – phosphate buffer; **PBS** – phosphate buffered saline; **TrisB** – tris(hydroxymethyl)aminomethane hydrochloride buffer.

Selectivity: when underlined – exhibited interference.

Comments: Ag|AgCl – silver|silver chloride electrode; **Ag|AgCl-pseudoRE** – silver|silver chloride pseudo-reference electrode; **AgE** – silver electrode; **SCE** – saturated calomel electrode.

N/A – not applicable.

Table 2. Comprehensive electroanalytical overview for the ANAs belonging to the group of antimetabolites.

Drug and its structure	Modification / Electrode	Technique	Medium	Linear range	LOD/LOQ	Application	Selectivity	Comments	Ref
Folic acid analogs									
methotrexate 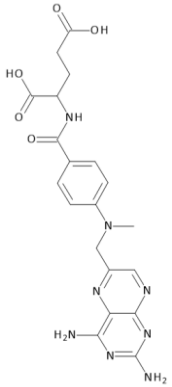	HMDE	LSAdSV	50.0 mM PB, pH 2.5	25.0 nM – 250.0 nM	N/A	**Real sample:** spiked urine.	**Tested interfering agents:** sodium dodecyl sulfate, chlorambucil, 6-fluorouracil, gelatin.	**Analytical signal:** methotrexate reduction (E_p ≈ – 0.5 V *vs* Ag|AgCl|KCl_{sat}).	[126]
	HMDE	DPAdCSV	10.0 mM PB, pH 7.0	350.0 pM – (~)5.5 nM	LOD = 350.0 pM	**Real sample:** spiked blood serum.	**Tested interfering agents:** sodium dodecyl sulfate, 5-fluorouracil, folinic acid.	**Analytical signal:** methotrexate reduction (E_p ≈ – 0.6 V *vs* Ag|AgCl|Cl^-_{3M}).	[127]
	HMDE	AdSV	BRB, pH 4.5	880.0 pM – 1.0 µM	N/A	**Real sample:** spiked blood plasma.	**Tested interfering agents:** folic acid, folinic acid, chlorpromazine, vincristine, dixyrazine, oxytetracycline, metachloropramidine.	**Analytical signal:** methotrexate reduction (E_p ≈ – 0.7 V *vs* SCE).	[128]
	m-AgSAE	DPV	40.0 mM BRB, pH 5.0	2.0 nM – 1.0 µM	LOD = 1.8 nM LOD = 2.6 nM	**Real sample:** pharmaceutical formulation	N/A	**Analytical signal:** methotrexate reduction (E_p ≈ – 0.3 V *vs* Ag|AgCl|KCl_{sat}). Proposed electrochemical reduction mechanism of methotrexate.	[130]
	p-AgSAE	DPAdSV	AcB, pH 5.0	1.0 nM – 3.0 µM	LOD = 150.0 pM LOQ = 220.0 pM	**Real sample:** pharmaceutical formulation.	N/A	**Analytical signal:** methotrexate reduction (E_p ≈ – 0.35 V *vs* Ag|AgCl|KCl_{sat}).	[129]
	HgF / CFBUME	ACAdSV	AcB, pH 5.0	500.0 pM – 20.0 nM	LOD = 500.0 pM	**Real sample:** spiked urine.	**Tested interfering agents:** gelatin, Triton X-100, cetyltrimethylammonium chloride, sodium dodecyl sulfate.	**Analytical signal:** methotrexate reduction.	[131]
	BDDE	DPV	50.0 mM H_2SO_4	50.0 nM – 20.0 µM	LOD = 10.0 nM	**Real sample:** pharmaceutical formulation, spiked urine.	**Tested interfering agents:** ascorbic acid, barbituric acid, oxalic acid, citric acid, tartaric acid, folic acid, uric acid, sucrose, glucose, urea, creatinine, leucovorin, K^+, Na^+, Zn^{2+}, Ca^{2+}, Mg^{2+}, Fe^{2+}, Fe^{3+}, Cl^-, SO_4^{2-}, PO_4^{3-}, CH_3COO^-.	**Analytical signal:** methotrexate oxidation (E_p ≈ +1.0 V *vs* Ag|AgCl|KCl_{sat}).	[160]
	GCE	SWV	200.0 mM AcB, pH 3.6	800.0 nM – 20.0 µM	LOD = 350.0 nM	**Real sample:** spiked urine.	**Tested interfering agents:** oxalic acid, uric acid, ascorbic acid, glucose, sucrose, L-valine, L-histidine, L-serine, L-threonine, L-arginine, Zn^{2+}, K^+, Ca^{2+}, Mg^{2+}, Fe^{3+}, Fe^{2+}, Cl^-, SO_4^{2-}, PO_4^{3-}, Ac^-.	**Analytical signal:** methotrexate oxidation (E_p ≈ +0.85 V *vs* SCE). Proposed electrochemical oxidation mechanism of methotrexate.	[161]
	ERGO – MWCNTs / GCE	DPV	100.0 mM PB, pH 6.0	700.0 nM – 10.0 µM 10.0 µM – 100.0 µM	LOD = 70.0 nM	**Real sample:** pharmaceutical formulation (tablets), spiked blood serum.	**Tested interfering agents:** ascorbic acid, dopamine, uric acid.	**Analytical signal:** methotrexate oxidation (E_p ≈ +0.75 V *vs* Ag|AgCl).	[162]
	(Ce-ZnO)NFLs / GCE	DPV	100.0 mM PBS, pH 7.0	10.0 nM – 500.0 µM	LOD = 6.3 nM	**Real sample:** pharmaceutical formulation	**Tested interfering agents:**	**Analytical signal:** methotrexate oxidation (E_p ≈ +0.75 V *vs* SCE).	[163]

						(injection), spiked blood serum, spiked urine.	uric acid, rutin, ascorbic acid, glucose, tyrosine, tryptophan, morphine.	Possible simultaneous determination of methotrexate and epirubicin.	
	NiONPs – NAF / GCE	Amp.	40.0 mM BRB, pH 2.0	10.0 nM – 70.0 nM	LOD = 100.0 pM LOQ = 1.3 nM	**Real sample:** pharmaceutical formulation.	**Tested interfering agents:** 5-fluorouracil, mitoxantrone, glucose, sucrose, urea, Cl^-.	**Applied potential in amperometry:** E = +0.95 V *vs* Ag|AgCl. Proposed electrochemical oxidation mechanism of methotrexate.	[82]
	CuNPs – CB – NAF / GCE	SWV	100.0 mM BRB, pH 3.0	2.2 µM – 25.0 µM	LOD = 95.0 nM	**Real sample:** spiked urine, spiked river water.	**Tested interfering agents:** urea, KCl, NaCl, KH_2PO_4, $CaCl_2$, NH_4Cl.	**Analytical signal:** methotrexate oxidation (E_p ≈ +0.9 V *vs* Ag|AgCl|KCl_{3M}). Determination of methotrexate was performed in the presence of doxorubicin (2.0 µM). Proposed electrochemical oxidation mechanism of methotrexate.	[164]
	(Pd-Ag)A – N-RGO / GCE	DPV	100.0 mM PB, pH 5.8	20.0 nM – 200.0 µM	LOD = 1.3 nM	**Real sample:** spiked urine.	**Tested interfering agents:** uric acid, ascorbic acid, glucose, dopamine.	**Analytical signal:** methotrexate oxidation (E_p ≈ +0.8 V *vs* Ag|AgCl|$NaCl_{3M}$).	[165]
	$(CoFe_2O_4)$NPs – RGO – IL (HMIM-PF_6) / GCE	DPV	100.0 mM PB, pH 2.5	50.0 nM – 7.5 µM	LOD = 10.0 nM	**Real sample:** pharmaceutical formulation (tablet).	**Tested interfering agents:** tartaric acid, dopamine, glucose, ascorbic acid, vitamin B_6, vitamin B_1, sucrose, Mg^{2+}, NH_4^+, Ca^{2+}, Fe^{3+}.	**Analytical signal:** methotrexate oxidation (E_p ≈ +0.8 V *vs* Ag|AgCl|KCl_{sat}).	[166]
	p-(p-ABSA) – f(Q)MWCNTs / GCE	DPV	PB, pH 7.0	100.0 nM – 8.0 µM	LOD = 15.0 nM	**Real sample:** spiked urine.	**Tested interfering agents:** ascorbic acid, uric acid, glucose, citric acid, tartaric acid, Na^+, K^+, NH_4^+, Ca^{2+}, Mg^{2+}, NO_3^-, SO_4^{2-}, Cl^-.	**Analytical signal:** methotrexate oxidation (E_p ≈ +0.85 V *vs* Ag|AgCl|KCl_{sat}). Determination of methotrexate in the presence of folinic acid (8.0 µM).	[167]
	p-(L-Lys) / GCE	SWV	100.0 mM PB, pH 2.0	5.0 nM – 200.0 nM	LOD = 1.7 nM	**Real sample:** pharmaceutical formulation (tablet).	**Tested interfering agents:** glucose, phenylalanine, alanine, leucine, cysteine, ascorbic acid, uric acid, Na^+, K^+, Zn^{2+}, Cl^-, Mg^{2+}, NO_3^-, SO_4^{2-}.	**Analytical signal:** methotrexate oxidation (E_p ≈ +0.85 V *vs* SCE). Determination of methotrexate in the presence of sodium dodecylbenzene sulfonate (100.0 µg mL^{-1}). Proposed electrochemical oxidation mechanism of methotrexate.	[168]
	AuNPs – p-(L-Cys) / GCE	SWASV	BRB, pH 2.0	40.0 nM – 2.0 µM	LOD = 10.0 nM	**Real sample:** pharmaceutical formulation (tablets), spiked blood serum.	**Tested interfering agents:** folic acid, epinephrine, dopamine, uric acid, glucose, sucrose, citric acid, tartaric acid, ascorbic acid, Zn^{2+}, Cl^-, SO_4^{2-}, PO_4^{3-}, Ac^-.	**Analytical signal:** methotrexate oxidation (E_p ≈ +0.95 V *vs* SCE). Proposed electrochemical oxidation mechanism of methotrexate.	[169]
	Pr_2O_3NPs – (p-Styr)MS / GCE	DPV	100.0 mM PB, pH 7.0	10.0 nM – 236.0 µM	LOD = 800.0 pM	**Real sample:** spiked blood serum, spiked urine.	**Tested interfering agents:** glucose, chlorpromazine, Br^-, Mg^{2+}, SO_4^{2-}, Ca^{2+}, Na^+, Co^{2+}, I^-.	**Analytical signal:** methotrexate oxidation (E_p ≈ +0.95 V *vs* Ag|AgCl). Proposed electrochemical oxidation mechanism of methotrexate.	[170]
	SiO_2NPs – p-DA / GCE	DPV	100.0 mM PB, pH 6.0	50.0 nM – 14.0 µM	LOD = 10.0 nM	**Real sample:** spiked blood serum.	**Tested interfering agents:**	**Analytical signal:**	[171]

							ascorbic acid, uric acid, folinic acid, tetrahydrofolic acid, pyridoxine, dopamine, 5-methyltetrahydrofolate,.	methotrexate oxidation (E_p ≈ +0.65 V *vs* Ag|AgCl). Proposed electrochemical oxidation mechanism of methotrexate.	
	PTC – p-EI – MoS_2NFLs / GCE	ECL	100.0 mM PBS containing 10.0 mM $K_2S_2O_8$, pH 7.4	1.0 pM – 10.0 µM	LOD = 150.0 fM	**Real sample:** spiked blood serum.	**Tested interfering agents:** ascorbic acid, uric acid, urea, glucose, L-lysine, L-cysteine, tryptophan, leucine, lactose, KCl, $CaCl_2$, Na_2CO_3, Na_2SO_4, $MgSO_4$.	**Analytical signal:** ECL reaction between perylenetetracarboxylic acid and $S_2O_8^{2-}$ *via* catalyzing the electrochemical reduction of peroxydisulfate ion to produce sulfate radical anions.	[149]
	Gr-C_3N_4 – CHIT – SnS_2NPLs / GCE	ECL	100.0 mM PBS containing 5.0 mM $K_2S_2O_8$, pH 7.4	1.0 pM – 10.0 µM	LOD = 270.0 fM	**Real sample:** spiked blood serum.	**Tested interfering agents:** uric acid, ascorbic acid, glucose, glycine, leucine, L-arginine, tryptophan, cysteine, KCl, $CaCl_2$, Na_2CO_3, Na_2SO_4, $MgSO_4$, $CuSO_4$.	**Analytical signal:** ECL reaction between graphite-like carbon nitride and $S_2O_8^{2-}$ *via* catalyzing the electrochemical reduction of peroxydisulfate ion to produce sulfate radical anions.	[150]
	(CFL-Ho^{3+}-NiO)NPs / GCE	DPV	100.0 mM PBS, pH 7.0	1.0 nM – 310.0 µM	LOD = 5.2 nM	**Real sample:** pharmaceutical formulation (ampoule), spiked blood serum, spiked urine.	**Tested interfering agents:** uric acid, rutin, ascorbic acid, glucose, tyrosine, tryptophan, morphine, Fe^{3+}, Fe^{2+}, Al^{3+}, Mg^{2+}.	**Analytical signal:** methotrexate oxidation (E_p ≈ +0.7 V *vs* SCE). Possible simultaneous determination of methotrexate and carbamazepine.	[172]
	β-CD – GO / GCE	DPV	100.0 mM PB, pH 6.0	100.0 nM – 1.0 µM	LOD = 20.0 nM	N/A	**Tested interfering agents:** ascorbic acid, uric acid.	**Analytical signal:** methotrexate oxidation (E_p ≈ – 0.6 V *vs* SCE).	[173]
	GrO – NAF / GCE	CV with accumulation step	30.0 mM $HClO_4$	400.0 nM – 20.0 µM	LOD = 9.0 nM	**Real sample:** pharmaceutical formulation (injection), spiked urine.	**Tested interfering agents:** oxalic acid, glucose, sucrose, citric acid, tartaric acid, uric acid, ascorbic acid, Na^+, K^+, Zn^{2+}, Mg^{2+}, Ca^{2+}, Fe^{3+}, Fe^{2+}, Cl^-, SO_4^{2-}, NO_3^-, CO_3^{2-}, Ac^-.	**Analytical signal:** methotrexate oxidation (E_p ≈ +0.95 V *vs* SCE).	[174]
	dsDNA / GCE	CCPSV	160.0 mM AcB, pH 4.2, containing 20% EtOH	2.0 µM – 3.6 µM	LOD = 2.0 µM	N/A	N/A	**Analytical signal:** indirect methotrexate sensing by monitoring the decrease in guanine oxidation peak current (E_p ≈ +0.9 V *vs* Ag|AgCl).	[143]
	dsDNA – ODA / AP-GCE	SWV	BRB, pH 2.0	20.0 nM – 4.0 µM	LOD = 5.0 nM	**Real sample:** spiked blood serum, spiked urine.	**Tested interfering agents:** ascorbic acid, oxalic acid, uric acid, glucose, sucrose, citric acid, tartaric acid, Zn^{2+}, K^+, Ca^{2+}, Mg^{2+}, Fe^{3+}, Na^+, Fe^{2+}, Cl^-, SO_4^{2-}, Ac^-, PO_4^{3-}.	**Analytical signal:** methotrexate oxidation (E_p ≈ +0.9 V *vs* SCE). Proposed electrochemical oxidation mechanism of methotrexate.	[175]
	DNA – GO / GCE	DPAdSV	100.0 mM AcB, pH 4.6	58.0 nM – 2.2 µM	LOD = 7.6 nM	**Real sample:** pharmaceutical formulation, spiked urine.	**Tested interfering agents:** uric acid and citric acid, glucose, lysine, ascorbic acid, dopamine, K^+, Ca^{2+}, Mg^{2+}, Fe^{3+}, Al^{3+}, Ni^{2+}, Cl^-, SO_4^{2-}, CO_3^{2-}, NO_3^-, PO_4^{3-}.	**Analytical signal:** indirect methotrexate sensing by monitoring the decrease in guanine oxidation peak current (E_p ≈ +0.7 V).	[144]
	dsDNA – SWCNTs – NAF / GCE	SWASV	BRB, pH 2.8	20.0 nM – 1.5 µM	LOD = 8.0 nM	**Real sample:** pharmaceutical formulation (tablets), spiked blood serum.	**Tested interfering agents:** glucose, glutamic acid, uric acid, epinephrine, dopamine, norepinephrine, K^+, Na^+, Ca^{2+}, Al^{3+}, NH_4^+, Hg^{2+}, Pb^{2+}, Zn^{2+}, Cd^{2+}, Cl^-, PO_4^{3-}, Ac^-.	**Analytical signal:** methotrexate oxidation (E_p ≈ +0.95 V *vs* Ag|AgCl|KCl_{sat}). Proposed electrochemical oxidation mechanism of methotrexate.	[176]

	AuNPs – f(–COOH)MWCNTs – CTAB – ZnONPs / SPCE	SWV	100.0 mM AcB, pH 4.5	20.0 μM – 1.0 μM	LOD = 10.0 nM	**Real sample:** pharmaceutical formulation (injection), spiked blood.	**Tested interfering agents:** glucose, dopamine, ascorbic acid, uric acid.	**Analytical signal:** methotrexate oxidation (E_p ≈ +0.75 V *vs* Ag|AgCl). Determination of methotrexate in the presence of epirubicin (5.0 nM).	[177]
	WP-N-f(–COOH)MWCNTs – NAF / SPCE	DPV	100.0 mM PB, pH 6.0	10.0 nM – (~)80 nM (~)80 nM – 540.0 μM	LOD = 45.0 nM	**Real sample:** spiked blood.	**Tested interfering agents**: glycine, cysteine, lysine, tryptophan, uric acid, citric acid, ascorbic acid, dopamine, glucose, K^+, Na^+, Ca^{2+}, Mg^{2+}, Zn^{2+}, Fe^{2+}, Fe^{3+}, Cl^-, NO_3^-, SO_4^{2-}.	**Analytical signal:** methotrexate oxidation (E_p ≈ +0.75 V *vs* Ag|AgCl).	[178]
	β-CD – MWCNTs / SPE	DPV	100.0 mM AcB, pH 4.0	100.0 nM – 5.0 μM 5.0 μM – 1.0 mM	LOD = 35.0 nM	**Real sample:** spiked rabbit blood plasma.	**Tested interfering agents:** dopamine, ascorbic acid, glucose.	**Analytical signal:** methotrexate oxidation (E_p ≈ +0.8 V). Multianalyte (methotrexate, urea, uric acid, lactate dehydrogenase) quantification based on the microfluidic technique and electrochemical sensor array.	[83]
	f(–COOH)MWCNTs / CPE	DPV	PB, pH 3.2	400.0 nM – 5.5 μM	LOD = 400.0 nM	**Real sample**: pharmaceutical formulation, spiked blood serum, spiked undiluted (artificial) urine.	**Tested interfering agents**: ascorbic acid, uric acid, dopamine, serotonin.	**Analytical signal:** methotrexate oxidation (E_p ≈ +0.75 V *vs* Ag|AgCl|KCl_{3N}).	[179]
	$(CuCr_2O_4$-CuO)NFBs – IL (BMIM-Br) / CPE	DPSV	100.0 mM BRB, pH 2.5	100.0 nM – 20.0 μM 20.0 μM – 300.0 μM	LOD = 25.0 nM	**Real sample:** spiked blood, spiked urine.	**Tested interfering agents:** dopamine, ascorbic acid, uric acid, citric acid, glucose, alanine, cysteine, Ca^{2+}, Mg^{2+}, Cl^-, NH_4^+, Fe^{3+}.	**Analytical signal:** methotrexate oxidation (E_p ≈ +1.0 V *vs* Ag|AgCl). Proposed electrochemical oxidation mechanism of methotrexate.	[180]
	L-Glox / CPE	Amp.	100.0 mM PB, pH 7.0	80.0 pM – 1.0 nM	4.0 fM	**Real sample:** pharmaceutical formulations (tablets, injections).	N/A	**Applied potential in amperometry:** E = +0.15 V *vs* Ag|AgCl. Determination of the enantiopurity of methotrexate. Determination of L-methotrexate.	[151]
	L-AAOD / CPE	Amp.	100.0 mM PB, pH 7.0	40.0 fM – 80.0 fM	10.0 fM	**Real sample:** pharmaceutical formulations (tablets, injections).	N/A	**Applied potential in amperometry:** E = +0.012 V *vs* Ag| AgCl. Determination of the enantiopurity of methotrexate. Determination of D-methotrexate.	[151]
	BiF / CuE	DPAdSV	100.0 mM PB, pH 6.0	12.0 nM – 1.7 μM	LOD = 900.0 pM	**Real sample:** pharmaceutical formulation.	**Tested interfering agents:** lactose, tartrazine, sodium stearate, starch.	**Analytical signal:** methotrexate oxidation (E_p ≈ – 0.7 V *vs* Ag|AgCl|$KCl_{3\ M}$). Proposed electrochemical oxidation mechanism of methotrexate.	[181]
	pTHMMAA – IgG-Mtx-Ab – GTA – CyA / AuE	EIS-MVA	PB, pH 7.0	276.0 pM – 270.0 μM	LOD = 165.0 pM	N/A	N/A	**Applied potential:** OCP The electrochemical cell consisted of two modified	[182]

								electrodes placed in a polydimethylsiloxane flow chamber.	
	pTHMMAA – IgG-Mtx-Ab – GTA – CyA / AuE	EIS-MVA	PB, pH 7.0	2.7 pM – 273.0 µM	LOD = 5.0 pM	**Real sample:** spiked blood serum.	N/A	**Applied potential:** E = 0.0 V *vs* Ag|AgCl|KCl_{sat}. The electrochemical cell consisted of two modified electrodes placed in a polydimethylsiloxane flow chamber.	[80]
	pTHMMAA – IgG-Mtx-Ab – NHS – EDC – eGCP / AuE	EIS-MVA	PB, pH 7.0	3.0 pM – 300.0 µM	LOD = 7.0 pM	N/A	N/A	**Applied potential:** E = 0.0 V *vs* Ag|AgCl|KCl_{sat}.	[81]
	Fe_3O_4NPs – p-ANI / ITOE	SWV	PBS, pH 7.4	10.0 fM – 10.0 nM	LOD = 400.0 aM	**Real sample:** spiked blood serum, blood serum collected from patients after their treatment with methotrexate.	N/A	**Analytical signal:** methotrexate oxidation (E_p ≈ –0.35 V *vs* Ag|AgCl).	[79]
	BM – p-VS / ITOE	SWV	AmAcB, pH 3.5	1.5 µM – 50.0 µM	LOD = 595.0 nM LOQ = 1.5 µM	N/A	N/A	**Analytical signal:** methotrexate oxidation (E_p ≈ +0.9 V *vs* SCE). Proposed electrochemical oxidation mechanism of methotrexate.	[183]
pemetrexed 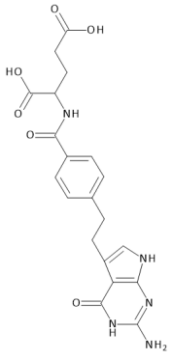	oop-Py – f(–COOH)MWCNTs / GCE	DPAdSV	100.0 mM PBS, pH 7.0	10.0 nM – 100.0 nM	LOD = 3.3 nM LOQ = 9.9 nM	**Real sample:** pharmaceutical formulation (injection).	**Tested interfering agents:** dopamine, ascorbic acid, uric acid, K^+, Ca^{2+}, Na^+, SO_4^{2-}, Cl^-, NO_3^-.	**Analytical signal:** pemetrexed oxidation (E_p ≈ +0.3 V *vs* Ag|AgCl). Proposed electrochemical oxidation mechanism of pemetrexed.	[184]
	PdNPs – CNFBs – IL($[M_3OA]^+[NTF_2]^-$) – NAF / CPE	SWV	100.0 mM PB, pH 6.0	1.0 nM – 35.0 nM	LOD = 330.0 pM LOQ = 990.0 pM	**Real sample:** pharmaceutical formulation (injection Alimta®), spiked cancerous plasma, spiked health urine.	**Tested interfering agents:** glucose, dopamine, caffeine, uric acid, paracetamol, maltose, citric acid, aspirin, ascorbic acid, Na^+, K^+, Mg^{2+}, Ca^{2+}, I^-, Cl^-.	**Analytical signal:** pemetrexed oxidation (E_p ≈ +0.3 V *vs* Ag|AgCl|KCl_{sat}). Proposed electrochemical oxidation mechanism of pemetrexed.	[84]
	MIP(o-PD) – CQDs / SPCE	DPV	AcB, pH 5.2	5.0 nM – 100.0 nM	LOD = 1.6 nM LOQ = 4.9 nM	**Real sample:** spiked synthetic urine.	**Tested interfering agents:** guanine, sulpiride, ascorbic acid.	**Analytical signal:** pemetrexed oxidation (E_p ≈ +0.3 V *vs* Ag|AgCl|KCl_{3M}).	[185]
Purine analogs									
6-mercaptopurine 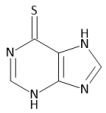	HCuADE	DPAdCSV	100.0 mM $LiClO_4$ and 500.0 mM $HClO_4$	360.0 pM – 5.3 µM	LOD = 120.0 pM	**Real sample:** pharmaceutical formulation (tablets).	**Tested interfering agents:** 6-thioguanine, azathioprine, Br^-, I^-.	**Analytical signal:** 6-mercaptopurine-Cu^{2+} complex reduction (E_p ≈ –0.2 V *vs* Ag|AgCl|KCl_{3M}).	[136]
	AP-BDDE	DPV	40.0 mM BRB, pH 2.0	1.0 µM – 275.0 µM 275.0 µM – 450.0 µM	LOD = 510.0 nM LOQ = 1.7 µM	**Real sample:** pharmaceutical formulation (tablets), spiked urine.	**Tested interfering agents:** starch, microcrystalline cellulose, titanium dioxide, magnesium stearate, ascorbic acid, uric acid, urea. polyvinylpyrrolidone.	**Analytical signal:** 6-mercaptopurine oxidation (E_p ≈ +1.6 V *vs* Ag|AgCl|KCl_{3M}). Proposed electrochemical oxidation mechanism of 6-mercaptopurine.	[186]
	MWCNTs – CTAB / GCE	LSV	200.0 mM PB, pH 3.0	500.0 nM – 3.0 µM	LOD = 8.4 nM LOQ = 28.0 nM	**Real sample:** spiked blood serum, spiked urine.	**Tested interfering agents:** citric acid, gum acacia, dextrose, oxalic acid,	**Analytical signal:** 6-mercaptopurine oxidation (E_p ≈ +1.6 V *vs* Ag|AgCl|KCl_{3M}).	[87]

							starch, tartaric acid, dopamine, ascorbic acid.	Proposed electrochemical oxidation mechanism of 6-mercaptopurine.	
	ERGO – IL(BMIM-PF_6) – CHIT / CSE	FIA-Amp.	100.0 mM PB, pH 7.0, containing 100.0 mM KCl	400.0 nM – 10.0 µM 10.0 µM – 400.0 µM	LOD = 110.0 nM	**Real sample:** pharmaceutical formulation.	N/A	**Applied potential in amperometry:** E = +0.3 V *vs* Ag|AgCl|KCl_{3M}. Proposed electrochemical oxidation mechanism of 6-mercaptopurine.	[187]
	AuNPs – CHIT – GO – IL(BMIM-PF_6) / CSE	AdSV	100.0 mM PB, pH 7.4, containing 1.0 M KCl	0 µM – 20.0 µM 20.0 µM – 200.0 µM	LOD = 30.0 nM	The interaction between dsDNA and 6-mercaptopurine.	N/A	**Analytical signal:** 6-mercaptopurine oxidation (E_p ≈ +0.7 V *vs* Ag|AgCl|KCl_{3M}).	[153]
	MWCNTs / CPE	LSV	pH 4.0	500.0 nM – 1.2 µM 1.2 µM – 900.0 µM	LOD = 100.0 nM	**Real sample:** pharmaceutical formulation (tablet), spiked urine from healthy or non-healthy volunteers (children with chronic lymphocytic leukemia).	**Tested interfering agents:** urea, fructose, glucose, sucrose, lactose, glycin, succinic acid, threonine, methanol, ethanol, thiourea, ascorbic acid, Na^+, NO_3^-, Cl^-.	**Analytical signal:** 6-mercaptopurine oxidation (E_p ≈ +0.55 V *vs* Ag|AgCl|KCl_{sat}). Determination of 6-mercaptopurine performed in the presence of isoprenaline (200.0 µM). Proposed electrochemical oxidation mechanism of 6-mercaptopurine.	[188]
	PtNPs – MWCNTs – IL (BMIM-PF_6) / CPE	SWV	100.0 mM PB, pH 8.0	50.0 nM – 550.0 µM	LOD = 9.0 nM	**Real sample:** pharmaceutical formulation (tablets), spiked urine.	**Tested interfering agents:** sucrose, lactose, methanol, glucose topotecan, 6-thioruric acid, thioguanylic acid, BMS-573188, Al^{3+}, Ca^{2+}, Mg^{2+}, SO_4^{2-}, CO_3^{2-}.	**Analytical signal:** 6-mercaptopurine oxidation (E_p ≈ +0.5 V *vs* Ag|AgCl|KCl). Possible simultaneous determination of 6-thioguanine and dasatinib.	[88]
	(ZnO-CuO)NPLs – 2-CBF / CPE	SWV	100.0 M PBS, pH 7.0	75.0 nM – 10.0 µM 10.0 µM – 500.0 µM	LOD = 45.0 nM	**Real sample:** pharmaceutical formulation, spiked urine.	**Tested interfering agents:** lactose, glucose, methanol, ethanol, fructose, saccharose, benzoic acid, NADH, acetaminophen, uric acid, ascorbic acid, dopamine, epinephrine, norepinephrine, histidine, glycine, tryptophan, phenylalanine, tyrosine, L-asparagine, L-lysine, L-serine, L-threonine, L-proline, Mg^{2+}, Al^{3+}, NH_4^+, Fe^{2+}, Fe^{3+}, F^-, SO_4^{2-}, S^{2-}.	**Analytical signal:** 6-mercaptopurine oxidation (E_p ≈ +0.55 V *vs* Ag|AgCl|KCl_{3M}). Possible simultaneous determination of 6-thioguanine and folic acid.	[189]
	MWCNTs – TiO_2NPs / CPE	DPV	100.0 mM BRB, pH 9.0	90.0 nM – 4.5 µM 4.5 µM – 350.0 µM	LOD = 65.0 nM	**Real sample:** pharmaceutical formulation, spiked urine.	**Tested interfering agents:** glucose, sucrose, lactose, fructose, citric acid, methanol, ethanol, glycine, citric acid, aspartic acid, folic acid, aspirin, Ca^{2+}, Mg^{2+}, SO_4^{2-}, Al^{3+}, NH_4^+, Fe^{2+}, Fe^{3+}, CO_3^{2-}, Cl^-, F^-.	**Analytical signal:** 6-mercaptopurine oxidation (E_p ≈ –0.05 V *vs* Ag|AgCl|KCl_{sat}). Possible simultaneous determination of 6-thioguanine and folic acid.	[190]
	NCCP – AHMT-Ag / CPE	DPV	100.0 mM PB, pH 7.0	12.0 µM – 62.0 µM	LOD = 21.0 nM	**Real sample:** pharmaceutical formulation (tablets), spiked blood serum, spiked urine.	**Tested interfering agents:** ethanol, glucose, starch, ascorbic acid, uric acid, dopamine.	**Analytical signal:** 6-mercaptopurine oxidation (E_p ≈ +0.5 V *vs* Ag|AgCl).	[191]
	[Co(III)-Sal] / MWCNTsPE	DPV	100.0 mM PB, pH 3.0	1.0 µM – 10.0 µM 10.0 µM – 100.0 µM	LOD = 100.0 nM	**Real sample:**	**Tested interfering agents:** ascorbic acid, uric acid.	**Analytical signal:** 6-mercaptopurine oxidation (E_p ≈ +1.6 V *vs* Ag|AgCl|KCl_{sat}).	[192]

						pharmaceutical formulation, spiked plasma.			
	$[Co(phen)_2(tatp)]^{3+}$ – SDS – MWCNTs / GCE	DPV	10.0 mM TrisB, pH 7.2, containing 50.0 mM NaCl	200.0 nM – 200.0 µM	LOD = 50.0 nM	N/A	**Tested interfering agents:** guanine, hypoxanthine, ascorbic acid, Zn^{2+}, Ni^{2+}.	**Analytical signal:** 6-mercaptopurine reduction (E_p ≈ 0.0 V *vs* SCE).	[135]
	$[Co(phen)_3]^{3+}$ – dsDNA – GO / GCE	DPV	10.0 mM TrisB, pH 7.2, containing 50.0 mM NaCl	50.0 µM – 2.0 µM	LOD = 15.0 nM	**Real sample:** spiked blood.	**Tested interfering agents:** 6-benzylaminopurine, 6-furfurylaminopurine, azathioprine, zeatin, glucose, lysine, caffeine, 6-hypoxanthine, ascorbic acid, uric acid, dopamine, K^+, Ca^{2+}, Mg^{2+}, Fe^{3+}, Al^{3+}, Ni^{2+}, Cl^-, SO_4^{2-}, CO_3^{2-}, PO_4^{3-}, NO_3^-.	**Analytical signal:** 6-mercaptopurine reduction (E_p ≈ –0.1 V *vs* Ag|AgCl).	[134]
	MIP(PTEOS – TEOS – TFA – p-Py) – ZnO-GQDs / PGE	DPV	100.0 mM PB, pH 8.0	10.0 nM – 50.0 µM 50.0 µM – 700.0 µM	LOD = 5.7 nM	**Real sample:** pharmaceutical formulation (tablet), spiked blood serum, spiked urine.	**Tested interfering agents:** 6-thioguanine, allopurinol, glucose, sucrose, ascorbic acid, uric acid, citric acid, tartaric acid, K^+, Na^+, Ca^{2+}, Mg^{2+}, NO_3^-, SO_4^{2-}, Cl^-.	**Analytical signal:** 6-mercaptopurine oxidation (E_p ≈ +0.45 V).	[85]
	MIP(N-AAsp – MBA – APS) – PdNPs – N-CSNS (CTAB – RES – TEOS – FM – MeI) – IL(BMIM-BF_4) / PGE	DPASV	100.0 mM PB, pH 5.0	4.1 nM – 508.0 nM	LOD = 722.8 pM	**Real sample:** pharmaceutical formulation, spiked water, spiked blood plasma, spiked urine.	**Tested interfering agents:** chlorambucil, ifosfamide, temozolomide, 5-fluorouracil, 6-thioguanine, ascorbic acid, uric acid, dopamine, glucose.	**Analytical signal:** 6-mercaptopurine oxidation (E_p ≈ +0.35 V *vs* Ag|AgCl|KCl_{3M}).	[86]
	dsDNA – p-Py – DBSA – f(–COOH)MWCNTs / PGE	DPV	TrisB, pH 7.0	200.0 nM – 8.0 µM 8.0 µM – 100.0 µM	LOD = 80.0 nM	**Real sample:** pharmaceutical formulation (tablets), spiked urine. The interaction of 6-mercaptopurine with dsDNA.	**Tested interfering agents:** glucose, fructose, lactose, sucrose, urea, glycine, valine, methionine, leucine, alanine, glycine, methanol, ethanol.	**Analytical signal:** indirect 6-mercaptopurine sensing by monitoring the decrease in oxidation peak currents of guanine ($E_{p\ guanine}$ ≈ +0.9 V *vs* Ag|AgCl|KCl_{sat}) and adenine ($E_{p\ adenine}$ ≈ +1.3 V *vs* Ag|AgCl|KCl_{sat}).	[145]
	Fe_3O_4NPs – p-Py – PtNPs / SPCE	DPV	100.0 mM PB, pH 7.0	40.0 nM – 330.0 µM	LOD = 10.0 nM	**Real sample:** pharmaceutical formulation (tablets), spiked urine.	**Tested interfering agents:** glucose, lactose, saccharose, benzoic acid, methanol, fructose and ethanol, dopamine, acetaminophen, uric acid, ascorbic acid, NADH, norepinephrine, epinephrine, tryptophan, L-serine, L-lysine, L-asparagine, threonine, histidine, glycine, L-proline, phenylalanine, L-tyrosine, Mg^{2+}, NH_4^+, F^-, Fe^{2+}, Fe^{3+}, Al^{3+}, S^{2-}, SO_4^{2-},	**Analytical signal:** 6-mercaptopurine oxidation (E_p ≈ +0.5 V *vs* Ag-pseudoRE). Possible simultaneous determination of 6-mercaptopurine and 6-thioguanine.	[89]
6-thioguanine 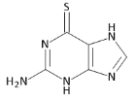	HMDE	SWV	50.0 mM AcB, pH 4.8	2.4 nM – (~)5 µM	LOD = 2.1 nM	**Real sample:** pharmaceutical formulation (tablets), spiked blood serum. The interaction of 6-thioguanine with ssDNA and dsDNA.	**Tested interfering agents:** fructose, sucrose, lactose, glucose, valine, glycine, leucine, urea, methanol, phenylalanine, ethanol, DL-tryptophane, cysteine.	**Analytical signal:** 6-thioguanine reduction (E_p ≈ –1.4 V *vs* Ag|AgCl|KCl_{sat}). Determination in the presence of dsDNA (2.0 mg L^{-1}) in the supporting electrolyte solution.	[132]

	CPE	SWV	100.0 mM BRB, pH 9.0	200.0 nM – 8.0 µM 8.0 µM – 350.0 µM	LOD = 80.0 nM	**Real sample:** pharmaceutical formulation (tablets), spiked urine.	**Tested interfering agents:** glucose, sucrose, lactose, fructose, starch, urea, K^+, Na^+, Ca^{2+}, Mg^{2+}, Fe^{2+}, Fe^{3+}, Cl^-, NO_3^-, F^-, SO_4^{2-}.	**Analytical signal:** 6-thioguanine oxidation ($E_p \approx -0.05$ V *vs* Ag|AgCl|KCl_{sat}).	[193]
	GO / CPE	SWSV	BRB, pH 5.0	100.0 nM – 20.0 µM	LOD = 18.0 nM LOQ = 60.0 nM	**Real sample:** pharmaceutical formulation (tablets Lanvis), spiked urine.	**Tested interfering agents:** acetaminophen, D-penicillamine, urea, ethanol, glucose, fructose, sucrose, lysine, asparagine, serine, proline, glycine, threonine, tryptophan, valine, phenylalanine, methionine, histidine, Ca^{2+}, Mg^{2+}, Fe^{2+}, Fe^{3+}, Al^{3+}, SO_4^{2-}, F^-.	**Analytical signal:** 6-thioguanine oxidation ($E_p \approx +1.3$ V *vs* Ag|AgCl|KCl_{3M}). Proposed electrochemical oxidation mechanism of 6-thioguanine.	[194]
	FDC – MWCNTs / CPE	DPV	100.0 mM BRB, pH 9.0	10.0 nM – 900.0 nM 900.0 nM – 100.0 µM	LOD = 8.5 nM	**Real sample:** pharmaceutical formulation (tablet), spiked urine.	**Tested interfering agents:** glucose, sucrose, lactose, fructose, citric acid, ascorbic acid, uric acid, urea, methanol, ethanol, methionine. aniline, cysteine, atenolol, starch, Ca^{2+}, Mg^{2+}, SO_4^{2-}, Al^{3+}, NH_4^+, Fe^{2+}, Fe^{3+}, F^-.	**Analytical signal:** 6-thioguanine oxidation ($E_p \approx +0.4$ V *vs* Ag|AgCl|KCl_{sat}). Possible determination in the presence of folic acid (10.0 µM). Proposed electrochemical oxidation mechanism of 6-thioguanine.	[91]
	PtNPs – MWCNTs – IL (BMIM-PF_6) / CPE	SWV	100.0 mM PB, pH 8.0	100.0 nM – 500.0 µM	LOD = 50.0 nM	**Real sample:** pharmaceutical formulation (tablets), spiked urine.	**Tested interfering agents:** sucrose, lactose, methanol, glucose, thioguanylic acid, 6-thiouric acid, topotecan, BMS-573188, Al^{3+}, Ca^{2+}, Mg^{2+}, SO_4^{2-}, CO_3^{2-}.	**Analytical signal:** 6-thioguanine oxidation ($E_p \approx +0.7$ V *vs* Ag|AgCl|KCl). Proposed electrochemical oxidation mechanism of 6-thioguanine.	[88]
	$MoWS_2$ – NFMF2A – IL(BPy-PF_6) / CPE	DPV	100.0 mM PB, pH 7.0	800.0 nM – 17.5 µM 17.5 µM – 600.0 µM	LOD = 90.0 nM	**Real sample:** pharmaceutical formulation (tablet), spiked urine, spiked blood serum.	**Tested interfering agents:** fructose, sucrose, lactose, glucose, asparagine, caffeine, uric acid, urea, ethanol, methanol, tryptophan, benzoic acid, L-proline, L-threonine, L-lysine, L-phenylalanine, L-histidine, L-serine, L-glycine, NH_4^+, Mg^{2+}, Al^{3+}, F^-, S^{2-}, SO_4^{2-}.	**Analytical signal:** 6-thioguanine oxidation ($E_p \approx +0.4$ V *vs* Ag|AgCl|KCl_{3M}).	[195]
	ERGO – IL (BMIM-PF_6) – CHIT / CSE	FIA-Amp.	100.0 mM PB, pH 7.0, containing 100.0 mM KCl	200.0 nM – 10.0 µM 10.0 µM – 250.0 µM	LOD = 50.0 nM	**Real sample:** pharmaceutical formulation.	N/A	**Applied potential in amperometry:** $E \approx +1.0$ V *vs* Ag|AgCl|KCl_{3M}. Proposed electrochemical oxidation mechanism of 6-thioguanine.	[187]
	AuNPs – CHIT – GO – IL (BMIM-PF_6) / CSE	AdSV	100.0 mM PB, pH 7.4, containing 1.0 M KCl	0 µM – 10.0 µM 10.0 µM – 150.0 µM	LOD = 20.0 nM	N/A	N/A	**Analytical signal:** 6-thioguanine oxidation ($E_p \approx -0.5$ V *vs* Ag|AgCl|KCl_{3M}).	[153]
	PGE	DPV	PB, pH 7.4	1.0 µM – 4.0 µM	LOD = 240.0 nM	The interaction of 6-thioguanine with ssDNA and dsDNA.	N/A	**Analytical signal:** 6-thioguanine oxidation ($E_p \approx +0.75$ V *vs* Ag|AgCl|KCl_{3M}).	[155]
	SWCNTs / PGE	DPV	PBS, pH 7.4	2.0 µM – 10.0 µM	LOD = 250.0 nM	The interaction of 6-thioguanine with ssDNA and dsDNA.	N/A	**Analytical signal:** 6-thioguanine oxidation ($E_p \approx +0.75$ V *vs* Ag|AgCl|KCl_{3M}).	[156]
	MIP (p-NR) – ERGO / PGE	DPAdSV	50.0 mM PB, pH 7.5	742.0 pM – 466.5 nM	LOD = 119.6 pM	**Real sample:**	**Tested interfering agents:**	**Analytical signal:**	[90]

						pharmaceutical formulation, spiked blood serum, spiked urine. The interaction of 6-thioguanine with dsDNA.	6-mercaptopurine, 5-fluorouracil, guanine, hypoxanthine, uric acid, dopamine, cytosine, adenine, thymine, glucose.	6-thioguanine oxidation (E_p ≈ +0.7 V *vs* Ag|AgCl|KCl_{3M}).	
cladribine (2-chlorodeoxyadenosine) 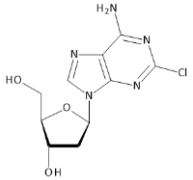	PyGE	DPAdSV	100.0 mM PB, pH 7.0	1.0 nM – 100.0 nM	LOD = 1.0 nM	**Real sample:** urine and blood serum taken from the patients treated with cladribine.	**Tested interfering agents:** cladribine metabolites.	**Analytical signal**: electrocatalytic reaction between cladribine oxidation product and NADH (E_p ≈ +0.1 V vs Ag|AgCl|KCl_{sat}). Determination of cladribine in the presence of NADH (500.0 µM).	[95]
clofarabine 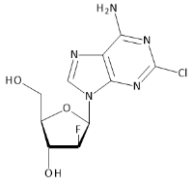	GCE	DPV	100.0 mM AcB, pH 4.3	1.6 µM – 25.3 µM	LOD = 80.0 nM LOQ = 260.0 nM	The interaction of clofarabine with dsDNA.	N/A	**Analytical signal**: clofarabine oxidation (E_p ≈ +1.45 V *vs* Ag|AgCl|KCl_{3M}). Proposed electrochemical oxidation mechanism of clofarabine.	[92]
fludarabine 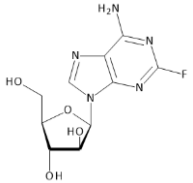	GCE	DPV	100.0 mM PB, pH 6.1	990.0 nM – 14.8 µM	LOD = 280.0 nM LOQ = 940.0 nM	The interaction of clofarabine with dsDNA.	N/A	**Analytical signal**: fludarabine oxidation (E_p ≈ +1.35 V *vs* Ag|AgCl|KCl_{3M}). Proposed electrochemical oxidation mechanism of fludarabine.	[93]
	f($-NH_2$)MWCNTs / GCE	SWAdSV	200.0 mM PB, pH 2.0	200.0 nM – 4.0 µM	LOD = 29.0 nM LOQ = 96.8 nM	**Real sample:** pharmaceutical formulation.	N/A	**Analytical signal**: fludarabine oxidation (E_p ≈ +1.45 V *vs* Ag|AgCl|KCl_{3M}).	[94]
	PyGE	DPAdSV	100.0 mM PB, pH 10.0	100.0 nM – 1.0 µM	LOD = 250.0 nM	**Real sample:** urine taked from the patients treated with fludarabine.	N/A	**Analytical signal**: electrocatalytic reaction between fludarabine oxidation product and NADH (E_p ≈ 0 V vs Ag|AgCl|KCl_{sat}). Determination of fludarabine in the presence of NADH (500.0 µM).	[96]
nelarabine 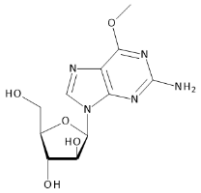	HMDE	AdSV	pH 6.0	100.0 nM – 10.0 mM	LOD = 100.0 nM	**Real sample:** pharmaceutical formulations, spiked urine.	N/A	**Analytical signal:** nelarabine reduction (E_p ≈ –0.8 V *vs* Ag|AgCl).	[133]
Pyrimidine analogs									
5-fluorouracil	SMDE	AdSV	250.0 mM BB, pH 10.0	25.0 nM – 150.0 nM	LOD = 3.0 nM	N/A	**Tested interfering agents**: gelatin, albumin, camphor, cyclophosphamide,	**Analytical signal:** 5-fluorouracil reduction (E_p ≈ –0.4 V *vs* Ag|AgCl).	[68]

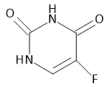							methotrexate, ascorbic acid, Cu^{2+}.		
	HMDE	SWCSV	100.0 mM Na_2SO_4, pH 6.7	10.0 pM – 90.0 pM	LOD = 7.7 pM	N/A	N/A	**Analytical signal:** 5-fluorouracil oxidation (E_p ≈ +0.05 V *vs* Ag|AgCl|KCl_{sat}). Determination of 5-fluorouracil in the presence of Cu^{2+} (50.0 pM).	[116]
	RGO – CHIT / GCE	SCV	100.0 mM BRB, pH 7.0	10.0 nM – 150.0 nM	LOD = 1.2 nM LOQ = 7.5 nM	**Real sample:** pharmaceutical formulation (injection), spiked urine, spiked blood serum.	**Tested interfering agents:** citric acid, dextrose, D-glucose, lactose, gum acacia, starch, sucrose.	**Analytical signal**: 5-fluorouracil oxidation (E_p ≈ +0.8 V *vs* Ag|AgCl|KCl_{sat}).	[97]
	f(–COOH)MWCNTs – BMB / GCE	CV	200.0 mM PB, pH 6.8	800.0 nM – 5.0 mM	LOD = 267.0 nM	**Real sample:** pharmaceutical formulation (injection).	N/A	**Analytical signal:** 5-fluorouracil oxidation (E_p ≈ +1.3 V *vs* Ag|AgCl|KCl_{3M}). Proposed electrochemical oxidation mechanism of 5-fluorouracil.	[98]
	p-ANI – ZnONPs – GQDs / GCE	DPV	BRB, pH 10.0	100.0 nM – 50.0 µM	LOD = 23.0 nM	**Real sample:** pharmaceutical formulation, spiked blood serum, spiked urine.	**Tested interfering agents:** oxaliplatin, ifosfamide, etoposide, flutamide, dopamine, folic acid, caffeine, ascorbic acid, citric acid, uric acid, glucose, dextrose, lactose, K^+, Na^+, Mg^{2+}, Ca^{2+}, CO_3^{2-}, NO^{3-}.	Analytical signal: 5-fluorouracil oxidation (E_p ≈ +1.1 V *vs* Ag|AgCl). Determination of 5-fluorouracil in the presence of irinotecan (10.0 µM).	[99]
	AuNPs – f(–COOH)MWCNTs – CHIT / GCE	DPV	40.0 mM BRB, pH 8.0	30.0 nM – 10.0 µM	LOD = 20.0 nM	**Real sample:** pharmaceutical formulation (injection), spiked artificial urine.	**Tested interfering agents:** ascorbic acid, uric acid, dopamine, 5-hydroxytryptamine.	**Analytical signal:** 5-fluorouracil oxidation (E_p ≈ +0.95 V *vs* Ag|AgCl|KCl_{3N}). Proposed electrochemical oxidation mechanism of 5-fluorouracil.	[100]
	N-CQDs – Fe_2O_3NPs – MWCNTs / GCE	DPV	100.0 mM PB, pH 7.0	500.0 nM – 126.0 µM	LOD = 19.0 nM	**Real sample:** spiked urine.	**Tested interfering agents:** dopamine, carbofuran, ascorbic acid, ibuprofen, catechol, naproxen, theophylline, uric acid, xanthine.	**Analytical signal:** 5-fluorouracil oxidation (E_p ≈ +0.95 V *vs* Ag|AgCl). Determination of 5-fluorouracil in the presence of uric acid (150.0 µM) and xanthine (100.0 µM). Proposed electrochemical oxidation mechanism of 5-fluorouracil.	[101]
	MoS_2 – Sm_2S_3 / GCE	DPV	100.0 mM PB, pH 7.0	100.0 nM – 1.2 mM	LOD = 15.0 nM	**Real sample:** spiked serum, spiked urine.	**Tested interfering agents:** ascorbic acid, uric acid, dopamine, glucose, caffeine, lactose, sucrose, dextrose, starch, xanthine.	**Analytical signal:** 5-fluorouracil oxidation (E_p ≈ +0.75 V *vs* Ag|AgCl). Proposed electrochemical oxidation mechanism of 5-fluorouracil.	[102]
	AuNPs – CHIT – p-MAA / GCE	DPV	100.0 mM PB, pH 7.0	100.0 nM – 497.0 µM	LOD = 30.0 nM	**Real sample:** spiked blood serum.	**Tested interfering agents:** ascorbic acid, uric acid, dopamine, acetaminophen, theophylline.	**Analytical signal:** 5-fluorouracil oxidation (E_p ≈ +1.25 V *vs* Ag|AgCl). Proposed electrochemical oxidation mechanism of 5-fluorouracil.	[103]
	p-NIPA – p-EDOT / GCE	DPV	50.0 mM PB, pH 7.0	30.0 nM – 182.0 µM	LOD = 15.0 nM	**Real sample:**	**Tested interfering agents:**	**Analytical signal:**	[104]

						spiked blood serum.	ascorbic acid, uric acid, dopamine, ibuprofen, naproxen, theophylline, catechol, carbofuran.	5-fluorouracil oxidation (E_p ≈ +0.95 V *vs* Ag|AgCl).	
	dsDNA – p-BCP / GCE	DPV	500.0 mM AcB, pH 4.8, containing 20.0 mM NaCl	7.7 µM – 65.3 µM 65.3 µM – 384.4 µM	LOD = 2.4 µM	**Real sample:** pharmaceutical formulation (injection). The interaction of dsDNA with 5-fluorouracil.	**Tested interfering agents:** ascorbic acid, dopamine, uric acid, urea, creatine, caffeine.	**Analytical signal:** indirect 5-fluorouracil sensing by monitoring the decrease in guanine oxidation peak current ($E_{p\ guanine}$ ≈ +0.75 V *vs* Ag|AgCl|$NaCl_{3M}$).	[146]
	AgNPs – p-ANI / PGE	DPV	40.0 mM BRB, pH 8.0	1.0 µM – 300.0 µM	LOD = 60.0 nM	**Real sample:** spiked blood serum.	**Tested interfering agents:** oxaliplatin, irinotecan, folic acid, dopamine, caffeine, glucose, lactose, ascorbic acid, tartaric acid, citric acid, uric acid.	**Analytical signal:** 5-fluorouracil oxidation (E_p ≈ +1.1 V *vs* Ag|AgCl|KCl_{sat}). Proposed electrochemical oxidation mechanism of 5-fluorouracil.	[105]
	GO – MWCNTs / SPCE	SWV	200.0 mM PB, pH 7.0	50.0 nM – 5.0 µM 5.0 µM – 1.2 mM	LOD = 16.0 nM	**Real sample:** spiked blood plasma.	**Tested interfering agents:** ascorbic acid, uric acid, dopamine, urea, glycine, benzoate sodium, glucose, fructose, lactose, starch, sulfate ammonium, caffeine, tyrosine, citrate sodium, phenylalanine, glycerol, vitamin B_2, vitamin B_1, vitamin B_6, vitamin B_{12}, NaCl, $BaCl_2$, $FeCl_3$, $Fe(NO_3)_3$.	**Analytical signal:** 5-fluorouracil oxidation (E_p ≈ +1.2 V *vs* Ag|AgCl|KCl_{3M}). Proposed electrochemical oxidation mechanism of 5-fluorouracil.	[106]
	MTB / CPE	DPV	200.0 mM PB, pH 7.0	100.0 nM – 40.0 µM	LOD = 2.0 nM LOQ = 6.8 nM	**Real sample:** pharmaceutical formulation (tablets), spiked urine.	**Tested interfering agents:** oxalic acid, citric acid, lactose, sucrose, dextrose, glucose, gum acacia, starch, caffeine, xanthine, uric acid, ascorbic acid, creatine, 5-hydroxytryptamine.	**Analytical signal:** 5-fluorouracil oxidation (E_p ≈ +1.1 V *vs* Ag|AgCl). Proposed electrochemical oxidation mechanism of 5-fluorouracil.	[107]
	Glu / CPE	DPV	200.0 mM PB, pH 7.0	400.0 nM – 10.0 µM	LOD = 5.2 nM LOQ = 17.2 nM	**Real sample:** pharmaceutical formulation (tablet), spiked urine.	**Tested interfering agents:** oxalic acid, citric acid, lactose, sucrose, gum acacia, starch.	**Analytical signal:** 5-fluorouracil oxidation (E_p ≈ +1.1 V *vs* Ag|AgCl|KCl_{3M}).	[108]
	IL (BPy-PF_6) / CPE	DPV	200.0 mM BRB, pH 7.0	500.0 nM – 2.0 µM 2.0 µM – 800.0 µM	LOD = 13.0 nM	**Real sample:** pharmaceutical formulation (injection).	**Tested interfering agents:** L-cysteine, L-valine, glycine, sucrose, Starch, guanine, adenine, cytosine, thymine, Mg^{2+}, Zn^{2+}.	**Analytical signal:** 5-fluorouracil oxidation (E_p ≈ +1.1 V *vs* SCE). Proposed electrochemical oxidation mechanism of 5-fluorouracil.	[109]
	($ZnFe_2O_4$)NPs – IL (DPIM-Br) / CPE	SWV	100.0 mM PB, pH 7.0	100.0 nM – 100.0 µM 100.0 µM – 1.4 mM	LOD = 70.0 nM	**Real sample:** pharmaceutical formulation (injection), spiked pharmaceutical serum, spiked urine.	**Tested interfering agents:** lysine, methionine, leucine, fructose, glucose, sucrose, isoleucine, phenylalanine, L-threonine, alanine, lactose, uric acid, albumin, glycine, urea, ascorbic acid, dopamine, ammonia, starch, Li^+, Na^+, Ca^{2+}, Cl^-, F^-.	**Analytical signal:** 5-fluorouracil oxidation (E_p ≈ +1.2 V *vs* Ag|AgCl|KCl_{sat}).	[110]
	(Pr-Er_2WO_6)NPs / CPE	SWV	100.0 mM PB, pH 7.0	10.0 nM – 50.0 µM	LOD = 980.0 pM	**Real sample:** pharmaceutical formulation	N/A	**Analytical signal:** 5-fluorouracil oxidation (E_p ≈ +1.1 V *vs* Ag|AgCl).	[111]

						(injection), spiked blood, spiked urine.			
	MWCNTsPE	DPV	200.0 mM PB, pH 7.0	100.0 nM – 5.0 µM	LOD = 39.4 nM LOQ = 130.0 nM	**Real sample:** pharmaceutical formulation (tablet), spiked urine.	**Tested interfering agents:** citric acid, dextrose, glucose, gum acacia, lactose, starch, sucrose.	**Analytical signal:** 5-fluorouracil oxidation (E_p ≈ +1.1 V *vs* Ag|AgCl|KCl_{3M}).	[112]
	AuNPs – PFR / GCPE	DPV	40.0 mM BRB, pH 8.0	29.9 µM – 234.0 µM	LOD = 670.0 nM LOQ = 2.2 µM	**Real sample:** pharmaceutical formulation (injection).	**Tested interfering agents:** D-glucose, ascorbic acid, urea, albumin, Na^+, K^+.	**Analytical signal:** 5-fluorouracil oxidation (E_p ≈ +1.05 V *vs* Ag|AgCl|KCl_{sat}). Proposed electrochemical oxidation mechanism of 5-fluorouracil.	[113]
	MIP (AMB – EGDMA – AIBN) – MWCNTs / AgE	DPASV	100.0 mM BB, pH 5.6	10.2 nM – 3.1 µM	LOD = 2.6 nM	**Real sample:** pharmaceutical formulation, spiked blood plasma.	**Tested interfering agents:** adenine, guanine, cytosine, thymine, dopamine, hypoxanthine, barbituric acid, ascorbic acid, caffeine, uric acid, creatine, urea, glucose.	**Analytical signal:** 5-fluorouracil oxidation (E_p ≈ –0.8 V *vs* Ag|AgCl|KCl_{3M}).	[114]
	MIP (TMPM – DAU – TEA – $CHCl_3$ – EGDMA) – f(–COOH)MWCNTs / CFBE	DPASV	100.0 mM BB, pH 6.0	76.8 nM – 3.3 µM	LOD = 10.0 nM	**Real sample:** pharmaceutical formulation, spiked blood plasma.	**Tested interfering agents:** adenine, guanine, thymine, cytosine, barbituric acid, hypoxanthine, caffeine, uric acid, ascorbic acid, dopamine, urea, glucose, creatine.	**Analytical signal**: 5-fluorouracil oxidation (E_p ≈ +0.6 V *vs* Ag|AgCl|KCl_{3M}).	[115]
capecitabine 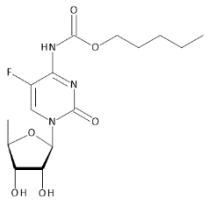	GCE	DPV	40.0 mM BRB, pH 2.5	800.0 nM – 50.0 µM	LOD = 113.0 nM LOQ = 378.0 nM	**Real sample:** pharmaceutical formulation.	**Tested interfering agents:** talc, glucose, starch, lactose, dextrose, gum acacia, magnesium stearate.	**Analytical signal:** capecitabine reduction (E_p ≈ –0.8 V *vs* Ag|AgCl|KCl_{3M}). Proposed electrochemical reduction mechanism of capecitabine.	[137]
	AuNPs – GNFBs / GCE	DPV	100.0 mM PB, pH 2.0	50.0 nM – 10.0 µM 10.0 µM – 80.0 µM	LOD = 17.0 nM	**Real sample:** spiked blood serum.	N/A	**Analytical signal:** capecitabine reduction (E_p ≈ –0.75 V *vs* SCE).	[139]
	MIP(MAA – EGDMA – AIBN) – Fe_3O_4NPs – GO / GCE	SWV	100.0 mM PB, pH 7.0	1.0 nM – 100.0 nM	LOD = 324.0 pM LOQ = 1.0 nM	**Real sample:** pharmaceutical formulation (tabet), spiked blood plasma.	**Tested interfering agents:** glucose, adenine, cysteine, cytidine, riboflavin, nitrophenol, ascorbic acid, citric acid, uric acid, flutamide, 5-fluorouracil.	**Analytical signal:** capecitabine reduction (E_p ≈ –0.3 V *vs* Ag|AgCl|KCl_{sat}).	[140]
	f(–COOH)MWCNTs – p-HU / p-PHF–PGE	DPV	50.0 mM PB, pH 7.0	7.7 µM – 142.0 µM	LOD = 110.0 nM LOQ = 330.0 nM	**Real sample:** spiked nail, spiked urine.	**Tested interfering agents:** chitosan, Triton X-100	**Analytical signal:** capecitabine oxidation (E_p ≈ +1.0 V *vs* Ag|AgCl|KCl_{3M}). Determination of capecitabine performed in the presence of erlotinib.	[117]
	ZnONPs – f(–COOH)MWCNTs / CPE	DPV	BRB, pH 2.0	100.0 nM – 10.0 µM 10.0 µM – 100.0 µM	LOD = 30.0 nM	**Real sample:** pharmaceutical formulation (tablets), spiked blood serum.	**Tested interfering agents:** glucose, sucrose, fructose, lactose, ascorbic acid, citric acid, uric acid, cysteinę, Na^+, NH_4^+, Ca^{2+}, K^+, NO_3^-, NO_2^-, Cl^-.	**Analytical signal:** capecitabine reduction (E_p ≈ –0.8 V *vs* Ag|AgCl). Proposed electrochemical reduction mechanism of capecitabine.	[138]
cytarabine (cytosine arabinose, tarabine)	HgF / GCE	OSWASV	100.0 mM SPB, pH 7.7	5.0 nM – 10.0 µM	LOD = 551.0 pM	**Real sample:** spiked urine. The interaction between ssDNA and cytarabine.	**Tested interfering agents:** ascorbic acid, uric acid, amino acids, gelatin, CTAB, SDS, Triton X-100, Fe^{3+}, Fe^{2+}, Zn^{2+}, Cd^{2+}, Mn^{2+}, Pb^{2+}, Cu^{2+}.	**Analytical signal:** cytarabine reduction (E_p ≈–1.1 V *vs* Ag|AgCl).	[141]

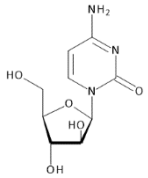	MIP (Cu^{2+} – MAC – EGDMA – AIBN) – AuNRs / PGE	DPASV	50.0 mM PB, pH 7.2	4.1 nM – 521.0 nM	LOD = 781.2 pM	**Real sample:** pharmaceutical formulation, spiked blood plasma, spiked urine.	**Tested interfering agents:** 6-mercaptopurine, 6-thioguanine, 5-fluorouracil, glycine, cytosine, cytidine, glucose, uric acid.	**Analytical signal:** cytarabine oxidation (E_p ≈ –0.1 V *vs* Ag|AgCl|KCl_{3M}).	[118]
	dsDNA – (Eu^{3+}-Cu_2O)NPs / CPE	DPV	100.0 mM AcB, pH 4.8	10.0 nM – 90.0 µM	LOD = 9.4 µM LOQ = 2.8 µM	**Real sample:** pharmaceutical formulations, spiked urine. The interaction of cytarabine with dsDNA.	**Tested interfering agents:** uric acid, sucrose, citrate, ascorbic acid, epinephrine, dopamine, L-tyrosine, folic acid.	**Analytical signal:** indirect cytarabine sensing by monitoring the decrease in guanine oxidation peak current ($E_{p\,guanine}$ ≈ +0.75 V *vs* Ag|AgCl).	[147]
floxuridine (5-fluorodeoxyuridine) 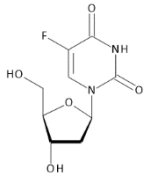	SMDE	Amp.	50.0 mM BB containing 10.0 mM KNO_3 and 100.0 mM HNO_3, pH 7.6	1.0 µM – 15.0 µM	N/A	N/A	N/A	**Applied potential in amperometry:** E = +0.2 V *vs* Ag|AgCl|KCl_{sat}.	[119]
gemcitabine 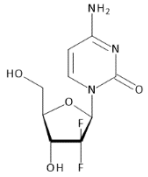	BDDE	Amp.	100.0 mM PBS, pH 5.5	1.9 µM – 247.0 µM	LOD = 570.0 nM LOQ = 1.9 µM	**Real sample:** pharmaceutical formulation (injection).	N/A	**Applied potential in amperometry:** E ≈ +2.0 V *vs* Ag|AgCl).	[120]
	CPE	DPSV	PB, pH 6.0	50.0 nM – 300.0 µM	LOD = 9.0 nM LOQ = 29.8 nM	**Real sample:** pharmaceutical formulations (vials), spiked urine, spiked blood serum.	N/A	**Analytical signal:** gemcitabine oxidation (E_p ≈ +1.0 V *vs* Ag|AgCl). Determination of gemcitabine performed in the presence of an anionic surfactant sodium dodecyl sulfate (800.0 µM) in the supporting electrolyte solution.	[123]
	MIP – dsDNA – AgNPs – MWCNTs / CPE	DPV	500.0 mM AcB, pH 4.8	1.5 µM – 93.0 µM	(a) LOD =12.5 nM (b) LOD = 48.8 nM	**Real sample:** spiked blood serum.	**Tested interfering agents:** ascorbic acid, uric acid.	**Analytical signal:** indirect gemcitabine sensing by monitoring the decrease in oxidation peak currents of (a) guanine ($E_{p\,guanine}$ ≈ +1.0 V *vs* Ag|AgCl|KCl_{3M}) and (b) adenine ($E_{p\,adenine}$ ≈ +1.3 V *vs* Ag|AgCl|KCl_{3M}).	[124]
	BiNPs – ERGO / GCE	DPV	PB, pH 3.0	100.0 nM – 51.1 µM	LOD = 50.0 nM LOQ = 150.0 nM	**Real sample:** pharmaceutical formulation (injection), spiked urine.	**Tested interfering agents:** glucose, cellulose, starch, ascorbic, uric acid.	**Analytical signal:** gemcitabine oxidation (E_p ≈ +1.1 V *vs* Ag|AgCl|$KCl_{3.5M}$).	[122]
	dsDNA – p-PDCA / GCE	DPAdSV	500.0 mM AcB, pH 4.8	3.8 µM – 114.0 µM	LOD = 1.1 µM LOQ = 3.5 µM	**Real sample:** pharmaceutical formulation, spiked blood serum.	**Tested interfering agents:** ascorbic acid, uric acid, D-glucose, L-cysteine.	**Analytical signal:** indirect gemcitabine sensing by monitoring the decrease in guanine oxidation peak current ($E_{p\,guanine}$ ≈ +0.75 V *vs* Ag|AgCl|$NaCl_{3M}$).	[148]
	AuE	DPV	200.0 mM PB, pH 10.4	100.0 nM – 15.0 µM	LOD = 60.0 nM LOQ = 200.0 nM	**Real sample:** pharmaceutical formulation, spiked urine.	N/A	**Analytical signal:** gemcitabine oxidation (E_p ≈ +1.55 V *vs* Ag|AgCl).	[196]
	MIP(p-(p-ATPh)) – MOF(AuNPs) / AuE	LSV	PBS, pH 7.2	3.8 fM – 38.0 nM	LOD = 3.0 fM	**Real sample:**	N/A	**Analytical signal:**	[142]

						pharmaceutical formulation (injection), spiked diluted serum (commercially available calf serum).		gemcitabine reduction $E_p \approx +0.1$ V *vs* SCE).	

Modification: 2-CBF – 2-chlorobenzoyl ferrocene; **AgNPs** – silver nanoparticles; **AHMT-Ag** – 4-amino-3-hydrazino-5-mercapto-1,2,4-triazole coordinated silver(I) ions; **AIBN** – 2-20-azobis (isobutyronitrile); **AMB** – N-acryloyl-2-mercaptobenzamide; **APS** – ammonium persulfate; **AuNPs** – gold nanoparticles; **AuNRs** – gold nanorods; **BiF** – bismuth film; **BiNPs** – bismuth nanoparticles; **BM** – natural polymer (*Orbignya phalerata*) babassu mesocarp; **BMB** – bromothymol blue; **BMIM-BF_4** – 1-butyl-3-methylimidazolium tetrafluorobarate; **BMIM-Br** – 1-butyl-3-methylimidazolium bromide; **BMIM-PF_6** – 1-butyl-3-methylimidazolium hexafluorophosphate; **BPy-PF_6** – 1-butylpyridinium hexafluorophosphate;**$CHCl_3$** – chloroform; **CHIT** – chitosan; **CNFBs** – carbon nanofibers; **CQDs** – carbon quantum dots; **CTAB** – hexadecyl(trimethyl)ammonium bromide; **CuNPs** – cooper nanoparticles; **CB** – carbon black; **CyA** – cysteamine; **DAU** – diacryl urea; **DBSA** – 4-dodecylbenzenesulfonic acid; **DNA** – deoxyribonucleic acid; **DPIM-Br** – 1,3-dipropylimidazolium bromide; **dsDNA** – double-stranded deoxyribonucleic acid; **EDC** – N-(3-dimetylaminopropyl)-N′-ethylcarbodimide; **eGCP** – electrografted carboxyphenyl; **EGDMA** – ethylene glycol dimethacrylate; **ERGO** – electrochemically reduced graphene oxide; **f(-COOH)MWCNTs** – functionalized (carboxyl) multi-walled carbon nanotubes; **f(–NH_2)MWCNTs** – functionalized (amine) multi-walled carbon nanotubes; **f(Q)MWCNTs** – functionalized (quaternary amine) multi-walled carbon nanotubes; **FDC** – ferrocenedicarboxylic acid; **Fe_2O_3NPs** – ferrite nanoparticles; **Fe_3O_4NPs** – magnetite nanoparticles; **FM** – formaldehyde; **Glu** – glucose; **GNFBs** – graphene nanofibers; **GO** – graphene oxide; **GQDs** – graphene quantum dots; **Gr-C_3N_4** – graphite-like carbon nitride; **GrO** – graphite oxide; **GTA** – glutaraldehyde; **HgF** – mercury film; **HgF** – mercury film; **HMIM-PF_6** – 1-hexyl-3-methylimidazolium hexafluorophosphate; **IgG-Mtx-Ab** – immunoglobulin G methotrexate antibody; **IL** – ionic liquid; **L-AAOD** – L-amino acid oxidase; **L-Glox** – L-glutamate: oxygen oxido reductase; **MAA** – methacrylic acid; **MAC** – N-methacryloyl-L-cysteine; **MBA** – N,N-methylene bis(acrylamide); **MeI** – melamine; **MIP** – molecularly imprinted polymer; **MOF** – metal organic framework; **MoS_2** – molybdenum disulfide; **MoS_2NFLs** – molybdenum disulfide nanoflowers; **$MoWS_2$** – molybdenum tungsten disulfide; **MTB** – methylene blue; **MWCNTs** – multi-walled carbon nanotubes; **MWCNTs** – multi-walled carbon nanotubes; **N-AAsp** – N-acryloyl aspartic acid; **NCCP** – nanocrystalline coordination polymers; **N-CQDs** – nitrogen-doped carbon quantum dots; **N-CSNS** – nitrogen-doped carbon-silica nanospheres; **NFMF2A** – N-(ferrocenylmethylidene)fluoren-2-amine; **NHS** – N-hydroxysuccinimide; **NiONPs** – nickel(II) oxide nanoparticles; **NAF** – Nafion; **N-RGO** – nitrogen-doped reduced graphene oxide; **ODA** – octadecylamine; **oop-Py** – over-oxidized poly-pyrrole; **o-PD** – o-phenylediamine; **p-(L-Cys)** – poly-(L-Cysteine); **p-(L-Lys)** – poly-(L-lysine); **p-(p-ABSA)** – poly-(p-aminobenzene sulfonic acid); **p-(p-ATPh)** – poly-(p-aminothiophenol); **p-(PDCA)** – poly-(2,6-pyridinedicarboxylic acid); **p-ANI** – poly-aniline; **p-BCP** – poly-bromocresol purple; **p-DA** – poly-dopamine; **PdNPs** – palladium nanoparticles; **p-EDOT** – poly-(3,4-ethylenedioxythiophene); **p-EI** – poly-ethyleneimine; **PFR** – porphyrin; **p-HU** – poly-(hydroxy urethane); **p-MAA** – poly-methacrylic acid; **p-NIPA** – poly-(N-isopropylacrylamide); **p-NR** – poly-neutral red; **p-Py** – poly-pyrrole; **Pr_2O_3NPs** – praseodymium(III) oxide nanoparticles; **PTC** – perylene tetracarboxylic derivative; **PTEOS** – phenyltriethoxysilane; **pTHMMAA** – N-[tris(hydroxyl-methyl)methyl]acrylamide; **PtNPs** – platinum nanoparticles;**p-VS** – poly-vinyl sodium sulfonate; **RES** – resorcinol; **RGO** – reduced graphene oxide; **SDS** – sodium dodecyl sulfate; **SiO_2NPs** – silicon dioxide nanopartciles; **Sm_2S_3** – samarium(III) sulfide; **SnS_2NPLs** – tin disulfide nanoplatelets; **SWCNTs** – single-walled carbon nanotubes; **TEA** – triethylamine; **TEOS** – tetraethoxysilane; **TFA** – trifluoroacetic acid; **TiO_2NPs** – titanium dioxide nanoparticles; **TMPM** – 3-(trimethoxysilyl) propyl methacrylate; **WP-N-f(-COOH)MWCNTs** – tungsten phosphide embedded nitrogen-doped functionalized (carboxyl) multi-walled carbon nanotubes; **ZnO-GQDs** – core-shell zinc oxide - graphene quantum dots; **ZnONPs** – zinc oxide nanoparticles; **β-CD** – β-cyclodextrin; **(Ce-ZnO)NFLs** – cerium-doped zinc oxide nanoflowers; **(CFL-Ho^{3+}-NiO)NPs** – cabbage flower-like holmium-doped nickel(II) oxide nanoparticles; **($CoFe_2O_4$)NPs** – cobalt-doped ferrite nanoparticles; **($CuCr_2O_4$-CuO)NFBs** – cooper chromate-copper oxide nanofibers; **(Eu^{3+}-Cu_2O)NPs** – europium(III)-doped copper(I) oxide nanoparticles; **(Pd-Ag)A** – palladium-silver alloy; **(Pr-Er_2WO_6)NPs** – praseodymium-erbium(III) tungstate nanoparticles; **(p-Styr)MS** – poly-styrene microspheres; **($ZnFe_2O_4$)NPs** – zinc-doped ferrite nanoparticles; **(ZnO-CuO)NPLs** – zinc oxide-copper oxide nanoplates; **[Co(III)-Sal]** – cobalt(III) salophen complex; **$[Co(phen)_2(tatp)]^{3+}$** – cobalt (III) complex, where phen is 1,10-phenanthroline and tatp is 1,4,8,9-tetra-aza-triphenylene); **$[Co(phen)_3]^{3+}$** – tris(1,10-phenanthroline)cobalt(iii) complex; **$[M_3OA]^+[NTF_2]^-$** – methyl (trioctyl)ammonium bis(trifluoromethylsulfonyl)imide.

Electrode: AgE – silver electrode; **AP-BDDE** – anodically pretreated boron-doped diamond electrode; **AP-GCE** – anodically pretreated glassy carbon electrode; **AuE** – gold electrode; **BDDE** – boron-doped diamond electrode; **CFBE** – carbon fiber electrode; **CFBUME** – carbon fiber ultramicroelectrode; **CPE** – carbon (graphite) paste electrode; **CSE** – carbositall electrode; **CuE** – copper electrode; **GCE** – glassy carbon electrode; **GCPE** – glassy carbon paste electrode; **HCuADE** – hanging copper amalgam dropping electrode; **HMDE** – hanging mercury drop electrode; **ITOE** – indium tin oxide electrode; **m-AgSAE** – meniscus modified silver solid amalgam electrode; **MWCNTsPE** – multi-walled carbon nanotubes paste electrode; **PGE** – pencil graphite electrode; **p-AgSAE** – polished modified silver solid amalgam electrode; **p-PHF–PGE** – poly-propylene hollow fiber pencil graphite electrode;**PyGE** – pyrolytic graphite electrode; **SMDE** – static mercury drop electrode; **SPCE** – screen printed carbon (graphite) electrode; **SPE** – screen printed electrode.

Technique:ACAdSV – alternating current adsorptive stripping voltammetry; **AdSV** – adsorptive stripping voltammetry; **AdSV** – adsorptive stripping voltammetry; **Amp.** – amperometry; **CCPSV** – constant current potentiometric stripping voltammetry; **CV** – cyclic voltammetry; **DPAdCSV** – differential pulse adsorptive cathodic stripping voltammetry; **DPAdSV** – differential pulse adsorptive stripping voltammetry; **DPASV** – differential pulse anodic stripping voltammetry; **DPSV** – differential pulse stripping voltammetry; **DPV** – differential pulse voltammetry; **ECL** – electrochemiluminescence; **EIS-MVA** – electrochemical impedance spectroscopy - multivariate data analysis; **LSV** – linear sweep voltammetry; **FIA-Amp.** – flow injection analysis coupled with amperometry; **LSAdSV** – linear sweep adsorptive stripping voltammetry; **OSWASV** – Osteryoung square-wave anodic stripping voltammetry; **SCV** – staircase voltammetry; **SWAdSV** – square-wave adsorptive stripping voltammetry; **SWASV** – square-wave anodic stripping voltammetry; **SWCSV** – square-wave cathodic stripping voltammetry; **SWSV** – square-wave stripping voltammetry; **SWV** – square-wave voltammetry.

Medium: AcB – acetate buffer; **AmAcB** – ammonium acetate buffer; **BB** – borate buffer; **BRB** – Britton-Robinson buffer; **EtOH** – ethanol; **PB** – phosphate buffer; **PBS** – phosphate buffered saline; **SPB** – Sorensen's phosphate buffer; **TrisB** – tris(hydroxymethyl)aminomethane hydrochloride buffer.

Selectivity: when underlined – exhibited interference.

Comments: Ag|AgCl – silver|silver chloride electrode; **Ag-pseudoRE** – silver pseudo-reference electrode; **SCE** – saturated calomel electrode.

N/A – not applicable.

Table 3. Comprehensive electroanalytical overview for the ANAs belonging to the group of plant alkaloids and other natural products.

Drug and its structure	Modification / Electrode	Technique	Medium	Linear range	LOD/LOQ	Application	Selectivity	Comments	Ref
Vinca alkaloids and analogs									
vinblastine 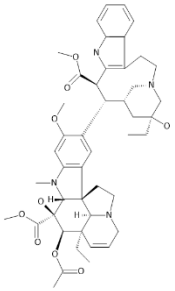	TUB – NHS – EDC – MPA – AuNPs / GCE	EIS	100.0 mM PBS, pH 7.4, containing 100.0 mM KCl	400.0 pM – 12.0 nM 12.0 nM – 65.0 nM	LOD = 84.0 pM	**Real sample:** spiked plant extracts, spiked serum.	**Tested interfering agents:** glucose, citric acid, tyrosine, tryptophan, uric acid, ascorbic acid, hemoglobin, bovine serum albumin, vincristine, vinorelbine, vindesine, Ca^{2+}, Na^{+}, Cu^{2+}, Zn^{2+} Cl^{-}, SO_4^{2-}.	**Analytical signal:** Indirect vincristine sensing by monitoring the redox reaction of $[Fe(CN)_6]^{3-/4-}$.	[209]
vincristine (leurocristine) 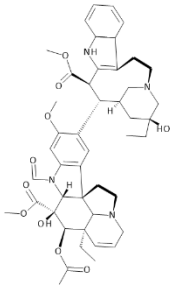	DME	LSAdSV	5 mM TrisB, pH 7.1, containing 50.0 mM NaCl	210.0 nM – 4.2 µM	LOD = 100.0 nM	The binding of vincristine to tubulin.	N/A	**Analytical signal:** vincristine reduction ($E_p \approx -1.6$ V *vs* SCE).	[206]
	MIP(MAA – EGMRA – AIBN) – RGO – AuNPs / GCE	DPV	PB, pH 7.2	50.0 nM – 5.0 µM	LOD = 26.0 nM	**Real sample:** Pharmaceutical formulation.	**Tested interfering agents:** daunorubicin, vinblastine, guanine, Ca^{2+}, Mg^{2+}, Zn^{2+}, K^{+}.	**Analytical signal:** Indirect vincristine sensing by monitoring the decrease in $[Fe(CN)_6]^{3-/4-}$ oxidation peak current ($E_{p\,[Fe(CN)6]3-/4-} \approx +0.35$ V *vs* SCE).	[208]
Podophyllotoxin derivatives									
etoposide 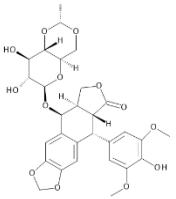	RGO / GCE	SWAdSV	100.0 mM BRB, pH 4.0	42.5 nM – 849.5 nM	LOD = 3.9 nM LOQ = 13.1 nM	**Real sample:** pharmaceutical formulation.	**Tested interfering agents:** glucose, fructose, saccharin, sucrose, ascorbic acid, dopamine, uric acid, Na^{+}, K^{+}, Ca^{2+}, Mg^{2+}.	**Analytical signal:** etoposide oxidation ($E_p \approx +0.6$ V *vs* Ag|AgCl|$NaCl_{3M}$). Proposed electrochemical oxidation mechanism of etoposide.	[221]
	CQDs / GCE	DPV	BRB, pH 6.0	20.0 nM – 10.0 µM	LOD = 5.0 nM LOQ = 16.0 nM	**Real sample:** prostate cancer cell line (PC3).	N/A	**Analytical signal:** etoposide oxidation ($E_p \approx +0.4$ V *vs* Ag|AgCl|KCl_{3M}). Proposed electrochemical oxidation mechanism of etoposide.	[222]
	p-(L-Cys) – RGO – AuNPs – PdNPs / AP-PGE	DPV	BRB, pH 6.0	1.0 nM – 1.0 µM 1.0 µM – 45.0 µM	LOD = 718.0 pM	**Real sample:** pharmaceutical formulation, spiked blood serum. spiked urine.	**Tested interfering agents**: glucose, sucrose, ascorbic acid, uric acid, citric acid, Na^{+}, K^{+}, Mg^{2+}, SO_4^{2-}, CO_3^{2-}, NO_3^{-}.	**Analytical signal:** etoposide oxidation ($E_p \approx +0.3$ V *vs* Ag|AgCl|KCl_{sat}). Possible simultaneous determination of etoposide and ifosfamide.	[199]
	dsDNA / SPCE	DPV	20.0 mM PB, pH 7.4	N/A	LOD = 5.0 nM LOQ = 50.0 nM	**Real sample:** spiked blood serum.	N/A	**Analytical signal:**	[217]

						The interaction of etoposide with dsDNA.		etoposide oxidation (E_p ≈ +0.4 V *vs* Ag|AgCl-pseudoRE).	
	f(-COOH)MWCNTs / SPCPE	CV	100.0 mM PBS, pH 7.4	34.0 µM – 102.0 µM	LOD = 50.0 nM	**Real sample:** spiked blood serum.	N/A	**Analytical signal:** etoposide oxidation (E_p ≈ +0.25 V *vs* Ag|AgCl).	[40]
	DNA – CHIT – GO – ($CoFe_2O_4$)NPs– (Zn-Al)-LDH / FTOE	DPV	20.0 mM PB, pH 7.4, containing 0.9% NaCl	200.0 nM – 10.0 µM	LOD = 1.0 nM	**Real sample:** spiked blood plasma, spiked urine.	**Tested interfering agents:** uric acid, glucose, ascorbic acid, citric acid, methionine, valine, caffeine, ibuprofen, acetaminophen, Na^+, K^+, Ca^{2+}, Mg^{2+}, Fe^{2+}.	**Analytical signal:** etoposide oxidation (E_p ≈ –0.1 V *vs* Ag|AgCl).	[223]
Taxanes									
paclitaxel (taxol) 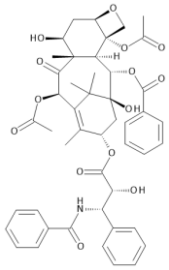	HMDE	SWCSV	50.0 mM BB, pH 9.0	4.1 nM – 138.2 nM	LOD = 6.1 nM LOQ = 12.9 nM	**Real sample:** spiked urine.	N/A	**Analytical signal:** paclitaxel reduction (E_p ≈ –1.6 V *vs* Ag|AgCl|KCl_{3M}).	[207]
	GCE	DPAdSV	200.0 mM PB, pH 7.0	1.0 µM – 10.0 µM	LOD = 12.3 nM LOQ = 41.0 nM	**Real sample:** pharmaceutical (injection), spiked urine.	**Tested interfering agents**: dextrose, glucose, gum acacia, lactose, starch, citric acid, tartaric acid, sucrose.	**Analytical signal:** paclitaxel oxidation (E_p ≈ +1.15 V *vs* Ag|AgCl|KCl_{3M}). Proposed electrochemical oxidation mechanism of paclitaxel.	[224]
	CPE	DPAdSV	200.0 mM PB, pH 7.0	2.0 µM – 20.0 µM	LOD = 4.6 nM LOQ = 15.3 nM	**Real sample:** pharmaceutical (injection), spiked blood, spiked urine.	**Tested interfering agents:** dextrose, glucose, gum acacia, lactose, starch, citric acid, tartaric acid, sucrose.	**Analytical signal:** paclitaxel oxidation (E_p ≈ +1.15 V *vs* SCE). Proposed electrochemical oxidation mechanism of paclitaxel.	[225]
	PGE	DPV	200.0 mM PB, pH 7.0	400.0 nM – 3.0 µM	LOD = 2.5 nM LOQ = 8.2 nM	**Real sample:** pharmaceutical formulation (injection), spiked blood, spiked urine.	**Tested interfering agents**: dextrose, glucose, gum acacia, lactose, starch, citric acid, tartaric acid, sucrose.	**Analytical signal:** paclitaxel oxidation (E_p ≈ +1.1 V *vs* Ag|AgCl|KCl_{3M}). Proposed electrochemical oxidation mechanism of paclitaxel.	[226]
	dsDNA – p-EDOT / PGE	DPV	50.0 mM PB, pH 7.4, containing 20.0 mM NaCl	585.5 nM – 150.0 µM	LOD = 164.0 nM	The interaction of paclitaxel with dsDNA.	N/A	**Analytical signal:** indirect paclitaxel sensing by monitoring the decrease in oxidation peak currents of (a) guanine ($E_{p\ guanine}$ ≈ +0.85 V *vs* Ag|AgCl).	[212]
	f(-COOH)MWCNTs – TiO_2NPs – ZrO_2NPs – CHIT / PGE	DPV	100.0 mM PB, pH 7.0, containing 20.0 mM NaCl	700.0 pM – 1.9 µM	LOD = 10.0 pM	**Real sample:** pharmaceutical formulation (injection), spiked blood serum, spiked urine. The interaction of paclitaxel with dsDNA.	**Tested interfering agents:** glucose, fructose, sucrose, lactose, urea, aspartic acid, citrate, ascorbic acid, Na^+, Mg^{2+}, Ca^{2+}, K^+, Br^-, F^-, NO_3^-, NO_2^-, SO_4^{2-}.	**Analytical signal:** paclitaxel oxidation (E_p ≈ +1.25 V *vs* Ag|AgCl).	[200]
	dsDNA / PGE	DPV	AcB, pH 4.8, containing 20.0 mM NaCl	200.0 nM – 10.0 µM	(a) LOD = 80.0 nM (b) LOD = 90.0 nM	**Real sample:** pharmaceutical formulation, spiked blood serum, spiked urine. The interaction of paclitaxel with dsDNA.	**Tested interfering agents:** glucose, sucrose, lactose, fructose, citric acid, ascorbic acid, methanol, ethanol, alanine, phenylalanine, methionine, glutamic acid, glycine, tryptophan, aspirin, thiourea, cysteine, cysteine,	**Analytical signal:** indirect paclitaxel sensing by monitoring the decrease in oxidation peak currents of (a) guanine ($E_{p\ guanine}$ ≈ +1.0 V *vs* Ag|AgCl|KCl_{3M}) and (b) adenine ($E_{p\ adenine}$ ≈ +1.3 V *vs* Ag|AgCl|KCl_{3M}).	[210]

							urea, uric acid, Ca^{2+}, Mg^{2+}, Al^{3+}, NH_4^+, SO_4^{2-}, F^-.		
	dsDNA – SAM(AHT) / AuE	DPV	10.0 mM TrisB, pH 7.4	120.0 nM – 1.5 µM	LOD = 12.0 nM	**Real sample:** spiked blood serum. The interaction of paclitaxel with dsDNA.	N/A	**Analytical signal:** indirect paclitaxel sensing by monitoring the decrease in guanine oxidation peak current ($E_{p\ guanine}$ ≈ +0.85 V *vs* Ag|AgCl|KCl_{3M}).	[211]
docetaxel 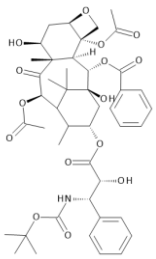	AuNPs – MWCNTs / GCE	DPASV	100.0 mM PB, pH 7.0	300.0 nM – 3.3 µM	LOD = 90.0 nM	**Real sample:** spiked urine, spiked blood serum.	**Tested interfering agents:** glucose, sucrose, fructose, lactose, ascorbic acid, dopamine, thiourea, alanine, methionine, glutamic acid, Na^+, K^+, Mg^{2+}, Fe^{3+}, Al^{3+}, Cl^-, CO_3^{2-}, NO_3^-.	**Analytical signal:** docetaxel oxidation (E_p ≈ +1.25 V *vs* Ag|AgCl|KCl_{sat}). Proposed electrochemical oxidation mechanism of docetaxel.	[198]
Topoisomerase 1 (TOP1) inhibitors									
irinotecan 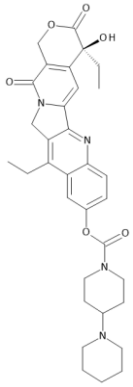	SMDE	SWAdSV	500.0 mM KNO_3, pH 5.0	5.0 nM – 120.0 nM	LOD = 2.6 nM LOQ = 8.7 nM	N/A	N/A	**Analytical signal:** irinotecan reduction (E_p ≈ –0.9 V *vs* Ag|AgCl|KCl_{3M}). Proposed electrochemical reduction mechanism of irinotecan.	[204]
	PGE	SWAdCSV	80.0 mM BRB, pH 5.0	79.4 nM – 403.0 nM	LOD = 1.7 nM LOQ = 5.6 nM	**Real sample:** spiked serum, spiked urine.	**Tested interfering species:** oxalic acid, glutaric acid, phenylalanine, alanine, ascorbic acid, TritonX-100, EDTA, Cd^{2+}, Ca^{2+}, Ba^{2+}, Mg^{2+}, Pb^{2+}, Co^{2+}, Ni^{2+}, Zn^{2+}.	**Analytical signal:** irinotecan reduction (E_p ≈ –1.0 V *vs* Ag|AgCl|KCl_{sat}). Possible determination of irinotecan in the presence of flutamide (31.0 µM).	[205]
	GCE	DPV	100.0 mM TBAHFP containing ACN, 730.0 µM Borax	200.0 nM – 9.0 µM	LOD = 112.0 nM LOQ = 376.0 nM	N/A	**Tested interfering species:** irinotecan metabolites.	**Analytical signal:** irinotecan oxidation (E_p ≈ +0.9 V *vs* Ag-pseudoRE). Proposed electrochemical oxidation mechanism of irinotecan.	[227]
	GCE	DPV	100.0 mM TBAHFP containing ACN, 730.0 µM Borax	250.0 nM – 9.0 µM	LOD = 110.0 nM LOQ = 374.0 nM	**Real sample:** spiked blood plasma collected from healthy volunteers, blood plasma collected from a patient undergoing chemotherapeutic treatment.	**Tested interfering species:** irinotecan metabolites.	**Analytical signal:** irinotecan oxidation (E_p ≈ +1.0 V *vs* Ag-pseudoRE).	[228]
	p-MTB – f(–COOH)MWCNTs / GCE	DPV	40.0 mM BRB, pH 10.0	8.0 µM – 80.0 µM	LOD = 214.0 nM LOQ = 650.0 nM	**Real sample:** pharmaceutical formulation (injection).	N/A	**Analytical signal:** irinotecan oxidation (E_p ≈ +0.6 V *vs* Ag|AgCl|KCl_{sat}). Proposed electrochemical oxidation mechanism of irinotecan.	[229]
	GQDs – p-ANI – ZnONPs / GCE	DPV	BRB, pH 10.0	50.0 nM – 30.0 µM	LOD = 11.0 nM	**Real sample:** pharmaceutical formulation	**Tested interfering species:** lactose, dextrose, glucose, uric acid, citric acid, ascorbic	**Analytical signal:** irinotecan oxidation (E_p ≈ +0.8 V *vs* Ag|AgCl).	[99]

						(injection), spiked serum, spiked urine.	acid, folic acid, caffeine, dopamine, ifosfamide, flutamide, etoposide, oxaliplatin, K^+, Na^+, Mg^{2+}, Ca^{2+}, CO_3^{2-}, NO^{3-}.	Determination of irinotecan performed in the presence of 5-fluorouracil (20.0 µM).	
	dsDNA – p-(MWCNTs-CTAB) / PGE	DPV	50.0 mM AcB, pH 4.8, containing 20.0 mM NaCl	3.4 µM – 17.1 µM 17.1 µM – 852.2 µM	LOD = 1.8 µM	**Real sample:** spiked blood serum. The interaction of irinotecan with dsDNA.	N/A	**Analytical signal:** indirect irinotecan sensing by monitoring the decrease in guanine oxidation peak current ($E_{p\ guanine}$ ≈ +0.95 V *vs* SCE).	[213]
	o-PD – AChE – ChOx – p-EI – BSA – GTA / PtE	CA	PB, pH 7.4	17.1 nM – 17.1 µM	LOD = 2.7 nM LOQ = 8.0 nM	**Real sample:** fetal bovine serum.	**Tested interfering species:** acetaminophen, irinotecan metabolites.	**Analytical signal:** acetylcholine esterase inhibition by irinotecan monitored by dropping H_2O_2 oxidation current. **Applied potential in CA:** E = +0.7 V (*vs* Ag|AgCl).	[214]
	AuME	FFTCCV with accumulation step	50.0 mM H_3PO_4	3.2 nM – 90.3 µM	LOD = 60.5 pM LOQ = 340.9 pM	**Real sample:** pharmaceutical formulation.	N/A	**Analytical signal:** irinotecan oxidation.	[203]
topotecan 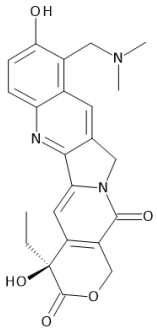	ABNPs / GCE	DPSV	100.0 mM PB, pH 7.0	4.8 nM – 949.1 nM	LOD = 3.4 nM	**Real sample:** spiked blood serum.	**Tested interfering species:** glucose, uric acid, glycine, histidine, hypoxanthine, dopamine, phenylalanine, adenine, vitamin C.	**Analytical signal:** topotecan oxidation (E_p ≈ +0.6 V *vs* SCE).	[230]
	TiO_2NPs – G – CHIT / GCE	SWV	BRB, pH 5.6	237.3 nM – 2.9 µM	LOD = 289.6 nM LOQ = 877.7 nM	**Real sample:** pharmaceutical formulation.	N/A	**Analytical signal:** topotecan oxidation (E_p ≈ +0.75 V *vs* Ag|AgCl|KCl_{3M}).	[231]
	WI-CPE	DPSV	100.0 mM PB, pH 4.0	2.0 pM – 10.0 pM 80.0 pM – 800.0 pM	LOD = 640.0 fM	**Real sample:** spiked urine.	**Tested interfering species:** urea, uric acid, Fe^{3+}, Al^{3+}, Na^+, Zn^{2+}, K^+, Cu^{2+}, Pb^{2+}, Ag^+, Mg^{2+}, SO_4^{2-}.	**Analytical signal:** topotecan oxidation (E_p ≈ +0.8 V *vs* SCE). Determination performed in the presence of sodium dodecyl sulfate (10.0 nM).	[201]
	N-RGO – IL (OMIM-Cl) / CPE	SWV	PB, pH 5.5	600.0 nM – 800.0 µM	LOD = 270.0 nM	**Real sample:** pharmaceutical formulation (injection), spiked pharmaceutical serum.	N/A	**Analytical signal:** topotecan oxidation (E_p ≈ +0.95 V). Simultaneous determination of topotecan and doxorubicin.	[232]
	dsDNA – GQDs – IL (BPy-PF_6) / CPE	DPSV	500.0 mM AcB, pH 4.8	350.0 nM – 100.0 µM	LOD = 100.0 nM	**Real sample:** spiked blood serum, spiked urine. The interaction of topotecan with dsDNA.	N/A	**Analytical signal:** topotecan oxidation (E_p ≈ +0.7 V *vs* Ag|AgCl|KCl).	[218]
	CuONPs – IL (BP-PF_6) / CPE	SWV	100.0 mM PB, pH 7.0	700.0 nM – 800.0 µM	LOD = 300.0 nM	**Real sample:** pharmaceutical formulation (injection).	N/A	**Analytical signal:** topotecan oxidation (E_p ≈ +0.95 V *vs* Ag|AgCl|KCl_{sat}). Simultaneous determination of topotecan and epirubicin.	[233]
	dsDNA – G / CPE	DPSV	500.0 mM AcB, pH 4.8	700.0 nM – 90.0 µM	LOD = 370.0 nM	**Real sample:** spiked urine, spiked blood serum.	N/A	**Analytical signal:** topotecan oxidation (E_p ≈ +0.7 V *vs* Ag|AgCl|KCl_{sat}).	[234]
	AuNPs – ABNPs / GCPE	SWSV	200.0 mM PB, pH 6.0	2.0 nM – 671.0 nM	LOD = 16.4 pM	**Real sample:** spiked serum, spiked urine.	**Tested interfering species:** uric acid.	**Analytical signal:** topotecan oxidation (E_p ≈ +0.7 V *vs* Ag|AgCl).	[202]
	CTAB-AuNRs – G / SPE	DPAdSV	100.0 mM PBS, pH 7.0	100.0 nM – 16.0 µM	LOD = 22.0 nM	**Real sample:** spiked blood serum.	**Tested interfering species:**	**Analytical signal:** topotecan oxidation (E_p ≈ +0.4 V).	[235]

							ascorbic acid, dopamine, glucose, uric acid, K^+, Na^+, Ca^{2+}, Cl^-, NO_3^-, SO_4^{2-}	Proposed electrochemical oxidation mechanism of topotecan.	
	ITIES	DPSV	10.0 mM Tris-AcB, pH 4.0	100.0 nM – 150.0 μM	LOD = 100.0 nM	**Real sample:** spiked serum.	**Tested interfering species:** azacytidine, carboplatin, gemcitabine, ascorbic acid, glucose, poly-L-lysine, Mg^{2+}.	**Analytical signal:** protonated topotecan interfacial ion transfer (E_{p+} ≈ +0.75 V *vs* Ag|AgCl).	[215]

Modification: ABNPs – acetylene black nanoparticles; **AChE** – acetylcholine esterase; **AHT** – 1-azidohexane-6-thiol; **AIBN** – 2-20-azobis (isobutyronitrile); **AuNPs** – gold nanoparticles; **BP-PF_6** – 1-butylpyridinium hexafluorophosphate; **BPy-PF_6** – 1-butylpyridinium hexafluorophosphate; **BSA** – bovine serum albumin; **CHIT** – chitosan; **ChOx** – choline oxidase; **CQDs** – carbon quantum dots; **CTAB-AuNRs** – hexadecyl(trimethyl)ammonium bromide-capped gold nanorods; **CuONPs** – copper oxide nanoparticles; **DNA** –deoxyribonucleic acid; **dsDNA** – double-stranded deoxyribonucleic acid; **EDC** – N-(3 dimethylaminopropyl)-N′-ethyl carbodiimide; **EGMRA** – ethylene glycol maleic rosinate acrylate; **f(-COOH)MWCNTs** – functionalized (carboxyl) multi-walled carbon nanotubes; **G** – graphene; **GO** – graphene oxide; **GQDs** – graphene quantum dots; **GTA** – glutaraldehyde; **IL** – ionic liquid; **MAA** – methyl acrylic acid; **MIP** – molecularly imprinted polymer; **MPA** – 3-mercaptopropionic acid; **MWCNTs** – multi-walled carbon nanotubes; **NHS** – N-hydroxy succinimide; **N-RGO** – nitrogen-doped reduced graphene oxide; **OMIM-Cl** – 1-methyl-3-octylimidazolium chloride; **o-PD** – o-phenylediamine; **p-(L-Cys)** – poly-(L-cysteine); **p-(MWCNTs-CTAB)** – poly-(multi-walled carbon nanotubes - hexadecyl(trimethyl)ammonium bromide); **p-ANI** – poly-aniline; **PdNPs** – palladium nanoparticles; **p-EDOT** – poly-(3,4-ethylenedioxythiophene); **p-EI** – poly-ethyleneimine; **p-MTB** – poly-methylene blue; **RGO** – reduced graphene oxide; **SAM** – self-assembled monolayer; **TiO_2NPs** – titanium dioxide nanoparticles; **TUB** – tubulin; **ZnONPs** – zinc oxide nanoparticles; **ZrO_2NPs** – zirconium dioxide nanoparticles; **($CoFe_2O_4$)NPs** – cobalt-doped ferrite nanoparticles; **(Zn-Al)-LDH** – zinc-aluminum layered double hydroxide.

Electrode: AP-PGE – anodically pretreated pencil graphite electrode; **AuE** – gold electrode; **AuME** – gold microelectrode; **CPE** – carbon (graphite) paste electrode; **DME** – dropping mercury electrode; **FTOE** – fluorine-doped tin oxide electrode; **GCE** – glassy carbon electrode; **GCPE** – glassy carbon paste electrode; **HMDE** – hanging mercury drop electrode; **ITIES** – interface between two immiscible electrolyte solutions; **PGE** – pencil graphite electrode; **PtE** – platinum electrode; **SMDE** – static mercury drop electrode; **SPCE** – screen printed carbon (graphite) electrode; **SPCPE** – screen-printed carbon (graphite) paste electrode; **SPE** – screen-printed electrode; **WI-CPE** – wax impregnated carbon (graphite) paste electrode;

Technique: CA – chronoamperometry; **CV** – cyclic voltammetry; **DPAdSV** – differential pulse adsorptive stripping voltammetry; **DPASV** – differential pulse anodic stripping voltammetry; **DPSV** – differential pulse stripping voltammetry; **DPV** – differential pulse voltammetry; **EIS** – electrochemical impedance spectroscopy; **FFTCCV** – fast Fourier transform continuous cyclic voltammetry; **LSAdSV** – linear sweep adsorptive stripping voltammetry; **SWAdCSV** – square-wave adsorptive cathodic stripping voltammetry; **SWAdSV** – square-wave adsorptive stripping voltammetry; **SWCSV** – square-wave cathodic stripping voltammetry; **SWSV** – square -wave stripping voltammetry; **SWV** – square-wave voltammetry.

Medium: AcB – acetate buffer; **ACN** – acetonitrile, **BB** – borate buffer; **BRB** – Britton-Robinson buffer; **PB** – phosphate buffer; **PBS** – phosphate buffered saline; **TBAHFP** – tetrabutylammonium hexafluorophosphate; **Tris-AcAB** – tris(hydroxymethyl)aminomethane hydrochloride - acetate buffer; **TrisB** – tris(hydroxymethyl)aminomethane hydrochloride.

Selectivity: when underlined – exhibited interference.

Comments: Ag|AgCl – silver|silver chloride electrode; **Ag|AgCl-pseudoRE** – silver|silver chloride pseudo-reference electrode; **Ag-pseudoRE** – silver pseudo-reference electrode; **SCE** – saturated calomel electrode.

N/A – not applicable.

Table 4. Comprehensive electroanalytical overview for the ANAs belonging to the group of cytostatic antibiotics and related substances.

Drug and its structure	Modification / Electrode	Technique	Medium	Linear range	LOD/LOQ	Application	Selectivity	Comments	Ref.
Anthracyclines and related substances									
doxorubicin 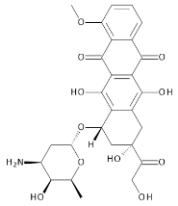	HMDE	SWV	100.0 mM AcB, pH 3.5	500.0 nM – 10.0 µM	LOD = 100.0 nM	N/A	N/A	**Analytical signal:** doxorubicin reduction ($E_p \approx -0.35$ V *vs* Ag|AgCl|KCl_{sat}). Proposed electrochemical reduction mechanism of doxorubicin.	[251]
	p-AgSAE	DPCSV	40.0 mM BRB, pH 6.0	600.0 nM – 10.0 µM	LOD = 440.0 nM	**Real sample:** spiked tap water, spiked urine.	N/A	**Analytical signal:** doxorubicin reduction ($E_p \approx -0.5$ V *vs* Ag|AgCl|KCl_{3M}).	[250]
	GCE	SWV	10.0 mM PBS, pH 6.5, containing 150.0 mM NaCl	10.0 nM – 3.0 µM	LOD = 400.0 pM	**Real sample:** spiked blood serum.	**Tested interfering agents:** thrombin, lysozyme, glucose oxidase, bovine serum albumin, paclitaxel, vinca alkaloids, 5-fluorouracil, cytarabine, methotrexate.	**Analytical signal:** doxorubicin reduction ($E_p \approx -0.55$ V vs. SCE). Dual-signal sensing of methylene blue (5.0 µM) and doxorubicin.	[252]
	GCE	DPV	100.0 mM AcB, pH 4.5	100.0 pM – 1.0 nM	LOD = 78.8 pM	N/A	N/A	**Analytical signal:** doxorubicin oxidation ($E_p \approx +0.5$ V *vs* SCE). Proposed electrochemical oxidation mechanism of doxorubicin.	[241]
	AgNPs – f(-COOH)MWCNTs / GCE	DPV	100.0 mM PB, pH 7.0	8.2 nM – 19.0 nM	LOD = 1.7 nM	N/A	N/A	**Analytical signal** doxorubicin reduction ($E_p \approx -0.65$ V *vs* SCE).	[253]
	AuNPs – f(-COOH)MWCNTs / GCE	LSV	100.0 mM PB, pH 7.0	10.0 pM – 1.0 µM 1.0 µM – 100.0 µM	LOD = 6.5 pM	**Real sample:** pharmaceutical formulation (injection).	N/A	**Analytical signal** doxorubicin reduction ($E_p \approx -0.8$ V *vs* SCE).	[237]
	o-MWCNTs – SDS / GCE	SWAdSV	BRB, pH 5.0	40.0 nM – 2.0 µM 2.0 µM – 90.0 µM	LOD = 9.4 nM	**Real sample:** spiked blood serum, spiked urine.	**Tested interfering agents:** glucose, tyrosine, L-cysteine, acetaminophen, citric acid, ascorbic acid, uric acid, levodopa, carbidopa, tryptophan, NaCl, KCl, $CaCl_2$, $MgSO_4$, $ZnCl_2$.	**Analytical signal:** doxorubicin oxidation ($E_p \approx +0.5$ V *vs* Ag|AgCl|KCl_{sat}). Determination of doxorubicin performed in the presence of dopamine (2.0 µM). Proposed electrochemical oxidation mechanism of doxorubicin.	[305]
	GQDs / GCE	DPV	20.0 mM PB, pH 4.0	18.0 nM – 3.6 µM	LOD = 16.0 nM	**Real sample:** spiked blood plasma.	N/A	**Analytical signal:** doxorubicin oxidation ($E_p \approx -0.55$ V *vs* Ag|AgCl). Proposed electrochemical oxidation mechanism of doxorubicin.	[306, 307]
	β-CD – GO / GCE	DPV	100.0 mM PB, pH 8.0	10.0 nM – 200.0 nM	LOD = 100.0 pM	N/A	**Tested interfering agents:** ascorbic acid, uric acid.	**Analytical signal:** doxorubicin oxidation ($E_p \approx -0.7$ V *vs* SCE).	[173]
	AgNPs – CHIT / GCE	SWV	100.0 mM PB, pH 5.8	103.0 nM – 8.6 µM	LOD = 103.0 nM	**Real sample:** untreated plasma. Determination of doxorubicin in	**Tested interfering agents:** arginine, leucine, tyrosine, acetate, aspartic acid, proline, NaCl, KCl, Cu^+.	**Analytical signal:** doxorubicin oxidation ($E_p \approx -0.5$ V *vs* Ag|AgCl|KCl_{sat}).	[308]

						murine melanoma cell line (B16F10).			
	p-TB / GCE	DPV	100.0 mM PB, pH 6.5	17.0 nM – 8.6 µM	LOD = 17.0 nM	**Real sample:** untreated plasma, plasma taken from patients treated with doxorubicin.	**Tested interfering agents:** ascorbic acid, aspartic acid, arginine, methionine, tyrosine, dopamine, serine, acetate, proline, leucine, glycine, cysteine, glucose, NaCl, KCl, Cu^{+}, Al^{3+}, Fe^{3+}, NH_4^{+}.	**Analytical signal:** doxorubicin oxidation ($E_p \approx -0.55$ V *vs* Ag|AgCl|KCl_{sat}). Possible determination of doxorubicin in mouse breast cancer cell line (4T1), human breast cancer cell line (MDA-MB-231). Proposed electrochemical oxidation mechanism of doxorubicin.	[309]
	AgNPs – CQDs – RGO / GCE	DPV	1.0 mM PB, pH 7.0	10.0 nM – 2.5 µM	LOD = 2.0 nM	**Real sample:** spiked blood serum.	**Tested interfering agents:** bovine serum albumin, lysozyme, glucose oxidase, 5-fluorouracil, methotrexate.	**Analytical signal:** doxorubicin oxidation ($E_p \approx$ +0.55 V *vs* SCE).	[310]
	(Pd-Pt)NPs – MWCNTs / GCE	SWAdSV	100.0 mM PBS, pH 6.0	3.8 nM – 8.4 µM	LOD = 730.0 pM	**Real sample:** spiked blood serum, spiked urine.	**Tested interfering agents:** dasatinib, bovine serum albumin, glucose, sucrose, lactose, ascorbic acid, urea, aspartic acid, KCl, NaCl.	**Analytical signal:** doxorubicin oxidation ($E_p \approx +0.5$ V *vs* Ag|AgCl|KCl_{3M}). Simultaneous determination of doxorubicin and dasatinib. Proposed electrochemical oxidation mechanism of doxorubicin.	[311]
	RGO – AuNPs – p-Py / GCE	CV	1.0 mM PB, pH 5.5	20.0 nM – 5.2 mM 5.2 mM – 25.0 mM	LOD = 20.0 nM	**Real sample:** pharmaceutical formulation (injection).	N/A	**Analytical signal:** doxorubicin oxidation ($E_p \approx +0.4$ V *vs* Ag|AgCl|KCl_{sat}).	[312]
	CuNPs – NAF – CB / GCE	SWV	100.0 mM BRB, pH 3.0	450.0 nM – 5.1 µM	LOD = 24.0 nM	**Real sample:** spiked urine, spiked river water.	**Tested interfering agents:** urea, KCl, NaCl, KH_2PO_4, $CaCl_2$, NH_4Cl.	**Analytical signal:** doxorubicin oxidation ($E_p \approx +0.65$ V *vs* Ag|AgCl|KCl_{3M}). Simultaneous determination of doxorubicin and methotrexate. Proposed electrochemical oxidation mechanism of doxorubicin.	[313]
	$FeVO_4$NPs – S-CNFBs / GCE	Amp.	100.0 mM PBS, pH 7.0	20.0 nM – 542.5 µM	LOD = 5.2 nM	**Real sample:** pharmaceutical formulation, spiked blood serum, spiked urine.	**Tested interfering agents:** folic acid, dopamine, uric acid, ascorbic acid, glucose, flutamide, methotrexate, riboflavin, pyrimethamine, epinephrine, avilamycin, ethopabate, clopidol, 5-fluorouracil, robenidine, halofuginone, etoposide, H_2O_2, nitrite, imatInib.	**Applied potential in amperometry:** $E \approx +0.25$ V *vs* Ag|AgCl). Proposed electrochemical oxidation mechanism of doxorubicin.	[314]
	CuNWs – (Mg_2-Al)-LDH / GCE	DPV	100.0 mM PB, pH 7.0	10.0 nM – 2.1 µM	LOD = 20.0 pM	**Real sample:** pharmaceutical formulation (injection), spiked urine, spiked blood.	**Tested interfering agents:** glucose, fructose, sucrose, lactose, urea, aspartic acid citrate, ascorbic acid, Na^{+}, Cl^{-}, F^{-}, Ca^{2+}, K^{+}, NO_3^{-}, SO_4^{2-}.	**Analytical signal:** doxorubicin oxidation ($E_p \approx +0.5$ V *vs* Ag|AgCl). Proposed electrochemical oxidation mechanism of doxorubicin.	[240]
	TiO_2NPs – NAF / GCE	LSAdSV	100.0 mM PB, pH 8.0	5.0 nM – 2.0 µM	LOD = 1.0 nM	**Real sample:** spiked blood plasma.	**Tested interfering agents:** uric acid, ascorbic acid, xanthine, L-cysteine,	**Analytical signal:** doxorubicin reduction ($E_p \approx -0.6$ V *vs* Ag|AgCl|KCl_{3M}).	[254]

							histidine, glucose, vitamin B6.	Determination of doxorubicin performed in the presence of a cationic surfactant cetyltrimethylammonium bromide (80.0 μM).	
	p-Styr – BPO – SDS – Fe_3O_4NPs – f(-SO_3H)GO / GCE	DPV	20.0 mM PB, pH 2.0	a) 43.0 nM – 3.5 μM b) 26.0 nM – 3.5 μM c) 860.0 nM – 13.0 μM	a) LOD = 4.9 nM b) LOD = 4.3 nM c) LOD = 14.0 nM	**Real sample:** a) spiked blood plasma, b) spiked urine, c) spiked cerebrospinal fluids.	**Tested interfering agents:** ascorbic acid, glucose, L-cysteine, tyrosine.	**Analytical signal:** doxorubicin oxidation (E_p ≈ –0.4 V *vs* Ag|AgCl). Proposed electrochemical oxidation mechanism of doxorubicin.	[315]
	p-Arg / GCE	DPV	120.0 mM PB, pH 7.4	a) 69.0 nM – 1.1 μM b) 103.0 nM – 3.5 μM	a) LOD = 69.0 nM b) LOD = 103.0 nM	**Real sample:** a) blood plasma, b) blood.	**Tested interfering agents:** alanine, arginine, aspartic acid, cysteine, glycine, histidine, leucine, lysine, methionine, phenylalanine, proline, tryptophan, tyrosine, valine, glucose, dopamine, ascorbic acid, acetate, Na^+, K^+, Zn^{2+}, Ca^{2+}, NH_4^+, Al^{3+}, Mg^{2+}, Fe^{3+}, Cl^-, $C_2O_4^{2-}$, NO_3^-.	**Analytical signal:** doxorubicin oxidation ($E_p \approx -0.7$ V *vs* Ag|AgCl|KCl_{sat}). Proposed electrochemical oxidation mechanism of doxorubicin.	[316]
	N-CNOs / GCE	DPV	100.0 mM PB, pH 7.0	200.0 pM – 10.0 μM	LOD= 60.0 pM	**Real sample:** spiked blood serum.	**Tested interfering agents:** glucose, urea, uric acid, ascorbic acid, dopamine, bilirubin, creatinine, vitamin B6, Na^+, K^+, Ca^{2+}, Mg^{2+}, CO_3^{2-}.	**Analytical signal** doxorubicin oxidation (E_p ≈ –0.6 V *vs* Ag|AgCl|KCl_{3M}). Proposed electrochemical oxidation mechanism of doxorubicin.	[317]
	MSNPs – ERGO / GCE	DPV	100.0 mM PB, pH 6.0	1.0 nM – 20.0 μM	LOD = 770.0 pM	**Real sample:** spiked blood.	N/A	**Analytical signal** doxorubicin oxidation (E_p ≈ –0.6 V *vs* Ag|AgCl|KCl_{sat}). Proposed electrochemical oxidation mechanism of doxorubicin.	[318]
	p-AMT – AuNPs – RGO / GCE	DPV	100.0 mM PB, pH 7.0	30.0 pM – 30.0 nM 30.0 nM – 30.0 μM	LOD = 9.0 pM	**Real sample:** spiked blood serum.	**Tested interfering agents:** glucose, fructose, valine, urea, ascorbic acid, uric acid, caffeine, xanthine, theophylline, Ca^{2+}, NO_3^-, SO_4^{2-}.	**Analytical signal** doxorubicin oxidation (E_p ≈ –0.6 V *vs* Ag|AgCl|KCl_{3M}).	[238]
	Cyst – L-GSH – MoS_2NPs / GCE	DPV	100.0 M PBS, pH 6.0	100.0 nM – 78.3 μM 98.3 μM – 1.2 mM	LOD = 31.0 nM	**Real sample:** spiked blood serum.	**Tested interfering agents:** Dopamine, glucose, lysine, uric acid, fructose, adenine, sucrose, folic acid, guaninę, ascorbic acid.	**Analytical signal** doxorubicin oxidation (E_p ≈ +0.5 V *vs* Ag|AgCl|KCl_{sat}). Proposed electrochemical oxidation mechanism of doxorubicin.	[319]
	DNA – OA – p-ANI / GCE	CV	HBS, pH 7.0	100.0 pM – 10.0 nM 10.0 nM – 200.0 μM	LOD = 10.0 pM	**Real sample:** pharmaceutical formulation. The interaction between DNA and doxorubicin.	**Tested interfering agents:** sulfanilamide, albumin, blood plasma electrolytes.	**Analytical signal:** Indirect doxorubicin sensing by monitoring the decrease in $[Fe(CN)_6]^{3-/4-}$ reduction peak current ($E_{p\ [Fe(CN)6]3-/4-}$ ≈ –0.5 V *vs* Ag|AgCl).	[267]
	DNA – p-Prof / GCE	EIS	10.0 mM $[Fe(CN)_6]^{3-/4-}$	1.0 nM – 100.0 nM	LOD = 300.0 pM	**Real sample:** pharmaceutical formulation, spiked solution simulating the plasma electrolytes.	**Tested interfering agents:** Ringer-Locke's solution, bovine serum albumin.	**Analytical signal** Indirect doxorubicin sensing by monitoring the redox reaction of $[Fe(CN)_6]^{3-/4-}$.	[266]

	dsDNA – PtNPs – AgNPs / SPCE	DPV	100.0 mM AcB, pH 4.7	184.0 nM – 920.0 nM	N/A	The interaction between DNA and doxorubicin.	N/A	**Analytical signal:** indirect doxorubicin sensing by monitoring the decrease in guanine ($E_{p\ guanine}$ ≈ +0.75 V *vs* Ag-pseudoRE) and adenine ($E_{p\ adenine}$ ≈ +1.0 V *vs* Ag-pseudoRE) oxidation peak currents.	[272]
	MSNPs / AP-GCE	DPV	100.0 mM PB, pH 6.0	500.0 pM – 2.0 µM 2.0 µM – 23.0 µM	LOD = 200.0 pM	**Real sample:** spiked blood.	**Tested interfering agents:** glucose, citric acid, L-leucine, L-threonine, glycine, acetaminophen, uric acid, ascorbic acid, dopamine, bovine serum albumin, Na^+, K^+, Mg^{2+}.	**Analytical signal:** doxorubicin oxidation ($E_p \approx -0.6$ V *vs* Ag|AgCl|KCl_{sat}). Proposed electrochemical oxidation mechanism of doxorubicin.	[320]
	CPE	DPAdSV	200.0 mM AcB, pH 4.5	100.0 nM – 10.0 µM	LOD = 10.0 nM	**Real sample:** spiked urine, urine from a patient with cancer undergoing treatment with doxorubicin.	N/A	**Analytical signal:** doxorubicin oxidation (E_p ≈ +0.5 V *vs* SCE).	[321]
	CPE	DPAdSV	40.0 mM BRB, pH 7.0	2.0 nM – 20.0 µM	LOD = 2.8 nM	N/A	N/A	**Analytical signal:** doxorubicin oxidation (E_p ≈ +0.45 V *vs* Ag|AgCl|KCl_{1M}).	[322]
	SDS / CPE	DPV	200.0 mM PBS, pH 6.2	2.0 µM – 24.0 µM	LOD = 390.0 nM	The interaction between DNA and doxorubicin.	**Tested interfering agents**: citric acid, oxalic acid, glucose, starch, succinic acid.	**Analytical signal:** doxorubicin oxidation (E_p ≈ +0.45 V *vs* SCE). Possible simultaneous determination of doxorubicin with dacarbazine. Proposed electrochemical oxidation mechanism of doxorubicin.	[76]
	f(-COOH)MWCNTs – ($CoFe_2O_4$)NPs / CPE	DPV	100.0 mM PB, pH 6.0	50.0 pM – 1.2 µM	LOD = 10.0 pM	**Real sample:** pharmaceutical formulation (injection), spiked blood serum, spiked urine.	**Tested interfering agents:** glucose, fructose, sucrose, lactose, urea aspartic acid citrate, ascorbic acid, Na^+, Ca^{2+}, K^+, Cl^-, F^-, NO_3^-, SO_4^{2-}.	**Analytical signal:** doxorubicin oxidation (E_p ≈ +0.5 V *vs* Ag|AgCl|KCl).	[239]
	ZnONPs – IL(BMIM-BF_4) / CPE	SWV	pH 5.0	70.0 nM – 500.0 µM	LOD = 9.0 nM	**Real sample:** pharmaceutical formulation (injection), spiked pharmaceutical serum.	**Tested interfering agents:** glucose, alanine, phenylalanine, methionine, glycine, valine, tryptophan.	**Analytical signal:** doxorubicin oxidation (E_p ≈ +0.7 V *vs* Ag|AgCl|KCl_{sat}). Possible simultaneous determination of doxorubicin and dasatinib. Proposed electrochemical oxidation mechanism of doxorubicin.	[323]
	($PtFe_3O_4$)NPs – MWCNTs / CPE	DPV	100.0 mM PB, pH 8.0	50.0 nM – 1.0 µM 1.0 µM – 70.0 µM	LOD = 1.0 nM LOQ = 33.0 nM	**Real sample:** spiked urine.	**Tested nterfering agents:** lactose monohydrate, urea, glucose, Ca^{2+}, Na^+, K^+, Mg^{2+}, NO_2^-, Cl^-, SO_4^{2-}, CO_3^{2-}.	**Analytical signal:** doxorubicin oxidation (E_p ≈ +0.4 V *vs* Ag|AgCl|KCl_{sat}).	[324]
	BPPDNi / (Pt-Co)NPs / CPE	SWV	PB, pH 7.4	500.0 nM – 300.0 µM	LOD = 100.0 nM	**Real sample:** pharmaceutical formulation (injection), spiked pharmaceutical serum, spiked hemolyzed erythrocyte.	**Tested interfering agents:** vitamin C, vitamin B_2, vitamin K_1, alanine, methionine, glycine, temadol, tamoxifen, tryptophan, epinephrine, dopamine.	**Analytical signal:** doxorubicin oxidation (E_p ≈ +0.45 V *vs* Ag|AgCl|KCl_{sat}). Possible simultaneous determination of doxorubicin, glutathione, and tyrosine.	[325]

	N-RGO – IL(OMIMCl) / CPE	SWV	PB, pH 5.5	6.0 nM – 750.0 µM	LOD = 3.1 nM	**Real sample:** pharmaceutical formulation (injection), spiked pharmaceutical serum.	**Tested interfering agents:** flutamide, dasatinib, 5-fluorouracil, ixabepilone, Na^+, K^+, Ca^{2+}, Ni^{2+}, Cl^-.	**Analytical signal:** doxorubicin oxidation ($E_p \approx +0.65$ V). Possible simultaneous determination of doxorubicin and topotecan. Proposed electrochemical oxidation mechanism of doxorubicin.	[232]
	dsDNA / AP-BPPyGE	SCP	AcB, pH 5.0	10.0 nM – 1.0 µM	LOD = 10.0 pM	N/A	N/A	**Analytical signal:** doxorubicin reduction and its coupling to catalytic oxygen reduction ($E_p \approx -0.5$ V *vs* Ag|AgCl|KCl_{3M}).	[255]
	mAb – AuNPs – f(–SH)-SG / AuE	EIS	100.0 µM PB, pH 5.0. 184.0 fM – 1.8 pM 4.6 pM – 92.0 pM	LOD = 165.9 fM	**Real sample:** spiked blood serum, spiked urine.	N/A	**Analytical signal:** Indirect doxorubicin sensing by monitoring the redox reaction of $[Fe(CN)_6]^{3-/4-}$.	[264]
	Ab_2 – HAuNSs – AG – BSA – Ab_1 –PrA– GMCNPs –AuNPs – p-AMAM / AuE	DPV	10.0 mM PB, pH 7.5	46.0 pM – 11.8 nM	LOD = 1.2 pM	**Real sample:** spiked blood serum.	N/A	**Analytical signal** Indirect doxorubicin sensing by monitoring the increase of penicillin binding protein 2a signal ($E_p \approx -0.65$ V *vs* Ag|AgCl|KCl_{sat}).	[265]
	NiHCF – (Ni-Al)-LDH / AuE	DPV	200.0 mM PB, pH 7.4	10.0 nM – 6.2 µM	LOD = 1.9 nM	**Real sample:** spiked blood serum.	**Tested interfering agents:** vitamin B_6, ascorbic acid, L-lysine, L-serine, glycine, glucose, sodium citrate.	**Analytical signal** doxorubicin reduction ($E_p \approx -0.65$ V *vs* Ag|AgCl|KCl_{sat}). Proposed electrochemical reduction mechanism of doxorubicin.	[256]
	SPDE	Amp.	40.0 mM BRB, pH 2.0	100.0 nM – 800.0 nM 800.0 nM – 2.5 µM	LOD = 36.0 nM LOQ = 104.0 nM	**Real sample:** pharmaceutical formulation (injection), spiked urine.	**Tested interfering agents:** ascorbic acid, dopamine, levodopa, uric acid, glucose, vitamin B_1, vitamin B_2, vitamin B_6, Na^+, K^+, Ca^{2+}, Mg^{2+}, Cu^{2+}, Zn^{2+}, Fe^{3+}, Cl^-, NO_3^-.	**Applied potential in amperometry:** $E \approx +1.1$ V *vs* Ag-pseudoRE). Proposed electrochemical oxidation mechanism of doxorubicin.	[326]
	CTAB – AuNRs – MoS_2NPs / SPE	DPAdSV	100.0 mM PBS, pH 6.0	10.0 nM – 9.5 µM	LOD = 2.5 nM	**Real sample:** spiked blood serum.	**Tested interfering agents:** 5-fluorouracil, ascorbic acid, dopamine, glucose, uric acid, Na^+, Mg^{2+}, Cl^-, SO_4^{2-}.	**Analytical signal:** doxorubicin oxidation ($E_p \approx +0.45$ V *vs* Ag-pseudoRE).	[327]
	AuNPs – AL – dsDNA – p-TTCA – AuNPs / SPE	Amp.	100.0 mM PBS, pH 7.4	7.5 pM – 50.0 pM	LOD = 3.6 fM	**Real sample:** spiked urine.	**Tested interfering agents:** ascorbic acid, uric acid, acetaminophen, dopamine.	**Applied potential in amperometry:** $E \approx -0.7$ V *vs* Ag|AgCl). Simultaneous determination of doxorubicin, daunorubicin, Idarubicin, and mitoxantrone.	[249]
	ITIES	DPV	1.0 mM HCl, pH 3.0	1.0 µM – 40.0 µM	LOD = 840.0 nM	N/A	N/A	**Analytical signal:** protonated doxorubicin interfacial ion transfer ($E_{p+} \approx +0.65$ V *vs* Ag|AgCl).	[250]
daunorubicin	HMDE	DPAdSV	100.0 mM AcB, pH 4.4	20.0 nM – 140.0 nM	N/A	**Real sample:** spiked urine.	**Tested interfering agents:** fluorouracil, methotrexate, dodecyl sodium sulfate, camphor, albumin, gelatin, ascorbic acid, Cu^{2+}.	**Analytical signal:** daunorubicin reduction ($E_p \approx -0.6$ V *vs* Ag|AgCl|KCl_{sat}). Proposed electrochemical mechanism of daunomycin.	[328]
	DNA – p-Prof / GCE	EIS	10.0 mM $[Fe(CN)_6]^{3-/4-}$	1.0 pM – 10.0 nM	LOD = 1.0 pM	**Real sample:**	**Tested interfering agents:**	**Analytical signal**	[266]

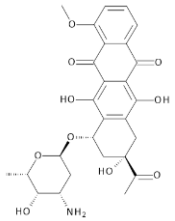						pharmaceutical formulation, spiked solution simulating the plasma electrolytes.	Ringer-Locke's solution, bovine serum albumin.	Indirect daunorubicin sensing by monitoring the redox reaction of $[Fe(CN)_6]^{3-/4-}$.	
	DNA – OA – p-ANI / GCE	CV	HBS, pH 7.0	500.0 pM – 10.0 µM	LOD = 100.0 pM	**Real sample:** pharmaceutical formulation. The interaction between DNA and daunorubicin.	**Tested interfering agents:** sulfanilamide, albumin, blood plasma electrolytes.	**Analytical signal:** Indirect daunorubicin sensing by monitoring the decrease in $[Fe(CN)_6]^{3-/4-}$ reduction peak current ($E_{p\ [Fe(CN)6]3-/4-} \approx -0.5$ V *vs* Ag|AgCl).	[267]
	AuNPs – PTTBA – PS – AuNPs / GCE	DPV	100.0 mM PB, pH 7.4, containing 0.9% NaCl	100.0 pM – 60.0 nM	LOD = 52.3 pM	**Real sample:** spiked urine.	**Tested interfering agents:** tetracycline, kanamycin, chloramphenicol, neomycin, anthraquinone, doxorubicin.	**Analytical signal:** daunorubicin reduction ($E_p \approx -0.6$ V *vs* Ag|AgCl|KCl_{sat}).	[257]
	dsDNA – PtNPs – SWCNTs / GCE	DPV	TrisB, pH 7.4	4.0 nM – 250.0 µM	LOD = 1.0 nM	**Real sample:** pharmaceutical formulation (injection). The interaction between DNA and daunorubicin.	**Tested interfering agents:** glycine, valine, methionine, vitamin B6, vitamin C, K^+, Na^+, Cl^-, F^-.	**Analytical signal:** indirect doxorubicin sensing by monitoring the decrease in guanine oxidation peak current ($E_{p\ guanine} \approx +0.9$ V *vs* Ag|AgCl|KCl_{sat}).	[276]
	dsDNA – 4-ATP – AgNPs – f(-COCl)MWCNTs / CPE	DPAdSV	500.0 mM AcB, pH 5.5	1.0 nM – 10.0 µM	LOD = 300.0 pM LOQ = 1.0 nM	**Real sample:** spiked blood serum, spiked urine. The interaction between dsDNA and daunorubicin.	**Tested interfering agents:** folic acid, glucose, urea, ascorbic acid.	**Analytical signal:** daunorubicin oxidation ($E_p \approx -0.65$ V *vs* Ag|AgCl|KCl_{sat}).	[279]
	AuNPs – AL – dsDNA – p-TTCA – AuNPs / SPE	Amp.	100.0 mM PBS, pH 7.4	8.0 pM – 50.0 pM	LOD = 5.5 fM	**Real sample:** spiked urine.	**Tested interfering agents:** ascorbic acid, uric acid, acetaminophen, dopamine.	**Applied potential in amperometry:** $E \approx -0.7$ V *vs* Ag|AgCl). Simultaneous determination of daunorubicin, Idarubicin, mitoxantrone, and doxorubicin.	[249]
	RGO / PGE	DPV	AcB, pH 4.8	1.0 nM – 6.0 µM	LOD = 550.0 nM	The interaction between DNA and daunorubicin.	N/A	**Analytical signal:** daunorubicin oxidation ($E_p \approx +0.5$ V *vs* Ag|AgCl|KCl_{3M}).	[277]
	p-AMAM / PGE	DPV	50.0 mM PB, pH 7.4	N/A	LOD = 128.0 nM	N/A	N/A	**Analytical signal:** daunorubicin oxidation ($E_p \approx +0.5$ V *vs* Ag|AgCl|KCl).	[329]
	COOH / ITOE	LSAdSV	5.0 mM PB, pH 7.1	200.0 nM – 5.0 µM	LOD = 100.0 nM	**Real sample:** spiked urine.	N/A	**Analytical signal:** daunorubicin reduction ($E_p \approx -0.65$ V *vs* Ag|AgCl).	[330]
	ITIES	DPV	10.0 mM TrisB, pH 7.2	12.0 µM – 82.0 µM	LOD = 800.0 nM	**Real sample:** spiked blood plasma.	**Tested interfering agents:** ascorbic acid, aspartic acid, arginine, glycine, lysine, glucose, sucrose, K^+, Zn^{2+}, Mg^{2+}.	**Analytical signal:** protonated daunorubicin interfacial ion transfer ($E_{p+} \approx +0.8$ V *vs* Ag|AgCl).	[271]
epirubicin	BDDE	DPV	100.0 mM H_2SO_4, containing and 20 % of MeOH	920.0 nM – 73.6 µM	LOD = 79.1 nM LOQ = 261.3 nM	**Real sample:** pharmaceutical formulation (injection).	N/A	**Analytical signal:** epirubicin oxidation ($E_p \approx +0.95$ V *vs* Ag|AgCl|KCl_{sat}). Determination of epirubicin in the presence of 1.0 mM sodium dodecyl sulphate. Proposed electrochemical oxidation mechanism of epirubicin.	[331]

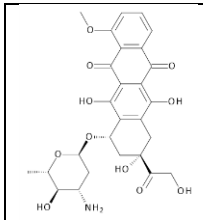	(Ce-ZnO)NFLs / GCE	DPV	100.0 mM PBS, pH 7.0	10.0 nM – 600.0 µM	LOD = 2.3 nM	**Real sample:** pharmaceutical formulation (injection), spiked blood serum, spiked urine.	**Tested interfering agents:** uric acid, rutin, ascorbic acid, glucose, tyrosine, tryptophan, morphine.	**Analytical signal:** epirubicin oxidation (E_p ≈ +0.7 V *vs* SCE). Possible simultaneous determination of epirubicin and methotrexate. Proposed electrochemical oxidation mechanism of epirubicin.	[163]
	AgNPs – f(-COOH)MWCNTs / GCE	SWAdSV	100.0 mM AcB, pH 4.7	3.0 nM – 250.0 nM	LOD = 1.0 nM	**Real sample:** pharmaceutical formulation (injection), spiked urine, spiked blood.	**Tested interfering agents:** ascorbic acid, glucose, uric acid, caffeine, vitamin A, vitamin E, dopamine, Na^+, K^+, Fe^{2+}, Fe^{3+}, Cu^{2+}, Hg^{2+}, Pb^{2+}, Ca^{2+}, Zn^{2+}, Cl^-, SO_4^{2-}, NO_3^-.	**Analytical signal:** epirubicin oxidation (E_p ≈ –0.5 V *vs* SCE). Proposed electrochemical oxidation mechanism of epirubicin.	[242]
	CuONPs – IL(BMIM-BF_4) / CPE	SWV	100.0 mM PB, pH 7.0	30.0 nM – 800.0 µM	LOD = 8.0 nM	**Real sample:** pharmaceutical formulation (injection).	**Tested interfering agents:** ascorbic acid, glycine, ampicillin, Li^+, K^+, Br^-.	**Analytical signal:** epirubicin oxidation (E_p ≈ +0.6 V *vs* Ag|AgCl|KCl_{sat}). Simultaneous determination of epirubicin and topotecan. Proposed electrochemical oxidation mechanism of epirubicin.	[233]
	Fe_3O_4NPs – SWCNTs – IL(OMIMCl) / CPE	SWV	PB, pH 5.0	20.0 nM – 700.0 µM	LOD = 7.0 nM	**Real sample:** pharmaceutical formulation (injection), spiked pharmaceutical serum.	**Tested interfering agents:** methionine, methionine, alanine, phenylalanine, dasatinib, abemaciclib, anastrozole.	**Analytical signal:** epirubicin oxidation (E_p ≈ +0.75 V *vs* Ag|AgCl|KCl_{sat}). Proposed electrochemical oxidation mechanism of epirubicin.	[332]
	($CoFe_2O_4$)NPs – IL(DPIM-Br) / CPE	SWV	100.0 mM PB, pH 7.0	40.0 nM – 450.0 µM	LOD = 10.0 nM	**Real sample:** pharmaceutical formulation (injection), spiked pharmaceutical serum.	**Tested interfering agents:** glucose, ascorbic acid, phenylalanine, isolucin, tryptophan, glycine, starch, K^+, Li^+, F^-, NO_3^-, Br^-.	**Analytical signal:** epirubicin oxidation (E_p ≈ +0.6 V). Proposed electrochemical oxidation mechanism of epirubicin.	[333]
	5'HS−DNA3' – AuNPs – (Fe_3O_4-SiO_2)NPs-DABCO / SPCE	LSV	100.0 mM PB, pH 7.4, containing 100.0 mM KCl	70.0 nM – 1.0 µM 3.0 µM – 21.0 µM	LOD = 40.0 nM	**Real sample:** pharmaceutical formulation (injection), spiked blood serum.	**Tested interfering agents:** paclitaxel, docetaxel, tamoxifen, imatinib.	**Analytical signal:** epirubicin reduction (E_p ≈ –0.7 V *vs* Ag-pseudoRE).	[334]
	AuNPs– f(-COOH)MWCNTs –CTAB – ZnONPs / SPCE	SWV	100.0 mM AcB, pH 4.5	5.0 nM – 200.0 nM	LOD = 2.5 nM	**Real sample:** pharmaceutical formulation (injection), spiked and diluted blood.	**Tested interfering agents:** glucose, ascorbic acid, dopamine, uric acid.	**Analytical signal:** epirubicin reduction (E_p ≈ –0.6 V *vs* Ag|AgCl). Determination of epirubicin performed in the presence of methotrexate (500.0 nM).	[177]
	dsDNA – AuNCs / SPCE	DPV	10.0 mM TrisB, pH 7.2	40.0 nM – 800.0 nM 800.0 nM – 20.0 µM	LOD = 10.0 nM	**Real sample:** spiked blood serum. The interaction between DNA and epirubicin.	**Tested interfering agents**: docetaxel, tamoxifen, paclitaxel.	**Analytical signal:** epirubicin reduction (E_p ≈ –0.75 V *vs* Ag-pseudoRE).	[283]
	dsDNA – PtNPs – AgNPs / SPCE	DPV	100.0 mM AcB, pH 4.7	552.0 nM – 1.8 µM	N/A	The interaction between DNA and epirubicin.	N/A	**Analytical signal:** indirect epirubicin sensing by monitoring the decrease in guanine ($E_{p\,guanine}$ ≈ +0.8 V *vs* Ag-	[272]

								pseudoRE) oxidation peak current.	
	dsDNA– N-RGO – p-Py / PGE	DPV	500.0 mM AcB, pH 4.8	4.0 nM – 55.0 µM	LOD = 1.0 nM	**Real sample:** pharmaceutical formulation (injection), spiked urine. The interaction between dsDNA and epirubicin.	**Tested interfering agents**: tryptophan, tyrosine, alanine, glucose, K^+, Na^+, Mg^{2+}, Br^-, Cl^-.	**Analytical signal:** indirect epirubicin sensing by monitoring the decrease in guanine oxidation peak current ($E_{p\ guanine}$ ≈ +0.9 V *vs* Ag|AgCl|KCl_{sat}).	[269]
idarubicin 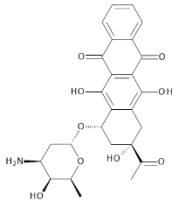	Ru – CB / GCE	DPAdSV	PB, pH 1.5	50.0 nM – 1.0 µM	LOD = 9.3 nM LOQ = 28.0 nM	**Real sample:** pharmaceutical formulation (vial), spiked blood serum.	N/A	**Analytical signal:** idarubicin oxidation (E_p ≈ +0.7 V *vs* Ag|AgCl).	[335]
	MWCNTs / GCE	DPAdSV	200.0 mM PB, pH 3.0	93.6 nM – 1.9 µM	LOD = 18.7 nM LOQ = 74.9 nM	**Real sample:** pharmaceutical formulation.	**Tested interfering agents**: dopamine, ascorbic acid, aspirin.	**Analytical signal:** idarubicin oxidation (E_p ≈ +0.6 V *vs* Ag|AgCl|KCl_{3M}). Proposed electrochemical oxidation mechanism of idarubicin.	[336]
	DNA – OA – p-ANI / GCE	CV	HBS, pH 7.0	1.0 nM – 100.0 µM	LOD = 200.0 pM	**Real sample:** pharmaceutical formulation. The interaction between DNA and idarubicin.	**Tested interfering agents:** sulfanylamides, albumin, blood plasma electrolytes.	**Analytical signal:** Indirect idarubicin sensing by monitoring the decrease in $[Fe(CN)_6]^{3-/4-}$ reduction peak current ($E_{p\ [Fe(CN)6]3-/4-}$ ≈ –0.5 V *vs* Ag|AgCl).	[267]
	dsDNA – PtNPs – AgNPs / SPCE	DPV	100.0 mM AcB, pH 4.7	201.0 nM – 1.0 µM	N/A	The interaction between DNA and idarubicin.	N/A	**Analytical signal:** indirect idarubicin sensing by monitoring the decrease in guanine ($E_{p\ guanine}$ ≈ +0.75 V *vs* Ag-pseudoRE) and adenine ($E_{p\ adenine}$ ≈ +1.0 V *vs* Ag-pseudoRE) oxidation peak currents.	[272]
	AuNPs – AL – dsDNA – p-TTCA – AuNPs / SPE	Amp.	100.0 mM PBS, pH 7.4	5.0 pM – 55.0 pM	LOD = 2.2 fM	**Real sample:** spiked urine.	**Tested interfering agents:** ascorbic acid, uric acid, acetaminophen, dopamine.	**Applied potential in amperometry:** $E \approx -0.7$ V *vs* Ag|AgCl). Simultaneous determination of. Idarubicin, mitoxantrone, daunorubicin, and doxorubicin.	[249]
	TiO_2NPs – CNFBs / CPE	SWV	100.0 mM PB, pH 2.0	12.0 nM – 10.0 µM	LOD = 3.0 nM	**Real sample:** spiked blood serum, spiked urine.	**Tested interfering agents:** epirubicin, doxorubicin, daunorubicin, cysteine, ascorbic acid, glucose, lactose, fructose, citric acid, uric acid, urea, acetaminophen, Ca^{2+}, Mg^{2+}, Fe^{2+}, Fe^{3+}, Cl^-.	**Analytical signal:** idarubicin oxidation (E_p ≈ +0.75 V *vs* Ag|AgCl|KCl_{sat}). Proposed electrochemical oxidation mechanism of idarubicin.	[243]
	MWCNTs / EPPyGE	DPAdSV	200.0 mM PB, pH 3.0	93.6 nM – 936.0 nM	LOD = 37.5 nM LOQ = 93.6 nM	**Real sample:** pharmaceutical formulation.	**Tested interfering agents**: dopamine, ascorbic acid, aspirin.	**Analytical signal:** idarubicin oxidation (E_p ≈ +0.6 V *vs* Ag|AgCl|KCl_{3M}). Proposed electrochemical oxidation mechanism of idarubicin.	[336]
mitoxantrone	GCE	SWV	160.0 mM BRB, pH 2.0, containing 1.3 M KCl and 30% EtOH	100.0 nM – 1.0 µM	LOD = 100.0 nM	N/A	N/A	**Analytical signal:** mitoxantrone oxidation (E_p ≈ +0.75 V *vs* Ag|AgCl|KCl_{3M}).	[337]

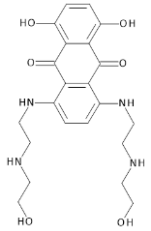								Proposed electrochemical oxidation mechanism of mitoxantrone.	
	f(-SO_3H)SiO_2NPs / GCE	DPV	50.0 mM TrisB, pH 7.4	500.0 nM – 173.0 µM	LOQ = 500.0 nM	**Real sample:** spiked blood serum.	N/A	**Analytical signal:** mitoxantrone oxidation (E_p ≈ +0.55 V *vs* Ag|AgCl). Proposed electrochemical oxidation mechanism of mitoxantrone.	[338]
	MIP(β-CD) / GCE	DPV	100.0 mM PB, pH 6.0	60.0 nM –10.0 µM	LOD = 30.0 nM	**Real sample:** pharmaceutical formulations, spiked urine.	**Tested interfering agents:** 1,4-diaminoanthraquinone, p-1-amino-anthraquinone, dihydroxybenzene, ketoprofen, piroxicam, sulfamethoxazole, tenoxicam, gatifloxacin, glucose, ascorbic acid, uric acid.	**Analytical signal:** mitoxantrone oxidation (E_p ≈ +0.45 V *vs* SCE).	[246]
	CPE	ACAdSV	100.0 mM $HClO_4$	5.0 nM – 150.0 µM	N/A	**Real sample:** spiked urine.	N/A	**Analytical signal:** mitoxantrone oxidation. Proposed electrochemical oxidation mechanism of mitoxantrone.	[339]
	CPE	ACAdSV	100.0 mM $HClO_4$	50.0 pM – 700.0 pM 700.0 pM – 2.0 nM	LOD = 50.0 pM	**Real sample:** spiked urine.	**Tested interfering agents:** surfactants (SDS, CTAC, Triton X-100, gelatin).	**Analytical signal:** mitoxantrone oxidation (E_p ≈ +0.65 V *vs* SCE).	[245]
	dsDNA – IL(BMIM-$MeSO_3$) – ZIF-8 / CPE	DPV	50.0. mM AcB, pH 4.8	8.0 nM – 110.0 µM	LOD = 3.0 nM	**Real sample:** pharmaceutical formulations (injection). The interaction between dsDNA and mitoxantrone.	**Tested interfering agents:** methionine, alanine, phenylalanine, vitamin C, vitamin B_2, Na^+, Li^+, Br^-, NO_3^-.	**Analytical signal:** indirect mitoxantrone sensing by monitoring the decrease in guanine oxidation peak current ($E_{p\ guanine}$ ≈ +0.8 V *vs* Ag|AgCl|KCl_{sat}).	[270]
	AuNPs – AL – dsDNA – p-TTCA – AuNPs / SPE	Amp.	100.0 mM PBS, pH 7.4	2.0 pM – 60.0 pM	LOD = 1.2 fM	**Real sample:** spiked urine.	**Tested interfering agents:** ascorbic acid, uric acid, acetaminophen, dopamine.	**Applied potential in amperometry:** E ≈ –0.7 V *vs* Ag|AgCl). Simultaneous determination of mitoxantrone, daunorubicin, doxorubicin, and idarubicin.	[249]
	Co^{2+} / CFBUME	LSAdSV	5.0 mM TrisB, pH 7.1	200.0 nM – 6.0 µM	LOD = 42.0 nM	**Real sample:** spiked urine.	N/A	**Analytical signal:** mitoxantrone reduction (E_p ≈ –0.8 V *vs* SCE).	[340]
valrubicin 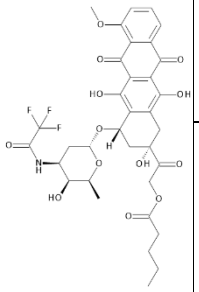	AuNPs – CeO_2NPs – f(-OH)MWCNTs – f(-OH)GCMSs / CPE	SWV	200.0 mM PB, pH 11.2	71.0 nM – 580.0 nM	LOD = 1.6 nM LOQ = 5.2 nM	**Real sample:** spiked urine, spiked blood serum. The interaction between dsDNA and valrubicin.	**Tested interfering agents:** ascorbic acid, glutamic acid, aspartic acid, caffeine, sucrose, glucose, NaCl, KCl.	**Analytical signal:** valrubicin oxidation (E_p ≈ +0.15 V *vs* Ag|AgCl|KCl_{sat}). Proposed electrochemical oxidation mechanism of valrubicin.	[244]
	AuNPs – en – MWCNTs / AuE	CV	10.0 mM CB, pH 4.0 containing 1.0 mM KCl	500.0 nM – 80.0 µM	LOD = 18.0 nM	**Real sample:** spiked urine, spiked blood serum. The interaction between DNA and valrubicin.	**Tested interfering agents:** caffeine, ascorbic acid, azithromycin, urea, glucose, sucrose, paracetamol, Na^+, K^+, Fe^{2+}, Mg^{2+}, Ca^{2+}.	**Analytical signal:** valrubicin reduction (E_p ≈ +0.55 V *vs* Ag|AgCl|3M KCl). Proposed electrochemical mechanism of valrubicin.	[258]
pirarubicin	dsDNA / DRCE	LSV	100.0 mM PB, pH 7.5 containing 10.0 mM KCl	1.0 pM – 50.0 pM	LOD = 112.0 pM	**Real sample**	**Tested interfering agents:**	**Analytical signal:**	[261]

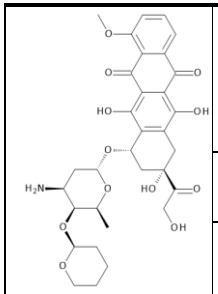						spiked fetal bovine serum.	acetaminophen, ascorbic acid.	pirarubicin reduction (E_p ≈ -0.5 V *vs* SCE). Possible determination of pirarubicin in the presence of acetaminophen and ascorbic acid.	
	AuNPs / ITOE	CV	10.0 mM PB, pH 7.9	5.0 nM – 1.5 µM	LOD = 1.0 nM	**Real sample:** spiked urine.	**Tested interfering agents:** ascorbic acid, glucose, urea.	**Analytical signal:** pirarubicin reduction (E_p ≈ -0.8 V *vs* SCE).	[259]
	COOH / ITOE	DPV	5.0 mM PB, pH 7.2	600.0 pM – 25.0 nM 14.0 µM – 2.8 µM	LOD = 200.0 pM	N/A	**Tested interfering agents** ascorbic acid, glucose, urea, NH_4^+, Ca^{2+}, Cu^{2+}, Ba^{2+}, Zn^{2+}, Mn^{2+}, Co^{2+}, I^-, Cl^-, SO_4^{2-}.	**Analytical signal:** pirarubicin reduction (E_p ≈ -0.5 V *vs* Ag|AgCl|KCl_{sat}).	[260]
Other cytotoxic antibiotics									
bleomycin 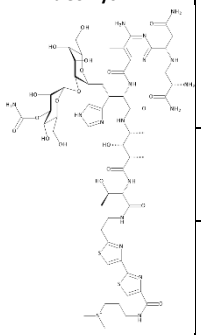	HMDE	LSAdSV	50.0 mM H_2SO_4	1.0 nM – 100.0 nM	LOD = 500.0 pM	**Real sample:** spiked mouse blood serum.	N/A	**Analytical signal:** bleomycin reduction (E_p ≈ –1.05 V *vs* Ag|AgCl|KCl_{sat}). Proposed electrochemical reduction mechanism of bleomycin.	[262]
	Fc-ssDNA – Zr(IV)-MOF (NH_2-UiO-66) / GCE	SWV	10.0 mM PB, pH 7.4	5.0 pM – 20.0 nM	LOD = 4.0 pM	**Real sample:** spiked diluted blood serum.	**Tested interfering agents:** mitomycin, daunorubicin, dactinomycin.	**Analytical signal:** bleomycin-Fe^{2+} complex oxidation (E_p ≈ +0.45 V *vs* Ag|AgCl|KCl_{3M}).	[248]
	MTB-DNA / ITOE	DPV	20.0 mM PB, pH 8.0	100.0 pM – 100.0 nM	LOD = 33.0 pM	**Real sample:** spiked blood serum.	**Tested interfering agents:** dactinomycin, daunorubicin, mitomycin, tryptophan, cysteine, lysine, L-threonine, ascorbate, urea, glucose.	**Analytical signal:** bleomycin-Fe^{2+} complex oxidation (E_p ≈ – 0.25 V *vs* Ag|AgCl).	[247]
	5'-HS-DNA3' / AuE	DPV	1.0 M KNO_3	1.0 pM – 100.0 nM	LOD = 740.0 fM	**Real sample:** spiked blood serum.	**Tested interfering agents:** daunorubicin, mitomycin, dactinomycin.	**Analytical signal:** Indirect bleomycin sensing by monitoring the increase in $[Fe(CN)_6]^{3-/4-}$ oxidation peak current (E_p ≈ +0.25 V *vs* SCE).	[341]
mitomycin 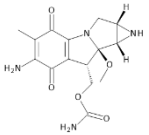	HMDE	SV	300.0 mM $HCOONH_4$, 50.0 mM Na_3PO_4, pH 6.9	10.0 nM – 200.0 nM	LOD = 10.0 nM	**Real sample:** spiked urine.	N/A	**Analytical signal:** mitomycin reduction (E_p ≈ -0.35 V *vs* SCE). Determination of mitomycin in the presence of 5-fluorouracil and cisplatin.	[263]
	dsDNA – p-EDOT / PGE	DPV	50.0 mM PB, pH 7.4 containing 20.0 mM NaCl	3.0 µM – 150.0 µM	LOD = 7.8 nM	The interaction between dsDNA and mitomycin.	N/A	**Analytical signal:** indirect mitomycin sensing by monitoring the decrease in guanine oxidation peak current ($E_{p\,guanine}$ ≈ +0.85 V *vs* Ag|AgCl).	[212]
	dsDNA – p-Gly – MWCNTs / PGE	DPV	50.0 mM PB, pH 7.4, containing 20.0 mM NaCl	15.0 µM – 448.7 µM	LOD = 5.3 µM	**Real sample:** spiked blood serum. The interaction between dsDNA and mitomycin.	N/A	**Analytical signal:** indirect mitomycin sensing by monitoring the decrease in guanine oxidation peak current ($E_{p\,guanine}$ ≈ +0.9 V *vs* Ag|AgCl).	[291]
	dsDNA – L-LysNFLs / AP-PGE	DPV	N/A	59.8 µM – 299.1 µM	LOD = 37.5 µM	The interaction between dsDNA and mitomycin.	N/A	**Analytical signal:** indirect mitomycin sensing by monitoring the decrease in guanine oxidation peak current ($E_{p\,guanine}$ ≈ +0.85 V *vs* Ag|AgCl|KCl_{3M}).	[289]

	dsDNA – p-oPD – MWCNTs / PGE	DPV	50.0 mM AcB, pH 4.8	1.5 µM – 74.8 µM	LOD = 35.9 nM LOQ = 116.7 nM	**Real sample:** spiked urine. The interaction between dsDNA and mitomycin.	N/A	**Analytical signal:** indirect mitomycin sensing by monitoring the decrease in guanine oxidation peak current ($E_{p\ guanine}$ ≈ +0.9 V *vs* Ag|AgCl).	[290]
plicamycin 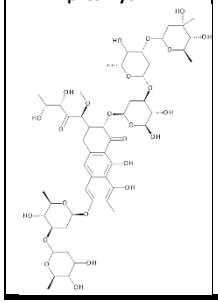	dsDNA – AuNPs / AuE	EIS	4.0 mM $[Fe(CN)_6]^{3-/4-}$ in 100.0 mM PB, pH 7.0, containing 300.0 mM $NaClO_4$	15.0 nM – 1.0 µM	LOD = 10.0 nM	The interaction between dsDNA and plicamycin.	N/A	**Analytical signal:** Indirect plicamycin sensing by monitoring the redox reaction of $[Fe(CN)_6]^{3-/4-}$.	[268]

Modification: 4-ATP – 4-aminothiophenol; **5'MB-DNA3'** – DNA probe labeled with methylene blue at the 5′ terminus; **5'HS–DNA3'** –5′-thiol terminated deoxyribonucleic acid probe; **Ab_1** – mouse anti-PbP2a antibody; **Ab_2** – rabbit anti-PbP2a (anti-penicilin binding protein) antibody; **AG** – PbP2a (penicillin binding protein) antigen; **AgNPs** – silver nanoparticles; **AL** – anionic lipid; **AuNCs** – gold nanocubes; **AuNPs** – gold nanoparticles; **AuNRs** – gold nanorods; **BMIM-BF_4** – 1-butyl-3-methylimidazolium tetrafluoroborate; **BMIM-$MeSO_3$** – 1-butyl-3-methylimidazolium methanesulfonate; **BPO** – benzoyl peroxide; **BPPDNi** – bis(1,10-phenanthroline) (1,10-phenanthroline-5,6-dione) nickel(II) hexafluorophosphate; **BSA** – bovine serum albumin; **CB** – carbon black; **CeO_2NPs** – cerium(IV) oxide nanoparticles; **CHIT** – chitosan; **CNFBs** – carbon nanofibers; **COOH** – $COOH^+$ ions produced from the ionization of the appropriate acid and implanted into indium tin oxide electrode; **CQDs** – carbon quantum dots; **CTAB** – cetyltrimethylammonium bromide; **CuNPs** – copper nanoparticles; **CuNWs** – copper nanowires; **CuONPs** – copper(II) oxide nanoparticles; **Cyst** – cysteamine; **DNA** – deoxyribonucleic acid; **DPIM-Br** – 1,3-dipropylimidazolium bromide; **dsDNA** – double-stranded deoxyribonucleic acid; **en** – ethylenediamine; **ERGO** – electrochemically reduced graphene oxide; **f(-COCl)MWCNTs** – functionalized (acyl chloride) multi-walled carbon nanotubes; **f(-COOH)MWCNTs** – functionalized (carboxyl) multi-walled carbon nanotubes; **f(-OH)GCMSs** – functionalized (hydroxyl) glassy carbon microspheres; **f(-OH)MWCNTs** – functionalized (hydroxyl) multi-walled carbon nanotubes; **f(-SH)-SG** – sol-gel functionalized with thiol functional groups; **f(-SO_3H)GO** – functionalized (sulfonic acid) graphene oxide; **f(-SO_3H)SiO_2NPs** – functionalized (sulfonic acid) silicon dioxide nanoparticles; **Fc-ssDNA** – ferrocene-labeled single-stranded deoxyribonucleic acid; **Fe_3O_4NPs** – magnetite nanoparticles; **$FeVO_4$NPs** – iron vanadate nanoparticles; **GMCNPs** – graphitized mesoporous carbon nanoparticles; **GO** – graphene oxide; **GQDs** – graphene quantum dots; **HAuNSs** – hollow gold nanospheres; **IL** – ionic liquid; **L-GSH** – L-glutathione; **L-LysNFLs** – L-Lysine nanoflowers; **mAb** – monoclonal antibody; **MIP** – molecularly imprinted polymer; **MoS_2NPs** – molybdenum disulfide nanoparticles; **MSNPs** – mesoporous silica nanoparticles; **MTB-DNA** – DNA labeled with methylene blue; **MWCNTs** –multi-walled carbon nanotubes; **NAF** – Nafion; **N-CNOs** – nitrogen-doped carbon nanoonions; **NiHCF** – nickel hexacyanoferrate; **N-RGO** – nitrogen-doped reduced graphene oxide; **OA** – oxalic acid; **OMIMCl** –1-methyl-3-octylimidazolium chloride; **o-MWCNTs** – electrochemically oxidized multi-walled carbon nanotubes; **p-AMAM** – poly-amidoamine dendrimers; **p-AMT** – poly(2-amino-5-mercapto-1,3,4-thiadiazole); **p-ANI** – poly-aniline; **p-Arg** – poly-arginine; **p-EDOT** – poly-(3,4-ethylenedioxythiophene); **p-Gly** – poly-glycine; **p-oPD** – poly-(o-phenylenediamine); **p-Prof** – poly-proflavine; **p-Py** – poly-pyrrole; **PrA** – penicillin-binding protein 2 a (PbP2a); **PS** – phosphatidylserine; **p-Styr** – poly-styrene; **p-TB** – poly-toluidine blue; **PtNPs** – platinum nanoparticles; **PTTBA** – 2,2′:5′,2′′-terthiophene-3′-(p-benzoic acid); **p-TTCA** – poly-(5,2:5,2-terthiophene-3-carboxylic acid); **RGO** – reduced graphene oxide; **Ru** – ruthenium; **S-CNFBs** – sulfur-doped carbon nanofibers; **SDS** – sodium dodecyl sulfate; **SWCNTs** – single-walled carbon nanotubes; **TiO_2NPs** – titanium dioxide nanoparticles; **ZIF-8** – zeolitic imidazolate framework-8; **ZnONPs** – zinc oxide nanoparticles; **Zr(IV)-MOF (NH_2-UiO-66)** – zirconium(IV)-based metal-organic framework; **β-CD** – β-cyclodextrin; **(Ce-ZnO)NFLs** – cerium-doped zinc oxide nanoflowers; **($CoFe_2O_4$)NPs** – cobalt-doped ferrite nanoparticles; **(Fe_3O_4-SiO_2)NPs-DABCO** – magnetite double-charged diazoniabicyclo [2.2.2] octane dichloride silica hybrid; **(Mg_2-Al)-LDH** – magnesium-aluminum layered double hydroxide; **(Ni-Al)-LDH** – nickel-aluminum layered double hydroxide; **(Pd-Pt)NPs** – palladium - platinum nanoparticles; **(Pt-Co)NPs** –platinum - cobalt nanoparticles; **(PtFe_3O_4)NPs** –core-shell platinum-doped magnetite nanoparticles.

Electrode: AP-BPPyGE – anodically pretreated basal-plane pyrolytic graphite electrode; **AP-GCE** – anodically pretreated glassy carbon electrode; **AP-PGE** – anodically pretreated pencil graphite electrode;

AuE – gold electrode; **BDDE** – boron-doped diamond electrode; **CFUME** – carbon fiber ultramicroelectrode; **CPE** – carbon (graphite) paste electrode; **DRCE** – direct writing carbon (graphite) electrode; **EPPyGE** – edge-plane pyrolytic graphite electrode; **GCE** – glassy carbon electrode; **HMDE** – hanging mercury drop electrode; **ITIES** – electrochemistry of two immiscible electrolyte solutions; **ITOE** – indium tin oxide electrode; **p-AgSAE** – polished silver solid amalgam electrode; **PGE** – pencil graphite electrode; **SPCE** – screen-printed carbon (graphite) electrode; **SPDE** – screen-printed diamond electrode; **SPE** – screen-printed electrode;

Technique: ACAdSV – alternating current adsorptive stripping voltammetry; **Amp.** – amperometry; **CV** – cyclic voltammetry; **DPAdSV** – differential pulse adsorptive stripping voltammetry; **DPCSV** – differential pulse cathodic stripping voltammetry; **DPV** – differential pulse voltammetry; **EIS** – electrochemical impedance spectroscopy; **LSAdSV** – linear sweep adsorptive stripping voltammetry; **LSV** – linear sweep voltammetry; **SCP** – stripping chronopotentiometry; **SV** – stripping voltammetry; **SWAdSV** – square-wave adsorptive stripping voltammetry; **SWV** – square-wave voltammetry.

Medium: AcB – acetate buffer; **BRB** – Britton-Robinson buffer; **CB** – citrate buffer; **EtOH** – ethanol; **HBS** – HEPES buffered saline; **MeOH** – methanol; **PB** – phosphate buffer; **PBS** – phosphate buffered saline; **TrisB** – tris(hydroxymethyl)aminomethane hydrochloride buffer.

Selectivity: when underlined – exhibited interference.

Comments: Ag|AgCl – silver|silver chloride electrode; **Ag-pseudoRE** – silver pseudo-reference electrode; **SCE** – saturated calomel electrode.

N/A – not applicable.

Table 5. Comprehensive electroanalytical overview for the antineoplastic agents belonging to the group of protein kinase inhibitors.

Drug and its structure	Modification / Electrode	Technique	Medium	Linear range	LOD/LOQ	Application	Selectivity	Comments	Ref.
BCR-ABL tyrosine kinase inhibitors									
imatinib 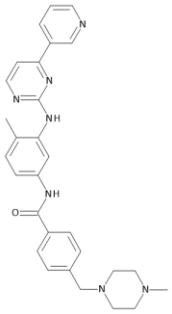	HMDE	SWAdSV	10.0 mM $HClO_4$, pH 2.0	10.0 nM – 480.0 nM	LOD = 5.2 nM LOQ = 17.3 nM	**Real sample:** spiked urine, urine from patients undergoing treatment with imatinib.	N/A	**Analytical signal:** imatinib reduction ($E_p \approx -0.7$ V *vs* Ag|AgCl).	[360]
	HMDE	SWAdCSV	40.0 mM BRB, pH 6.0	900.0 pM – 30.0 nM	LOD = 260.0 pM LOQ = 870.0 pM	**Real sample:** pharmaceutical formulation (tablets), spiked urine.	N/A	**Analytical signal:** imatinib reduction ($E_p \approx -1.15$V *vs* Ag|AgCl|$KCl_{sat.}$). Proposed electrochemical reduction mechanism of imatinib.	[361]
	AP-BDDE	DPV	40.0 mM BRB, pH 2.0	30.0 nM – 250.0 nM	LOD = 6.3 nM LOQ = 21.0 nM	**Real sample:** spiked urine.	**Tested interfering species:** ascorbic acid, uric acid, paracetamol, dopamine, paroxetine, epinephrine, estradiol, K^+, Na^+, Ca^{2+}, Mg^{2+}.	**Analytical signal:** imatinib oxidation ($E_p \approx +1.0$ V *vs* Ag|AgCl|KCl_{3M}). Proposed electrochemical oxidation mechanism of imatinib.	[347]
	RGO – AgNPs / GCE	DPV	100.0 mM PB, pH 7.0	10.0 nM – 280.0 µM	LOD = 1.1 nM	**Real sample:** spiked urine.	**Tested interfering species:** glucose, ascorbic acid, uric acid, paracetamol, dopamine, folic acid, ibuprofen, aspirin, Na^+, K^+, Cu^{2+}, Mg^{2+}.	**Analytical signal:** imatinib oxidation ($E_p \approx +0.45$ V *vs* Ag|AgCl|KCl_{3M}).	[345]
	(NiO-ZnO)NPs – f(–COOH)MWCNTs / GCE	DPV	40.0 mM BRB, pH 4.5	15.0 nM – 2.0 µM	LOD = 2.4 nM	**Real sample:** spiked urine, spiked blood serum.	**Tested interfering species:** ascorbic acid, uric acid, dopamine, glucose, lysine, serine, valine, bovine serum albumin, Ca^{2+}, Na^+, K^+, Mg^{2+}, Cl^-.	**Analytical signal:** imatinib oxidation ($E_p \approx +1.1$ V *vs* Ag|AgCl|KCl). Determination of imatinib performed in the presence of itraconazole (900.0 nM). Proposed electrochemical oxidation mechanism of imatinib.	[372]
	MOF (CuNPs) – MWCNTs / GCE	DPV	100.0 mM PB, pH 7.0	10.0 nM – 20.0 µM 20.0 µM – 220.0 µM	LOD = 4.1 nM	**Real sample:** pharmaceutical formulation (tablets), spiked blood serum, spiked urine.	**Tested interfering species:** glucose, fructose, ascorbic acid, paracetamol, uric acid, thiourea, urea, sodium benzoate, dopamine, epinephrine, hexadecyl(trimethyl)ammonium bromide, Na^+, K^+, Mg^{2+}, Ca^{2+}, Cd^{2+}, Fe^{3+}, Fe^{2+}, Cl^-, NO_3^-, PO_4^{3-}.	**Analytical signal:** imatinib oxidation ($E_p \approx +0.85$ V *vs* Ag|AgCl|KCl_{sat}). Proposed electrochemical oxidation mechanism of imatinib.	[373]
	MOF (HKUST-1) – GONRBs / GCE	DPV	40.0 mM BRB, pH 7.0	40.0 nM – 1.0 µM 1.0 µM – 80.0 µM	LOD = 6.0 nM	**Real sample:** spiked urine, spiked blood serum.	**Tested interfering species:** lysine, ascorbic acid, cysteine, glucose, sucrose, fructose, uric acid, urea, Na^+, K^+, Ca^{2+}, Mg^{2+}, SO_4^{2-}, CO_3^{2-}, Cl^-.	**Analytical signal:** imatinib oxidation ($E_p \approx +0.9$ V *vs* Ag|AgCl). Proposed electrochemical oxidation mechanism of imatinib.	[346]
	p-ANFBs – Fe_3O_4NPs – MWCNTs / CPE	DPV	40.0 mM BRB, pH 6.0	1.7 nM – 850.0 nM 8.5 µM – 34.0 µM	LOD = 400.0 pM	**Real sample:** spiked urine.	**Tested interfering species:** glucose, fructose, sucrose, lactose, maltose, metoclopramide, gefitinib, dexamethasone, sunitinib,	**Analytical signal:** imatinib oxidation ($E_p \approx +0.85$ V *vs* Ag|AgCl|KCl_{sat}).	[344]

							Na^+, K^+, Ca^{2+}, Cl^-, HPO_4^{2-}, $H_2PO_4^-$, Fe^{3+}, Mg^{2+}, NO^{3-}.	Proposed electrochemical oxidation mechanism of imatinib.	
	p-AMAM – RGO – IL (BDMIM-BF_6) – p-PHFBs) / AP-PGE	DPV	40.0 mM BRB, pH 4.5	10.0 nM – 10.0 µM 10.0 µM – 200.0 µM	LOD = 7.4 nM LOQ = 24.6 nM	**Real sample:** spiked urine, spiked blood serum.	**Tested interfering species:** nilotinib, ponatinib, dasatinib, tartaric acid, citric acid, sucrose, lactose, dextrose, glucose.	**Analytical signal:** imatinib oxidation (E_p ≈ +0.95 V *vs* Ag|AgCl|KCl_{sat}).	[374]
	f(–COOH)MWCNTs / SPCE	d-SWAdSV	20.0 mM PB, pH 7.0	50.6 – 912.0 nM	LOD = 7.0 nM LOQ = 23.0 nM	**Real sample:** spiked clinical urine samples from patients with chronic myeloid leukemia.	**Tested interfering species:** uric acid, urea, creatinine, ascorbic acid.	**Analytical signal:** imatinib oxidation (E_p ≈ +0.75 V *vs* Ag|AgCl-pseudoRE).	[375]
dasatinib 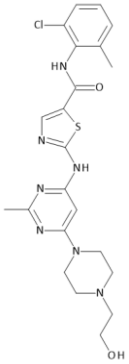	GCE	DPV	100.0 mM AcB, pH 3.4	200.0 nM – 2.0 µM	LOD = 130.0 nM LOQ = 430.0 nM	**Real sample:** spiked blood serum.	N/A	**Analytical signal:** dasatinib oxidation (E_p ≈ +0.9 V *vs* Ag|AgCl|KCl_{sat}). Proposed electrochemical oxidation mechanism of dasatinib.	[350]
	(Pd-Pt)NPs – MWCNTs / GCE	SWAdSV	100.0 mM PBS, pH 6.0	37.0 nM – 9.7 µM	LOD = 5.8 nM	**Real sample:** spiked blood serum, spiked urine.	**Tested interfering agents:** doxorubicin, bovine serum albumin, glucose, sucrose, lactose, ascorbic acid, urea, aspartic acid, KCl, NaCl.	**Analytical signal:** dasatinib oxidation (E_p ≈ +0.8 V *vs* Ag|AgCl|KCl_{3M}). Simultaneous determination of dasatinib and doxorubicin. Proposed electrochemical oxidation mechanism of dasatinib.	[311]
	dsDNA – AuNPs – RGO / GCE	DPV	N/A	30.0 nM – 5.5 µM	LOD = 9.0 nM	**Real sample:** pharmaceutical formulation, spiked urine. The interaction between dsDNA and dasatinib.	**Tested interfering species:** niclosamide, sulfonamide, amoxicillin, ascorbic acid, glucose, phenylalanine, Ca^{2+}, Na^+, F^-.	**Analytical signal:** indirect dasatinib sensing by monitoring the decrease in the guanine oxidation current (E_p ≈ +0.9 V *vs* Ag|AgCl|KCl).	[364]
	PGE	SWAdSV	20.0 mM BRB, pH 3.0	9.2 nM – 1.0 µM	LOD = 2.8 nM LOQ = 9.2 nM	**Real sample:** spiked urine.	**Tested interfering species:** uric acid, ascorbic acid, glucose, L-glutamic acid, L-cysteine.	**Analytical signal:** dasatinib oxidation (E_p ≈ +0.95 V *vs* Ag|AgCl|$NaCl_{3M}$). Proposed electrochemical oxidation mechanism of dasatinib.	[349]
	PtNPs – MWCNTs – IL (BMIM-PF_6) / CPE	SWV	100.0 mM PB, pH 8.0	5.0 µM – 500.0 µM	LOD = 1.0 µM	**Real sample:** pharmaceutical formulation (tablets), spiked urine.	**Tested interfering agents:** sucrose, lactose, methanol, thioguanylic acid, glucose, 6-thiouric acid, topotecan, BMS-573188, Al^{3+}, Ca^{2+}, Mg^{2+}, SO_4^{2-}, CO_3^{2-}.	**Analytical signal:** dasatinib oxidation (E_p ≈ +0.8 V *vs* Ag|AgCl|KCl). Possible simultaneous determination of dasatinib, 6-mercaptopurine, and 6-thioguanine. Proposed electrochemical oxidation mechanism of dasatinib.	[88]
	ZnONPs – IL (BMIM-BF_4) / CPE	SWV	pH 5.0	1.0 µM – 1.2 mM	LOD = 500.0 nM	**Real sample:** pharmaceutical formulation (injection), spiked pharmaceutical serum.	**Tested interfering agents:** glucose, alanine, phenylalanine, methionine, glycine, valine, tryptophan.	**Analytical signal:** dasatinib oxidation (E_p ≈ +1.0 V *vs* Ag|AgCl|KCl_{sat}). Simultaneous determination of dasatinib and doxorubicin.	[323]

	Fe_3O_4NPs – f(–COOH)SWCNTs – IL(HMIM-BF_4) / CPE	SWV	PB, pH 6.0	1.0 nM – 100.0 µM 100.0 µM – 220.0 µM	LOD = 700.0 pM	**Real sample:** pharmaceutical formulation (tablets), spiked dextrose saline.	**Tested interfering agents:** ascorbic acid, vitamin B_2, glucose, sucrose, methionine, glycine, alanine, Na^+, Li^+, Br^-, CO_3^{2-}.	**Analytical signal:** dasatinib oxidation (E_p ≈ +0.6 V *vs* Ag|AgCl|KCl_{sat}). Proposed electrochemical oxidation mechanism of dasatinib.	[348]
nilotinib 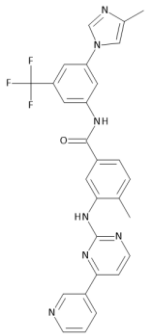	GCE	SWAdSV	100.0 mM H_2SO_4, containing 20% MeOH	400.0 nM – 40.0 µM	LOD = 106.0 nM LOQ = 321.0 nM	N/A	N/A	**Analytical signal:** nilotinib oxidation ($E_{p,1}$ ≈ +1.1 V and $E_{p,2}$ ≈ +1.6 V *vs* Ag|AgCl|$NaCl_{3M}$). Proposed electrochemical oxidation mechanism of nilotinib.	[351]
	GCE	SWAdSV	100.0 mM H_2SO_4, containing 20% MeOH	20.0 nM – 2.0 µM	LOD = 3.4 nM LOQ = 10.2 nM	**Real sample:** spiked blood serum, spiked urine.	**Tested interfering agents:** ascorbic acid, dopamine, paracetamol, Ca^+, Na^+, K^+, Cl^-, NO_3^-.	**Analytical signal:** nilotinib oxidation ($E_{p,1}$ ≈ +1.2 V and $E_{p,2}$ ≈ +1.6 V *vs* Ag|AgCl|$NaCl_{3M}$). Determination in the presence of 200.0 nM sodium dodecyl sulfate.	[351]
Epidermal growth factor receptor tyrosine kinase inhibitors									
gefitinib 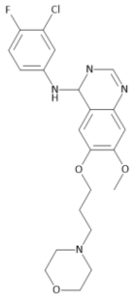	HMDE	AdSV	200.0 mM BRB, pH 4.0	10.0 nM – 100.0 µM	LOD = 12.0 nM	**Real sample:** pharmaceutical formulation (tablets), spiked urine.	N/A	**Analytical signal:** gefitinib reduction (E_p ≈ –0.8 V *vs* SCE). Proposed electrochemical reduction mechanism of gefitinib.	[362]
erlotinib 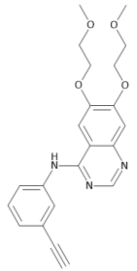	β-CD / GCE	SWAdSV	100.0 mM PB, pH 3.0, containing 20% MeOH	10.0 nM – 8.0 µM	LOD = 1.1 nM LOQ = 3.6 nM	**Real sample:** pharmaceutical formulations (tablets).	N/A	**Analytical signal:** erlotinib oxidation (E_p ≈ +1.15 V *vs* Ag|AgCl|KCl_{3M}). Proposed electrochemical oxidation mechanism of erlotinib.	[353]
	f(–COOH)MWCNTs – p-HU / p-PHF–PGE	DPV	BRB, pH 7.0	110.0 nM – 23.5 µM	LOD = 20.0 nM LOQ = 70.0 nM	**Real sample:** spiked nail, spiked urine.	**Tested interfering agents:** chitosan, Triton X-100	**Analytical signal:** erlotinib oxidation (E_p ≈ +0.5 V *vs* Ag|AgCl|KCl_{3M}). Determination of erlotinib performed in the presence of capecitabine.	[117]
Cyclin-dependent kinase inhibitors									
palbociclib	HMDE	SWAdSV	BRB, pH 7.0	100.0 nM – 1.0 µM	LOD = 88.0 pM LOQ = 290.0 pM	**Real sample:** spiked blood plasma, spiked urine.	N/A	**Analytical signal:** palbociclib reduction (E_p ≈ –1.05 V Ag|AgCl|KCl_{3M}).	[363]

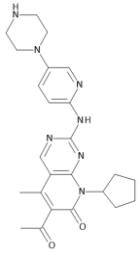								Proposed electrochemical reduction mechanism of palbociclib.	
Human epidermal growth factor receptor 2 tyrosine kinase inhibitors									
lapatinib 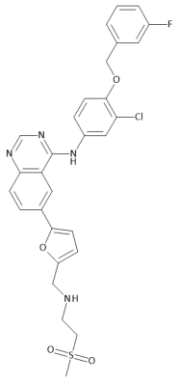	GCE	SWAdSV	100.0 mM H_2SO_4, containing 20% MeOH	20.0 nM – 1.0 µM	LOD = 3.5 nM LOQ = 10.6 nM	**Real sample:** pharmaceutical formulations (tablets), spiked blood serum. The interaction between dsDNA and lapatinib.	N/A	**Analytical signal:** lapatinib oxidation (E_p ≈ +1.0 V *vs* Ag|AgCl|$NaCl_{3M}$). Determination in the presence of 50.0 µM Triton X-100. Proposed electrochemical oxidation mechanism of lapatinib.	[352]
	GCE	SWAdSV	100.0 mM H_2SO_4, containing 20% MeOH	20.0 nM – 1.0 µM	LOD = 1.6 nM LOQ = 4.8 nM	**Real sample:** pharmaceutical formulations (tablets), spiked blood serum.	N/A	**Analytical signal:** lapatinib oxidation (E_p ≈ +1.2 V *vs* Ag|AgCl|$NaCl_{3M}$). Determination in the presence of 50.0 µM Triton X-100. Proposed electrochemical oxidation mechanism of lapatinib.	[352]
Janus-associated kinase inhibitors									
ruxolitinib 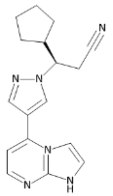	MIP (T – HOBtMA – TEA – HEMA – EGDMA – AIBN – p-VA) / GCE	DPV	5.0 mM $[Fe(CN)_6]^{3-/4-}$ in 10 mM AcB, pH 5.2	10.0 fM – 100.0 fM	LOD = 1.9 fM LOQ = 6.4 fM	**Real sample:** pharmaceutical formulations (tablets), spiked synthetic blood serum.	**Tested interfering agents:** axitinib, imatinib, dasatinib, dopamine, uric acid, paracetamol, ascorbic acid, Na^+, SO_4^{2-}.	**Analytical signal:** indirect ruxolitinib sensing by monitoring the decrease in $[Fe(CN)_6]^{3-/4-}$ oxidation peak current ($E_{p\ [Fe(CN)6]3-/4-}$ ≈ +0.3 V *vs* Ag|AgCl).	[365]
Vascular endothelial growth factor receptor tyrosine kinase inhibitors									
axitinib	GCE	DPAdSV	BRB, pH 2.0, containing 20% MeOH	80.0 nM – 2.0 µM	LOD = 1.1 nM LOQ = 3.7 nM	**Real sample:** pharmaceutical formulations (tablets), spiked blood serum, spiked urine.	**Tested interfering agents:** ascorbic acid, dopamine, uric acid, Na^+, NO_3^-, K^+, Fe^{3+}, Mg^{2+}, SO_4^{2-}, Cl^-.	**Analytical signal:** axitinib oxidation (E_p ≈ +1.0 V *vs* Ag|AgCl|KCl_{3M}). Proposed electrochemical oxidation mechanism of axitinib.	[366]
	BDDE	DPV	AcB, pH 3.7, containing 20% MeOH	600.0 nM – 80.0 µM	LOD = 36.8 nM LOQ = 123.0 nM	**Real sample:** pharmaceutical formulations (tablets), spiked blood serum, spiked urine.	**Tested interfering agents:** ascorbic acid, dopamine, uric acid, Na^+, NO_3^-, K^+, Fe^{3+}, Mg^{2+}, SO_4^{2-}, Cl^-.	**Analytical signal:** axitinib oxidation (E_p ≈ +0.9 V *vs* Ag|AgCl|KCl_{3M}). Proposed electrochemical oxidation mechanism of axitinib.	[366]

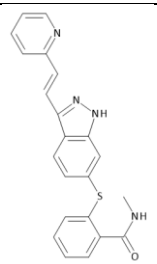	MIP (p-(o-PD)) / GCE	DPV	5.0 mM $[Fe(CN)_6]^{3-/4-}$ in 100.0 mM KCl	100.0 fM – 1.0 pM	LOD = 27.0 fM LOQ = 89.0 fM	**Real sample:** pharmaceutical formulations (tablets), spiked blood serum.	**Tested interfering agents:** erlotinib, dasatinib, nilotinib, imatinib, ascorbic acid, dopamine, K^+, Cl^-, Na^+, SO_4^{2-}.	**Analytical signal:** indirect sunitinib sensing by monitoring the decrease in $[Fe(CN)_6]^{3-/4-}$ oxidation peak current ($E_{p\ [Fe(CN)6]3-/4-}$ ≈ +0.2 V *vs* Ag|AgCl|KCl_{3M}).	[376]
Other protein kinase inhibitors									
sunitinib 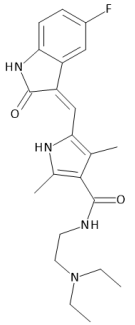	p-ANNFBs – ($NiZnFe_2O_4$)NPs / CPE	DPSV	40.0 mM BRB, pH 8.5	7.0 nM – 337.0 nM 337.0 nM – 18.8 µM	LOD = 900.0 pM	**Real sample:** spiked blood serum, spiked urine.	**Tested interfering species:** ranitidine, dexamethasone, ascorbic acid, cysteine, citric acid, glucose, sucrose, lactose, fructose, imatinib, gefitinib, Na^+, K^+, Ca^{2+}, Mg^{2+}, NO_3^-, Cl^-.	**Analytical signal:** sunitinib oxidation (E_p ≈ +0.65 V *vs* Ag|AgCl).	[355]
sorafenib 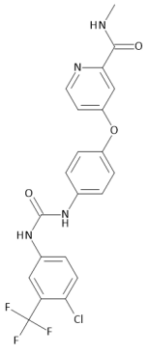	CHIT – f(–COOH)MWCNTs / GCE	DPAdSV	100.0 mM PB, pH 7.0, containing 50% MeOH	10.0 nM – 80.0 nM 100.0 nM – 1.0 µM	LOD = 440.0 pM LOQ = 1.5 nM	**Real sample:** spiked blood serum.	**Tested interfering species:** uric acid, dopamine, Na^+, K^+, Ca^{2+}, Mg^{2+}, Cl^-, SO_4^{2-}.	**Analytical signal:** sorafenib oxidation (E_p ≈ +0.8 V Ag|AgCl|$NaCl_{sat}$). Proposed electrochemical oxidation mechanism of sorafenib.	[377]
	Na-MMT / CPE	SWAdASV	BRB, pH 3.0	2.0 nM – 120.0 nM	LOD = 73.8 pM LOQ = 246.0 pM	**Real sample:** pharmaceutical formulation (tablets), spiked urine.	**Tested interfering species:** vitamin A, vitamin C, vitamin E, aspirin, ketoprofen, ketorolac, ibuprofen, gabapentin, oxalic acid, uric acid, glucose, sucrose, starch, gelatin, lactose, Na^+, K^+, Ca^{2+}, Mg^{2+}, Zn^{2+}, Al^{3+}, Se^{4+}, Cu^{2+}, Fe^{3+}, Cl^-, SO_4^{2-}, PO_4^{3-}, Ac^-.	**Analytical signal:** sorafenib oxidation (E_p ≈ +1.0 V *vs* Ag|AgCl|KCl_{sat}). Proposed electrochemical oxidation mechanism of sorafenib.	[378]
pazopanib	CuONPs – C-WM / GCE	SWAdSV	100.0 mM PB, pH 7.0	200.0 pM – 1.0 µM	LOD = 49.4 pM LOQ = 150.0 pM	**Real sample:** pharmaceutical formulation (tablets), spiked synthetic blood serum.	**Tested interfering species:** uric acid, dopamine, ascorbic acid, KCl, NaCl, $NaNO_3$, $CaCl_2$.	**Analytical signal:** pazopanib oxidation (E_p ≈ +0.9 V *vs* Ag|AgCl|KCl_{3M}). Proposed electrochemical oxidation mechanism of pazopanib.	[357]

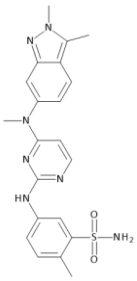									
regorafenib 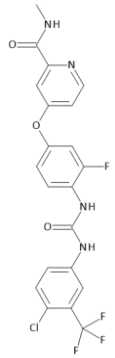	ZrO_2NPs – RGO / GCE	DPV	100.0 mM PBS, pH 7.0	11.0 nM – 343.0 nM	LOD = 17.0 nM LOQ = 59.0 nM	**Real sample:** pharmaceutical formulation, spiked blood serum.	**Tested interfering species:** ascorbic acid, uric acid, folic acid, glutathione, L-cysteine, Ca^{2+}, Mg^{2+}, Zn^{2+}.	**Analytical signal:** regorafenib oxidation ($E_p \approx +0.3$ V *vs* Ag|AgCl). Possible simultaneous determination of regorafenib, ascorbic acid, and uric acid. Proposed electrochemical oxidation mechanism of regorafenib.	[359]
	CPE	DPV	100.0 mM BRB, pH 5.0, containing MeOH	1.0 µM – 26.9 µM	LOD = 207.1 nM LOQ = 606.0 nM	**Real sample:** spiked plasma, spiked urine.	**Tested interfering species:** ascorbic acid, riboflavin, Cl^-.	**Analytical signal:** regorafenib oxidation ($E_p \approx +0.9$ V *vs* Ag|AgCl|$NaCl_{3M}$).	[379]
	fMWCNTs / GCE	DPAdSV	100.0 mM H_2SO_4	500.0 nM – 25.0 µM	LOD = 20.8 nM LOQ = 69.3 nM	**Real sample:** pharmaceutical formulation (tablets), spiked synthetic blood serum.	**Tested interfering species:** ascorbic acid, dopamine, paracetamol, uric acid, Na^+, Cl^-.	**Analytical signal:** regorafenib oxidation ($E_p \approx +1.0$ V *vs* Ag|AgCl). Proposed electrochemical oxidation mechanism of regorafenib.	[358]

Modification: AgNPs – silver nanoparticles; **AIBN** – 2-20-azobis (isobutyronitrile); **AuNPs** – gold nanoparticles; **BDMIM-PF_6** – 1-butyl-2,3-dimethylimidazolium hexafluorophosphate; **BMIM-BF_4** – 1-butyl-3-methylimidazolium tetrafluoroborate; **BMIM-PF_6** – 1-butyl-3-methylimidazolium hexafluorophosphate; **CHIT** – chitosan; **CuNPs** – copper nanoparticles; **CuONPs** – copper oxide nanoparticles; **C-WM** – carbon material obtained from hydrothermal carbonization of waste masks; **dsDNA** – double-stranded deoxyribonucleic acid; **EGDMA** – ethylene glycol dimethacrylate; **f(–COOH)MWCNTs** – functionalized (carboxyl) multi-walled carbon nanotubes; **f(–COOH)SWCNTs** – functionalized (carboxyl) single-walled carbon nanotubes; **Fe_3O_4NPs** – magnetite nanoparticles; **fMWCNTs** – functionalized multi-walled carbon nanotubes; **GONRBs** – graphene oxide nanoribbons; **HEMA** – 2-hydroxyethyl methacrylate; **HKUST-1** – cooper^{2+}-1,3,5-benzenetricarboxylate ($[Cu_3(H_2O)_3(BTC)_2]_n$); **HMIM-BF_4** – 1-hexyl-3-methylimidazolium tetrafluoroborate; **HOBtMA** – 1-hydroxybenzotriazole methacrylate; **IL** – ionic liquid; **MIP** – molecularly imprinted polymer; **MOF** – metal-organic framework; **MWCNTs** – multi-walled carbon nanotubes; **Na-MMT** – sodium montmorillonite clay; **p-(o-PD)** – poly-(o-phenylenediamine); **p-AMAM** – poly-amidoamine dendrimer; **p-ANNFBs** – poly-acrylonitrile nanofibers; **p-HU** – poly-hydroxy urethane; **p-PHFBs** – poly-propylene hollow fibers; **PtNPs** – platinum nanoparticles; **p-VA** – poly-vinyl alcohol; **RGO** – reduced graphene oxide; **T** – thymine; **TEA** – trimethylamine; **ZnONPs** – zinc oxide nanoparticles; **ZrO_2NPs** – zirconia oxide nanoparticles; **β-CD** – β-cyclodextrin; **(NiO-ZnO)NPs** – nickel oxide-zinc oxide nanoparticles; **(Ni-Zn-Fe_2O_4)NPs** – nickel- and zinc-doped ferrite nanoparticles; **(Pd-Pt)NPs** – palladium-platinum nanoparticles.

Electrode:

AP-BDDE – anodically pretreated boron-doped diamond electrode; **AP-PGE** – anodically pretreated pencil graphite electrode; **BDDE** –boron-doped diamond electrode; **CPE** – carbon (graphite) paste electrode; **GCE** – glassy carbon electrode; **HMDE** – hanging mercury drop electrode; **PGE** – pencil graphite electrode; **p-PHF–PGE** – poly-propylene hollow fiber pencil graphite electrode; **SPCE** – screen-printed carbon (graphite) electrode.

Technique: AdSV –adsorptive stripping voltammetry; **DPAdSV** – differential pulse adsorptive stripping voltammetry; **DPSV** – differential pulse stripping voltammetry; **DPV** – differential pulse voltammetry; **d-SWAdSV** – derivative square-wave adsorptive stripping voltammetry; **SWAdASV** – square-wave adsorptive anodic stripping voltammetry; **SWAdCSV** – square-wave adsorptive cathodic stripping voltammetry; **SWAdSV** – square-wave adsorptive stripping voltammetry; **SWV** – square-wave voltammetry.

Medium: AcB – acetate buffer; **BRB** – Britton-Robinson buffer; **MeOH** – methanol; **PB** – phosphate buffer; **PBS** – phosphate buffered saline.

Selectivity: when underlined – exhibited interference.

Comments: Ag|AgCl – silver|silver chloride electrode; **Ag|AgCl-pseudoRE** – silver|silver chloride pseudo-reference electrode; **SCE** – saturated calomel electrode.

N/A – not applicable.

Table 6. Comprehensive electroanalytical overview for the antineoplastic agents belonging to the group of monoclonal antibodies and antibody-drug conjugates.

Drug	Modification / Electrode	Technique	Medium	Linear range	LOD/LOQ	Application	Selectivity	Comments	Ref.
Clusters of Differentiation 20 inhibitors									
rituximab (rituxan)	dsDNA – p-AMAM – RGO / PGE	DPV	100.0 mM PB, pH 7.4	7.0 – 60.0 µM 60.0 – 300.0 µM	LOD = 560.0 nM LOQ = 1.9 µM	**Real sample:** pharmaceutical formulation (injection), spiked blood serum. The interaction between rituximab and dsDNA.	**Tested interfering agents:** ascorbic acid, uric acid, tartaric acid, citric acid, sucrose, lactose, dextrose, glucose.	**Analytical signal:** indirect rituximab sensing by monitoring the decrease in guanine oxidation peak current ($E_{p\ guanine} \approx$ +0.85 V *vs* Ag|AgCl|KCl_{3M}).	[382]
Human Epidermal Growth Factor Receptor 2 inhibitors									
trastuzumab	SAM (CH19 – CS7) / AuE	EIS	PBS, pH 7.4	0 nM – 110.0 nM	LOD = 1.5 nM	**Real sample:** spiked blood serum.	**Tested interfering agents:** bevacizumab, ofatumumab, obinutuzumab, panitumumab, rituximab.	**Analytical signal:** change in the impedance caused by the trastuzumab-peptide mimotope binding.	[387]
Epidermal Growth Factor Receptor inhibitors									
cetuximab	ConAL – EEL – BSA – (ZnO-CdSe)QDs / GCE	SWSV	10.0 mM PB, pH 7.0	68.6 pM – 2.7 µM	LOD = 23.3 nM	N/A	N/A	**Analytical signal:** indirect cetuximab sensing by monitoring the reduction peak current of Cd^{2+} ($E_{p\ Cd2+} \approx$–0.7 V *vs* SCE). Simultaneous determination of cetuximab with carcinoembryonic antigen (colorectal cancer biomarker).	[390]

Modification: BSA – bovine serum albumin; **CH19** – cysteine-containing peptide mimotope, sequence CGSGSGSQLGPYELWELSH; **ConAL** – Concanavalin A lectin; **CS7** – spacer peptide, sequence CGSGSGS; **dsDNA** – double-stranded deoxyribonucleic acid; **EEL** – Euonymus europaeus lectin; **p-AMAM** – poly-amidoamine dendrimers; **RGO** – reduced graphene oxide; **SAM** – self-assembled monolayer; **(ZnO-CdSe)QDs** – zinc oxide - cadmium selenide core-shell quantum dots.

Electrode: AuE – gold electrode; **GCE** – glassy carbon electrode; **PGE** – pencil graphite electrode.

Technique: DPV – differential pulse voltammetry; **EIS** – electrochemical impedance spectroscopy; **SWSV** – square-wave stripping voltammetry.

Medium: PB – phosphate buffer; **PBS** – phosphate buffered saline.

Comments: Ag|AgCl – silver|silver chloride electrode; **SCE** – saturated calomel electrode.

N/A – not applicable.

Table 7. Comprehensive electroanalytical overview for the antineoplastic agents belonging to the group of other antineoplastic agents.

Drug and its structure	Modification / Electrode	Technique	Medium	Linear range	LOD/LOQ	Application	Selectivity	Comments	Ref.
Platinum compounds									
cisplatin 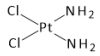	HMDE	DPAdSV	360.0 mM H_2SO_4 containing 10.0 mM N_2H_4 and 37% HCHO	1.0 µM – 8.3 µM	LOD = 100.0 nM LOQ = 400.0 nM	The effect of cell culture medium (Dulbecco's Modified Eagle Medium) on cisplatin determination.	N/A	**Analytical signal:** indirect cisplatin sensing by monitoring the increase in Pt^{2+}-formazone complex reduction peak current ($E_p \approx -0.9$ V *vs* Ag|AgCl|KCl_{3M}).	[421]
	HMDE	DPSV	360.0 mM H_2SO_4 containing 10.0 mM N_2H_4 and 37% HCHO, pH 1.8	660.0 pM – 83.0 nM	LOD = 200.0 pM LOQ = 700.0 pM	The interaction between cisplatin and metallothionein proteins.	N/A	**Analytical signal:** indirect cisplatin sensing by monitoring the increase in Pt^{2+}-formazone complex reduction peak current ($E_p \approx -0.9$ V *vs* Ag|AgCl|KCl_{3M}).	[401]
	MT / HMDE	DPAdSV	500.0 mM NaCl, pH 6.4	25.0 µM – 375.0 µM	LOD = 500.0 nM	**Real sample:** spiked blood serum.	N/A	**Analytical signal:** cisplatin reduction ($E_p \approx -0.65$ V *vs* Ag|AgCl|KCl_{3M}).	[397]
	Thio – GQDs / np-GCE	DPASV	100.0 mM PB containing 0.1 M KCl, pH 7.0	200.0 nM – 30.0 µM 30.0 µM – 110.0 µM	LOD = 90.0 nM LOQ = 300.0 nM	**Real sample:** spiked blood serum, spiked urine.	**Tested interfering agents:** dopamine, ascorbic acid, NH_4^+, Al^{3+}, Li^+, K^+, Na^+, Ca^{2+}, Mg^{2+}, Cl^-.	**Analytical signal:** cisplatin oxidation ($E_p \approx +0.65$ V *vs* Ag|AgCl).	[399]
	CPE	CV with accumulation step	1.0 M NH_3 containing 200.0 µM $AgNO_3$	10.0 nM – 100.0 nM	LOD = 3.2 nM	N/A	N/A	**Analytical signal:** indirect cisplatin detection based on anodic stripping signal of electrodeposited Ag^+ ($E_p \approx +0.1$ V *vs* Ag|AgCl).	[398]
	GST / CPE	SWV	50.0 mM PB, pH 6.5	50.0 µM – 140.0 µM	LOD = 8.8 µM	N/A	**Tested interfering agents:** glucose, glycine, tyrosine, histidine, glutamic acid, carboplatin, oxaliplatin, gemcitabine, doxorubicin, pirarubicin.	**Analytical signal:** the enzymatic reaction inhibition by the addition of cisplatin ($E_p \approx +0.1$ V *vs* Ag|AgCl|KCl_{3M}).	[422]
	f(–COOH)MWCNTs / SPCE	DPSV	100.0 mM NaCl, pH 7.0	14.5 µM – 100.0 µM	LOD = 4.6 µM LOQ = 14.0 µM	**Real sample:** spiked blood serum.	N/A	**Analytical signal:** Pt^{2+} oxidation ($E_p \approx -0.25$ V *vs* Ag|AgCl|KCl_{sat}). Determination in the presence of sodium dodecyl sulfate (800.0 µM).	[423]
	5'HS–$(CH_2)_6$–AGAGAG–MTB3' / AuE	ACV	50.0 mM HBS, pH 5.0, containing 100.0 mM $NaClO_4$	200.0 nM – 2.0 µM	LOD = 200.0 nM	**Real sample:** spiked saliva, spiked urine.	**Tested interfering agents:** carboplatin, satraplatin, tetracycline, ampicillin, trimethoprim, nitrofurantoin, sulfamethoxazole, amoxicillin, levofloxacin	**Analytical signal:** the electrocatalytic reaction between the Pt(IV) center of cisplatin and leucomethylene blue ($E_p \approx -0.15$ V *vs* Ag|AgCl|KCl_{3M}).	[400]
carboplatin 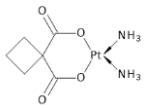	HMDE	DPSV	360.0 mM H_2SO_4 containing 10.0 mM N_2H_4 and 37% HCHO, pH 1.8	540.0 pM – 67.0 nM	LOD = 100.0 pM LOQ = 400.0 nM	The interaction between carboplatin and metallothionein proteins.	N/A	**Analytical signal:** indirect carboplatin sensing by monitoring the increase in Pt^{2+}-formazone complex reduction peak current ($E_p \approx -0.9$ V *vs* Ag|AgCl|KCl_{3M}).	[401]
	ssDNA / GCE	DPV	100.0 mM AcB, pH 4.6 containing 5% TCAA	7.7 µM – 2.4 mM	LOD = 5.7 µM (in blood serum)	**Real sample:**	N/A	**Analytical signal:**	[403]

				(5.7 µM – 40.0 µM in blood serum)		blood serum collected from the patients with ovarian cancer undergoing treatment with carboplatin. The interaction between ssDNA and carboplatin.		indirect carboplatin sensing by monitoring the decrease in adenine oxidation peak current ($E_{p\ adenine}$ ≈ +1.15 V *vs* SCE).	
	PtE	LSV	172.0 mM PBS, pH 7.0	30.0 µM – 1.0 mM	LOD = 30.0 µM LOQ = 50.0 µM	Monitoring of carboplatin consumption in ovarian cancer cells.	N/A	**Analytical signal:** carboplatin oxidation (E_p ≈ +0.8 V *vs* Ag|AgCl|$NaCl_{3M}$).	[402]
oxaliplatin 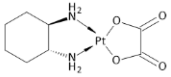	HMDE	DPSV	360.0 mM H_2SO_4, containing 10.0 mM N_2H_4 and 37% HCHO, pH 1.8	250.0 pM – 63.0 nM	LOD = 80.0 pM LOQ = 300.0 pM	The interaction between oxaliplatin and metallothionein proteins.	N/A	**Analytical signal:** indirect oxaliplatin sensing by monitoring the increase in Pt^{2+}-formazone complex reduction peak current (E_p ≈ –0.9 V *vs* Ag|AgCl|KCl_{3M}).	[401]
	MIP (p-Py)– AgNPs – MOF(Cu-TPA) –N-MWCNTs / GCE	DPV	100.0 mM PB, pH 7.0	141.0 pM – 503.4 nM	LOD = 40.3 pM	**Real sample:** pharmaceutical formulation (injection), spiked blood plasma, spiked urine.	**Tested interfering agents:** dopamine, uric acid, ascorbic acid, glutathione, 5-fluorouracil, capecitabine, cisplatin, carboplatin, satraplatin, flutamide, doxorubicin, Na^+, K^+, Cd^{2+}, Pb^{2+}, Cu^{2+}, Zn^{2+}, Mg^{2+}, Ca^{2+}, Cl^-, SO_4^{2-}.	**Analytical signal:** indirect oxaliplatin sensing by monitoring the decrease in the cooper-terephthalic acid reduction peak (E_p ≈ –0.15 V *vs* Ag|AgCl|KCl_{3M}).	[404]
	MIP (MAA – AIBN – EGDMA) – Zr(IV)-MOF(NH_2-UiO-66) – CHIT – CQDs – HBNNSs / GCE	DPV	100.0 mM KCl, pH 7.0	1.0 nM – 20.0 nM 20.0 nM – 250.0 nM	LOD = 370.0 pM	**Real sample:** pharmaceutical formulation (injection), spiked blood serum, spiked urine.	**Tested interfering agents:** ascorbic acid, uric acid, glucose, cisplatin, carboplatin, picoplatin, satraplatin, Na^+, K^+, Ca^{2+}, Cu^{2+}, Mg^{2+}, Zn^{2+}, Cl^-, SO_4^{2-}.	**Analytical signal:** indirect oxaliplatin sensing by monitoring the decrease in $[Fe(CN)_6]^{3-/4-}$ oxidation peak current ($E_{p\ [Fe(CN)6]3-/4-}$ ≈ +0.2 V *vs* Ag|AgCl).	[405]
satraplatin 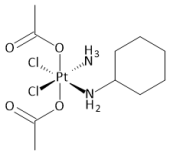	MTB – C2 / AuE	CA	20.0 mM AcB, pH 4.5, containing 2.0 M $NaClO_4$	1.0 µM – 1.0 mM	LOD = 1.0 µM	**Real sample:** spiked 50% bovine calf serum.	**Tested interfering agents:** cisplatin, carboplatin.	**Analytical signal:** the electrocatalytic reaction between the Pt(IV) center of satraplatin and leucomethylene blue. **Applied potential in CA:** *E* = –0.3 V *vs* Ag|AgCl|KCl_{3M}.	[414]
Methylhydrazines									
procarbazine 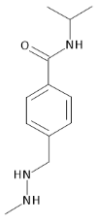	FISE	Pot.	10.0 mM BB, pH 9.0	100.0 µM – 5.0 mM	LOD = 90.0 µM	**Real sample:** pharmaceutical formulation (capsules Natulan®).	N/A	**Analytical signal:** reaction between 1-fluoro-2,4-dinitrobenzene and procarbazine releases fluoride ions that can be detected using ion selective electrode**.**	[411]
Retinoids fo cancer treatment									

tretinoin 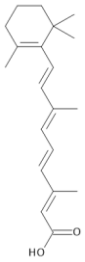	GCE	DPASV	BRB, pH 7.0	1.0 µM – 10.0 mM	LOD = 7.5 nM LOQ = 24.9 nM	**Real sample:** spiked urine, spiked blood serum.	N/A	**Analytical signal:** Tretinoin oxidation (E_p ≈ +0.75 V *vs* Ag|AgCl|KCl_{3M}). Proposed electrochemical oxidation mechanism of tretinoin.	[412]
Histone deacetylase inhibitors									
vorinostat 	AuNPs – ChCl / AuE	Amp.	100.0 mM PB, pH 7.4	4.0 µM – 52.0 µM	LOD = 1.4 µM LOQ = 4.6 µM	**Real sample:** pharmaceutical formulation.	N/A	**Applied potential in Amp.:** E = +0.48 V *vs* Ag|AgCl|$KCl_{sat.}$ Proposed electrochemical oxidation mechanism of vorinostat.	[413]
Other non-classified antineoplastic agents									
amsacrine (acridinyl anisidide) 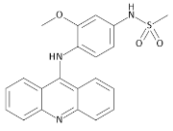	dsDNA – G / CPE	DPAdSV	30.0 mM PB, pH 7.5	700.0 nM – 100.0 µM	LOD = 300.0 nM	**Real sample:** spiked blood serum, spiked urine. The interaction between dsDNA and amsacrine.	N/A	**Analytical signal:** amsacrine oxidation (E_p ≈ +0.35 V *vs* Ag|AgCl|KCl_{sat}).	[407]
	dsDNA – (Eu^{3+}-NiO)NPs / CPE	DPV	100.0 mM PB, pH 7.0	100.0 nM – 100.0 µM	LOD = 50.0 nM	The interaction between dsDNA and amsacrine.	**Tested interfering agents:** uric acid, citrate, sucrose, epinephrine, ascorbic acid, folic acid, dopamine, L-tyrosine, K^+, Cl^-, Ca^{2+}.	**Analytical signal:** indirect amsacrine sensing by monitoring the decrease in guanine oxidation peak ($E_{p\ guanine}$ ≈ +0.85 V *vs* Ag|AgCl|KCl).	[406]
hydroxycarbamide (hydroxyurea) 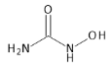	CPE	DPV	100.0 mM PB, pH 7.0	200.0 µM – 1.0 mM	LOD = 6.5 µM LOQ = 21.7 µM	**Real sample:** pharmaceutical formulation (HYDROX-L capsule), spiked urine.	**Tested interfering agents:** citric acid, glucose, lactose, tartaric acid, sucrose, urea.	**Analytical signal:** hydroxycarbamide oxidation (E_p ≈ +1.05 V *vs* Ag|AgCl|KCl_{3M}). Proposed electrochemical oxidation mechanism of hydroxycarbamide.	[424]
	TiO_2NPs / CPE	DPV	300.0 mM PB, pH 2.0	105.2 µM – 2.4 mM	LOD = 2.1 µM	**Real sample:** spiked blood serum.	**Tested interfering agents:** glucose, urea, ascorbic acid.	**Analytical signal:** hydroxycarbamide oxidation (E_p ≈ +1.15 V *vs* Ag|AgCl|KCl_{sat}).	[425]
	MoS_2 / AuE	DPV	PBS, pH 7.4	0 – 500.0 µM	LOD = 22.0 nM	**Real sample:** spiked blood serum.	**Tested interfering agents:** uric acid, ascorbic acid.	**Analytical signal:** hydroxycarbamide oxidation (E_p ≈ +0.1 V *vs* Ag|AgCl|$NaCl_{3M}$). Possible simultaneous determination of	[426]

								hydroxycarbamide, uric acid, and ascorbic acid. Proposed electrochemical oxidation mechanism of hydroxycarbamide.	
	(Ag-Pt)NPs – HEH –f(–COOH)MWCNTs / CPE	DPV	100.0 mM PB, pH 7.0	50.0 nM – 1.0 µM 1.0 µM – 50.0 µM 50.0 µM – 1.0 mM	LOD = 23.0 nM	**Real sample**: spiked blood plasma.	**Tested interfering agents:** uric acid, glucose, tryptophan, glutathione, ascorbic acid, folic acid.	**Analytical signal:** hydroxycarbamide oxidation (E_p ≈ +0.15 V *vs* SCE). Possible simultaneous determination of hydroxycarbamide and uric acid.	[427]
	PGE	DPV	200.0 mM PB, pH 8.0	10.0 µM – 1.0 mM	LOD = 7.9 µM LOQ = 26.3 µM	**Real sample:** pharmaceutical formulation (capsule), spiked urine.	**Tested interfering agents:** citric acid, glucose, lactose, tartaric acid, sucrose, urea.	**Analytical signal:** hydroxycarbamide oxidation (E_p ≈ +0.85 V *vs* Ag|AgCl|KCl_{3M}). Proposed electrochemical oxidation mechanism of hydroxycarbamide.	[428]
	MIP (HPPD – EGDMA) – N-GQDs-COCl – (Au-Ag)NRs / SPCE	DPASV	100.0 mM PB, pH 7.5	7.2 nM – 1.4 µM	LOD = 657.4 pM	**Real sample:** pharmaceutical formulation, spiked blood plasma, spiked urine.	**Tested interfering agents:** temozolomide, dacarbazine, ifosfamide, chlorambucil, urea, uric acid, citric acid, cysteine, phenyl alanine, ascorbic acid, dopamine.	**Analytical signal:** hydroxycarbamide oxidation (E_p ≈ +0.3 V *vs* Ag|AgCl-pseudoRE).	[408]
arsenic trioxide 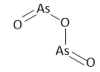	CYC / BDDE	SWV	100.0 mM PB, pH 7.0	0 – 10.0 µM	LOD = 22.0 µM	N/A	N/A	**Analytical signal:** Indirect arsenic trioxide sensing by monitoring the decrease in cytochrome C reduction peak (E_p = –0.4 V *vs* Ag|AgCl|KCl_{3M}).	[429]
celecoxib 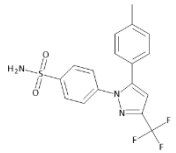	HMDE	SWAdCSV	BRB, pH 7.0	1.0 nM – 20.0 nM	LOD = 186.0 pM LOQ =620.0 pM	**Real sample:** pharmaceutical formulation (capsules), spiked blood serum.	**Tested interfering agents:** starch, gelatin, lactose, talc, magnesium stearate.	**Analytical signal:** celecoxib reduction (E_p ≈ –1.55 V *vs* Ag/AgCl/KCl_{sat}). Proposed electrochemical reduction mechanism of celecoxib.	[410]
	AuNPs – IL (EMIM-PF_6) – RGO / CPE	DPV	100.0 mM PB, pH 7.4	500.0 nM – 15.0 µM	LOD = 200.0 nM	**Real sample:** pharmaceutical formulation (capsules), spiked blood serum.	**Tested interfering agents:** diclofenac, acetaminophen, aspirin, ibuprofen, naproxen, glucose, tyrosine.	**Analytical signal:** celecoxib reduction (E_p ≈ –1.1 V *vs* SCE).	[430]
	AgNPs – ChCl – GO / CPE	DPV	40.0 mM BRB, pH 5.0	9.6 nM – 740.0 nM	LOD = 2.5 nM LOQ = 6.6 nM	**Real sample:** spiked plasma.	N/A	**Analytical signal:** celecoxib reduction (E_p ≈ –1.0 V *vs* Ag|AgCl).	[431]
	MIP(p-Py) – f(–COOH)MWCNTs / PGE	DPV	40.0 mM BRB, pH 4.0	5.0 nM – 20.0 µM	LOD = 2.4 nM	**Real sample:** pharmaceutical formulation, spiked blood serum.	**Tested interfering agents:** fluoxetine, pantoprazole, tetracycline, acetaminophen, famotidine, letrozole.	**Analytical signal:** celecoxib reduction (E_p ≈ –1.05 V *vs* Ag|AgCl).	[432]
	p-ANI – f(–NH_2)MWCNTs / ITOE	SWSV	40.0 mM BRB, pH 7.0	10.0 pM – 1.0 µM	LOD = 10.0 pM	N/A	N/A	**Analytical signal:** celecoxib reduction (E_p ≈ –1.1 V *vs* Ag|AgCl).	[409]
anagrelide	(Zn-$CoFe_2O_4$)NPs / SPCE	SWSV	40.0 mM BRB, pH 7.0	2.5 µM – 31.9 µM	LOD = 1.2 µM LOQ = 3.7 µM	**Real sample:** pharmaceutical formulation (tablet), spiked blood serum, spiked urine.	N/A	**Analytical signal:** anagrelide oxidation (E_p ≈ +0.9 V *vs* Ag|AgCl|KCl_{3M}). Proposed electrochemical oxidation mechanism of anagrelide.	[433]

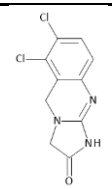									

Modification: 5'HS–(CH_2)$_6$–AGAGAG–MTB3' – oligo-adenine (A)-guanine (G) DNA probe (5' AGAGAG 3') terminated with methylene blue on the 3' terminus and C6-disulfide linker on the 5' terminus; **AgNPs** – silver nanoparticles; **AIBN** – 2-20-azobis (isobutyronitrile); **AuNPs** – gold nanoparticles;**C2** – 2-mercaptoethanol; **ChCl** – choline chloride; **CHIT** – chitosan; **CQDs** – carbon quantum dots; **Cu-TPA** –cooper-doped terephthalic acid; **CYC** – cytochrome C; **dsDNA** – double-stranded deoxyribonucleic acid; **EGDMA** – ethylene glycol dimethacrylate; **EMIM-PF_6** – 1-ethyl-3-methylimidazolium hexafluorophosphate; **f(–COOH)MWCNTs** – functionalized (carboxyl) multi-walled carbon nanotubes; **f(–NH_2)MWCNTs** – functionalized (amine) multi-walled carbon nanotubes; **G** – graphene; **GO** – graphene oxide; **GQDs** – graphene quantum dots; **GST** – glutathione-s-transferase; **HBNNSs** – hexagonal boron nitride nanosheets; **HEH** – 2,2'-(1, 6-hexanediylbisnitrilo-ethylidine)-bis-hydroquinone; **HPPD** – 1-(2-(3,4-dihydroxy -phenyl)-ethyl)-pyrrole-2,5-dione; **IL** – ionic liquid; **MAA** – methacrylic acid; **MIP** – molecularly imprinted polymer; **MOF** – metal organic framework; **MoS_2** – molybdenum disulfide; **MT** – metallothionein; **MTB** – methylene blue; **N-GQDs-COCl** – acrylated nitrogen-doped graphene quantum dots; **N-MWCNTs** – nitrogen-doped multi-walled carbon nanotubes; **p-ANI** – poly-aniline; **p-Py** – poly-pyrrole; **RGO** – reduced graphene oxide; **ssDNA** – single-stranded deoxyribonucleic acid; **Thio** – thionine; **TiO_2NPs** – titanium dioxide nanoparticles; **Zr(IV)-MOF (NH_2-UiO-66)** – zirconium(IV)-based metal-organic framework; **(Ag-Pt)NPs** – silver - platinum nanoparticles; **(Au-Ag)NRs** – gold-silver nanorods; **(Eu^{3+}-NiO)NPs** – europium(III)-doped nickel(II) oxide nanoparticles; **(Zn-$CoFe_2O_4$)NPs** – zinc- and cobalt co-doped ferrite nanoparticles.

Electrode: AuE – gold electrode; **BDDE** – boron-doped diamond electrode; **CPE** – carbon (graphite) paste electrode; **FISE** – fluoride ion selective electrode; **GCE** – glassy carbon electrode; **HMDE** – hanging mercury drop electrode; **ITOE** – indium tin oxide electrode; **np-GCE** – nanoporous glassy carbon electrode; **PGE** – pencil graphite electrode; **PtE** – platinum electrode; **SPCE** – screen printed carbon (graphite) electrode;

Technique: ACV – alternating current voltammetry; **Amp.** – amperometry; **CA** – chronoamperometry; **CV** – cyclic voltammetry; **DPAdSV** – differential pulse adsorptive stripping voltammetry; **DPASV** – differential pulse anodic stripping voltammetry; **DPSV** – differential pulse stripping voltammetry; **DPV** – differential pulse voltammetry; **LSV** – linear sweep voltammetry; **Pot.** – potentiometry; **SWAdCSV** – square-wave adsorptive cathodic stripping voltammetry; **SWSV** – square-wave stripping voltammetry; **SWV** – square-wave voltammetry.

Medium: AcB – acetate buffer; **BB** – borate buffer; **BRB** – Britton-Robinson buffer; **HBS** – HEPES buffered saline; **PB** – phosphate buffer; **PBS** – phosphate buffered saline; **TCAA** – trichloroacetic acid.

Application: when underlined – exhibited interference.

Comments: Ag|AgCl – silver|silver chloride electrode; **Ag|AgCl-pseudoRE** – silver|silver chloride pseudo-reference electrode; **SCE** – saturated calomel electrode.

N/A – not applicable.